

**MENDELOVA UNIVERZITA V BRNĚ**

**LESNICKÁ A DŘEVAŘSKÁ FAKULTA**

**ÚSTAV HOSPODÁŘSKÉ ÚPRAVY LESŮ  
A APLIKOVANÉ GEOINFORMATIKY**

**Design of Application for Assessing the Height of Trees in Forest Stands  
Based on Images from an Unmanned Aerial Vehicle.**

**Doctoral Thesis**

Návrh aplikace pro vyhodnocování výšky stromů v lesním porostu na základě  
snímků z bezpilotního letadlového prostředku.

Disertační práce

*I would like to dedicate  
this work to my father,  
Ing. Antonín Machala*

*Prohlašuji, že jsem práci: Design of Application for Assessing the Height of Trees in Forest Stands Based on Images from an Unmanned Aerial Vehicle / Návrh aplikace pro vyhodnocování výšky stromů v lesním porostu na základě snímků z bezpilotního letadlového prostředku; vypracoval samostatně a veškeré použité prameny a informace uvádím v seznamu použité literatury. Souhlasím, aby moje práce byla zveřejněna v souladu s § 47b Zákona č. 111/1998 Sb., o vysokých školách ve znění pozdějších předpisů a v souladu s platnou Směrnicí o zveřejňování vysokoškolských závěrečných prací.*

*Jsem si vědom, že se na moji práci vztahuje zákon č. 121/2000 Sb., autorský zákon, a že Mendelova univerzita v Brně má právo na uzavření licenční smlouvy a užití této práce jako školního díla podle §60 odst. 1 autorského zákona. Dále se zavazuji, že před sepsáním licenční smlouvy o využití díla jinou osobou (subjektem) si vyžádám písemné stanovisko univerzity, že předmětná licenční smlouva není v rozporu s oprávněnými zájmy univerzity a zavazuji se uhradit případný příspěvek na úhradu nákladů spojených se vznikem díla, a to až do jejich skutečné výše.*

*V Brně, dne: ..... podpis studenta:*

## **Acknowledgements**

First of all I would like to thank to doc. Ing. Martin Klimánek, Ph.D. for supervising this work, for his advices and for providing all the ground and aerial equipment, which was needed for acquisition of all the required kinds of data for the purposes of this work. Big thanks belong also to Ing. Miloš Cibulka, Ph.D. for skilled help with field surveys and all the measurements and to Ing. Přemysl Janata, Ph.D. for expert acquirement of the remote sensing data, both fundamental parts necessary for realisation of this work.

Large thanks then belong to Ing. Pavla Kratochvílová for her patience and very significant help in the field. Last but not least I would like to thank to Ing. et Ing. Stanislav Carbol and his Petra and to Ing. Zdeněk Patočka for collaboration during the ground truth data acquisition. Thanks also to my family and friends for the support and confidence. Finally apologies for all those, whom I had to refuse for the lack of the time, which I devoted to this thesis.

## Abstract / Abstrakt

**Doctoral thesis name:** Design of Application for Assessing the Height of Trees in Forest Stands Based on Images from an Unmanned Aerial Vehicle.

Various remote sensing methods are being utilized to assess fundamental properties of forest stands, such as the height of trees, already for decades. Nevertheless, the use of Unmanned Aerial Vehicles in the combination with Structure from Motion software for these purposes, experiences its boom right now and thus not many pertinent studies exist yet. Such system producing image-based point clouds was utilized in this work to gain the canopy elevation data. To identify individual trees and to extract their height from these remote sensing data, a unique software tool called "UAV Forest Explorer" was developed. Twenty forest study plots was established to acquire the field measurements ground truth data about almost 1 500 trees to thoroughly test the tool and calculate demanded statistics. The research proved, that the tool is fully applicable on all types of forest stands.

**Key words:** Unmanned Aerial Vehicle (UAV) / System (UAS), Height of Trees, Photogrammetry, Image-Based Point Cloud, UAV Forest Explorer.

**Název disertační práce:** Návrh aplikace pro vyhodnocování výšky stromů v lesním porostu na základě snímků z bezpilotního letadlového prostředku.

K hodnocení elementárních vlastností lesních porostů, jako je výška stromů, jsou v posledních desetiletích využívány nejrůznější metody dálkového průzkumu Země (DPZ). Nicméně použití bezpilotních prostředků v kombinaci se softwarem využívajícím principů „Structure from Motion“ k tomuto účelu zažívá svůj vzestup právě nyní a proto zatím neexistuje mnoho příslušných studií. Takovýto systém, vytvářející ze snímků mračno bodů, byl v této práci použit k získání informací o výšce korunového zápoje. Pro identifikaci jednotlivých stromů a pro extrakci jejich výšek z těchto dat DPZ byl vytvořen unikátní softwarový nástroj nazvaný „UAV Forest Explorer“. Dále bylo založeno dvacet výzkumných lesních ploch pro získání referenčních dat pozemního měření pro důkladné otestování nástroje a výpočet potřebných statistik na vzorku téměř 1 500 stromů. Výzkum prokázal, že nástroj je plně použitelný pro všechny typy porostů.

**Klíčová slova:** bezpilotní prostředek (UAV) / systém (UAS), výška stromů, fotogrammetrie, mračno bodů získané ze snímků, UAV Forest Explorer.

# Table of Contents

<b>1. Introduction</b> .....	<b>1</b>
<b>2. Aim of the Work</b> .....	<b>5</b>
<b>3. Literature Overview</b> .....	<b>7</b>
3.1. Terrestrial Tree Height Measurements .....	7
3.2. Tree Height Assessment Via Remote Sensing .....	11
3.2.1. LiDAR Technology .....	11
3.2.2. Photogrammetric Processing of Image Data .....	14
3.2.2.1. Development of the Technology .....	14
3.2.2.2. Image-Based Point Clouds .....	19
3.2.3. Comparison of ALS and Image-Based Point Clouds .....	22
3.2.4. Forest Stands Assessment Approaches .....	25
3.2.4.1. Area-Based Approach .....	25
3.2.4.2. Individual Tree Approach .....	27
3.2.4.3. Data Segmentation Methods .....	30
3.2.4.3.1. Overview of the Methods .....	30
3.2.4.3.2. Inverse Watershed Segmentation .....	33
3.3. Unmanned Aerial Vehicles and Systems .....	35
3.3.1. Terminology .....	35
3.3.2. Unmanned Aerial Systems and their Advantages .....	39
3.3.3. Surveying Using Unmanned Aerial Systems .....	41
3.3.4. UASs and Photogrammetry .....	43
3.3.5. Employment of UAS in Forestry .....	45
3.3.6. Recent Studies of Interest .....	50
<b>4. Methodology</b> .....	<b>55</b>
4.1. Characterisation of Research Area .....	55
4.2. Specification of Study Plots .....	56
4.3. Forest Stands Measurements .....	59
4.3.1. Equipment .....	59
4.3.2. Measurements of Trees .....	61
4.4. Data Acquisition Using Unmanned Aerial Vehicle .....	65
4.4.1. Equipment .....	65
4.4.2. Image Data Acquisition using UAV .....	69

4.5. Hardware and Software .....	72
4.5.1. Hardware.....	72
4.5.1.1. Desktop PC.....	72
4.5.1.2. Notebook PC .....	72
4.5.2. Software.....	73
4.5.2.1. Agisoft PhotoScan® Professional Edition .....	73
4.5.2.2. ArcGIS® for Desktop Advanced.....	75
4.5.2.3. PythonWin.....	79
4.6. Image Data Processing .....	80
4.6.1. Automated Image Registration .....	80
4.6.2. Photogrammetric Image Processing.....	81
4.6.3. Auxiliary data.....	87
4.7. UAV Forest Explorer Software Tool Development.....	89
4.7.1. General Description of the UAV Forest Explorer.....	89
4.7.2. User-Defined Entries and Input Data for Initial Settings.....	92
4.7.3. Processing Principles and Tool Outputs .....	97
4.7.3.1. Identification of Trees and Computation of their Height .....	97
4.7.3.2. Comparison with Field Measurements Data.....	116
4.7.4. Specific Workflow Applied in this Study .....	137
4.7.4.1. Running the Tool .....	137
4.7.4.2. Assessing the Tool Outputs .....	142
<b>5. Results .....</b>	<b>147</b>
5.1. Results of the Field Measurements .....	147
5.1.1. Counts of Field-Measured Trees.....	147
5.1.2. Forest Stands Composition.....	148
5.1.3. Field-Measured Height of Trees .....	152
5.2. Results of the UAV Forest Explorer Runs .....	154
5.2.1. Individual Tree Approach Results .....	154
5.2.1.1. Root Mean Square Error (RMSE).....	155
5.2.1.2. Pearson’s Correlation Coefficient (R) .....	158
5.2.1.3. Pearson’s Correlation Coefficient (R) for Matched Trees Only...	161
5.2.1.4. Mean Difference of Heights for Matched Trees Only .....	162
5.2.1.5. Suitable CS, IM and FS Settings of the Tool within the ITA.....	163

5.2.2. Area-Based Approach Results .....	168
5.2.2.1. Count Difference, Height Difference and Standard Deviation. ...	168
5.2.2.2. Suitable CS, IM and FS Settings of the Tool within the ABA. ....	173
5.3. Interpretation of Results. ....	178
5.3.1. Interpretation of DTM Processing Results .....	178
5.3.2. Interpretation of Field Measurements Results .....	178
5.3.2.1. Counts of Trees and Species Composition .....	178
5.3.2.2. Height of Trees .....	180
5.3.3. Interpretation of UAV Forest Explorer Results .....	182
5.3.3.1. Individual Tree Approach Results .....	182
5.3.3.1.1. Root Mean Square Error .....	183
5.3.3.1.2. Pearson's Correlation Coefficient .....	184
5.3.3.1.3. Pearson's Correlation Coefficient for Matched Trees Only ...	185
5.3.3.1.4. Mean Difference of Heights for Matched Trees Only .....	186
5.3.3.1.5. Suitable CS, IM and FS Settings of the Tool within the ITA ...	187
5.3.3.2. Area-Based Approach Results .....	189
5.3.3.2.1. Count Difference, Height Difference and Standard Deviation	189
5.3.3.2.2. Suitable CS, IM and FS Settings of the Tool within the ABA ..	192
5.4. Summarization of Results .....	193
<b>6. Discussion .....</b>	<b>196</b>
<b>7. Conclusion .....</b>	<b>201</b>
<b>8. Souhrn .....</b>	<b>203</b>
<b>9. References .....</b>	<b>205</b>
List of Abbreviations .....	223
List of Appendices .....	226



# 1. Introduction

Acquisition of various forest stand parameters, such as height of trees, diameter at breast height, stand density or stocking is a fundamental precondition for successful forest management or ecological research and applications (van Leeuwen & Nieuwenhuis, 2010). Especially the height of trees is an elemental measurement in most of the forest inventories and is a critical variable for quantitative assessment of further forest characteristics, such as volume of trunks, carbon stocks, growth of stand, forest site quality or its productive capacity (Andersen et al., 2006). For decades the ascertainment of the basic forest stand properties was performed principally by means of field surveys and manual tree measurements (West, 2004).

The field measurements are relatively accurate, but are generally time-consuming and costly (Kant & Alavalapati, 2014). Therefore various applications capable of estimating demanded forest characteristics based on remote sensing technologies are being developed, ever since such technologies are available. The aim of such endeavour is to acquire the required parameters efficiently for large forest areas with less manpower and effort compared to field surveys, which should lead to reduction of expenses (Andersen et al., 2006).

Originally airborne and later also spaceborne images were the remote sensing data used for retrieval of information about forest stands' health and structure. They were analyzed primarily in their inherent form as two-dimensional images (in an analogue and later also in digital form) enabling to study conditions and also physical proportions of forest stands and even shapes, sizes and distribution of single tree crowns. As the field of aerial photogrammetry and stereo image matching was being developed, also three-dimensional mapping and measurements were made feasible. This enabled to obtain much more detailed metrics of individual trees including their height (Baumann, 2014; Korpela, 2004).

Since these methods had some significant limitations in typical forest environments (mainly poor visibility of the ground below forest stands with dense canopy), also the measurements of height could be performed with demanded accuracy mainly in some, relatively sparse forest stands. An inception of a new technology of light detection and ranging (LiDAR) prefigured a way how to circumvent these deficiencies of photogrammetric methods (Næsset, 2007).

Since laser pulses can penetrate the forest canopy and measure both, elevation of the canopy as well as elevation of the ground below, LiDAR seemed to be an ideal mediator for acquisition of high-accuracy three-dimensional information about forest structure. Many research studies affirmed the usability of this technology for mensuration of various forest- and tree-level quantities (an overview give e.g. van Leeuwen & Nieuwenhuis, 2010). Aerial laser scanning campaigns even became an integral part of national forest inventories of several (mainly Scandinavian) countries (Carson et al., 2004). Nevertheless, the technical complexity of the LiDAR devices and relatively high costs of the data acquisition via this technique make it still unavailable for many target groups of potentially interested customers (Erdody & Moskal, 2010).

The fast development of Unmanned Aerial Vehicles and Systems (also called Remotely Piloted Aircraft Systems) transcending beyond the purely military applications in recent years, outlined the possibilities of photogrammetry comeback, not only for forestry purposes (Haala, 2009). Even though these devices cannot be equipped with high-quality aerial surveying cameras, but rather with normal digital compact cameras, the contemporaneous development of software allows to reach very satisfactory outputs with these relatively very cheap and available systems. Particularly implementation of multiple image matching, computer vision and Structure from Motion principles into this software made it possible to process images from classical user-grade cameras and from them to acquire the elevation data of forest canopy surface in the form of high-density 3D point clouds (Dey et al., 2012).

Although also these methods need the information on the elevation of the ground below the forest stand for the proper canopy height assessment. One option is to utilize the LiDAR-derived digital terrain models in the areas, where is available (e.g. from national campaigns providing otherwise not enough-quality digital surface models for good tree height assessment, as is the situation e.g. in the Czech Republic). Another option is to use the terrain model retrieved from the photogrammetric point cloud, preferably from images gained within the leaf-off season, as some authors also proved to be applicable (Dandois & Ellis, 2013).

The cost-effectiveness, high flexibility and adaptable employment regarding the time requirements, weather conditions or various phenological stages and ecological phenomena make the UAS-based photogrammetry a versatile tool for support of decision-making in forestry management or diverse ecological

studies (Anderson et al., 2013). Even though the use of aerial photogrammetry in forestry is a relatively old branch, for its highly different principles the UAS-based photogrammetry and its application for tree parameters assessment is still a very young discipline. Therefore only few research studies dealing with tree height estimation using this technology have been published so far (Puliti et al., 2015).

The fundamental quantity - height of trees, which was examined within this study, can be assessed basically from two points of view. One is referred as the area-based approach, and the more-detailed one is the individual tree approach (Vastaranta et al., 2009). To appropriately evaluate the estimation of tree height from the remote sensing data, it is important to compare the calculated results with the ground truth, obtained usually using accurate field measurements (Vauhkonen & Mehtätalo, 2015). When assessing the accuracy of applied procedure and statistical model, it is important to consider not only the comparison of field-measured and calculated tree heights, but also the numbers of trees being identified and thus compared.

As can be seen in the very few available scientific papers, the achieved results of identification of trees and of estimation of their height using UAS image-based technology are very varying. The reached accuracies are disputable, since in some cases the correlation with field-measured data can be very poor, e.g.  $R^2 = 0.1$  even in two studies (Dandois & Ellis, 2013; Díaz-Varela et al., 2015). In some studies where the results seem to be more satisfactory, the authors had to use very sophisticated statistical methods to find a suitable regression equation giving them acceptable results (e.g. Lisein et al., 2013; Puliti et al., 2015). The practical applicability of such workflows is then questionable.

The methods of identification of individual trees as such are then usually very weakly described, or the authors utilized area-based approach only (e.g. Díaz-Varela et al., 2015). Some authors used visual interpretation of point cloud data and subsequent manual identification of trees (e.g. Sperlich et al., 2014; Wallace et al., 2016). Other authors compared their models only with few tallest trees on their study subplots (Dandois & Ellis, 2010, 2013). The authors who “showed their hand” and stated the success rate of trees identification then achieved diverse, and sometimes not very satisfactory results, e.g. between 13 % for broadleaf and 90 % for coniferous forest stands (Sperlich et al., 2014).

The remaining studies then seem to ignore to compare the numbers of field-measured trees with the numbers of identified trees (e.g. Lisein et al., 2013). The

results of height assessment can then come out very well, but when the numbers of identified trees do not correspond to those of measured trees, or when the authors selected only some portion of the trees to assess their heights, without showing the selection key, such results seem to be rather irrelevant.

Since none of the discovered studies describes any tool which would enable to find the appropriate results of trees identification suitable for particular forest stands, either concerning the numbers of identified trees, or the accuracies of height estimation, this seems to be still relatively unexplored field of research. The tool should enable to select the proper settings to achieve the numbers of identified trees maximally corresponding to the numbers of field measured trees on the one hand, with the height differences kept at the minimum on the other hand. Since such tool suitable to process image-based point clouds from a UAS and derive the required height of trees from these remote sensing data was missing, development of such tool and its practical testing on own study plots was the main goal of this work.

## 2. Aim of the Work

The height of trees is a fundamental quantity, the knowledge of which enables to assess and derive a series of parameters of the forest stands. For instance in the combination with other properties such as the age of the stand or species composition it enables to evaluate the growing conditions present at particular forest areas and indicates their potential. Together with the information about the diameter at breast height (DBH) or other parameters it can serve as an input for computation of the growing stock at particular forest stands, and many more.

Assessing the height of standing trees is therefore a crucial operation when evaluating the properties of forest stands being under any type of management. Nevertheless, the most common way of acquiring this quantity, i.e. manual measurement by any type of hypsometer in the field, is highly demanding and time-consuming, and therefore expensive. The common method of measuring only some portion of trees in the forest of interest and subsequent generalization then often cannot be sufficiently accurate, since it cannot guarantee that different conditions and all the various parts of the forest stand are comprehended enough.

For this reason a series of methods utilizing the remote sensing data for the assessment of the height of trees are being developed and applied in recent years, enabling to evaluate large areas of forests at one time. The most common method is still usage of the aerial LiDAR data. This data can be highly accurate, but they still suffer one disadvantage - generally high price and with that connected relatively low accessibility for many potential users.

The elementary aim of this work was therefore to utilize an alternative source of the remote sensing data which would enable to assess the height of trees in the forest stands. The image data gained using the digital cameras mounted on an Unmanned Aerial Vehicle (UAV) were chosen for this purpose. UAVs are relatively cheap (compared to LiDAR technology, or aerial photogrammetry) and can be therefore afforded by even smaller forest management subjects, companies or institutions. The image data from such device, when photogrammetrically processed, then provide similar data as the LiDAR technology. Particularly a point cloud in the form of \*.las file, which enables to build a Digital Surface Model of the forest canopy (or particularly a Canopy Height Model) can be acquired.

Even having such data available, it can be still quite demanding to process them efficiently and to extract the height of examined trees from them with

satisfactory results. The main aim of this work is therefore to design and to create an original application, i.e. a software product, which would enable to process the UAV-based data effectively and to extract the heights of trees from them.

The basic logic of such tool then is to facilitate testing of various kinds of settings of inverse watershed segmentation inputs to enable to find the most suitable ones fitting to particular forest stands. To have the adequate UAV-based image data of various forest stands for the tool development and for the subsequent testing, a series of flight campaigns is to be performed. Since the outputs of such application have to be verified, best on the ground truth data, the next aim of this work is the acquisition of the field measurements data which can make it possible. Therefore all the photographed forest stands are to be visited and all the demanded properties of trees should be manually acquired.

Since for the purposes of this work both approaches are to be tested, i.e. the one working generally with all the trees present at examined study plots (area-based approach), as well as the one working also with particular trees (individual tree approach), also the exact positions of the trees are to be measured using the high-accuracy geodetic equipment (surveying GNSS devices and total stations).

Such field-measurements data including the height of trees, their exact positions and other properties, such as determined species, health and morphological conditions, DBH etc., then can serve as a sufficient ground truth. The various outputs of the own tool then can be compared with this field data based on specific statistical computations. This enables to find the settings of the application leading to the results the most fitting to the ground truth in each particular forest stand. Such results should differ minimally regarding the number of identified trees and their height, from the ground truth data. The developed application therefore should enable to test the settings on a field-measured portion of the explored forest stands and then potentially to apply these settings on the whole extent of the forest stands with minimal additional effort.

## 3. Literature Overview

### 3.1. Terrestrial Tree Height Measurements

Tree height (or also total or actual height when referred in the forestry context) is defined as the vertical distance between the tip of the tree and mid-slope point of the base at ground level (Husch et al., 1972). As emphasizes Andersen et al. (2006), tree height is one of the most fundamental measurements in forest inventory and is a critical variable in the quantitative assessment of forest biomass, carbon stocks, stand growth, and site productivity. Individual tree height and stem diameter are the primary variables used in the estimation of tree and stand volume, and tree height at a given age is often used as an index of forest site quality (Schreuder et al., 1993).

As states Bragg (2007), foresters have measured height in many ways since the earliest years of the profession (e.g., Schlich, 1911). As broadly describes Larjavaara & Muller-Landau (2013), tree heights have long been measured as part of efforts to quantify timber resources (Avery & Burkhart, 2011), and more recently also forest carbon stocks (Chave et al., 2005; Feldpausch et al., 2012). In addition, tree heights are often measured in ecological studies characterizing life histories of individual tree species and populations (King & Clark, 2011; Banin et al., 2012).

A number of different methods are used to measure tree heights from the ground (Clark & Clark, 2001; Chave, 2005; CTFS, 2007). Perhaps the simplest method involves lifting the top of a pole of known length to the same level as the top of the tree using, for example, a telescoping height measuring pole. This method is easy to learn but requires two field technicians because the relative height of the tops is difficult to judge from directly below. More importantly, this method is limited to relatively small trees (approximately below 10 m in height). It is possible to apply a similar methodology to larger trees, but only by having a technician climb the tree (or an adjacent structure). This approach is used to measure potentially record-breaking trees (Goodwind, 2004), but is obviously very slow and potentially dangerous, and thus not suitable for measuring large numbers of trees in inventories (Larjavaara & Muller-Landau, 2013).

For larger trees, height measurements typically involve light, handheld instruments used to examine trees from a distance. Between the most common methods belong tangent and sine methods utilizing clinometer or rangefinder devices. Both methods can be explained on Figure 1. Tree height is defined as distance

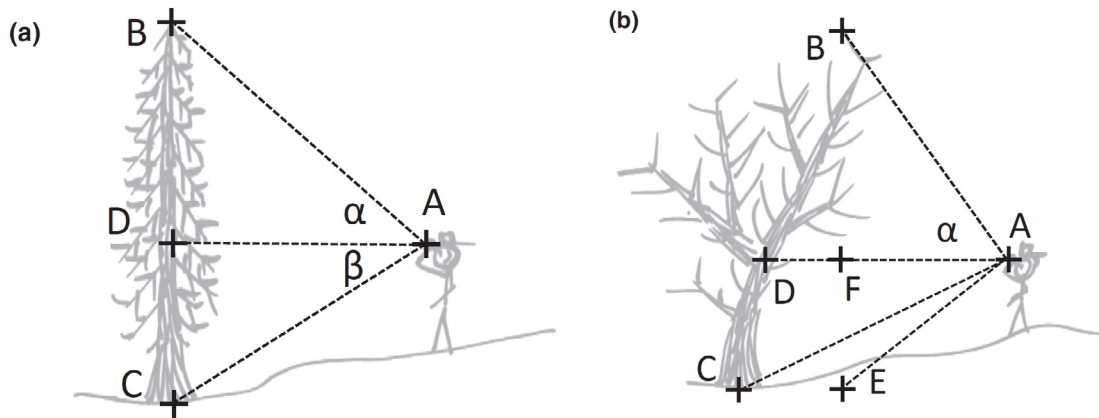


Fig. 1. Tree height measurements using tangent and sine methods shown on a vertical tree (a) and a leaning tree (b). Source: Larjavaara & Muller-Landau (2013).

BC in (a) and BE in (b). For a vertical tree in which the top is directly above the trunk (a), the tangent method requires measuring angle  $\alpha$  from horizontal to the top (B) and distance AD and computing  $BD = \tan \alpha \cdot AD$ , where BD is the distance from B to D and AD the distance from A to D.

If the ground is not flat and thus the vertical distance to the base, CD, cannot be easily estimated from the height of the technician, then CD can be estimated in the same way:  $CD = \tan \beta \cdot AD$ . The tree height is  $BC = BD + CD$ . The sine method is based on measuring the angle  $\alpha$  and distance AB to the top of the tree and computing:  $BD = \sin \alpha \cdot AB$ . As with the tangent method, CD can be estimated from the height of the technician alone on flat ground, or using the sine method. When the tree is leaning (b), or more generally when the topmost branch is not located above a vertical trunk, the tangent method risks severely biased estimates. For example,  $\tan \alpha \cdot AD$  severely overestimates the height to the top of the tree in (b). Instead, this height is correctly estimated as  $\tan \alpha \cdot AF$ , where AF is the distance to an imaginary plumb line hanging down from the top of the tree.

Similarly, if the bottom part of the tree (below A) is also estimated with the tangent method, the angle needs to be measured to E which is at the same level with C but directly below B. In contrast, lean of the tree does not influence field procedures for the sine method as  $BF = \sin \alpha \cdot AB$  and  $EF = \sin DAC \cdot AC$ , where DAC is the angle between DA and AC (Larjavaara & Muller-Landau, 2013).

Before laser rangefinders were easily available, the tangent method predominated. This method involves measuring angles ( $\alpha$  and  $\beta$ ) from horizontal with a clinometer and combining these with measurements of either horizontal distance or of angles to a pole of known length (Korning & Thomsen, 1994). Historically horizontal distances were often measured with measuring tapes or simple distance prisms; more recently, ultrasound technology and laser rangefinders have been used for the same purpose.



The actual height measurement processes look superficially similar with the tangent and sine methods. Most of the measurement time is spent searching for a spot from which the top of the tree can be seen clearly. The main differences are that the sine method lacks the horizontal distance (AD in Fig. 1a) measurement and can be carried out from closer to the trunk (the precision of the tangent method declines quickly at higher angles and thus shorter distances).

Many newer laser rangefinders, especially those designed for forestry, can also be set to return the distance based on the reflection from a more distant object – this is very useful for measuring height of canopy trees from directly under the canopy. Regardless, there must be some direct, unblocked path to the top of the tree in order for measurements to be taken using the sine method, and it can be difficult to find such a path in the dense and multi-layered canopies of some forests. In contrast, the use of the tangent method and a clinometer is capable of yielding good results even without visibility to the top. For example, if the crowns of the target species are normally symmetrical with the top in the middle and other parts of the crown can be seen, the technician can estimate the location of the top and measure the angle to it even if the top is not directly visible (Larjavaara & Muller-Landau, 2013).

For the tangent method, the technician has to stand at a large enough distance that the angle from horizontal to the top remains fairly small. An oft-repeated recommendation is that this angle should be smaller than  $45^\circ$  (Goodwind, 2004), which means that the observer stands at a distance equivalent to at least one tree height.

The main reason for this recommendation is that the tangent of an angle increases very rapidly for larger angles, and thus, the precision of the height measurement declines disproportionately. In addition, the closer the observer is to the tree, the greater the bias if the tree is leaning or if the technician shoots not to the top directly above the base, but to parts of the crown closer to the technician. Various errors which can appear within application of both sine and tangent methods, can be seen in Figure 2.

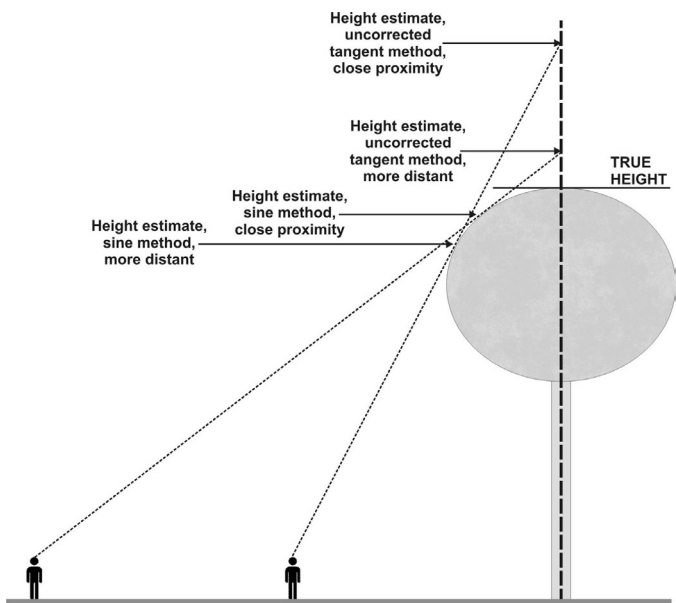


Fig. 2. The proximity effects on misread crown heights for the sine and tangent height measurements methods. Source: Bragg (2007).

Especially in dense and tall forests such as many tropical forests, intervening vegetation often makes it difficult if not impossible to find a spot that has a sufficiently good view of the tree crown at a sufficiently large distance that the angle is  $<45$  degrees. This contrasts with the sine method, in which the technician is free to make measurements at shorter distances to the tree, and even under the canopy. The specific visibility conditions of the forest will determine whether in practice it is easier to see where the top is from a distance greater than the tree height (tangent method) or to find an unblocked view of the top from anywhere (sine method) (Larjavaara & Muller-Landau, 2013).

Field ecologists and foresters have often discussed the best method and instrument to measure tree height and the scale of the uncertainty involved. Of the studies on uncertainty in tree height measurements that have been carried out, many focused on comparing instruments in ideal conditions of perfect visibility (Skovsgaard et al., 1998; Wing et al., 2004). Based on these studies, most instruments and both methods seem to have low systematic and random errors when measuring the height of a perfectly vertical tree with both top and bottom perfectly visible. However, these tests provide limited insight into the performance of these methods under typical measurement conditions in forests, with limited visibility and leaning trees.

Other studies have described the risks involved in the tangent method (Goodwind, 2004; Blozan, 2006; Bragg, 2007), or compared measurements from handheld instruments based on the tangent method with actual heights obtained by climbing. For instance Rennie (1978) compared measured heights among six methods and with actual heights; he found height measurements obtained using a simple clinometer and a measuring tape to be fast and relatively unbiased on easy to measure pines in a plantation.

Similarly, Williams et al. (1994) compared measured heights among methods and with actual heights in another pine dominated research site with similar results. Da Silva et al. conducted two separate studies; one in a eucalypt plantation (da Silva et al., 2012a) and another in natural forest nearby Rio de Janeiro (da Silva et al., 2012b). In the plantation, mechanical clinometers performed better than electronic ones, and bias was significant only when distance to the tree was much smaller than tree height. In the natural forest, the random errors were larger, while bias remained unimportant (Larjavaara & Muller-Landau, 2013).

## **3.2. Tree Height Assessment Via Remote Sensing**

As described in the previous chapter, it can be often very difficult to implement any of the common manual methods of measuring the height of standing trees in some rather closed stands, where the treetops are not easily visible. Also for this reason, measurement of tree height is usually time-consuming, and therefore expensive component of forest inventories (Andersen et al., 2014). Collection of information from forests is the main task of the forest inventory and making correct decision in forest management is based on the quality of the collected information (Benko & Balenović, 2011). Forest economic planning is a basis for decisions of the forest industry, the official forest policy and the forest owners in order to be able to optimally exploit forest resources and products. Typically, forests are operationally assessed with two scales: economic planning of forests at stand level, when the forest stand is a homogeneous forest area with respect to forest resources and treatments needed (small-area inventory), and monitoring of forest resources at the national level (large-area inventory) (Hyypä et al., 2000).

Due to the rapid development of technology, in the second half of the 20<sup>th</sup> century, there have been major changes in the way of data collection, particularly in developed countries. In addition to conventional terrestrial methods of data collection, data on forests are increasingly being collected with remote sensing methods. Using remote sensing methods leads to reducing the scope of the fieldwork, and opens the possibility of saving time and money (Benko & Balenović, 2011).

Various kinds of remote sensing data have been utilized for gathering the information about different properties of forest stands, including the height of trees, in recent decades. Between the most common belong aerial or also satellite images (formerly analogue, recently mainly digital ones with various spatial and spectral resolution) which are often also being photogrammetrically processed. Lately were utilized also technologies such as synthetic aperture radar (SAR) or widely deployed Light Detection and Ranging (LiDAR), from which especially the last mentioned became very popular, but its relatively high cost demands are still an often limiting factor for its availability.

### **3.2.1. LiDAR Technology**

In the forestry, as well as in many other fields of human activity, the LiDAR technology finds a place as a very powerful tool for data acquisition. Since it is nowadays a widely utilized and at the same time still thoroughly studied technology

enabling to gain similar type of data and to process them in a resembling way as were the data treated in this work, the possibilities of the LiDAR application in height assessment in forestry will be also described.

LiDAR is a technology that uses laser pulses to generate large amounts of data about the physical layout of terrain and landscape features. All varieties of LiDAR operate using the same basic principle. The LiDAR instrument fires rapid pulses of light (laser pulses) to the landscape and a sensor mounted on the instrument measures the amount of time taken for each light pulse to bounce back. Because light moves at a constant and known speed, the LiDAR instrument can then calculate the distance between itself and the target with high accuracy. By rapidly repeating the process, the LiDAR instrument builds up a complex 'picture' of the surface it is measuring, in the form of a point cloud LAS file (Schuckman & Renslow, 2012).

The LAS file format is, according to ASPRS (2012), a public file format for the interchange of 3-dimensional point cloud data between data users. Although developed primarily for exchange of LiDAR point cloud data, this format supports the exchange of any 3-dimensional X, Y, Z triplet. The intention of the data format is to provide an open format that allows different hardware and software tools to output data in a common format.

Airborne LiDAR (or ALS - Aerial Laser Scanner) has advantages over other airborne remote sensing techniques, such as multispectral or hyperspectral imaging, in that it generates three-dimensional structural data because the laser pulses can penetrate the forest canopy to reach the ground (Figure 3.). ALS systems then have the capacity to directly measure the vertical distribution of vegetation and the underlying topography, resulting in the accurate estimation of both vegetation height and ground elevation (White et al., 2013a).

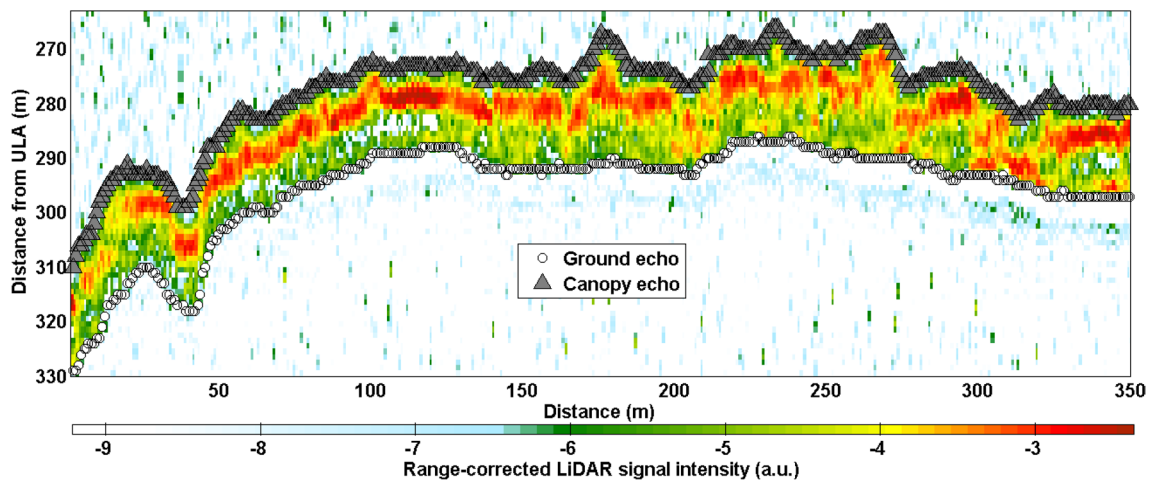


Fig. 3. Example of ground echo and canopy top detection from a LiDAR signal for a section of flight over a forest. The difference between these two point layers yields the canopy height. The used y-axis is the distance from the emitter (aircraft). Source: Shang et al. (2016).

The actual points collected are dependent on the hardware, but the most common are first hit (usually the canopy layers), last hit (usually the ground), and a secondary hit or hits that land somewhere in between. Many scanners can also collect the information about surface laser is reflected by. While there are many different types of LiDAR systems, discrete-return ALS systems are the most common type used in forestry applications (Wulder et al., 2008).

As widely describes Edson & Wing (2011), LiDAR has recently emerged as significant technology for forest measurement applications. Forest measurements derived from LiDAR include ground and vegetation surfaces, which are used to assess tree height, volume, and biomass measurements (Popescu et al., 2004). Many forest attributes can be measured by LiDAR over large areas including canopy height, sub-canopy topography, vertical canopy distribution (Lim et al., 2003), and individual tree heights (Andersen et al., 2014). Tree height may also be used to estimate diameter at breast height (DBH), based on allometric equations (Lucas et al., 2008).

Edson & Wing (2011) continue, that when measuring tree heights using LiDAR, accuracy is impacted by several factors including size and reflectivity of the tree, shape of the tree crown, and LiDAR pulse density and footprint (pulse diameter). A primary source of error in LiDAR tree height measurement associated with conifer species occurs when laser pulses miss the sharp apex of the tree resulting in an underestimation of tree height (Anderson et al., 2006; Popescu et al., 2002). Lewis & Hancock (2007) confirm, that due to the low probability of hitting the absolute highest point in the canopy for a given pulse (and a given species of tree), canopy height surfaces derived from LiDAR are consistently lower than field measurements, but this effect can be accounted for with empirical corrections.

Discrete returns from LiDAR pulses that strike the canopy may be used to estimate tree heights, or canopy elevations may be derived from a canopy height model (CHM) (Lovell et al., 2005). In order to reduce the computational burden in processing mass points, the trees are usually detected from a 2.5-dimensional CHM interpolated from the height data (Vauhkonen, 2010). A CHM is raster surface model interpolated from points acquired on the upper surface of the canopy. It can be generated by subtracting the digital terrain model (DTM) from the digital surface model (DSM), resulting in normalized aboveground object heights.

LiDAR tree height estimates are therefore calculated by subtracting the terrain surface from the top of the vegetation, so that highest points - local maxima, can be associated with individual trees (Lim et al., 2003; Kraus & Pfeifer, 1998). Tree height can be estimated as the values of these maxima, but other measurements require

the tree crowns to be delineated from their surroundings. Mainly image analysis techniques are used also for that purpose, but the segmentation can equally be done by point-based techniques (Vauhkonen, 2010). Based on the tree structure, errors in LiDAR tree height measurement are also dependent on the algorithm used to create the CHM (Hyyppä et al., 2004). (Edson & Wing, 2011).

Van Leeuwen & Nieuwenhuis (2010) confirm, that most attention in retrieving structural parameters from LiDAR data has been paid to the retrieval of tree height, and plot height averages such as Lorey's mean height, predominant tree height, and average tree height, but the technique also allows for individual tree measurements after segmentation of the LiDAR point cloud. Various segmentation approaches have been proposed in a number of studies with varying degrees of success (e.g. Heurich, 2008; Chen et al., 2006).

Validation of field and remotely sensed tree height is sometimes difficult due to differences in scale of the field observations and LiDAR acquisitions (Zhao et al., 2009), and challenges to collocate the two (Popescu et al., 2002). These aspects of scale need to be taken into consideration when the suitability of LiDAR remote sensing for forest inventory is assessed and comparisons with other sources of information are made. Furthermore, differences in definition of height measures complicate the task of comparing LiDAR-derived height metrics among different studies (Lovell et al., 2005). For example, mean tree height may be taken as the average height of dominant and codominant trees (Lefsky et al., 2007), whereas others may attempt to include the contribution of suppressed trees (Lee & Lucas, 2007; Maltamo et al., 2004). (Van Leeuwen & Nieuwenhuis, 2010).

### **3.2.2. Photogrammetric Processing of Image Data**

#### **3.2.2.1. Development of the Technology**

The capacity to acquire information characterizing the three-dimensional structure of forest canopies has revolutionized forest inventories around the globe (van Leeuwen & Nieuwenhuis, 2010). Airborne laser scanning has been the primary data source for three-dimensional information on forest vertical structure (Reutebuch et al., 2005; Evans et al., 2006; Wulder et al., 2008; Hyyppä et al., 2008), however, there is an increasing interest in the use of high spatial resolution digital aerial imagery to generate information analogous to ALS data (Leberl et al., 2010; Bohlin et al., 2012a; Järnstedt et al., 2012) to support forest inventory and monitoring. This interest in alternative technologies for acquiring accurate height

information can be attributed to needs to control costs, but also to provide data that is complementary to traditional inventory practices, available technical capacity, and current regulatory requirements (White et al., 2013a).

As broadly describes Balenović et al. (2015), widely used remote sensing methods for estimating tree heights include besides LiDAR also photogrammetric measurements of aerial images. Manual methods of stereophotogrammetry have been used in forestry since the 1940s (Korpela, 2004). Estimating the height of an individual tree and mean stand height, by photogrammetric measurements of stereo pairs using classical analogue aerial photographs from analogue or analytical stereo instruments (analogue and analytical photogrammetry) has been studied by a number of authors (e.g., Worley & Landis, 1954; Næsset, 1996; Kovats, 1997; Anttila, 1998; Eid et al., 2004; Magnusson & Fransson, 2005). Aerial photographs and digital aerial images have become an integral part of forest inventories in a number of countries (e.g., Finland, Norway, Sweden, Canada) (Spencer & Hall, 1988; Næsset, 2002a; Magnusson et al., 2007; Tuominen et al., 2014).

During a classical photogrammetric stereo-measurement of analogue aerial photographs, tree height is determined by placing stereo markers of the instrument on the top of the tree and ground next to the tree and the elevation difference between the two markers is then calculated as the height. The main disadvantage of this process is the limited potential of identifying the bottom of a tree in densely canopied stands, if the terrain surface in the vicinity of the tree is not visible (Korpela, 2004; Paine & Kiser, 2012). Another reason for the limited practical application is related to the amount of manual processing required when using the classical photogrammetric methods (Balenović et al., 2011). Due to above-mentioned reasons it has been generally accepted that the extraction of forest and tree data from classical analogue aerial photographs had certain limitations, especially in the densely canopied forests. Therefore, except for the above-mentioned countries the usefulness of classical photogrammetric method for forest inventories remained a controversial issue (van Laar & Akça, 2007).

However, advancements in computer technology in the 1980s and 1990s have enhanced the development of remote sensing methods and techniques. Over the past thirty years, photogrammetry has also crossed a developmental path from analogue and analytical to digital photogrammetry, which has replaced analogue aerial photographs and analogue and analytical stereo instruments with digital aerial images and digital photogrammetric workstations (DPWs) (Magnusson et al., 2007; Linder, 2009). By the development of digital photogrammetry, primarily as a result of improvement in digital aerophotogrammetric cameras (DACs) that

can capture digital images of high spatial, radiometric and spectral resolution, as well as by digital photogrammetric workstations, possibilities of application of the photogrammetry in practical forestry were highly increased and extended (Balenović et al., 2010).

Current digital aerial photogrammetric cameras make it possible to capture digital aerial images of extremely high spatial resolution with Ground Sampling Distance (GSD) values of only several centimetres (Sandau, 2010). With the application of DPWs, a number of photogrammetric processes, such as the creation of digital terrain models or digital orthophotos, have generally become automated and the manipulation of aerial images has improved (Honkavaara et al., 2009; Lemmens, 2011). (Balenović et al., 2015).

Balenovic et al. (2011) then further broadly explains, that digital (softcopy) photogrammetry can be defined as the newest development phase of photogrammetry which includes the use of digital images captured by DACs or scanned analogue images as well as the use of DPWs in order to perform photogrammetric processing and to obtain photogrammetric products. Although the term digital photogrammetry has been in use for a long time, namely when scanners were used to obtain digital image from analogue photographs, only with the appearance of digital cameras we can talk of fully digital photogrammetry. The first commercial solutions of DACs were presented at the ISPRS (International Society for Photogrammetry and Remote Sensing) congress in 2000 in Amsterdam (Cramer, 2005; Sandau, 2010).

The appearance of DACs which, by its characteristics, could replace the existing analogue technology meant a big change for photogrammetry. During a single aerial survey, the majority of digital cameras simultaneously record panchromatic, red, blue, green and infrared part of electromagnetic spectrum. With the help of GPS (Global Positioning System) and IMU (Inertial Measurement Unit), it is possible to get oriented images right after airplane landing. Then the images are directly loaded into DPWs for further processing. The additional benefits of using DACs are that there are no longer needs for films, photolab developing and scanning. In this way, a whole phase of photogrammetric work process disappeared, resulting in time and costs savings (Ciceli, 2004; Petrie & Walker, 2007).

Furthermore, digital images have improved radiometric properties of the image which enables much more information to be extracted, especially from shadowed areas of the image. Digital images also outperformed the analogue ones in terms of spatial resolution. This led to the improved stereoscopic view and better possibility for interpretation from stereomodel derived from digital images. Electronic forward motion compensation device enables recording of high spatial



resolution images at great flying speed, so the time interval between two recordings can be shorter than one second. Due to the properties of DACs, aerial recordings can be made under relatively low light conditions. This increased the length of the season suitable for recording, as well as extended daily time appropriate for aerial photo flight sessions (Cramer, 2005; Jacobsen, 2009).

Balenovic et al. (2011) further describes, that a digital camera, in its main parts, is almost identical to the analogue one. The basic difference is in the media for light registration and the process of creating images. In analogue cameras the media is a film and the image is created photographically, i.e. by chemical reaction of light and film. In digital cameras, the film is replaced by an electronic photosensitive sensor which could be CCD (Charge-Coupled Device) or CMOS (Complementary Metal Oxide Semiconductor) (Ciceli, 2004; Petrie & Walker, 2007). Concerning the digital photogrammetric workstations, the first DPW was presented at the XVI ISPRS congress held in Kyoto in 1988. The DPW was defined as "a hardware and software connection to derive photogrammetric products from digital imagery". The advances in computer technology in the 1990s had great influence on the DPWs evolution and their expansion at the market. At the end of the same decade many photogrammetric companies and research institutions were using DPWs which gradually took domination over the analytical plotters (Petrie, 1997; Ahmad, 2008).

As any other ordinary computer, the DPW also consists of hardware and software. The main characteristic of DPW is a powerful hardware which implies powerful and fast processor (CPU), large memory (RAM) and large storage units. A part of the hardware which makes DPW significantly different from normal computer is the stereo viewing system consisted of graphic card, high resolution stereo monitor as well as a monitor suitable stereo glasses. Today the most widely used stereo viewing system is the one comprised of monitor with active polarization display and stereo glasses with polarization filters (Schenk, 2005; Ahmad, 2008; Ruzgiené, 2007). The most important part of DPW is its software. Generally, photogrammetric tasks which can be performed using DPW are the following: basic photogrammetric functions such as image orientation, aerial triangulation or image block adjustment; mono or stereo vectorization, more or less automated creation of digital terrain model and digital elevation model, digital orthophoto, digital map, etc. (Heipke, 2001; Lemmens, 2009). (Balenovic et al., 2011).

Haala (2009 and 2013) widely discusses, that both improvements in camera technology and the rise of new matching approaches triggered the development of suitable software tools for image based 3D reconstruction by research groups and vendors of photogrammetric software. Based on dense pixel-wise matching, the

photogrammetric generation of dense 3D point clouds and Digital Surface Models from highly overlapping aerial images has become feasible. Recent innovations in matching algorithms considerably improved the quality of elevation data, generated automatically from aerial images. The use of digital image matching for automatic point transfer within photogrammetric applications is today a well known standard procedure. The restriction to matches of selected points usually provides correspondences at high certainty.

Similar to automatic aerial triangulation, software tools for image based surface reconstruction are being developed for more than two decades. Since then such software, which integrates feature or intensity based algorithms in stereo-matching is also commercially available. This trend is currently supported by the development

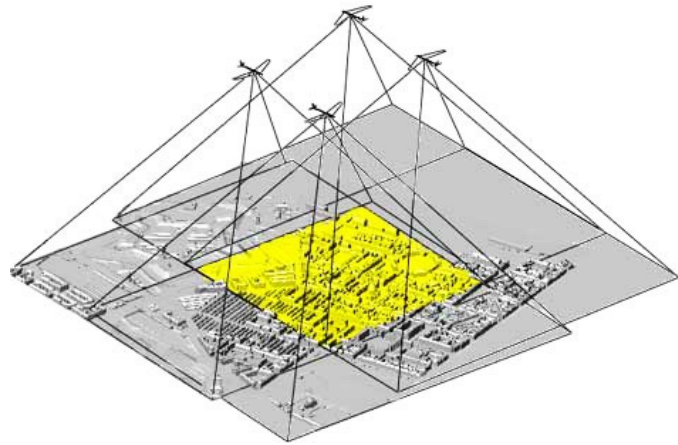


*Fig. 4. Overlapping aerial images and resulting 3D model of the land surface. Source: SharpGIS (2016).*

of improved software tools which for example extend traditional stereo- to multi-image matching. The utilized algorithms first extract feature points and then search the corresponding features in the overlapping images. Meanwhile, the automatic identification of corresponding points is also implemented within close range applications, where the situation is even more complex compared to airborne applications. In such scenarios affine invariant feature detectors are combined with robust orientation estimation techniques to cope with matching problems caused by perspective distortions within images of arbitrary rotation and scale.

In contrast to the great relevance of image matching for orientation purposes, the importance of this technique for 3D surface reconstruction is subordinated. However, automatic stereo image matching was frequently substituted by LiDAR measurements. Compared to image based surface reconstruction, LiDAR measurements were more competitive especially while aiming at very accurate and dense elevation data. Meanwhile, this gap could be considerably narrowed since now imagery from digital airborne camera systems is available as standard data source. Compared to scanned film, these images feature an increased dynamic and improved signal-to-noise-ratio. As a result, the quality and accuracy of image based point transfer as basic observation for 3D surface reconstruction could be improved considerably. In addition to the better radiometric quality, digital airborne

camera systems can also capture largely overlapping images at a relatively little additional effort. The availability of such high redundant multi-image information is especially beneficial in situations, where standard stereo matching is hindered due to occlusions. The increasing potential of such data for surface reconstruction based on automatic image matching additionally triggered a renaissance in the research and development of suitable software tools (Haala, 2009, 2013).

### 3.2.2.2. Image-Based Point Clouds

As broadly describes White et al. (2013a), when an object is imaged from two different perspectives, stereophotogrammetry enables the measurement of its three-dimensional position relative to a reference datum (e.g., sea level). The process is analogous to our own visual perception of depth with normal binocular vision. Like human vision, stereophotogrammetry is based upon the principle of parallax, which refers to the apparent change in the relative position of stationary objects resulting from a change in viewing position (Lillesand & Kiefer, 1987).

In simple terms, stereophoto-grammetry involves identifying a common point on each image. A line of sight (also referred to as a ray) is constructed from the camera viewpoint to the common point on each image. The intersection of the two rays is found using triangulation, and the three-dimensional position of the point is determined (i.e., X, Y, Z). Repetition of this process for the many points that make up the object or surface being viewed results in the image-based point cloud.

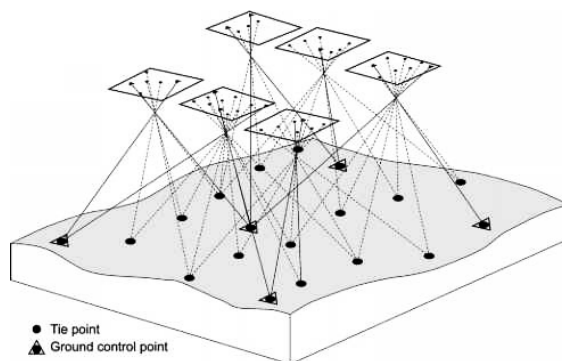


*Fig. 5. Scheme of aerotriangulation principles. Source: GISBOX (2016).*

The photogrammetric processing of data generally utilizes the principles of aerial triangulation (Figure 5.). As describes Whitehead et al. (2014) aerial triangulation refers to the process by which the true positions and orientations of the images from an aerial survey are re-established. This process includes project setup, measurement of GCPs and manual tie points, and bundle-block

adjustment (Whitehead et al., 2013). During aerial triangulation, a large number of automated tie points are generated for conjugate points identified across multiple images. A bundle-block adjustment then uses these automated tie points, along with manually observed ground control points (GCPs) and tie points, to optimise the photo positions and orientations, with the goal being to recreate the positions and

orientations associated with each image at the time of its capture (Hugenholtz et al., 2013). The bundle-block adjustment process generates a high number of redundant observations, which are used to derive an optimal solution through a rigorous least-squares adjustment. After aerial triangulation, the oriented images may be used to generate a dense point cloud by matching features across multiple image pairs. From the dense point cloud a digital surface model can be produced, which provides a detailed representation of the terrain surface, including the elevations of raised objects, such as trees or buildings (Whitehead et al., 2013, 2014).

White et al. (2013a) extensively continues, that two noteworthy innovations in digital photogrammetry have resulted in the capacity to generate image-based point clouds that are similar in several respects to ALS point clouds. First, digital aerial cameras facilitate the easy acquisition of multiple overlapping images, without the previous level of effort and expense required to capture, develop, and scan analog photos. From overlapping images, an object can be visible on multiple image pairs, allowing for multi-view matching (not just stereo-matching), which reduces the opportunity for occlusions and improves geometric accuracy (Leberl et al., 2010; Zitová & Flusser, 2003). Second, rapid advances in the development of computer technology have made complex algorithms for image matching practical. The result of these innovations has been the generation of image-based point clouds and DSMs that are much more detailed and more accurate than was previously possible with traditional manual stereophotogrammetric processing.

The creation of an image-based point cloud (Figure 6.) and DSM requires high-spatial resolution aerial images with multi-image overlap (Leberl et al., 2010; Baltsavias et al., 2008). Spatial resolution is defined by the Ground Sampling Distance, which depends on flying height and sensor characteristics. For forestry applications, the need for highly redundant (i.e., many overlapping images with at least 60 % – 90 % along-track and 30 % – 60 % across-track overlap), multi-image information is especially acute to overcome occlusions that are common in the canopy (Baltsavias et al., 2008; Haala et al., 2010).

The aim of image matching is to find corresponding points (objects) in images based on their radiometric and geometric similarity. The main automated photogrammetric image matching methods can be divided into area- or feature-based methods (Zitová & Flusser, 2003). Area-based methods typically use a window of image pixels to search for the best match between images. Feature-based methods rely on matching between basic mapping entities, such as points, lines, and polygons. Current image processing software often uses a combination of these two methods for image matching (Bohlin et al., 2012a; Järnstedt et al., 2012).



*Fig. 6. Visualisation of very high-density coloured image-based point cloud representing boreal forest stand and several buildings, generated from UAV-borne RGB images. Source: Nyström (2015).*

A variant of the area-based method to image matching is termed “Global Image Matching”. Global Image Matching methods seek to match each pixel in the image (as opposed to a window of pixels), and although these methods may be considered state-of-the-art in terms of the quality and resolution of the point clouds and DSMs that they can produce, they are computationally intensive and slow to process (Gehrke et al., 2010). Hence, a method referred to as Semi-Global Matching (SGM) has emerged, which is a hybrid between global image and area-based matching approaches. SGM constrains the possibilities for pixel-wise matching using a cost function, thereby making the matching process markedly more efficient (Hirshmüller, 2008).

Regardless of the image-matching method used, stereo-matching parameters, image resolution, and differences in sun-angle and viewing geometry have a significant impact on the quality of image-based point clouds and DSMs. While technological innovations can improve image matching capacity, issues of sun angle and viewing geometry will be a factor in any optical image product that is acquired and used for point cloud and DSM generation (St-Onge et al., 2008). Photogrammetric matching of digital aerial images using approaches such as SGM results in the production of a three-dimensional point cloud with similarities to an ALS point cloud. However, as indicated above, the aforementioned photogrammetric matching process produces three-dimensional points for the upper canopy surface only, in contrast to the ALS data points, which are distributed between the ground surface and the upper canopy (White et al., 2013a).

### 3.2.3. Comparison of ALS and Image-Based Point Clouds

White et al. (2013a) states that the ALS instruments typically used for forestry applications are able to record several, often up to five returns for each pulse emitted. Therefore, a DSM built from an image-based point cloud is similar to a DSM that is built from first ALS returns only. Similar to an ALS-derived DSM, a DTM can be subtracted from an image-based DSM to give an estimate of aboveground object heights; however, the DTM must have a sufficiently high spatial resolution and vertical accuracy to enable this normalization. Finally, metrics may be calculated from the image-based point cloud that resemble – but are not necessarily the same – as those generated from the ALS point cloud. In terms of processing, ALS data currently have an advantage over image-based approaches. The time required to acquire and process ALS data into a useable point cloud is generally less than for imagery, however as digital image workflows become increasingly efficient, this advantage will likely become less relevant over time.

Leberl et al. (2010) then concludes that novel photogrammetric approaches deliver point clouds at comparable accuracy but higher density and superior throughput than LiDAR. Given the advantages of a single workflow and the existence of images for a variety of applications, Leberl finds that image-based methods are superior to LiDAR-surveys in the creation of 3D point clouds. With regards to resolution of airborne data from both sources, the image-based point cloud is capable of a greater point density than ALS data, for a given cost, as a function of the GSD and the number of independent three-dimensional pixel matches.

Typical aerial LiDAR point density may be in the range of 1 to 5 points/m<sup>2</sup>. Aerial photogrammetry point density may at first be seen as defined by the two-dimensional ground sampling distance, thus pixel size. At a 10 cm pixel, one would produce 100 points/m<sup>2</sup>, but these are not 3D elevation values. The 3D sampling interval depends on the image overlap to achieve independent 3D matches. If 50 percent of the pixels were to get matched for independent 3D elevation values, one would achieve 50 points/m<sup>2</sup> from 10 cm pixels (Leberl et al., 2010).

White et al. (2013a) continues, that concerning comparison of the accuracy of both approaches when estimating forest inventory attributes including the height, only few studies were conducted so far. The available studies of Bohlin et al. (2012a) and Järnstedt et al. (2012) indicate, that the performance of ALS- and image-based predictive models of forest inventory attributes are more or less similar. Since both ALS and image-based DSMs are capable of characterizing canopy height with similar levels of accuracy in more homogenous forest environments (i.e., even-aged, single

layer stands) where it has been tested thus far, and since height is an important predictor of dominant height, basal area, and volume (Næsset, 2002b; Maltamo et al., 2006) it is not surprising that the predictions based on the image-based metrics in these studies are similar to those generated from the ALS metrics.

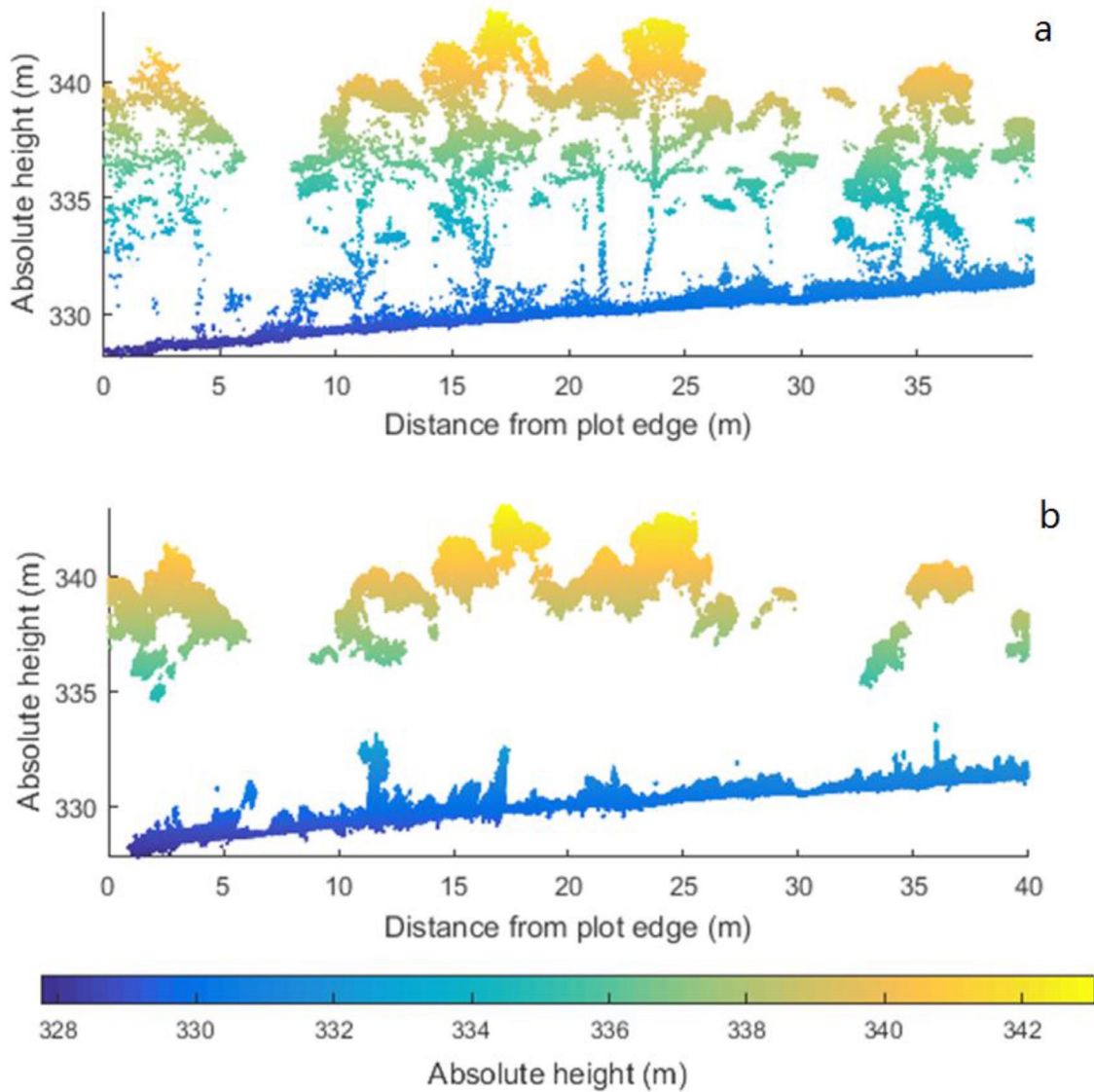


*Fig. 7. Example of height assessment of individual trees based on two sources of remote sensing data. a) Side-view of a transect through the study plot generated from the point cloud of the ALS system and (b) image-based point cloud produced using RGB photography. Source: Wallace et al. (2016).*

Regarding the economical efficiency, interest in exploring alternatives to ALS data stems from a need to control and reduce costs. The cost-effective reduction of the inventory cycle is consistently demanded by forest managers and other jurisdictions, and represents a significant research need (Pitt & Pineau, 2009). Without delving into specific pricing, which is in constant flux and highly situation-dependent, aerial imagery is currently about one-half to one-third of the cost of ALS data. Thus, if

ALS-equivalent area-based predictions can be made from imagery (something that has yet to be demonstrated for a range of forest types and stand structures), forest managers could potentially realize more frequent inventory cycles.

Since it is envisioned that image acquisition will always play a role in forest inventory development and update, the ability to also estimate forest inventory attributes with robust area-based predictions from image-based point clouds – rather than the current practice of projecting attributes forward based on averaged growth or yield curves – would be an attractive option for forest managers. However, to reiterate, the use of image-based point clouds is predicated on the availability of high spatial resolution DTMs and therefore, an initial investment in ALS data is generally required before the potential cost savings afforded by image-based point clouds could be realized (White et al., 2013a).

Regardless the method used, an important aspect is that in most cases not all trees can be detected. Korpela (2004) analyzed the discernibility of trees in varying species and development classes by visually interpreting colour-infrared images with multiple views on the targets. The trees with heights of less than 40–60 % relative to the dominant height were most probably missed, this proportion being dependent on forest structure and density. Most of the dominant trees, and thus 88–100 % of the total volume could still be detected from the images. ALS-based studies have led to similar conclusions, as Persson et al. (2002), for example, detected 71 % of the stems, but 91 % of their volume as measured in the field. Pitkänen et al. (2004), on the other hand, performed tree detection in a more heterogeneous forest, reporting a 40 % detection rate for all trees, but that of 70 % for the dominant trees (Vauhkonen, 2010).

Considering automatic interpretation, the algorithm has a major effect on the tree detection result (Kaartinen & Hyypä, 2008), which is often affected by the parameterization of the method (e.g. Solberg et al., 2006). In addition to omission errors caused by the undetected trees, also commission errors, i.e. segmentation of objects that are not trees, can occur. Solberg et al. (2006), for example, reported a 26 % commission error rate in an inventory that found 66 % of the field-measured trees. In this sense the conifers are less problematic than the deciduous trees, which often have multiple crowns of irregular shapes (Brandtberg et al., 2003; Koch et al., 2006). (Vauhkonen, 2010).

When comparing the two data sources, White et al. (2013a) also notes that imagery is a key data source for forest inventory, enabling the implementation of standard inventory practices, including stand delineation and visual interpretation of attributes like species, which cannot (at this time) be estimated from ALS exclusively.



As a result, any new forest inventory for a given area for which ALS will be acquired will also require some consideration of how attributes that are not readily generated from ALS will be acquired. Typically, imagery of some kind will be necessary.

A main advantage of ALS data is the ability to generate a detailed DSM, but also a DTM under the forest canopy, which, in addition to its utility for inventory, affords a broad range of operational and engineering applications. In contrast, it is usually not possible to generate a DTM from an image-based point cloud if the ground is obscured by vegetation. Given that a detailed DTM is a necessary prerequisite for normalizing an image-based point cloud to aboveground heights, it is therefore likely that the use of image-based point clouds for forest inventory will be limited to those areas which already have a pre-existing high spatial resolution DTM (likely derived from ALS data) (White et al., 2013a). A recent study of (Dandois & Ellis, 2013) nevertheless indicates a possibility to create sufficient-quality DTMs also from image-based point clouds at least in leaf-off deciduous forests.

### **3.2.4. Forest Stands Assessment Approaches**

As states Vauhkonen et al. (2011), currently, there are two main approaches for using point clouds to characterize forest resources: 1. an area-based approach typically providing data at stand level and 2. a single-tree approach where individual trees are the basic unit of the assessment.

#### **3.2.4.1. Area-Based Approach**

According to Wang & Weng (2013), the area-based prediction of forest variables is based on a statistical dependency between the variables measured in the field from ground plots and predictor features derived from remote sensing (RS) data. In the case of point cloud data, the method in which this kind of two-stage procedure is used to produce stand-level information from wall-to-wall grid-level predictions is called an Area-Based Approach (ABA) (Næsset, 2002b). In a more general context, two-stage predictions using field and RS data have a long history in forestry inventory (Poso et al., 1984), and this process could also be called ABA.

As states Tompalski et al. (2015), the ABA is now routinely applied in operational forestry applications, and results in generalized plot- or stand-level attribute predictions. Area-based approaches, rather than explicitly extracting or identifying each individual tree crown, are based on aggregations of ALS or image-based point clouds to develop a series of canopy density and height metrics (Næsset,

2002b). These metrics become independent variables that are used to predict the desired forest inventory attributes. The successful application of the area-based approach is predicated on accurate measurements of forest height and height variation from point cloud data (White et al., 2013b). When ABA is applied, accurate training data must be on hand (Poso et al., 1984; Næsset, 2002b). Training plots should represent the whole population and cover the full range of variability in the attributes of interest. The efficient selection of the training plot locations requires preknowledge of the inventory area (Maltamo et al., 2011).

Area-based approaches use circular plots, grids or forest stands as reference units (Maltamo et al., 2014). When a grid cell is used as a sample unit in ABA, its size refers to the size of the field-measured training plot. Then, the point cloud-derived features are extracted from the grid cell areas and used as possible predictors. The statistical relation between the predictors and response variables is modelled using training data when both of them are on hand. The response variables are predicted for grid cells without training data using regression or other statistical methods. If stand-level variables are needed, they are calculated by weighting the grid-level predictions inside the stand (Wang & Weng, 2013).

White et al. (2013b) summarizes, that area-based approach is accomplished in two stages. In the first stage, remote sensing data is acquired for the entire area of interest, tree-level measures are acquired from sampled ground plots, and predictive models are developed (e.g., regression or non-parametric methods). For the purposes of model development, the point cloud is clipped to correspond to the area of each ground plot. Metrics (descriptive statistics) are calculated from the clipped normalized point cloud and include measures such as mean height, standard deviation of height, height percentiles, and canopy cover. Attributes of interest are measured by ground crews (i.e., height, diameter) or modelled (i.e., volume, biomass) for each ground plot. Predictive models are then constructed using the ground plot attributes as the response variable and the point cloud-derived metrics as predictors.

In the second stage of the area-based approach, the models are applied to the entire area of interest to generate the desired wall-to-wall estimates and maps of specific forest inventory attributes. The same metrics that are calculated for the clipped point cloud (as described above) are generated for the wall-to-wall point cloud data. The predictive equations developed from the modelling in the first step are then applied to the entire area of interest using the wall-to-wall metrics. Once the predictive equations are applied, each part of the examined forest stand will have an estimate for the attribute of interest. The foremost advantages of the area-based

approach compared with traditional stand-level forest inventories include having complete spatial knowledge of X and predicted Y, more precise predictions of certain forest variables, and the capability to calculate confidence intervals for estimates (e.g., Woods et al., 2011). Forest attributes, such as mean height, dominant height, stem number, mean diameter, basal area, stem volume or biomass, are predicted with better or comparable quality to traditional field inventories (e.g., Næsset et al., 2004). (White et al., 2013b).

### **3.2.4.2. Individual Tree Approach**

An alternative to Area-Based Approach is Individual Tree Approach (ITA) also known as Individual Tree Crown (ITC) technique, Individual Tree Crown Detection / Delineation (ITCD), Single Tree Approach or its variants. Generally it is a procedure of recognizing individual trees, including tree top/trunk detection and crown boundary delineation (Maltamo et al., 2004). Individual tree-based forest inventory is based on measurements of all trees in a given area. This is attainable only if all trees are observable and measurable for the needed variables (Korpela, 2004).

As in detail describe Breidenbach & Astrup (2014) due to the visibility of single trees in high-resolution ALS data, several researchers (mainly Hyyppä & Hyyppä, 1999; Hyyppä & Inkinen, 1999; Borgefors et al., 1999) started using automatically detected tree crowns to estimate forest properties. The aim of the individual tree approach is to derive tree attributes of interest from trees or tree crowns detected in point cloud data. The ITA approach is conceptually similar to earlier approaches used in high-resolution photography and basically consists of five steps:

- I. Detection of tree crowns in canopy height models or point clouds covering the areas of interest for which estimates of forest parameters are required.

2. Linking detected crowns with trees observed on field plots with known tree locations. The primary assumption in the traditional ITA is that one field-measured tree can be linked to one crown detected in the point cloud data.

3. Fitting statistical models that regress field-measured tree characteristics, such as maximum height within the detected crown, against metrics derived from the detected tree crowns.

4. Application of the fitted model to the detected tree crowns within areas of interest such as stands in order to estimate tree characteristics of interest.

5. Typically, the estimates for crown segments within each stand are averaged or summed in order to estimate mean or total forest characteristics within the stand.

Popular methods for crown detection in canopy height models are watershed algorithms. Since the canopy height model is segmented, the detected tree crowns are often denoted “segments”. Usually, only dominant trees are correctly identified in step 1 in the sense that exactly one field-measured tree is within one detected crown segment (Persson et al., 2002). Frequently, only “correctly identified” segments with one linked field tree are used to fit regression models in step 3. However, the number of field-measured trees within a segment influences the response variable such as timber volume or DBH of the segment. In general, it can be said that omitting observations from a regression model based on the response variable, for example empty segments or segments with several held trees, will result in biased regression models (Breidenbach & Astrup, 2014).

Tompalski et al. (2015) states, that using ITA approaches, individual treetops are located from either the raw point clouds directly (Reitberger et al., 2009), or from a canopy height model (Popescu & Wynne, 2004; Solberg, et al., 2006). The main tree detection methods belong to the latter and are usually based on finding local maxima on a smoothed CHM. After the local maxima are found, the boundaries of the crown are extracted, e.g. using a watershed-based region detector. The accuracy of the CHM and the corresponding accuracy of the ITA depend on the point cloud density (Wang & Weng, 2013).

Tree variables such as height and location can be measured directly from the laser point cloud. The XY location of the tree is generally the location of the treetop, that is, the XY location of the highest point or CHM value. The estimate for tree height can be the highest point or the CHM value within the tree crown. Besides tree height and crown dimensions, the use of other geometric features and point height distributions has become more common in ITA predictions (Holmgren & Persson, 2004; Yu et al., 2011). With respect to the plot level training data used in ABA, ITA training data should cover the whole population variation at the tree level. However, ITA can be carried out without any field measurements if desired. In this case, missing variables are measured straight from the point cloud and/or modelled with existing models (Wang & Weng, 2013).

Zhen et al. (2016) ascertained, that in the last two decades, various semi- and fully-automatic algorithms have been developed for individual tree detection and crown delineation. However, even if one method is best for a specific application, it may not be optimal for other situations. For example, many approaches that worked well on softwood stands have demonstrated lower accuracy for hardwood or mixed forests, particularly those with high variation in terms of tree spacing, age or size,

or when the crowns have a high degree of overlap (Larsen et al., 2011; Zhen et al., 2015). It is challenging to assess the accuracy of ITA results because there is no standardized accuracy assessment procedure (Ke & Quackenbush, 2011), which makes it more difficult to compare ITA algorithms unless multiple approaches are tested on a single study area using the same accuracy metrics (Kaartinen et al., 2012). However, researchers have generally had greater successes in implementing ITA algorithms on even-spaced, even-aged, and even-sized softwood forests (Ke & Quackenbush, 2011).

According to Tompalski et al. (2015), ITA-based estimates provide detailed information for individual trees, but are typically biased due to challenges associated with individual tree detection. ITA approaches are still in research mode (Breidenbach et al., 2010; Vastaranta et al., 2011). Tree properties can subsequently be estimated using the segment properties, such as segment area or point cloud-derived height metrics as explanatory variables.

As discussed by Breidenbach et al. (2010), ITA approaches are more intuitive than ABA since the response variable refers to the single tree, which is in fact the smallest unit on which forest management is carried out. Trees can be often clearly seen in the point clouds, especially when the density of points is much greater than individual crown sizes. In addition, ITA provides the tree coordinates which may be of use in single tree harvesting operations and in growth predictions with distance-dependent growth models.

However, ITA approaches are prone to bias, as a result of over or under segmentation of tree crowns, whereby some trees are undetected, whilst others are split into multiple trees. These issues result in omission and commission errors, which can have a significant impact on overall estimate for forest inventory (Maltamo et al., 2004). As further describes Breidenbach et al. (2010) the segmentation errors of any segmentation algorithm can be attributed to i) missing trees, ii) segmentation of objects that are not actually trees, iii) oversegmentation of tree crowns (i.e., one crown is split into several segments), and iv) clustering of several crowns in one segment. In terms of classification accuracy assessment, errors of type i) and ii) will result in errors of omission and commission, respectively (e.g., Campbell, 2008).

Oversegmentation, i.e., type iii) errors, can also be seen as a special case of type ii) errors which result in one correct segmentation and one or several errors of commission. Likewise, clustering of several crowns would result in one correct classification and one or more errors of omission. The absolute and relative frequencies of errors of the different types will depend on factors such as algorithm design, parameter settings, and complexity of the forest. Since these errors usually

do not level out, the estimate of the response variable of interest is likely to be biased if aggregated to a larger geographical unit such as a forest stand (Maltamo et al., 2004)

Vauhkonen (2010) agrees, that as the forest stand-level estimates are aggregated from single trees, their precision is a function of the errors in the tree detection phase. Two types of solutions for taking the tree detection errors into account have been presented. First, statistical approaches can be used for estimating the proportion of the undetected trees, and the tree detection result is then added to an estimate for those (Mehtätalo, 2006; Flewelling, 2008). Second, the estimation procedures can be modified to provide segments with a summation of field reference attributes rather than treating them as single trees (Lindberg et al., 2010; Breidenbach et al., 2010). Both of these approaches reduce the bias at the area-level, the latter being potentially able to also take the commission errors into account.

### **3.2.4.3. Data Segmentation Methods**

#### **3.2.4.3.1. Overview of the Methods**

As described in the previous chapter, in the scope of ITA the examined point cloud or raster data are usually segmented to smaller parts representing individual tree crowns. There are various segmentation methods of the RS data. Between the most promising in the recent years belongs e.g. semiautomatic OBIA, i.e. Object-Based Image Analysis segmenting the datasets on homogenous objects using fuzzy logic (Machala, 2012; Machala & Zejdová, 2014; Machala et al., 2014, 2015; Novotný et al., 2014). Even though some authors try to apply OBIA for the purposes of tree detection (overview gives e.g. Cheng & Han, 2016) this modern approach as such is in classical forest conditions usually not sufficiently applicable for distinguishing of individual trees with the demanded accuracy. Several more suitable methods were developed for this purpose.

As broadly describe Strîmbu & Strîmbu (2015), regardless of the remote sensing data type, a variety of tree detection and delineation algorithms have been proposed in the last two decades. Those that according to the authors most often recur in the literature are following:

Gougeon's valley following technique (Gougeon, 1989; Gougeon et al., 1992) is among the earliest attempts to tackle this problem. The algorithm starts at local minima and searches for adjacent pixels that lie in between pixels of higher value, with the resulting paths assumed to correspond to tree crown boundaries.

Local maxima filtering (LMF) (Figure 8.) has been extensively employed in tree top detection (Wulder et al., 2000; Pitkänen, 2001). Edson & Wing (2011) speaks about TreeVaW which operates on a CHM using a variable window filter that varies its search window size, (convolution kernel), by passing a local maxima filter over the CHM and determines a tree location based on elevation data contained in individual pixels. The highest elevation value is taken to indicate the tree apex. When the filter determines a local maxima value, a tree X and Y coordinate location is identified (Popescu & Wynne, 2004). LMF is often used to provide seed points for algorithms that delineate entire tree crowns based on the allometric relationship to height (Holmgren & Persson, 2004; Yu et al., 2011).

Region growing algorithms (Culvenor, 2002; Hirschmugl et al., 2007) start with seed pixels and progressively grow regions by iteratively including adjacent pixels until a threshold of expansion or stopping criteria are met. The borders of regions found by region growing are perfectly thin and the algorithm is also very stable with respect to noise. The fundamental drawback of histogram-based region growing detection is that histograms provide no spatial information, only the distribution of grey levels (Kamdi & Krishna, 2011).

Watershed segmentation (Kwak et al., 2007; Tang et al., 2007) (Figure 8.) is a particular instance of region growing that operates on topologically inverted data by the analogy of pouring water in the local minima, and considering the basins limits as the water level rises. According to Edson & Wing (2011) inverse watershed segmentation, is the most common method applied to determining locations of individual tree crowns using a CHM by segmenting the inverted raster canopy surface into the equivalent of individual hydrologic drainage basins (Goerndt, 2010; Andersen, 2009). Following inversion, a watershed segmentation algorithm separates the CHM into distinct tree polygons with raster crown diameter and height values (Goerndt & Monleon, 2010).

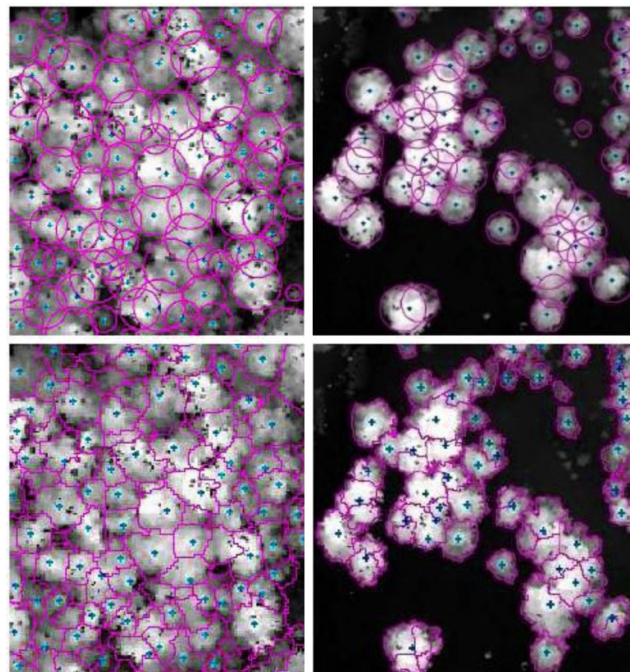


*Fig. 8. The extracted crowns from a CHM model by the means of the local maxima filtering using variable window filter (upper images) and inverse watershed segmentation (bottom images). Source: Wannasiri et al. (2013).*

Pouring algorithm, which is similar in spirit to watershed segmentation, was described e.g. by Koch et al. (2006). The smoothed CHM tree tops are detected with a local maximum filter. A pixel counts as a local maximum, if all of its neighbours have got a lower height value. Then regions are extended, as long as neighbouring pixels with a lower or the same height value exist. Overlapping regions in “height-valleys” are finally distributed evenly to all involved trees. This algorithm resembles water being poured onto mountains, thus being similar to an inverted, classical watershed-algorithm (Soille, 1999). The pouring algorithm produces already a first approximation to the actual shape of the tree crown.

Template matching segmentation methods rely on a generalized tree model. The choice of tree model varies from illumination patterns (Hung et al., 2012) to ellipses (Larsen & Rudemo, 1998), ellipsoids (Wolf & Heipke, 2007), Gaussian blobs (Brandtberg et al., 2003), conic and parabolic surfaces (Persson et al., 2002).

Clustering algorithms have been employed at pixel level (Gupta et al., 2010), voxel level (Reitberger et al., 2009) and subsegment level (Lee et al., 2010). Finally, global optimization algorithms segment trees simultaneously in an iterative process with the aim to reach a state of fitness for the segmented forest as a whole.

Strîmbu & Strîmbu (2015) summarize, that while most of the above mentioned methods have reported relatively satisfactory performance, an international benchmarking project (Kaartinen et al., 2012) revealed however, that when applied to the same dataset, most of the tested methods showed a high variability in their performance. In fact, they did not perform much better and often worse than simple local maxima and watershed based methods used by the authors of the report.

In another comparative study, Larsen et al. (2011) compared the accuracy of six segmentation methods when applied to six different forest types. The algorithms were fundamentally different and were based on: local maxima filtering, valley following, region growing, template matching, scale-space theory, and stochastic processes. The results revealed that while all methods were relatively accurate when applied to a young plantation, they performed significantly different on other forest types. For instance, the region growing algorithm outperformed all the methods in a mixed forest area as well as an area with high stem density but was poor on areas with isolated trees. Isolated trees on the other hand, were best extracted by the template matching method.

While the first study reveals that the method of segmentation is the main source of variability in segmentation accuracy, the second study shows that the methods behave differently when applied to certain forest types. In other words, they are inherently more or less appropriate to segment forests of certain structure. The



inherent inability to adapt to various forest conditions sometimes stems in reliance on overly simplified assumptions regarding the structure of tree crowns and their layout in the forest. Tree crowns have an extremely complex structure that varies greatly from species to species as well as with the context in which they developed (Strîmbu & Strîmbu, 2015).

#### **3.2.4.3.2. Inverse Watershed Segmentation**

The principles of Inverse Watershed Segmentation (IWS) also known as Watershed Transform(ation) or Watershed Algorithm were utilized in this work and therefore this method is described in more detail. According to Mohan et al. (2003) watershed transformation as a non-parametric method was first developed for contour extraction in greyscale images, which relied in defining the contours as watersheds. This method has been considerably improved with the tools of mathematical morphology. As inform Belaid & Mourou (2009), the watershed transformation is one of the oldest segmentation techniques which was initially proposed by Beucher (Beucher & Lantu'éjoul, 1979; Beucher, 1990; Beucher, 1992). According to Chen et al. (2006) watershed segmentation is a well-known and powerful image segmentation method that incorporates the advantages of other segmentation methods such as region growing and edge-detection.

As Mohan et al. (2003) continues, watershed analysis is well recognized as being useful for image segmentation and has been made computationally practical thanks to a fast technique presented by Vincent & Soille (1991). Watershed analysis uses an image's gradient magnitude as input to subdivide the image into low-gradient catchment basins surrounded by high-gradient watershed lines. The catchment basins consist of locally homogeneous connected sets of pixels. The watershed lines are made up of connected pixels exhibiting local maxima in gradient magnitude; to achieve a final segmentation, these pixels are typically absorbed into adjacent catchment basins.

As describes van Henten et al. (2009) the watershed transform is a region-based segmentation approach in which a grey-level image is considered as a topographic surface. The intuitive idea underlying this method comes from geography: it is that of a landscape or topographic relief that is flooded by water, with watersheds being the dividing lines between the domains of attraction of rain falling over the region (Serra, 1982). During a successive pseudo flooding of the grey value relief, watersheds with adjacent catchment basins are constructed.

Beginning with a rasterized greyscale height image, this method locates local maxima throughout the data by first inverting the data (Miller, 2014). Schardt et al. (2002) explains, that the tree height model has to be inverted in order to adapt the given information to the needs and properties of classical watershed algorithms. In short, watershed algorithms find local minima in a greyscale image and try to assign each pixel of the image to a local minimum. The problem to solve in crown delineation is exactly vice versa. Each tree is represented by a single local maximum, and the pixels around the maxima should be assigned to the most probable maximum (treetop). When the CHM is inverted, watershed algorithm can be applied to the inverted data in order to delineate single trees.

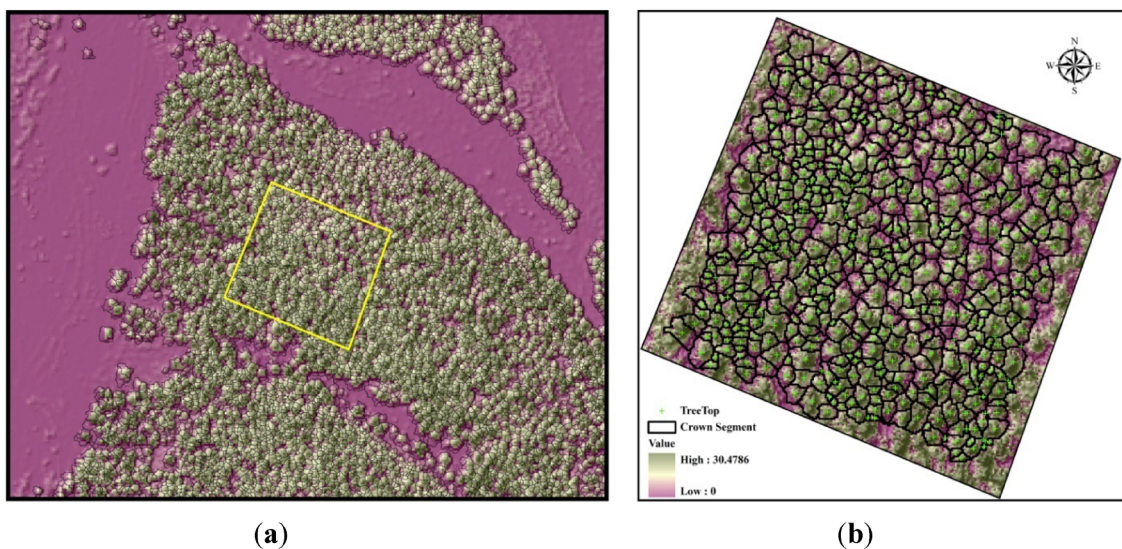


Fig. 9. Canopy height model overlaid with tree crown segments derived from watershed segmentation. Larger context (a) and detailed view (b). Source: Li et al. (2014).

Amoda & Kulkarni (2013) then describe the concept of watershed transform based on visualizing an image in three dimensions: two spatial coordinates versus gray levels. They consider three types of points: A. Points belonging to a regional minimum. B. Points at which a drop of water would fall with certainty to a single minimum. C. Points at which water would be equally likely to fall to more than one minimum. For a particular regional minimum, the set of points satisfying condition B is called the catchment basin or watershed of that minimum. The points satisfying condition C form crest lines on the topographic surface and are termed divide lines or watershed lines. The principal objective of segmentation algorithms based on these concepts is to find the watershed lines (Figure 9.).

Following advantages of the watershed segmentation technique can be emphasized. Grau et al. (2004) describes, that it is a fast, simple, intuitive method, can be computationally parallelized, and produces a complete division of the image

in separated regions even if the contrast is poor, thus avoiding the need for any kind of contour joining. Amoda & Kulkarni (2013) continue, that the resulting boundaries form closed and connected regions, which always correspond to contours which appear in the image as obvious boundaries of objects. Important is also, that the union of all the regions forms the entire image region. Belaid & Mourou (2009) see both, pros and cons. The main advantage is that the watershed transformation requires low computation times in comparison with other segmentation methods. However, using a watershed transformation often results in over-segmentation.

According to Zhao & Popescu (2007) among the segmentation approaches, watershed transform is the most popular technique in segmenting a CHM because it is intuitively straightforward to treat each concave tree crown in the inverted CHM as a catchment basin. However, cautions should be exercised as to how to appropriately select local maxima as candidates of treetops. For example, within a single crown, there may be multiple local maxima that result primarily from the real irregularity of crowns or partly from random errors in the procedures of creating the CHM; therefore over-segmentation is usually observed in such situations. As remedies, common strategies are to pre-process the CHM using a smoothing filter, or to merge over-segmented regions ad hoc; but too strong filter could possibly smear out small trees; as a result, smoothing filters with adaptive parameters are often desired to alleviate such situations.

### **3.3. Unmanned Aerial Vehicles and Systems**

An Unmanned Aerial System composed of one Unmanned Aerial Vehicle and the ground segment was utilized in this work to obtain the appropriate remote sensing data suitable for creation of image-based point clouds. This chapter is therefore devoted to this technology.

#### **3.3.1. Terminology**

According to Ministry of Defence of the UK (Joint Doctrine Note, 2010) the origins of unmanned aircrafts can be traced back to World War I; but it is mainly the last decade that has seen extraordinary development and progress in unmanned aircraft technology and capability. Much of the original terminology has, as a result, become outdated and manufacturers and operators have created a new descriptive language for the aircraft, their capabilities and consequent issues. As systems have

matured, there is an increasing requirement for standardised terminology. It should be noted that much existing manned aircraft terminology remains equally relevant to unmanned aircraft operations.

An Unmanned Aerial Vehicle (UAV) is a type of aircraft that operates without a human pilot onboard. UAVs can be remote controlled aircraft (e.g. flown by a pilot at a ground control station) or can fly autonomously based on pre-programmed flight plans or more complex dynamic automation systems. The acronym UAV has been expanded in some cases to UAVS (Unmanned Aircraft Vehicle System). The Federal Aviation Administration (FAA) has adopted the acronym UAS (Unmanned Aircraft System) to reflect the fact that these complex systems include ground stations and other elements besides the actual air vehicles. The term UAS, however, is not widely used as the term UAV has become part of the modern lexicon (TheUAV, 2016).

Recent technologies have allowed for the development of many different kinds of advanced unmanned aerial vehicles used for various purposes. Many of these applications were developed in the military, and the general public has seen UAVs evolve as spy or reconnaissance vehicles used during wartime. However, recently consumers have also seen rapid development of these types of aircraft for public markets. Remote control airplanes and helicopters can also be classified as UAVs when they have particular kinds of performance and remote control capabilities (Technopedia, 2016).

According to UK Ministry of Defence unmanned aircraft grow in numbers comparable to, or in future exceeding, manned aircraft. When building a descriptive taxonomy to describe such mixed systems, it is logical to use the same root word, aircraft, for both. Appropriate prefixes or suffixes might then be added, for example to indicate how they are controlled, or to indicate a specific role, capability or environment. The generic terms can be defined as follows (Joint Doctrine Note, 2010):

An Unmanned Aircraft (sometimes abbreviated to UA) is defined as an aircraft that does not carry a human operator, is operated remotely using varying levels of automated functions, is normally recoverable, and can carry a lethal or non-lethal payload. According to FAA this device excludes missiles, weapons, or exploding warheads, but includes all classes of airplanes, helicopters, airships, and powered-lift aircraft without an onboard pilot. UA do not include traditional balloons, rockets, tethered aircraft and un-powered gliders.

An Unmanned Aircraft System (UAS) is defined as a system, whose components include the unmanned aircraft and all equipment, network and personnel necessary to control the unmanned aircraft. Its parts may include control stations, data links, telemetry, communications and navigation equipment, control links, support equipment, payloads, flight termination systems, or launch/recovery equipment (Fig. 10.).

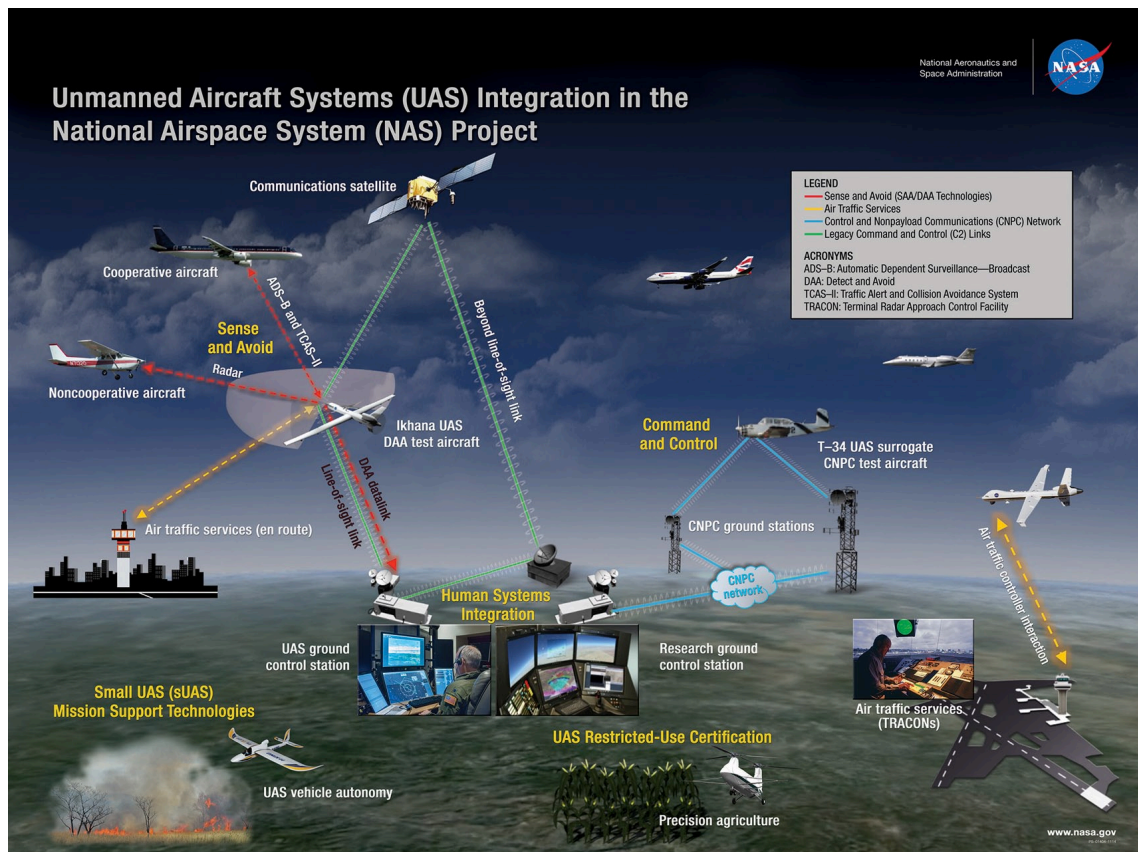


Fig. 10. A scheme showing integration of Unmanned Aircraft Systems in NASA's National Airspace System Project. Source: NASA Image (2014).

Remotely Piloted Aircraft and Remotely Piloted Air(craft) System. Although unmanned aircraft is the preferred term in many environments, there are occasions when such a generic term is unhelpful. The term 'unmanned' can cause confusion or uncertainty over the actual level of human control and has led to safety and legal concerns being raised. These concerns can be addressed in part by using terminology that describes the level of human control of such aircraft as being equivalent to that of piloted aircraft; the pilot is simply physically remote from the aircraft itself. Consequently, it may be appropriate to use the term Remotely Piloted Aircraft (RPA) to describe the actual aircraft, and Remotely Piloted Air(craft) System (RPAS) to describe the entirety of that which it takes to deliver the overall capability. Future RPA might carry passengers but not pilots to, for example, provide medical evacuation or tactical troop transport. Such systems would be manned, but remotely piloted. RPA and RPAS are defined as follows:

A Remotely Piloted Aircraft is defined as an aircraft that, while it does not carry a human operator, is flown remotely by a pilot, is normally recoverable, and can carry a lethal or non-lethal payload.

A Remotely Piloted Air(craft) System is the sum of the components required to deliver the overall capability and includes the Pilot, Sensor Operators (if applicable),

RPA, Ground Control Station, associated manpower and support systems, Satellite Communication links and Data Links.

**Pilot and Piloted.** The use of the terms pilot and piloted can cause confusion when trying to equate unmanned with manned aircraft operations. Some unmanned aircraft are required to be controlled by personnel who are already qualified to pilot manned aircraft, while most are not. By the standard Concise Oxford English Dictionary definition the use of the terms pilot and 'piloted' is only technically correct where the remote operator is operating the flying controls, which is not the case for all unmanned aircraft. An alternative description of 'operator' may be used instead, if appropriate. As with manned aircraft, where pilots will be qualified to different standards, unmanned aircraft pilots may be qualified to fly only certain classes of unmanned aircraft.

**Automation and Autonomy.** There are many different industry and academic descriptions of what comprises an automatic or autonomous unmanned aircraft. The following definitions have been chosen to be as simple as possible, while making clear the essential differences in meaning between the two:

In the unmanned aircraft context, an automated or automatic system is one that, in response to inputs from one or more sensors, is programmed to logically follow a pre-defined set of rules in order to provide an outcome. Knowing the set of rules under which it is operating means that its output is predictable.

An autonomous system is capable of understanding higher level intent and direction. From this understanding and its perception of its environment, such a system is able to take appropriate action to bring about a desired state. It is capable of deciding a course of action, from a number of alternatives, without depending on human oversight and control, although these may still be present. Although the overall activity of an autonomous unmanned aircraft will be predictable, individual actions may not be.

Any or none of the functions involved in the operation of an unmanned aircraft may be automated. Examples include: take-off and landing; navigation and route following; pre-programmed response to events such as loss of a command and communication link; and automated target detection and recognition. Unmanned aircraft which execute some elements of their operation without relying on human intervention or control may be described as partially automated. Those which carry out their entire mission from take-off to landing without human intervention may be said to be fully automated. At the moment, all but the very simplest and most limited of unmanned aircraft missions will be partially automated with a human controlling most aspects.

Autonomous systems will, in effect, be self-aware and their response to inputs indistinguishable from, or even superior to, that of a manned aircraft. As such, they must be capable of achieving the same level of situational understanding as a human. This level of technology is not yet achievable and so none of the currently fielded or in-development unmanned aircraft can be correctly described as autonomous. As computing and sensor capability increases, it is likely that many systems, using very complex sets of control rules, will appear and be described as autonomous systems, but as long as it can be shown that the system logically follows a pre-written set of rules or instructions and is not capable of human levels of situational understanding, then they should only be considered to be automated. (Joint Doctrine Note, 2010).

### **3.3.2. Unmanned Aerial Systems and their Advantages**

As describes Puliti et al. (2015) UAS typically consists of 1) an unmanned aerial vehicle, 2) a sensor payload (e.g., digital camera), 3) a navigational computer, 4) a UAV operator with remote controller, and 5) when necessary one or more spotters. Such systems have been in use for military purposes for several years, but have only recently become available for civilian purposes (Nex & Remondino, 2014). In recent years, the civilian market for UASs has increased rapidly and has become a highly dynamic and diverse market to meet the objectives of diverse applications.

A variety of flying vehicles is able to transport cameras and / or other sensors (Hollaus et al., 2014). Most common forms are small, electrically powered fixed-wing planes with wingspans from 1 to 3 meters and rotary-wing multi-rotor platforms (e.g. quadcopters, hexacopters or octocopters) or miniature helicopters (Figure 11.). Fixed wing UAVs typically have greater speed and longer range, rotary-wing UAVs have shorter flight durations, but offer greater manoeuvrability. They are piloted by an operator via remote control (RC), assisted by an onboard autopilot. Fixed-wing UAVs are typically launched by hand or by catapult, and land with or without some form of arresting mechanism, such as a parachute or by flying into a net. Rotary-wing UAVs often need some manual operation for take-off, and may or may not require manual operation for landing (Whitehead et al., 2014).

According to Wallace et al. (2016) small-size unmanned aerial vehicles (UAVs of less than 5 kg) represent a low-cost remote sensing alternative to airborne and satellite platforms that, when equipped with suitable sensors, can produce cost-effective data at local scales (e.g., for areas the size of traditional forest stands up to areas of several km<sup>2</sup>) with an unrivalled combination of spatial and temporal

resolution (Matese et al., 2015). Equipping UAVs with sensors capable of detecting 3D structure has led to the systems being increasingly used to provide an understanding of the structure and variability of forests (Dandois & Ellis, 2013; Jaakkola et al., 2011; Lisein et al., 2013; Wallace et al., 2014). UAS environmental applications benefit from a greater operational flexibility due to the possibility of acquiring RS data at precise moments in time under a variety of atmospheric and accessibility conditions. Due to these advantages, rapid growth of the UAS sector is predicted for the next decade (Puliti et al., 2015).

Hollaus et al. (2014) agrees, that Unmanned Aerial Vehicles are a rapidly upcoming method for remote-sensing data acquisition, mostly aerial images and derived products. By now, the systems are light-weight and effective, the development of the sensors and their reliability enable a relative safe operation with good chance of success. UAVs are quickly ready for operation almost anywhere and anytime. One of the greatest advantages of this new technique is its high flexibility and the relatively low operational costs. The miniaturisation of the sensors and the increasing reliability of the navigation systems make UAVs to an instrument for operational applications. In contrast to standard aerial imagery, the often even better spatial resolution of the data offers possibilities for new developments in image analysis.

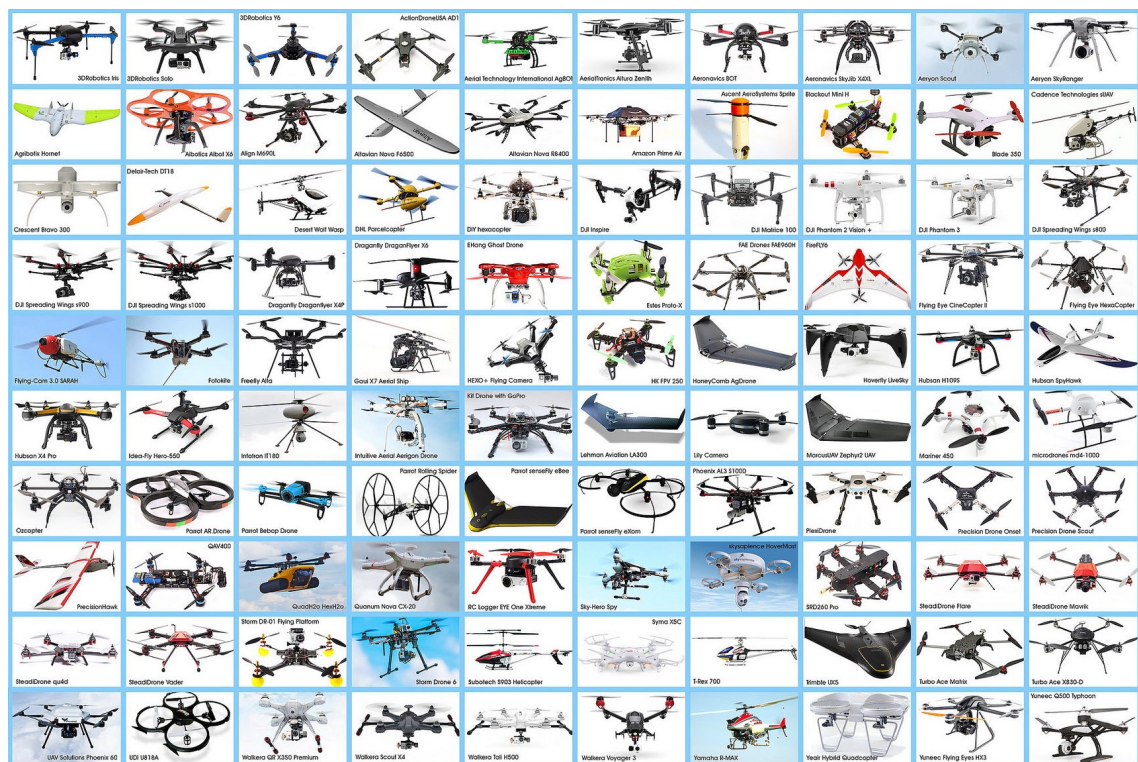
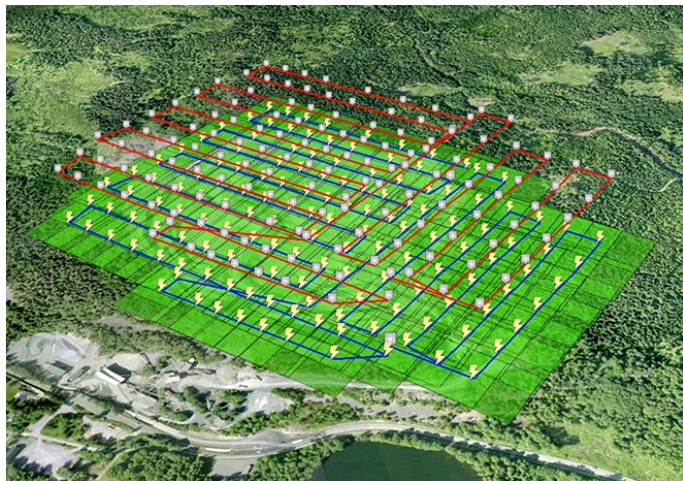


Fig. 11. A selection of 100 unmanned aerial vehicles showing the variability of UAVs present in the contemporary commercial airspace worldwide. Source: Stephens (2015).



### 3.3.3. Surveying Using Unmanned Aerial Systems

Whitehead et al. (2014) describes general principles concerning UAS survey and flight planning. The remote sensing workflow for small UASs is essentially an adaptation of the same steps and processes used for piloted aircraft surveys, and in both cases, aviation regulations place certain restrictions on how the surveys are configured. Though each UAS survey is unique in nature, the same generic workflow is normally followed. Typically, a UAS survey starts with flight planning (Hugenholtz et al., 2013). This stage relies on specialised flight-planning software and uses a background map or satellite image to define the survey area (Fig. 12.). Additional information is then added, such as the desired flying height, the focal length, shutter speed and orientation of the camera, the desired amount of overlap between images, and the desired flight direction. The flight-planning software will then calculate the optimal solution to obtain overlapping stereo imagery covering the area of interest. During this process, the various parameters can be adjusted until the operator is satisfied with the flight plan.



*Fig. 12. A flight plan for a UAV survey showing flight route, series of waypoints and expected image overlap on the ground. Source: One Drone Cloud (2016).*

Once a flight plan has been generated, it is uploaded to the UAS autopilot. The instructions contained in the flight plan are used by the autopilot to calculate the necessary climb rates and positional adjustments that enable the aircraft to follow the planned course as closely as possible. Readings from the GNSS (Global Navigation Satellite System) and IMU (Inertial Measurement Unit) are typically logged by the autopilot several times per second throughout the flight. The mission itself can run fully automatically, wireless communication allows tracking the actual position of the platform and adapting the flight plan if possible. A semiautomatic mode or manual mode, e.g. for landing, in case of signal loss or other unexpected problems is always available. The flight has to be supervised by a qualified pilot, who is able to take over the direct control of the UAV anytime. Flight telemetry data are logged and either transmitted to the ground station in real time or downloaded after the flight (Hollaus et al., 2014).

Whitehead et al. (2014) continues, that on completion of the flight, a log file is usually downloaded from the aircraft autopilot. This file contains details about the recorded aircraft position and attitude throughout the flight, as well as details about when the camera was triggered. The log file from the UAS autopilot can be used to provide initial estimates for the position and orientation of each image. In addition, it is usual to include a number of accurately surveyed ground control points in the photogrammetric adjustment. These usually consist of specially placed targets whose position is precisely measured with a GNSS device (preferably geodetic) at the time of the UAS survey (e.g., Hugenholz et al., 2013).

Hollaus et al. (2014) specifies, that automated UAVs are navigated by a small onboard GNSS/INS (Inertial Navigation System) unit. The main components of the navigation unit are gyroscopes for measuring roll, pitch and yaw rotations and thus inclination angles of the platform, air pressure sensor, magnetometer and accelerometer. Concerning the accurate positioning of the data being acquired by the UAV, he describes, that georeferencing can be done in several ways:

- Direct georeferencing (defined as direct measurement of camera position and orientation for each image) can be done with telemetry data from the GNSS/IMU unit (Pfeifer et al., 2012; Blaha et al., 2011). Real time monitoring systems are also described by several authors (Kim et al., 2012; Rieke et al., 2011).

- Georeferencing with (additional) use of ground control points. In practice, extensive field work can be necessary for installation and accurate measurement of ground control in rough and densely forested terrain.

- Combination of direct georeferencing and ground control. Because of the relatively inaccurate position and orientation data from the onboard sensors the direct georeferencing method is rarely sufficient without ground control measurements. So, GNSS and INS data are used for an initial estimation of the exterior orientation parameters (EOP), which can help to speed up the further image processing significantly.

Regarding the equipment, Hollaus et al. (2014) describes, that because of limited payload and space, UAVs are equipped with light-weight consumer compact cameras or DSLRs. They usually deliver images in high quality and resolution, but are often unstable concerning the parameters of inner orientation (IOP). This problem can be solved, while the camera lens is mechanically fixed or a fixed focal length is used. The camera is triggered by the RC and takes images either in predefined intervals (eg. every two seconds) or at predefined locations. The images are usually stored on a memory card and downloaded after the mission.

### 3.3.4. UASs and Photogrammetry

Lisein et al., 2013 describes, that along with the rising use of UASs, dense three-dimensional reconstruction through the combined use of photogrammetry and Structure from Motion (SfM) state-of-the-art techniques has triggered the “comeback of photogrammetry”. Indeed, the ubiquitous use of digital photography instead of analogue photography and the continuous improvements in computer computation power have turned digital photogrammetry into a viable surrogate for laser scanning.

The SfM algorithms originate from the field of computer vision and aim to automatically determine scene geometry, camera calibration, position and orientation from an unordered overlapping collection of images. This results in a sparse 3D point cloud and camera orientations that are subsequently used for multi-view dense image-matching. Hollaus et al. (2014) continues stating, that it is possible in a highly automated way to estimate camera geometry and calculate a 3D model from a set of overlapping images, invariant to scale, orientation, distortion and illumination changes. Point clouds as a result from image matching can be further processed in a similar manner like point clouds from airborne or terrestrial laser scanning and can be even combined with laser scanning data.

Whitehead et al. (2014) agrees, that the most common non-military application of UASs to date has been for large-scale photogrammetric mapping. Nevertheless, issues, such as platform stability and the use of nonmetric cameras, usually mean that the geometry of the imagery collected is of a lower quality than that obtained during traditional photogrammetric surveys carried out from manned aircraft (Hardin & Jensen, 2011). UAS surveys also tend to collect images with large amounts of overlap. This is partly because the low flying height and comparatively low accuracy of onboard navigational sensors, which can lead to significant differences between the image footprints estimated during flight planning and the actual ground coverage of each image, especially in undulating terrain (Haala et al., 2011; Zhang et al., 2011).

Image footprints can also drift from expectation because of changes in the roll, pitch, and yaw of the UAV caused by wind and navigation corrections. In spite of these drawbacks, the low flying heights normally make it possible to gather imagery with few-centimetre spatial resolution. This level of detail combined with low costs, flexibility in the timing of image acquisition, and short turn-around times makes UAS-based photogrammetry an attractive option for many potential users across a broad spectrum of research and professional applications.

Also Hollaus et al. (2014) discusses, that regarding the processing of UAV-based, high resolution and small format images, there are a few main differences between images from low altitude UAV platform compared to classical aerial platforms flying at higher altitudes. He states, that UAVs have:

- Larger rotational and angular variations between images,
- Often not systematic flight lines, due to wind, visibility, terrain conditions,
- Large perspective distortions due to relatively large height differences in a scene,
- Small footprint of the images, therefore a lot of images have to be collected (and processed) for a good overlap,
- Parameters of exterior orientation often unknown or not accurate,
- IOP unstable because often light-weight and low-cost compact cameras are used

Whitehead et al. (2014) adds, that UAS imagery is subject to variable scales, high amounts of overlap, variable image orientations, and often has high amounts of relief displacement arising from the low flying heights relative to the variation in topographic relief. For these reasons standard aerotriangulation methods often fail for images acquired with UAVs (Haala & Rothermel, 2012). A variety of open-source and commercial dense stereo matching tools are now available to deal with these challenges. Over the last few years a number of Structure from Motion software packages have been developed. The SfM approach uses algorithms originally developed for computer vision, such as a Scale-Invariant Feature Transform (SIFT), which identifies similar features in conjugate images. Unlike conventional photogrammetry, which is bound by rigid geometric constraints, SfM is able to accommodate large variations in scale and image acquisition geometry.

Dandois & Ellis (2013) state, that SfM differs from prior photogrammetric applications in that camera position and orientation data, that are conventionally acquired using GNSS and IMU instruments carried by the aircraft, are removed from the 3D modelling equation, and instead the 3D reconstruction of surface feature points is determined automatically based on the inherent “motion” of numerous overlapping images acquired from different locations. The result is an extremely simple remote sensing instrument: an ordinary digital camera taking highly overlapping images while moving around or along objects. SfM techniques have already proved successful for accurate generating of 3D models of open fields, forests and trees from aerial images acquired from a remote-controlled multi-rotor aircraft (Rosnell & Honkavaara, 2012; Tao et al., 2011).

As adds Wallace et al. (2016), SfM has built onto traditional stereoscopic techniques as a result of advances in computer vision algorithms and parallel bundle adjustments on graphics processing units. These developments have made

it possible to match image features in many overlapping photographs (hundreds-thousands) acquired from different angles, which makes SfM ideally suited to photographs acquired from small UAVs. Whitehead et al. (2014) predicts, that, due to the comparatively low cost and ability to handle unconventional imagery, it is likely that SfM packages will increasingly become the software of choice for UAS photogrammetric surveys.

Wallace et al. (2016) specifies, that the use of SfM packages, such as Bundler or Agisoft Photoscan allow for a high degree of automation, and makes it possible for non-specialists to produce accurate DSMs and orthophoto mosaics in less time that it would take using conventional photogrammetric software. Various researchers utilize Agisoft PhotoScan in their studies, since it has been proven to be effective in the production of dense and accurate point clouds over forest areas (Dandois & Ellis, 2013; Puliti et al., 2015). Photoscan offers a user-friendly processing pipeline that combines proprietary algorithms from computer vision SfM and stereo-matching algorithms to accomplish the tasks of image alignment and multiview stereo-reconstruction (Verhoeven et al., 2012).

Another software package used by scientists recently is Ecosynth (e.g. Dandois & Ellis, 2010, 2013). It is a suite of tools for mapping and measuring vegetation in three-dimensions using off-the-shelf digital cameras and open-source computer vision software, from the ground or using low altitude hobbyist aircraft. Ecosynth is capable of generating 3D and spectral imaging data useful for ecological research and applications (Ecosynth, 2016). Ecosynth is the entire processing pipeline and suite of hardware involved in generating ecological data products, such as canopy height models, aboveground biomass estimates, and canopy structural and spectral vertical profiles (Dandois & Ellis, 2013).

### **3.3.5. Employment of UAS in Forestry**

Wallace et al. (2016) prefaces, that remote sensing generally can complement existing ground-based techniques, providing spatially representative characteristics of investigated forest stands in a more efficient manner. Data captured over varying spatial, spectral, and temporal scales has been shown to contain information, which can be used to measure and monitor various aspects of a complex forest structure. Advances in acquisition of this information have led to high spatial resolution three-dimensional remote sensing becoming an important tool in forest modelling.

As states Lisein et al. (2013) the recent development of operational small unmanned aerial systems opens the door for their extensive use in forest mapping,

as both the spatial and temporal resolution of UAS imagery better suit local-scale investigation than traditional remote sensing tools. The spatial resolution of UAS imagery can easily reach a sub-decimeter ground sampling distance, and the revisit period between two acquisitions can be selected in order to fit diverse needs of forest management or various scales of ecological phenomena. Small and lightweight UASs, in particular, are likely to become a versatile tool also for environmentalists and scientists (Anderson et al., 2013; Turner et al., 2012).

Gatziolis et al. (2015) summarizes, that recently unmanned aerial vehicles equipped with user-grade cameras and inexpensive GPS devices have emerged as a flexible, economic alternative data source that supports the retrieval of tree dimensionality and location information. Flying at low altitude above the trees and with the camera oriented at a nadir view, UAVs acquire high-resolution images with a high degree of spatial overlap. In such conditions, a point on the surface of a tree crown or a small object on exposed ground is visible from many positions along the UAV trajectory and is depicted in multiple images.

Automated photogrammetric systems based on computer vision SfM algorithms explore this redundancy to retrieve the camera location in the moment an image was acquired, calculate an orthographic rendition of each original image, and ultimately produce a precise 3D point cloud that represents objects (Rosnell & Honkavaara, 2012). Dey et al. (2012) underlines, that application of SfM techniques on UAV imagery has enabled accurate 3D modelling of forest canopies (Fig. 13.).

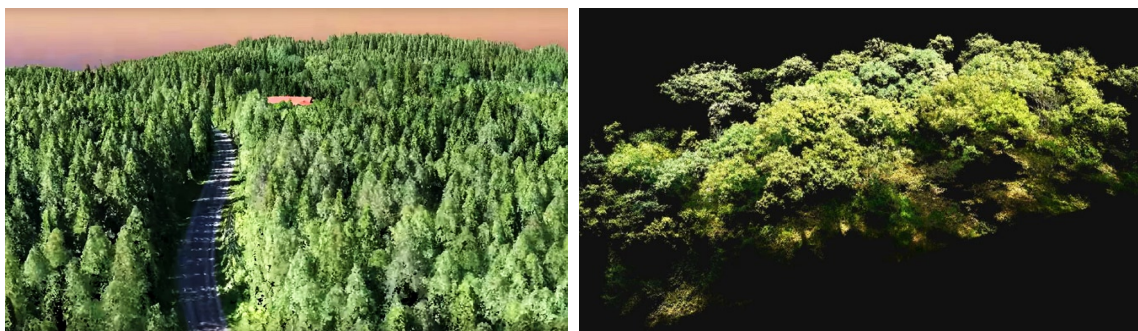


*Fig. 13. The image-based point clouds gained from images obtained by Unmanned Aerial Vehicles by the means of Structure from Motion software. Point cloud on the left represents coniferous forest in Finland, point cloud on the right broadleaf forest in Germany. Sources: Left image: VideoDrone (2016), Right image: Sperlich et al. (2014).*

Hollaus et al. (2014) adds, that the quick setup, the easy transport and operation makes a UAV system a perfect instrument for forest monitoring, because of the arbitrary frequency of repeating flights (Häme, 2012). This is also a great advantage for detection and assessment of damages from wind (Böhm, 2010), forest fire (Casbeer et. al., 2006) or mapping of biotic infections (Böhm, 2010).

But at the same time Hollaus et al. (2014) counters, that technical limitations can hinder the acquisition of images, especially in remote and steep forested regions. For fixed-wing UAVs suitable landing places are required. Narrow, rough forest roads or clearings are often the only possibilities in dense forested areas, but bear a high risk of damage of the vehicle. In case of no or low-quality GNSS signal, a manual flight control can be essential, with all drawbacks for image processing (overlap, area coverage, high rotational and angular deviations, oblique images, no exterior orientation parameters). Furthermore, ground control points often are simply not visible, and are hard to establish or measure by GNSS devices with reasonable accuracy in forested areas.

Puliti et al. (2015) adds, that the use of user-grade cameras leads to large perspective distortions, poor camera geometry, and a lack of spectral consistency. In addition, the use of inexpensive GPSs and the lack of inertial measurement units lead to poor positioning accuracy. Forest surveys are further affected by the presence of moving objects (swinging tree tops, shade), and pronounced distortion due to perspective shown as trees leaning towards the sides of the image.

All these factors posed challenges in the past with respect to 3D geometry generation from UAS imagery. Creating suitable image-based point clouds for assessing the required forest variables can be therefore a demanding task. As explains also Lisein et al. (2013), image matching in an area of vegetation is well known to be quite challenging, due to the numerous vegetation characteristics that hinder image matching: omissions, repetitive texture, multi-layered or moving objects. The abrupt vertical changes occurring between the trees crowns and the microtopography of the canopy (characterized by high variations of the relief) cause multiple omissions that can mar the dense-matching process.

Nevertheless, these issues can be partly or fully overcome, and previous investigations have shown that a photogrammetric digital canopy surface model may be generated by automatic image matching with a very satisfactory level of accuracy and resolution (St-Onge et al., 2008). Puliti et al. (2015) agrees, that the recent adoption of SfM algorithms in photogrammetric pipelines has made UAS-SfM systems a suitable tool for forest inventory purposes. As already mentioned, compared with traditional digital photogrammetry, for which accurate camera interior and exterior parameters are a prerequisite, SfM algorithms have the advantage of allowing 3D geometry generation from overlapping but otherwise unordered images acquired with uncalibrated cameras.

The resulting photogrammetric digital surface models (photo-DSMs) can be advantageously combined with a DTM generated from topographic or LiDAR data in order to produce a hybrid photo-topo or photo-LiDAR canopy height model.

Photogrammetry could be advantageously used to update LiDAR canopy height models and to constitute multi-temporal canopy height series. As already mentioned, on a local scale, UAS imagery is characterized by a high image overlap and, thus, a high level of information redundancy. It therefore has the potential to accurately model the canopy surface at a very high spatial (but also temporal) resolution (Lisein et al., 2013).

Hollaus et al. (2014) comments, that when using high resolution UAV images in forestry, generally the main outcomes of the image-survey are the photogrammetric evaluation in terms of derivation of digital surface models and orthorectified image mosaics. Like traditional aerial imagery, UAV-based images provide important basic data for various subsequent geospatial analyses. For high resolution UAV-based images all standard image processing, analyses and interpretation methods are used, possibly in combination with other remote sensing data. The images allow forest delineation and segmentation on relatively homogenous parts and further vegetation mapping (Machala & Zejdová, 2014), or even tree species classification (Yu et al., 2006; Gini et al., 2012).

Hollaus et al. (2014) further discusses, that particular attention lies in single-tree-extraction, tree crown detection, height estimation or assessment and derivation of tree density, age-classes and further structure parameters, like stem or timber volume. Such parameters can be derived from point cloud data as a result of image matching and are a valuable support for forest inventory as well as for forest management (Bohlin et al., 2012b). This also includes silvicultural methods and planning and monitoring of harvesting.

For vegetation-analyses, besides classical RGB cameras, also other sensors, such as near-infrared cameras, multispectral or even hyperspectral sensors, are being combined with UAVs. Recently small and light-weight models of sensors are offered, which are designed especially for application with UAVs (Bendig, 2012). In the last years also spectrometers (Jaakkola, 2010), thermal cameras (Zarco-Tejada, 2012), radars (Koo et al., 2012), or laser scanners (Esposito et al., 2014), are being mounted and tested on UAVs.

The application of UAV-borne laser data for forest change detection is documented e.g. by Wallace et al. (2012a; 2012b). Jaakkola et al. (2011) tested laser data from UAVs for single tree measurements. The application of IR-, hyper-, multispectral- or thermal sensors gets also operational, e.g. for estimation of leaf area index (Corcoles, 2013), calculation of narrow-band indices for detection of water stress in orchards (Zarco-Tejada, 2012), mapping states of vegetation and vegetation health (Knoth, 2011) or assessing the temperature (Bendig, 2012).

Regarding the practical fields of utilization of the UAV-borne RGB imagery, Dandois & Ellis (2013) summarize, that it may be used to observe forest canopy



structure and height (Machala & Janata, 2014; Baltsavias et al., 2008). Canopy height measurements are of great interest for the monitoring of harvests and recruitment (Næsset et al., 2004), the estimation of forest biomass and carbon stock (Corona & Fattorini, 2008) and, generally, in ecosystem process modelling.

In the field of multi-source forest inventory, structural forest attributes are commonly extracted from the canopy height model by means of regression models predicting forest variables with metrics (i.e., descriptive statistic of the canopy height model on a particular area) (Næsset, 2002b; Næsset et al., 2004). The practical outcomes of utilization of canopy height models, in combination with field measurements, are the predictions of forest attributes of interest, such as stand density and maturity indicators (Lisein et al., 2013).

The described SfM principles often used for processing UAV imagery relies on photogrammetric methods that have already been used for estimating tree height from overlapping images acquired using large-format, photogrammetric-grade cameras coupled with flight time GPS and IMU data. Including automated feature extraction, matching and bundle adjustment (Hirschmugl et al., 2007; Ofner et al., 2006), these methods are currently being discussed as a highly viable alternative to LIDAR for 3D forestry applications (Leberl et al., 2010).

As states Puliti et al. (2015) retrieving the necessary data to plan silvicultural activities may be one of several relevant areas of UAS applications. Currently, forest inventories in many countries are conducted by adopting an area-based approach using a combination of field samples and wall-to-wall airborne laser scanning data (Næsset, 2007; Vauhkonen et al., 2014). ALS is cost effective at a large scale, and in some countries (e.g. Norway, Finland), this technique has resulted in coordinated forest inventories that aggregate a multitude of private forest properties. However, in countries where these types of inventories are not carried out, access to accurate data at a small scale becomes too costly. Furthermore, for larger forest properties, timely and accurate data over specific forest areas are needed in the case of more specific pre-harvest, post-harvest, and post-disturbance inventories.

Given this context, the main advantage of UASs is the possibility to map areas effectively with very high spatial and temporal resolution, even under cloud cover, because UAS flights are often conducted below the cloud layer. Additionally, relevant cost reductions can be achieved compared with traditional manned airborne remote sensing data acquisitions when the forest inventory areas are small and require a high spatial and/or temporal resolution. The use of UASs in forest inventory research is also of great interest, especially with respect to the finely detailed, multi-temporal component of the data and their potential use in sampling applications (Wallace et al., 2014).

### 3.3.6. Recent Studies of Interest

Only a very few researchers have used UAS platforms and SfM software for image-based point cloud creation for forest inventory purposes so far (e.g. Lisein et al., 2013; Dandois & Ellis, 2013; Wallace et al., 2016). Also a review of the main achievements of these studies is lacking in the literature (Puliti et al., 2015). The need for studying this young phenomenon is therefore obvious. The discovered scientific papers dealing with these issues are summed up in this chapter.

Probably one of the earliest studies assessing, besides other quantities, also height of trees based on the estimates derived from CHM created using low-cost RS device and SfM computer vision, is the study of Dandois & Ellis (2010). Within this study, two 100 m × 225 m (2.25 ha) test sites were selected to assess 3D vegetation measurements by Ecosynth software against tree measurements made in the field. The study plots were divided into a grid of 25 m × 25 m subplots. Test site 1 was covered by a mixed-age forest composed of various broadleaf trees. Test site 2 was covered by a few-species broadleaf forest. Heights of all trees greater than 12.7 cm in DBH were measured across each test site before leaf-off in fall 2009 using a Haglöf Vertex laser hypsometer.

Aerial photographs for Ecosynth were acquired using an off-the-shelf Canon A470 digital camera and a kite aerial photography rig composed of an ITW Alpine Delta Conyne kite and of 100-lb Dacron kite line (not a UAV). Aerial photographs were uploaded into Bundler software for processing into 3D point clouds. Canopy height models were produced from the non-ground points in Ecosynth. Summary height statistics (CHM height metrics) were calculated across all CHM points with height >2 m. The relative accuracy of tree height estimates from Ecosynth CHMs was then tested based on the predictive strength of the strongest models obtained for the prediction of field-measured mean tree heights (average of the 5 tallest trees in each subplot; representative of dominant canopy height) across the set of subplot CHM height metrics using stepwise multiple linear regression.

Ecosynth predicted field-measured tree heights well at the site 2, where the largest terrain errors were observed (Adj.  $R^2 = 0.80$ , RMSE = 2.9 m), yet performed rather poorly at the site 1 (Adj.  $R^2 = 0.53$ , RMSE = 4.2 m). Since within this study the authors assessed only the 5 tallest trees at each subplot, the success rate of individual trees identification could not be determined.

Three years later, the same authors presented a new study (Dandois & Ellis, 2013). This study was carried out across three 6.25 ha (250 m × 250 m) forest research

study sites in Maryland USA. First two sites were centred on and expanded from the study sites described in the previous study. The third site was then also populated only by broadleaved species. Tree location, species, DBH and height of trees greater than 1 cm DBH were hand mapped within the subplot grid between June 2012 and March 2013. Tree heights were measured by laser hypsometer during leaf-off conditions for the five largest trees per subplot, based on DBH. Subplot canopy height was then estimated as the mean height of the 5 tallest trees, i.e., average maximum height.

A hobbyist-grade multi-rotor “Mikrokopter Hexakopter” was purchased as a kit, constructed, calibrated and programmed for autonomous flight. The flying system included a manufacturer-provided wireless telemetry downlink to a field computer, enabling real-time ground monitoring of aircraft altitude, position, speed, and battery life. A Canon SD4000 point-and-shoot camera was mounted under the hexakopter to point at nadir and set to “Continuous Shooting mode” to collect 10 megapixel resolution photographs continuously at a rate of 2 frames  $\cdot s^{-1}$ .

Three-dimensional RGB point clouds were generated from the sets of aerial photographs using a Agisoft PhotoScan software (v0.8.4 build 1289). Agisoft was used for its greater computational efficiency over the open source Bundler software used previously (Dandois & Ellis, 2010) for vegetation point cloud generation (estimated at least 10 times faster for photo sets >2000). The authors also used Ecosynth software for vegetation structure measurements and derived also DTMs from the point cloud data using Ecosynth.

At all sites, Ecosynth CHM metrics were compared with field measured heights of the five tallest trees within each subplot using simple linear regressions. At the sites 1 and 2, results demonstrate that Ecosynth CHMs adequately predicted field-measured average maximum height, when either Ecosynth leaf-off ( $R^2$  0.82–0.83) or LiDAR DTMs ( $R^2$  0.83–0.84) were used. When Ecosynth leaf-on DTMs were used, the quality of canopy height predictions was lower ( $R^2$  0.62–0.67). For the third site, Ecosynth predictions were very low for all DTMs ( $R^2$  0.07–0.30). For Ecosynth, field height prediction errors with the leaf-off DTM (3.9–9.3 m RMSE) were generally higher than when the LiDAR DTM was used (3.2–6.8 m RMSE) but lower than when the leaf-on DTM was used (7.1–10.9 m RMSE). Similarly as in the previous study, the numbers of identified trees were not the subject of research.

Lisein et al. (2013) carried out a forest inventory in autumn 2012, in order to compare digital canopy height models with field measurements. The forest inventory used variable-area circular plots installed on a systematic grid and focused exclusively on deciduous stands. The plot radius was adapted to keep to a minimum number of 20 trees and ranged between 7.4 m and 18 m (10 ares) in the case of low tree density.

For each plot, dominant height ( $h_{dom}$ ) was calculated as the average of dominant tree heights, which have to be representative of the 100 tallest trees per hectare. The number of dominant trees measured varied for each plot and corresponded to the number of the plot area plus 1 (e.g., 11 dominant trees were measured on a plot of 10 ares). In total, 36 plots located in irregular deciduous stands were inventoried.

A fixed-wing UAV Gatewing X100 was employed in this study, equipped with Ricoh GR3 still 10-megapixel camera adapted for near-infrared acquisition. For the SfM processing of the acquired data authors used the open source toolbox, MICMAC software, developed by the French mapping agency (the National Institute of Geographic and Forestry Information). An ABA was used to model  $h_{dom}$ , and an individual tree crown approach was used for single-tree height.

The ABA results showed adjusted  $R^2$  of 0.82 and RMSE of 1.65 m. For the individual tree crown approach, concerning 86 field-measured trees, the results were slightly better, with adjusted  $R^2$  value of 0.91 and RMSE of 1.04 m. Unfortunately the authors do not state how many dominant trees they measured within their study plots together, or based on what key those 86 trees whose height was assessed, were selected. Therefore the success rate of the detection of individual trees cannot be evaluated.

In another study Puliti et al. (2015) used a research area in a Norwegian boreal mainly coniferous forest. Field measurements were conducted in 38 circular fixed-area sample plots (400 m<sup>2</sup>). The plot data were collected by measuring the DBH for all trees with DBH  $\geq$  4 cm. Sample trees for height measurements were selected based on a probability proportional to stem basal area and height measured using a Vertex hypsometer. For trees without height measurements, height was predicted using height-DBH models.

In this study, a SenseFly eBee fixed-wing UAV was used for the remotely sensed data acquisition. The eBee was equipped with a Canon S110 near-infrared camera as the payload. Authors used the proprietary software Agisoft PhotoScan Professional Edition 1.1.0 (64 bit) to generate 3D dense point clouds from the entire set of images. The accuracy of the predictions of statistical models was validated at a plot level using leave-one-out cross-validation (CV). For each biophysical property of interest, the selected independent variables were used to fit the models to the field data by iteratively leaving one observation out at a time. The estimated parameters were then used to predict each variable of interest for the remaining observation. The root mean square error (RMSE) and mean difference ( $\bar{D}$ ) were determined.

The leave-one-out CV of the selected models revealed that the errors with respect to the RMSE for Lorey's mean height (i.e. mean height weighted by basal

area; referred as  $h_L$ ) were limited to 1.5 m and with respect to dominant height were limited to 0.7 m. Adjusted  $R^2$  then was 0.68 for  $h_L$  and 0.95 for  $h_{dom}$ . The mean difference had an absolute value of maximally 0.36 % of the ground reference value. As the authors confess, the error was larger for stem number, for which the RMSE was 538 trees  $\cdot$  ha $^{-1}$  which is 39.2 % (!) compared to field-measured counts.

A few more studies assessing vegetation height based on SfM principles applied on UAS image data was found. Briefly, their core methods and findings are following. The study of Zahawi et al. (2015) was focused on the use of lightweight UAVs to monitor tropical forest recovery while assessing also the height of trees. This study was carried out at 13 1-ha restoration sites established in tropical premontane wet forest zone. Images were acquired using a commercially available, hobbyist 'multirotor hexacopter' UAV (not further specified) equipped with Canon ELPH 520 HS 'point-and-shoot' digital camera pointed at nadir. 3D multispectral RGB point clouds (mean density 55 points  $\cdot$  m $^{-2}$ ) were generated from the digital images collected at each site using Agisoft PhotoScan software. The median Ecosynth height metric was the best overall predictor of field height for CHM with  $R^2$  equal to 0.87 and RMSE equal to 1.37 m.

Another study dealt with using UAV imagery to assess olive tree crown parameters (Díaz-Varela et al., 2015). Two olive tree plantations were studied, one with trees in 4 x 2 m grid, another with 3.75 x 1.35-m spacing between trees (narrow hedgerow). The UAV platform used for image acquisition was a 2-m wingspan fixed-wing platform with up to a 1-h endurance, equipped with Panasonic Lumix DMC-GF1 camera. The pix4UAV software was used to generate each orthomosaic and the DSM for each orchard. Tree height was retrieved from the DSM based on the identification of local maxima, likely to correspond to tree tops. Linear fits of the measured vs. estimated height at the individual tree/hedgerow level showed an  $R^2 = 0.07$  only and RMSE = 0.45 m at study plot 1 (isolated trees), while at study plot 2 (hedgerows), it reached the value of  $R^2 = 0.53$  and RMSE = 0.20 m. Numbers of trees were not assessed in this study.

A case study of Wallace et al. (2016) then analysed data collected from a 30 x 50 m plot in a dry eucalypt forest with a spatially varying canopy cover. The UAV used in this study was a multi-rotor Droidworx Skyjib Oktokopter equipped with Canon 550D digital 18 Megapixel single lens reflex (DSLR) camera. The image data were processed in Agisoft Photoscan v1.0.0. The SfM dataset contained sufficient spatial detail on the upper canopy to manually identify 112 tree top locations from 136 measured trees (82.4 %). The correlation found between field-measured and point cloud measured individual trees height reached  $R^2 = 0.68$ , the RMSE was 1.30 m.

The last relevant study found in scientific journals is a brief research of Sperlich et al. (2014) studying the potential of UAV-based photogrammetric point clouds for single tree detection. A coniferous (1.11 ha) and a broadleaved (1.28 ha) forest stands were situated in Germany. The utilized UAV was a octocopter MK Okto2 equipped with Panasonic Lumix G3. The DSM and DTM were calculated from the point cloud using TreesVis software. The tree crowns were detected manually based on visual interpretation of the data. The 1m and 2 m radii were created around each reference tree to seek for the modelled trees within them. On a deciduous study plot only 16 trees were detected, out of the 120 reference trees, for the 1 m search radius (i.e. 13.3 %) and 36 for the 2 m search radius (i.e. 30 %). The average success rate was therefore 21.65 % for broadleaf trees. On the coniferous study plot 192 out of 219 trees was detected within the 1 m radius (i.e. 87.7 %) and 198 trees were detected within the 2 m radius (i.e. 90.4 %). That makes the average of 89.05 % of detected coniferous trees.

The pertinent information from the described research articles and the achieved accuracy of results of height assessment are summed up in the Table 1.

*Table 1. The significant information and summarized results characterizing the discovered recent research papers focused on the assessment of height of trees using the image-based point clouds from UAV and various SfM software. B stands for Broadleaf trees, C for Coniferous trees, tr. means tropical and pl. means plantation.*

Authors & Year	Forest	UAV	Software	Height: R <sup>2</sup>	Height: RMSE	Matched Trees
Dandois & Ellis (2010)	B	kite (not "UAV")	Bundler & Ecosynth	0.53 - 0.80	2.9 m - 4.2 m	-
Dandois & Ellis (2013)	B	hexacopter	Agisoft PS & Ecosynth	0.07 - 0.84	3.2 m - 10.9 m	-
Lisein et al. (2013)	B	fixed-wing	MICMAC	0.82 (ABA) 0.91 (ITA)	1.65 m (ABA) 1.04 m (ITA)	?
Sperlich et al. (2014)	B & C	octocopter	TreesVis	-	-	21.7 % (B) 89.1 % (C)
Zahawi et al. (2015)	B - tr.	hexacopter	Agisoft PS & Ecosynth	0.87	1.37 m	?
Díaz-Varela et al. (2015)	B - pl.	fixed-wing	pix4UAV	0.07 - 0.53	0.20 m - 0.45 m	-
Puliti et al. (2015)	C	fixed-wing	Agisoft PhotoScan	0.68 (h <sub>L</sub> ) 0.95 (h <sub>dom</sub> )	1.5 m (h <sub>L</sub> ) 0.7 m (h <sub>dom</sub> )	rel. RMSE = 39.2 %
Wallace et al. (2016)	B	octocopter	Agisoft PhotoScan	0.68	1.30 m	82.4 % manually

## 4. Methodology

The methods applied in this work could be divided into several parts, all generally focused on studying particular characteristics of selected forest stands. The first part involved selection of forest study plots and thorough field measurements of trees present on them with the emphasis on measuring their height and also their position. These study plots were then the subject of UAV flight campaigns acquiring the images suitable for further photogrammetric processing. A parallel part then consisted of development and programming of unique software tool enabling to calculate the height of trees based on the remote sensing data, its application on the own data from the UAV, statistical comparison with the field-measured data and assessment of the results.

### 4.1. Characterisation of Research Area

Array of measurements of forest stands and series of UAV flight campaigns for photographing these stands were performed for the purposes of this work. All of those operations were held on a Training Forest Enterprise (TFE) Masaryk Forest Křtiny belonging to Mendel university in Brno. The enterprise is situated in the Czech Republic, in the South-Moravian District, north-east of the city of Brno - the second largest city in the country (Figure 14.).

The TFE spreads over 10 492 ha of land with the forest land covering 10 265 ha. The forests are situated at altitudes ranging from 210 to 575 meters above sea level and are characteristic with a variety of natural conditions, which predetermined the establishment of the special-purpose facility of the university. The area which is dominated mostly by mixed woods with 46 % of coniferous and 54 % of deciduous tree species contains 116 forest types situated in 4 forest altitudinal vegetation zones.

Mean annual temperature of 7.5 °C and mean annual precipitation of only 610 mm are limiting factors. Topography is very broken with deep-incised valleys and glens, especially those of the Svitava river and the Křtinský potok brook. Parent rock is formed by granodiorites, Culmian greywackes and limestone. About a third of the TFE area is situated within the Protected Landscape Area of the Moravian Karst. Main local tree species are spruce, pine, larch for conifers and beech and oak for broadleaves (TFE Křtiny, 2013).

The field activities in this work were situated mainly around towns Kanice, Řícmanice, Bílovice nad Svitavou, Soběšice, Ořešín, Útěchov, Vranov, Adamov, Babice nad Svitavou, Habrůvka, Křtiny and Březina.

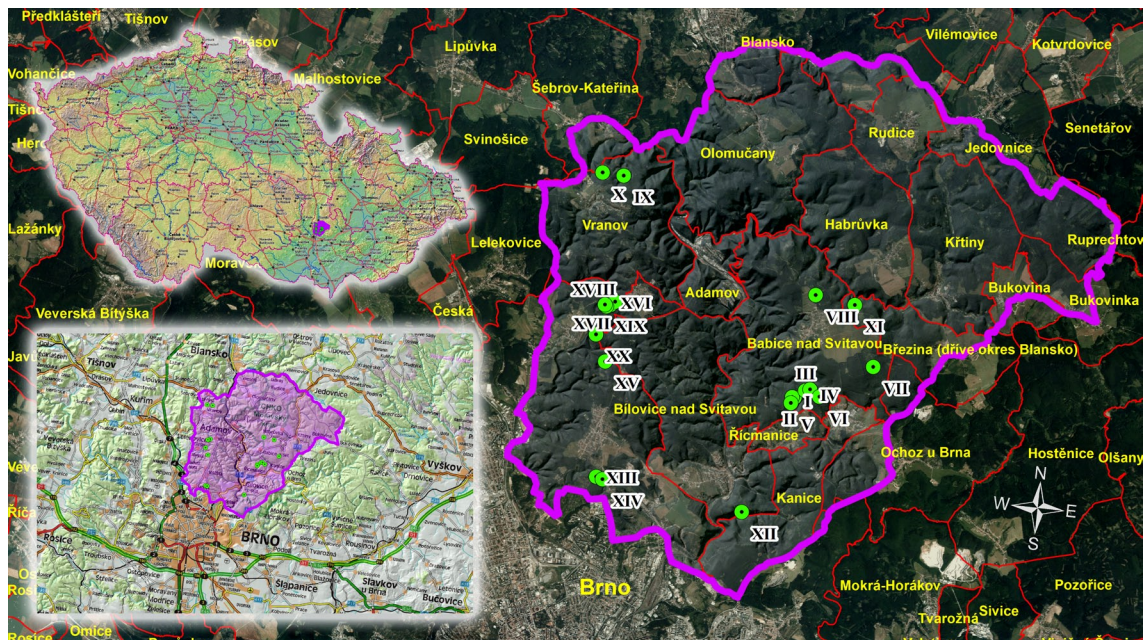


Fig. 14. The localization of the Training Forest Enterprise (purple borderline) in the context of the Czech Republic (top-left corner - topographic map) and the city of Brno (bottom-left corner - road map). The background orthophoto is supplemented with boundaries of individual municipalities (red borderlines and yellow names). The shapes of terrain in the TFE area are accentuated using a shaded relief. The 20 study plots are depicted by the green circles which are numbered with Roman numerals. Source of maps and background layers: WMS servers of CENIA (2015) and ČÚZK (2015).

## 4.2. Specification of Study Plots

Field measurements of relevant tree parameters were performed as an essential part of this work. Besides the health status and species determination of each tree of interest, a height of the tree was measured together with diameter at breast height (DBH). Also the exact positions of all the studied trees were measured using the total station. To embrace a sufficient variability of forest stand properties such as species composition, age of the trees, terrain conditions etc., together 20 different study plots were established to perform the measurements.

The study plots had circular shape and varied in size from minimal required area of 1000 m<sup>2</sup> (diameter 35.68 m) to maximally 3300 m<sup>2</sup> (diameter 64.82 m). The sizes of particular study plots can be seen in Table 2. The minimal required amount of trees in a single plot was 60 as being a double of conventional statistical



minimal sample size. Only trees with DBH larger than 7 cm were taken into account, according to Czech national forest inventorying standards (UHUL, 2003). If the basic plot area of 1000 m<sup>2</sup> did not contain the required amount of trees, the size of the plot was enlarged (with the step of 100 m<sup>2</sup>) until the amount of at least 60 trees was reached.

The field measurements were performed between August and October 2014, which is during the leaf-on season. The age of stands was ranging from 31 to 141 years. (The age was ascertained from the Forest Management Plan (FMP) of Masaryk Forest Křtiny. The plan was created in 2012 with the validity from 1.1.2013 to 31.12.2022. Since the age data about the forest stands in the FMP were related to year 2012, two years had to be added to gain the correct age in the year of the measurements). The stand ages can be seen in Table 2.

The localisations of the study plots were selected based on the multiple-criteria decision analysis. The most important variables were the species composition, age of stands, shape and minimal size of stands, slope of the terrain and accessibility. Last but not least, the proximity of an open area suitable for launching and landing of the UAV with good viewing conditions for the pilot had to be taken into the consideration. Based on these criteria a variety of forest stands with required properties was determined. The stands were then visited and some of the unsuitable stands were discarded - usually because of the presence of very dense undergrowth which would make the measurements enormously complicated or even impossible.

In the end 20 study plots were established to perform the measurements and to be photographed by the UAV. These particular plots were situated in the heights between 310 and 500 meters above sea level. By the analysis of a Digital Terrain Model (DTM 5G - see chapter 4.6.3. Auxiliary data) some terrain conditions were ascertained and derived. The average slope ranged between 1,1 and 28,5 degrees and the shapes of terrain varied from almost flat areas to very curved and steep terrain. Since the slope of terrain does not give overall information about the terrain conditions, also the curvature values were calculated for each plot. The rate of terrain curvature was calculated as a range of curvature values, which means as the difference between maximal and minimal values of the second derivatives of the surface. The quantity was reaching values from 0,4 on flat areas to 13,8 on curved areas (dimensionless units). Slope and curvature rate values are visualised in Figure 15. The values calculated for each plot can be seen in Table 2.

Table 2. List of the 20 study plots showing ages of the forest stands, areas of the circular study plots and various terrain characteristics such as average altitude, slope of the terrain or a rate of its curvature.

Plot Number	Age of the Stand (2014)	Area of the Plot (m <sup>2</sup> )	Average Slope (°)	Average Altitude (m.a.s.l.)	Curvature Rate
I.	61	1 000	3.60	361.53	0.38
II.	61	1 000	3.13	365.18	1.26
III.	102	1 300	3.81	376.51	4.29
IV.	102	1 300	2.97	384.31	1.52
V.	70	1 000	4.49	360.01	0.50
VI.	76	1 000	3.68	381.67	0.64
VII.	99	3 300	1.99	487.29	0.41
VIII.	92	1 500	1.09	499.44	1.26
IX.	92	1 500	12.16	443.53	6.82
X.	47	1 000	8.73	453.23	1.37
XI.	125	2 000	25.14	457.92	13.80
XII.	141	1 500	23.34	310.01	7.04
XIII.	90	1 200	4.20	360.56	0.55
XIV.	90	1 200	3.53	361.18	1.91
XV.	100	1 200	6.80	360.95	1.32
XVI.	31	1 000	4.25	441.95	0.47
XVII.	31	1 000	9.10	435.72	0.83
XVIII.	71	1 400	6.81	437.67	1.14
XIX.	36	1 000	4.37	443.05	0.44
XX.	110	1 300	28.48	365.83	7.00

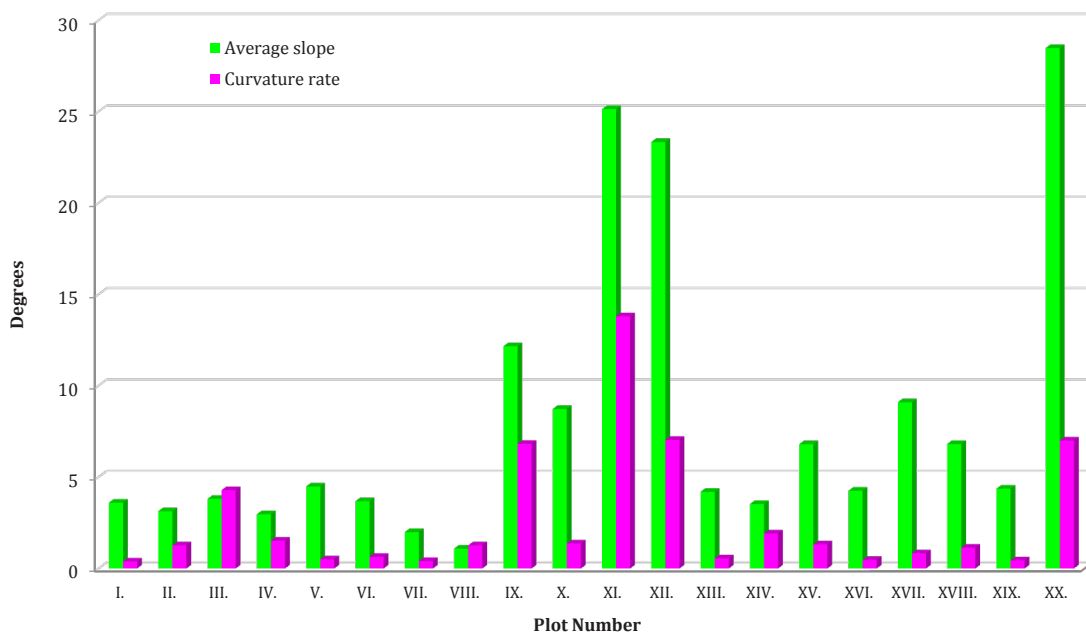


Fig. 15. A diagram showing the average slope of the terrain in degrees together with the rate of terrain curvature (non-dimensional quantity) calculated for each study plot.

## 4.3. Forest Stands Measurements

### 4.3.1. Equipment

Two different total stations and two different high-accuracy GNSS devices were employed for the geodetic measurements in this work. Also one hypsometer was utilized for measuring tree height. Particularly following devices were used:

- Total station TOPCON GTS-105N (Fig. 16.) having specification (TOPCON, 2007):

Distance Measurement:

- Range 1 / 3 / 9 prism: 2000 m / 2700 m / 3400 m
- Accuracy:  $\pm(2 \text{ mm} + 2 \text{ ppm} \times D)$  m.s.e.

Angle Measurement:

- Method: Absolute encoder reading
- Detecting system: H:2 sides V:1 side
- Accuracy: 1.5 mgon (5")

Telescope:

- Length: 150 mm
- Objective Lens Diameter: 45 mm
- Magnification: 30x
- Resolving Power: 3"



*Fig. 16. Total station TOPCON Green Label GTS-105N.*

- Total station TOPCON GPT-9003M (Fig. 17.) with specification (TOPCON, 2008):

Distance Measurement:

- Range 1 / 3 / 9 prism 3000m / 4000m / 5000m
- Accuracy:  $\pm(2 \text{ mm} + 2 \text{ ppm} \times D)$  m.s.e.

Angle Measurement:

- Method: Absolute encoder reading
- Accuracy: 1 mgon (3")

Telescope:

- Magnification: 30x

User Interface:

- OS Microsoft Windows® CE.NET 4.2
- Processor Intel PXA255 400 MHz



*Fig. 17. Motorized total station TOPCON GPT-9003M.*

- GNSS receiver TOPCON HiPer Pro (Fig. 18.) with description (TOPCON, 2004):

- 40 channel, dual frequency, dual-constellation RTK GPS+ tracking
- Tracking Channels (TCH) Standard: 40 L1 GPS (20 GPS L1+L2)
- Optional TCH: 20 GPS L1+L2 (GD), GPS L1 + GLONASS (GG), 20 GPS L1+L2+GLONASS (GGD)
- Performance: Static, Rapid Static:  
H: 3 mm, V: 5 mm + 0.5 ppm  
RTK: H: 10 mm, V: 15 mm + 1 ppm



*Fig. 18. TOPCON HiPer Pro GNSS receiver (left) and TOPCON FC-200 Windows field Bluetooth controller (right).*

Used with controller TOPCON FC-200 with specification (TOPCON, 2006):

- Microprocessor Intel PXA270 XScale, 520 MHz, Memory 256MB SDRAM
- Operating System Windows® CE.NET 5.0, Connectivity: Built-in Bluetooth™
- TopSURV GPS+ Integrated Controller Software

- GNSS receiver / controller TRIMBLE GeoExplorer 6000 Series GeoXH™ Handheld (Fig. 19.) with following specification (Trimble, 2011):

- 220 channel dual frequency receiver with real-time H-Star technology
- GNSS Receiver Trimble Maxwell™ 6
- Systems GPS (L1C/A, L2C, L2E), GLONASS (L1C/A, L1P, L2C/A, L2P)
- GNSS Accuracy (HRMS):  
Real-time H-Star: 10 cm + 1 ppm  
Real-time code corrected VRS or local base 75 cm + 1 ppm
- Processor TI OMAP 3503
- RAM 256 MB, Flash 2 GB
- OS Windows Mobile® 6.5 (Professional edition), Integrated Wi-Fi Bluetooth®
- TerraSync™ Trimble GPS Controller software



*Fig. 19. Trimble GeoXH 6000 GNSS receiver handheld (left) and Trimble Zephyr 2 broad frequency tracking antenna (right).*

Used with Trimble Zephyr 2 antenna having this specification (Trimble, 2008):

- Frequencies: L1/L2/L5/G1/G2/LBand/E1/E2/E5ab/E6; 1176 to 1575 MHz
- Signal Tracking: GPS, Glonass, OmniSTAR, SBAS (EGNOS), Galileo

- Laser rangefinder / hypsometer TruPulse 360B (Fig. 20.) having following specification (Laser Technology, 2004):
  - Professional laser rangefinder which measures horizontal distance (HD), vertical distance (VD), slope distance (SD), height (HT), inclination (INC), missing line (ML) and azimuth (AZ).
  - Optics: 7x magnification, In-scope LCD
  - Field of View: 100 m @ 915 m away
  - Built-in Targeting Modes: Closest, Farthest, Continuous and Reflector
  - Max range to reflective targets: 2000 m; to non-reflective targets: 1000 m
  - Accuracy: Azimuth:  $\pm 1.0^\circ$ ; Inclination:  $\pm 0.25^\circ$  typical; Distance:  $\pm 30$  cm to typical targets,  $\pm 0.3$  to 1 m to very distant, weak targets.



*Fig. 20. Laser rangefinder / hypsometer TruPulse 360B from Laser Technology Inc.*

#### **4.3.2. Measurements of Trees**

The procedure of the field measurements was following. First of all the centre of the circular plot was allocated and stabilized by the wooden stake. The stake was numbered and its position was measured by a metal tapeline in the relation to at least three nearest trees, and documented. Subsequently a total station was used and a polygonal traverse was led from the stake to a nearest open area where another two stakes sufficiently distant from each other could be stabilized and localized by a high-accuracy GNSS device. The position of these stakes was then measured by geodetic GNSS devices TOPCON HiPer Pro (Figure 18.) and TRIMBLE GeoExplorer 6000 (Figure 19.).

As the centre of the new study plot was geodetically localized, the radius of the plot was determined. The minimal radius was set to 17.84 m, which corresponds to the area of 1000 m<sup>2</sup>. In 8 cases this area was sufficient already as it contained 60 or more (up to 110) individual trees; in other cases the area had to be enlarged to reach this amount of trees. After demarcation of the area of interest, all the trees within the circular borderline were given a paper label with an individual number. The trees were numbered in a spiral, from plot centre to the border. Only trees with a DBH over 7 cm were numbered and inconvenient trees with smaller DBH were not taken into the consideration.

When the preparation of the study area was complete, the species of each tree was determined and recorded into a table. In the case the tree was noticeably leaning or curved, it was recorded as well. Also when some damages (e.g. leafless crown top) or abnormalities (such as double trunk) were recognized on the tree, it was written as a comment to the particular field. Examples of several typical abnormalities can be seen in Figure 21. Afterwards the required measurements were performed (Figures 22. - 26.).



*Fig. 21. Most common tree abnormalities such as double trunks or highly leaning trunks.*

First of all the diameter at breast height was measured using a caliper. The diameter was measured always twice in mutually perpendicular positions and the average of both gained values was counted as a final DBH. In several cases, when the diameter of measured tree was larger than the range of the caliper (which was 60 cm) a circumferential tape was used to measure the DBH. The recorded accuracy of the DBH measurements was 1 cm. Since the DBH was measured mainly for the purposes of a parallel study, these data were not fully utilized in this work and were used mainly to decide which trees should be accepted for further measurements based on the minimal DBH.



*Fig. 22. Measurements of the tree parameters shown on two different study plots.*

Besides the DBH, the height of trees as a principal parameter in this work, was measured. All the heights were measured using a TruPulse 360B laser rangefinder / hypsometer device (Fig. 20.). The measuring person was usually standing in the distance of about one tree height far from the trunk or further. The height was measured by the device in three steps. First of all the horizontal distance to the trunk was measured by the laser pulse (Fig. 23.). If the trunk could not be hit by the pulse in the horizontal level, the device calculated the horizontal distance itself based on the actual measured slope distance and the inclination, when measuring in the HD (Horizontal Distance) mode.

In the second step the base of the tree was focused and the bottom angle was measured. If the base was not sufficiently visible from the observation position (e.g. because of the presence of the dense undergrowth), the assisting person could place a sign on the nearest visible point on the ground preserving the distance between the measuring person and the trunk. Then the measuring person could focus on this sign and measure the correct angle in this way.



*Fig. 23. Measurements of tree height (left) and other parameters at various study plots.*

Afterwards the top of the tree was aimed by the device and the upper angle was measured. In the case that the treetop was not visible well (e.g. was partly hidden by other trees), usually a new observation point had to be chosen since there is no accurate way how to measure the proper angle in such case. Sometimes the thinner trees were shaken by the assisting person to make the apex of the tree of interest more evident. When measuring the conifers, the treetop was considered the highest living verticil of the tree. In the case of broadleaved trees the highest living part of the crown was the target of the measurements.

When all the values - horizontal distance, bottom angle and upper angle were measured, TruPulse automatically performed the triangulation and calculated the final height of the tree. The device was measuring with the accuracy of 0.1 m. The

height of each tree was measured at least two times from mutually perpendicular observer points and the gained values were averaged.

When the tree was leaning or there were not very ideal observing conditions, three up to seven measurements were performed from suitable positions to calculate the average. On a steep terrain the observer positions were situated preferably along the contour line on both sides of a tree. In the case of leaning trees, the observer positions were situated on the perpendiculars to the direction of leaning. When enough measurements were performed for each tree, the resulting average values were recorded into a table. The final height values were recorded with rounding to 0.5 m.

The last ascertained property of the trees was their position. The precise location of each single tree was geodetically measured using the total station (Fig. 24., 25.). Two total stations, particularly TOPCON GTS-105N (Fig. 16.) and TOPCON GPT-9003M (Fig. 17.) were utilized for this purpose. The total station was on each study plot positioned into the plot centre just above the central wooden stake (Fig. 24.). The assisting person then put the ranging pole of defined height with attached reflective prism on a proper place beside each tree just next to the trunk centre (i.e. on an imaginary circle intersecting the trunk midpoint and having the center in the total station). The operator then measured the position of the prism.



*Fig. 24. The total station situated above the wooden stake just at the plot centre, ready for measurements of the positions of all the trees being thoroughly examined.*



*Fig. 25. Geodetic measurements of the positions of the trees on different study plots.*





*Fig. 26. Geodetic measurements of the tree trunk centre with a total station using a horizontal offset.*

Since the total station allows to make a horizontal offset, the middle of the trunk was subsequently aimed by the total station and up to now the particular measurement was finished and saved (Fig. 26.). This technique ensured, that the precise position of the trunk centre was measured. In this way all the numbered trees in the study area were localized one by one. When any distant tree was hidden by some nearer tree the ranging pole was put to the closest visible place next to the tree and the trunk middle was localized using a larger horizontal offset. When the tree was obviously leaning, the measuring procedure did not change, but the direction of the leaning was noted.

## 4.4. Data Acquisition Using Unmanned Aerial Vehicle

### 4.4.1. Equipment

All the twenty study plots, in which all the trees were thoroughly manually measured, were also examined by the means of remote sensing. One remotely piloted aircraft system (RPAS) equipped with appropriate digital cameras was deployed for this mission. Particularly system composed of following elements was utilized:

- A professional UAV Hexa-Rotor Platform DJI Spreading Wings S800 (Fig. 27., 28.) having specification (DJI, 2015):

- 6 Rotors and Carbon Fibre Propellers

Carbon Fibre Frame:

- Diagonal Wheelbase: 800 mm
- Total Weight: 2.6 Kg

Flight Parameters:

- Takeoff Weight: 5.0 Kg ~ 7.5 Kg
- Load Weight: 0 Kg ~ 2.5 Kg
- Power Battery: LiPo 16 000 mAh
- Hover Time: Max: 18 min



*Fig. 27. Unmanned Aerial Vehicle (UAV) DJI Spreading Wings S800.*



*Fig. 28. Landing DJI S800.*

#### Components:

- Main flight Controller (MC)
- Inertial Measurement Unit (IMU) containing a 3-axis accelerometer, a 3-axis angular velocity meter and a barometric altimeter.
- GPS module with embedded digital compass
- Power Monitoring Unit (PMU)
- Electronic Speed Controllers (ESC)
- On-Screen Display (OSD) iOSD MK II module with 5.8 GHz Video Link Kit DJI AVL58
- Telemetry module LK24 with 2.4 GHz Bluetooth Data Link

- Microcomputer Radio Remote Control System composed of Graupner MX-20 HoTT Transmitter and Graupner GR-24 HoTT Receiver with following specifications (Fig. 29), (Graupner, 2015):

#### Transmitter:

- 12 channels (4 x trim)
- Modulation: 2,4 GHz FHSS HoTT
- Range: 4000 m
- Operating voltage: 3,4 - 4.8 V
- Charging rate: 210 mA
- Battery: built-in NiMH 2000 mAh

#### Receiver:

- 12 channels
- Modulation: 2,4 GHz FHSS HoTT
- Operating voltage: (2,5) 3,6 - 8,4 V
- Charging rate: 70 mA

Two Graupner transmitters were utilized, one for UAV remote control, another equipped with external display receiving data from the OSD unit.



*Fig. 29. Graupner MX-20 HoTT Transmitter with attached display showing live image and telemetry UAV data.*

- DJI Ground Station PC Software for route planning and waypoint setting (Fig. 30.), (DJI, 2015b):

- Adjustable Properties: Altitude, Latitude, Longitude, Forward Flight Speed, Turn Mode, Head Degree, Hold Time

- Assignments: Camera Shutter, Gimbal Control, Airdrop Control, General Purpose Control

- Flight Instruments: General Speed Indicator, Attitude Indicator, Signal Strength Indicator, GPS Coordinates Indicator, Helicopter Position Tracker, Pitch Position, Throttle Position, Servo Voltage

- Communication:

Hardware Interface: RS-232,

Radio Frequency: 2.4 GHz, Data-

Throughput: Max. 115,200 bps.

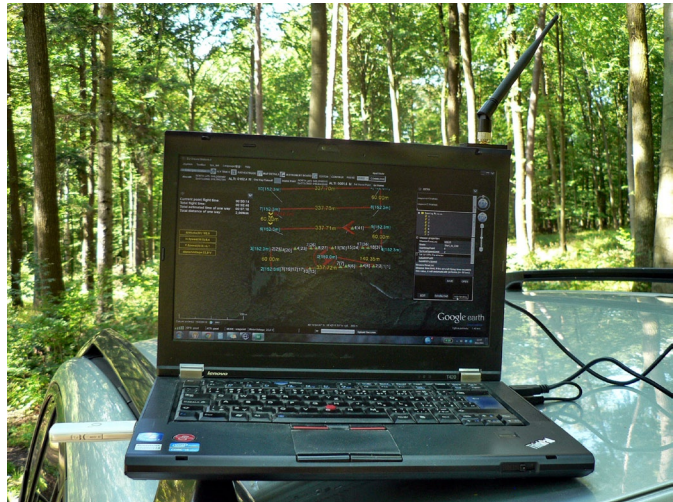
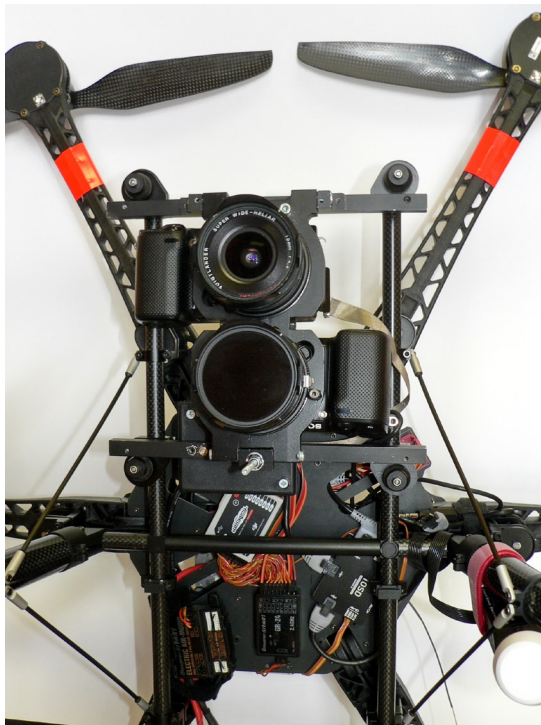


*Fig. 30. The laptop with running DJI Ground Station software during the actual flight operation.*

- Two Sony NEX-5R Cameras mounted on the DJI S800 (Fig. 31.), (Sony, 2015):

- Imaging Sensor: Exmor™ APS-C HD CMOS sensor (23.5 X 15.6 mm)



- Effective Picture Resolution: 16.1 megapixel
- Focal Length Conversion Factor: 1.5x
- Colour Filter System: RGB primary colour filters
- Color Space: sRGB, AdobeRGB
- Still Image Mode: JPEG (Standard, Fine), RAW
- Still Image Size: 4912 x 3264 (3:2, 16M)
- ISO: Auto 100 - 3200, Selectable 100 - 25600
- Shutter Speeds: 1/4000 to 30s (Bulb)
- Battery Type: InfoLITHIUM® NP-FW50 (7.2V)

*Fig. 31. Two Sony NEX-5R cameras with Voigtländer Super Wide Heliar 15 mm lenses mounted on the DJI S800 machine. One camera shooting in NIR, the other in RGB bands.*

- Two Voigtländer Super Wide Heliar Aspherical II 15 mm Lenses (Fig. 31.), (Voigtländer, 2015):
  - Lens Construction: 8 elements in 6 groups
  - Focal Length: 15 mm
  - Aperture Ratio: 1:4,5
  - Minimum Aperture: F 22
  - Minimum Focus: 0,5 m
  - Angle of View: 110°
  - Mount: M-Bayonet
  - Filter Size: 52 mm
- Hoya R72 Near-Infrared Filter (blocking visible light) (Fig. 31., 32.), (Hoya, 2015):
  - Blocking wavelengths below 720 nm
  - Transmits 50 % of light at the wavelength of 750 nm
  - Transmits 90 % of light from 800 nm up to longer wavelengths
  - Filer diameter: 52 mm

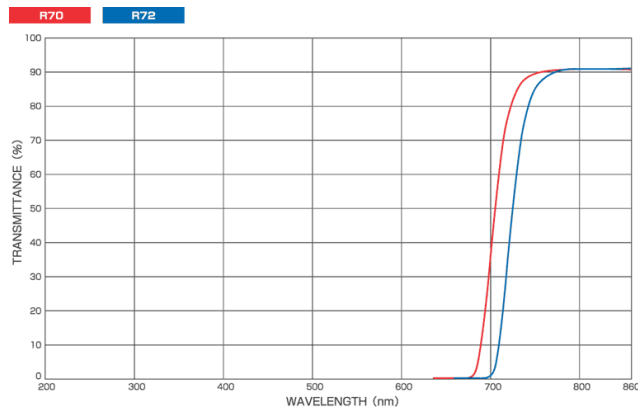


Fig. 32. Transmission curve of R72 filter (blue line).

- Two SanDisk 32GB Extreme PRO SDHC UHS-II Memory Cards (SanDisk, 2015):
  - Storage Capacity: 32GB
  - Type: UHS-II Class U3
  - Max. Write Speed: 250 MB/s
  - Max. Read Speed: 280 MB/s

As two digital cameras were utilized during the flights, each of them was capturing different part of the electromagnetic radiation. One camera had the Hot-Mirror (a built-in filter blocking near-infrared (NIR) light generally used in digital cameras) manually removed, so that also NIR light could be captured by the CMOS sensor in required amount. The lens of that camera was at the same time equipped with the NIR filter Hoya R72 which was efficiently blocking all the electromagnetic radiation with the wavelengths shorter than 720 nm (which is all the visible light and the UV radiance, see Fig. 32.). As a result mainly near-infrared light was captured by that particular camera.

The second camera was not adjusted anyhow, so it was recording images in standard RGB colours. Both cameras were put together by their bottoms, so that their lenses were in one axis and as close to each other as possible. This construction caused, that one camera was capturing mirror images compared to the ones from the other camera. Both cameras were mounted into a special light duralumin frame and connected to the frame of the UAV (Fig. 31.).

#### 4.4.2. Image Data Acquisition using UAV

Together 12 UAV flights were carried out to gain the required remote sensing data of the 20 study plots (some of the study plots were close to each other and could be overflown during single flight). The UAV flights were performed between August and October 2014. When the locality was reached with all the equipment, several operations had to be done before starting the flight itself. First of all the Ground Control Point (GCP) markers had to be positioned on selected places in or around the study plot. Metal plates with the size of 35 x 35 cm painted white with a black cross in the middle were used as the markers (Fig. 33.).



*Fig. 33. Operator setting the GNSS receiver TRIMBLE GeoExplorer 6000 for iterative measuring of the accurate position of a GCP marker (left) and the same device positioned above a marker situated on a very steep terrain (right).*

The sites suitable for placing the GCP markers had to be in a sufficiently open space (not covered by shrubbery or tree crowns) to be visible from above by the UAV cameras. The site also had to offer a good-quality GNSS signal to locate the GCP markers with required accuracy. Usually 5 to 7 GCP markers were positioned on such places on the ground around the forest stands containing the study plots, before each flight. The precise position of each marker was then measured using the GNSS devices TOPCON HiPer Pro (chapter 4.3.1., Fig. 18.) or TRIMBLE GeoExplorer 6000 (chapter 4.3.1., Fig. 19. and 33.).

When the accurate coordinates of the GCP markers were measured, the flight itself was approached. Each flight was planned in the DJI Ground Station software before anything else. All the essential properties of the flight, such as waypoints position, altitude, flight speed, cameras shutter frequency etc. were set before the flight. All those data and instructions were then transmitted into the UAV using Bluetooth Data Link.

Then also the cameras mounted on the machine were prepared. If needed, settings such as the shutter speed or aperture ratio, were adjusted according to the current weather and light conditions (different settings were used during sunny weather and different during the overcast). All the automatic software image enhancement techniques in the cameras such as the noise reduction, vignetting control or chromatic aberration corrections were turned off during all flights.

To make the UAV ready to fly, the battery pack was connected to the machine and carefully positioned to make the device fully balanced out. The machine was then placed on a suitable flat open plane. The pilot then manually took off and then handed the control over to the Ground Station software, so that the machine fluently reached the required altitude level and the position of the first waypoint (Fig. 34.).



*Fig. 34. The pilot and the DJI S800 just before the takeoff (left) and the machine on another site rising above the forest stand, heading to the given position when starting a new mission (right).*

The average altitude kept during the flights was usually between 100 and 150 meters above ground. After reaching the given coordinates, the UAV could begin the image shooting mission and started to visit one waypoint after another. The average flight speed was usually kept around 10 m/s. The UAV was usually flying fully automatically in this part of the flight. Nevertheless the pilot was keeping continuous eye-contact with it and had always full control over the machine. Therefore, if any unexpected circumstances would appear, he could intervene into the flight any time, and for instance abort the mission and land manually using radio remote controller Graupner MX-20.

To receive the telemetry data and for live transmission of image data from the RGB camera onboard the UAV a separate LCD screen mounted on another Graupner remote controller was utilized (Fig. 29.). The data from the OSD unit (On-Screen Display unit) were transmitted using the LK24 Bluetooth Data Link. This enabled the pilot to see continuously the places which is the machine flying above and the particular scenes which are the cameras shooting.

During the flight, both cameras were automatically capturing orthogonal images of the forests below. The average shooting rate was usually 1 image per second (taken parallelly in both cameras). To serve as a good source of images for the further photogrammetric processing, it was essential to guarantee sufficient overlapping of neighbouring images. The route was therefore usually planned to ensure approximately 80 % to 90 % overlapping between following photos in each line (forward overlap) and approximately 70 % to 80 % overlapping between adjacent flight lines (lateral overlap). The average amount of flight lines was ranging between 4 and 8 and the size of the horizontal rectangle drawn by the UAV during one mission was usually varying between 100–200 m by 200–300 m. The average amount of images taken by each camera during single missions was then ranging between 60 and 260.

The duration of average flight was between 7 and 15 minutes. When the machine went through the whole planned path and visited all the waypoints, it automatically flew back to the first waypoint position (Fig. 35.). Then the pilot usually took over the full control over the machine and landed manually. Afterwards the GCP markers could be collected. In this way the flight mission was completed.



*Fig. 35. The pilot (person on the right) and the assistant watching the UAV during the flight mission. A GNSS device measuring the position of a GCP marker can be seen on the left.*

## **4.5. Hardware and Software**

### **4.5.1. Hardware**

One desktop PC and one notebook PC were utilized within this work. One of the machines was used for processing of the image data from the UAV, one for programming and performing the full operation of the UAV Forest Explorer.

#### **4.5.1.1. Desktop PC**

For the photogrammetric processing of the UAV data in the AgiSoft Photoscan software a desktop PC with following specification was utilized:

- Processor Intel ® Core™ i7-4770 CPU @ 3.40 GHz (4 cores, 8 logical processors), 8 MB Intel Smart Cache
- RAM 32 GB, DIMM, 1333 MHz
- HDD1: 250 GB, HDD2: 1 TB
- 64bit operation system
- Windows 8.1 Pro
- NVIDIA GeForce GT 640 (2 Cores @ 941 MHz, 2048 MB) Graphic Card
- Two 24" HP Compaq LA2405x LCD screens

#### **4.5.1.2. Notebook PC**

For the purposes of running the UAV Forest Explorer tool within the ArcGIS Desktop 10 software a notebook PC with following specification was used:

- HP ProBook 4530s Notebook
- Processor Intel ® Core™ i5-2450M CPU @ 2.50 GHz (2 cores, 4 logical processors), 3 MB Intel Smart Cache
- RAM 8 GB, DDR3
- HDD: 750 GB
- 64bit operation system
- Windows 7 Home Premium
- AMD Radeon HD 7470M (1 Core @ 750 MHz, 1024 MB) Graphic Card
- One built-in 15,6" LCD screen and one external 24" LG 24MP55 IPS screen



## **4.5.2. Software**

The three main software products, which were for different purposes utilized in this work, are briefly described in this chapter.

### **4.5.2.1. Agisoft PhotoScan® Professional Edition**

The software Agisoft PhotoScan Professional Edition (Fig. 36.), version 1.0.4. build 1847 (64bit) was employed in this work for the photogrammetric processing of the images from the UAV. The software is developed by Agisoft LLC located in St. Petersburg in Russia.

As states the Agisoft PhotoScan User Manual (2014), Agisoft PhotoScan is an advanced image-based 3D modelling solution aimed at creating professional quality 3D content from still images. Based on the latest multi-view 3D reconstruction technology, it operates with arbitrary images and is efficient in both controlled and uncontrolled conditions. Photos can be taken from any position, providing that the object to be reconstructed is visible on at least two photos. Both image alignment and 3D model reconstruction are fully automated. Generally the final goal of photographs processing with PhotoScan is to build a textured 3D model. The procedure of photographs processing and 3D model construction comprises four main stages:

1. The first stage is camera alignment. At this stage PhotoScan searches for common points on photographs and matches them, as well as it finds the position of the camera for each picture and refines camera calibration parameters. As a result a sparse point cloud and a set of camera positions are formed. The sparse point cloud represents the results of photo alignment and will not be directly used in the further 3D model construction procedure. On the contrary, the set of camera positions is required for further 3D model construction by PhotoScan.

2. The next stage is building dense point cloud. Based on the estimated camera positions and pictures themselves a dense point cloud is built by PhotoScan. Dense point cloud may be edited and classified prior to export or proceeding to 3D mesh model generation.

3. Another stage is building a mesh. PhotoScan reconstructs a 3D polygonal mesh representing the object surface based on the dense point cloud. Additionally there is a Point Cloud based method for fast geometry generation based on the sparse point cloud alone. Generally there are two algorithmic methods available in PhotoScan that can be applied to 3D mesh generation: Height Field - for planar type of surfaces and Arbitrary - for any kind of objects.

Having built the mesh, it may be necessary to edit it. Some corrections, such as mesh decimation, removal of detached components, closing of holes in the mesh, etc. can be performed by PhotoScan. For more complex editing user can engage external 3D editor tools. PhotoScan allows to export mesh, edit it by another software and import it back.

4. After geometry (i.e. mesh) is reconstructed, it can be textured and / or used for orthophoto generation. Several texturing modes are available in PhotoScan, such as Generic, Adaptive Orthophoto, Orthophoto or Spherical.

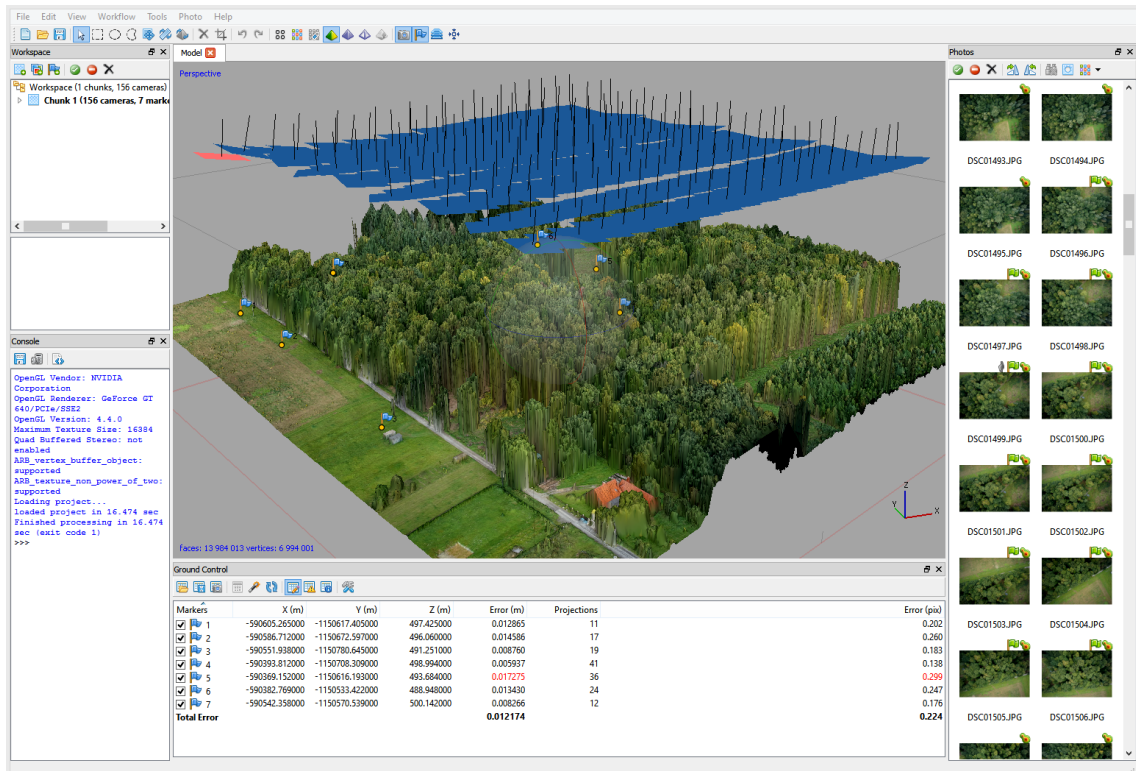


Fig. 36. The graphical user interface of the Agisoft PhotoScan Professional Edition software. The individual modifiable windows represent following content: Model, Workspace, Console, Ground Control and Photos.

#### 4.5.2.2. ArcGIS® for Desktop Advanced

ArcGIS® for Desktop Advanced software in the version 10.2.2. was used for running the UAV Forest Explorer tool in this work (Fig. 37.). ArcGIS is a collection of software products developed by Environmental Systems Research Institute (Esri®) having its headquarters in Redlands, California, United States. The software suite includes desktop, server, mobile, hosted, and online GIS products. The desktop GIS products allow users to integrate and edit data, create new map layers, and author maps. ArcGIS for Desktop includes a series of scalable products (Hillier A., 2011).

As stated by Esri (2016) ArcGIS for Desktop is available at different product levels, with increasing functionality. Besides the ArcReader which is freeware, the core products are following:

- ArcGIS for Desktop Basic, formerly known as ArcView, is the entry level of ArcGIS licensing offered. With ArcGIS for Desktop Basic, one is able to view and edit GIS data held in flat files, or view data stored in a relational database management system by accessing it through ArcSDE.

- ArcGIS for Desktop Standard, formerly known as ArcEditor, is the midlevel software suite designed for advanced editing of spatial data published in the proprietary Esri format. It provides tools for the creation of map and spatial data used in GIS, including the ability of editing geodatabase files and data, multiuser geodatabase editing, versioning, raster data editing and vectorization, advanced vector data editing, managing coverages, coordinate geometry, and editing geometric networks. ArcGIS for Desktop Standard is not intended for advanced spatial analysis.

- ArcGIS for Desktop Advanced, formerly known as ArcInfo, is the highest level of licensing (and therefore functionality) in the ArcGIS Desktop product line. It allows users the most flexibility and control in all aspects of data building, modelling, analysis, and map display. ArcGIS for Desktop Advanced includes increased capability in the areas of spatial analysis, geoprocessing, data management, and others. ArcGIS for Desktop Advanced was utilized in this work.

According to Esri (2016) and Introduction to GIS Using ArcGIS Desktop 10 (2012) ArcGIS Desktop is comprised of a set of integrated applications, which are accessible either from the Start menu of a computer (ArcMap and ArcCatalog) or from the software itself (ArcToolbox):

- ArcMap is the main mapping application which allows user to create maps, query attributes, analyze spatial relationships, and layout final projects.
- ArcCatalog organizes spatial data contained on a computer and various other locations and allows to search, preview, and add data to ArcMap as well as manage metadata and set up address locator services.
- ArcToolbox is the third application of ArcGIS Desktop. It is easily accessed and used within ArcMap and ArcCatalog. ArcToolbox contains series of tools for geoprocessing, data conversion, coordinate systems, projections, and many more.

ArcGIS enables also to create custom tools with Python. As states the ArcMap Help (2016), geoprocessing system tools (those installed with ArcGIS) are designed to perform one small but essential operation on geographic data. Using ModelBuilder or Python, user executes these geoprocessing tools in a sequence, feeding the output of one tool to the input of another. The script may be an essential part of user's workflow – a task user needs to repeat again and again.

Scripts that user creates can be executed either outside or within ArcGIS. Outside ArcGIS means that the script is executed from the operating system command prompt, or within a development application, such as PythonWin. Scripts executed in this manner are referred to as stand-alone scripts. Within ArcGIS means user accesses a script through a tool inside a toolbox. Such tool is like any other tool – it can be opened and executed from the tool dialog box, used in models and the Python window, and called from other scripts and script tools.

Concerning Python, it is a free, cross-platform, open-source, general-purpose programming language used also as a scripting language in ArcGIS geoprocessing. Geoprocessing functionality is accessible through Python using ArcGIS software's ArcPy site-package. ArcPy provides access to geoprocessing tools as well as additional functions, classes, and modules that allow user to create simple or complex workflows effectively.

The additional power of using ArcPy within Python is the fact that Python is a general-purpose programming language that is relatively easy to learn and use. It is interpreted and dynamically typed, which provides user with the ability to quickly prototype and test scripts in an interactive environment while still being powerful enough to support the writing of large applications.

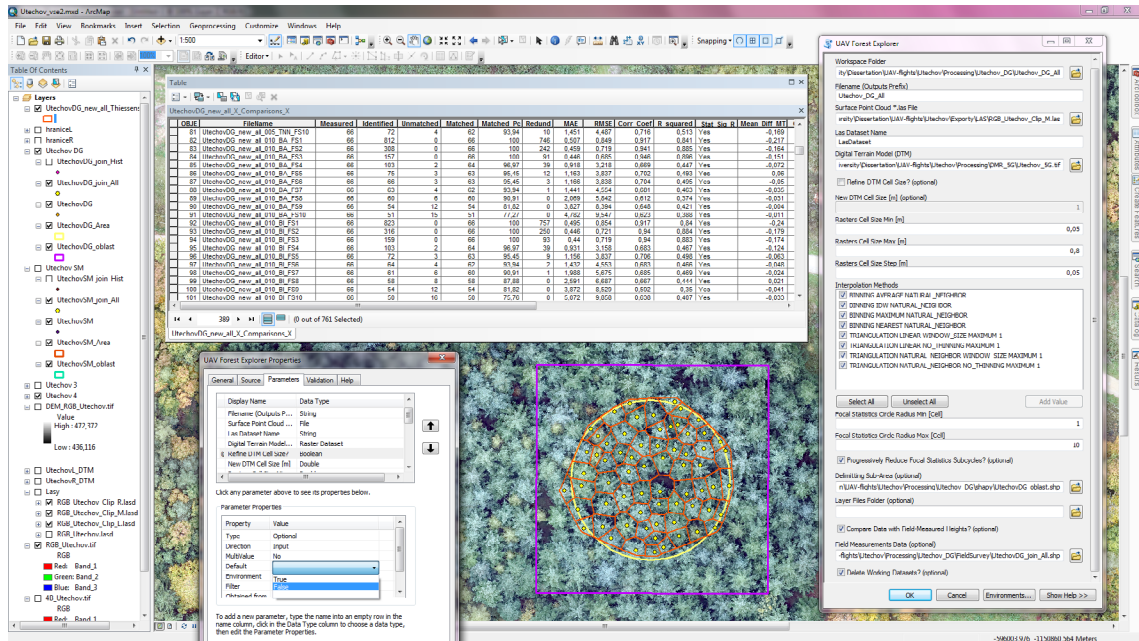


Fig. 37. Example of the work with ArcGIS software, particularly in the environment of ArcMap. Several dialog boxes, including the one of the UAV Forest Explorer (right), the one for setting its Properties (bottom mid-left) or a table containing summary of the tool's results (upper mid-left) (all to be described later) can be seen at this screenshot.

Broadly speaking, ArcPy is organized in tools, environments, functions, classes, and modules. These can be described as follows:

- **Tools** – A geoprocessing tool has a fixed set of parameters that provide the tool with the information it needs for execution. Tools usually have input parameters that define the dataset or datasets that are typically used to generate new output data. Parameters have several important properties: Each parameter expects a specific data types, such as feature class, integer, string, or raster. A parameter expects either an input or output value and either requires a value or is optional. Each tool parameter has a unique name. When a tool is used in Python, its parameter values must be correctly set so it can execute when the script is run. Once a valid set of parameter values is provided, the tool is ready to be executed. Parameters are specified as either strings or objects.

When a geoprocessing tool is executed, the results of the tool are returned in a Result object. Typically, this object is the path to the output dataset produced or updated by the tool. In other cases, it may contain other value types, such as a number or Boolean. If an output for a tool is a multivalued parameter, the values can be returned as a list within a list.

- **Environments** – Geoprocessing environment settings can be thought of as additional parameters that affect a tool's results. They differ from normal tool parameters in that they are set separately from the tool and are interrogated and used by tools when they are run. Environment settings, such as an area of interest, the coordinate system of the output dataset, and the cell size of a new raster dataset, can all be specified and honoured by the tools. Environment settings are available from the *env* class as properties, which can be used to retrieve the current environment values and set them.

- **Functions** – A function is a defined bit of functionality that does a specific task and can be incorporated into a larger program. In addition to tools, ArcPy exposes a number of functions to better support geoprocessing workflows. Functions can be used to list certain datasets, retrieve a dataset's properties, check for existence of data, validate a table name before adding it to a geodatabase, or perform many other useful scripting tasks.

- **Classes** – ArcPy classes, such as the SpatialReference and Extent classes, are often used as shortcuts to complete geoprocessing tool parameters that would otherwise have a more complicated string equivalent. A class is analogous to an architectural blueprint. The blueprint provides the framework for how to create something. Classes can be used to create objects; this is often referred to as an instance.

- **Modules** – ArcPy includes modules covering other areas of ArcGIS. ArcPy is supported by a series of modules, including a data access module (*arcpy.da*), a mapping module (*arcpy.mapping*), an ArcGIS Spatial Analyst extension module (*arcpy.sa*), and an ArcGIS Network Analyst extension module (*arcpy.na*).

For example, the tools of the `arcpy.sa` module use tools in the Spatial Analyst toolbox but are configured to support Map Algebra. Thus, executing for instance `arcpy.sa.Slope` is the same as executing the Slope tool from the Spatial Analyst toolbox.

### 4.5.2.3. PythonWin

PythonWin software was utilized for creating the source script of the UAV Forest Explorer tool (Fig. 38.). PythonWin is the integrated development environment (IDE) and graphical user interface (GUI) framework for Python that is part of the Python for Windows extensions. It provides a simple graphical interface for writing, editing and running Python programs on computers running the Microsoft Windows operating systems. It has an integrated debugger, and a rich Python editing environment. The Copyright to PythonWin belongs to Mark Hammond.

The program uses IDLE (Integrated Development and Learning Environment) extensions by Guido van Rossum (the author of Python programming language) which is bundled with the default implementation of the language. The PythonWin 2.7.5 as `pywin32` build 218 version was used in this work.

```

PythonWin - [UAV_Forest_Explorer.py]
PythonWin 2.7.5 (default, May 15 2013, 22:43:36) [MSC v.1500 32 bit (Intel)] on win32
Portions Copyright 1994-2008 Mark Hammond - see 'Help/About PythonWin' for further copyright information.

1019 -         for rs in rsts:
1020 -             arcpy.Delete_management(rs)
1021 -             arcpy.AddMessage("\nWorking rasters from IM cycle " + str(IMcycleSubtotal) + " were deleted.")
1022 -
1023 -
1024 -         else:
1025 -             arcpy.AddMessage("\nWorking datasets were not deleted.")
1026 -
1027 -         # - - - Updates counters before the completion of the IM cycle:
1028 -         IMcycleResidue = IMcycleTotal - IMcycleSubtotal
1029 -
1030 -         arcpy.AddMessage("\n\nIM cycle " + str(IMcycleSubtotal) + " completed! Remaining IM cycles: " + str(IMcycleResidue))
1031 -         arcpy.AddMessage("\n-----")
1032 -
1033 -         IMcycleSubtotal = IMcycleSubtotal + 1
1034 -
1035 -         # - - - End of IM cycle.
1036 -
1037 -         # - - - Updates counters before the completion of the CS cycle:
1038 -         CScycleResidue = CScycleTotal - CScycleSubtotal
1039 -
1040 -         arcpy.AddMessage("\n\nCS cycle " + str(CScycleSubtotal) + " completed! Remaining CS cycles: " + str(CScycleResidue))
1041 -         arcpy.AddMessage("\n*****")
1042 -
1043 -         outCellSize = outCellSize + outCellSizeStep
1044 -
1045 -         CScycleSubtotal = CScycleSubtotal + 1
1046 -
1047 -         # - - - Progressively reduces number of FS subcycles, if required:
1048 -         if str(checkBoxRFS) == 'true':
1049 -             if CScycleResidue < FScycles:
1050 -                 FScircleRadiusMax = FScircleRadiusMax - 1
1051 -                 FScycles = FScycles - 1
1052 -                 arcpy.AddMessage("\n\nNumber of FS subcycles was reduced by 1 to actual value of " + str(FScycles) + ".")

```

Fig. 38. The graphical user interface of PythonWin IDE containing the source script of the UAV Forest Explorer tool.

## 4.6. Image Data Processing

The hundreds of images of the explored forest stands acquired during the twelve flight campaigns were gradually processed using different computer-aided techniques. The main employed processes are described in this chapter.

### 4.6.1. Automated Image Registration

Airborne images from the UAV were processed in several steps. Generally images from both cameras were registered before further photogrammetric processing. Based on the construction of the cameras holder, when the two cameras were mounted adjacent to each other by their bottoms, the images from one camera were mirror images in relation to the images from the other camera. Therefore all the images from one camera had to be rotated by the angle of 180° first. This was done using the “Rotate” tool in ArcGIS.

Afterwards all pairs of corresponding images could be registered. For this purpose the “Register Raster” tool in ArcGIS was utilized with the Transformation Type “ADJUST”. This transformation type proved to provide most satisfactory results, since it optimizes for both global and local accuracy. It is accomplished by first performing a polynomial transformation, then adjusting the control points locally, to better match the target control points, using a triangulated irregular network (TIN) interpolation technique (ArcGIS 10.2.2. Tool Help).

Because in some cases the edges of registered images could be partially distorted a Processing Extent was defined to clip the scene and get rid of the unwanted borders. To compile the registered raster with the reference raster into one single raster the tool “Composite Bands” was utilized. As the inputs were inserted the first band of the image captured in the Near-Infrared light together with all three bands of the image captured in the visible light (red, green, blue). The output was then saved as the 4-band TIFF image. An illustration showing the process can be seen in Figure 39.

To make the procedure highly efficient, an original python script containing all the described functions was created to process the data continuously and fully automatically. The script including description of all its parts can be found in Appendix 1. This procedure would not be needed in cases when only RGB or only



NIR images would be sufficient. Since it required relatively little effort and the results could be subsequently used to support some visual assessment procedures of the forest stands, the combination of visible and Near-Infrared light into one multispectral image was carried out using images from all investigated areas.

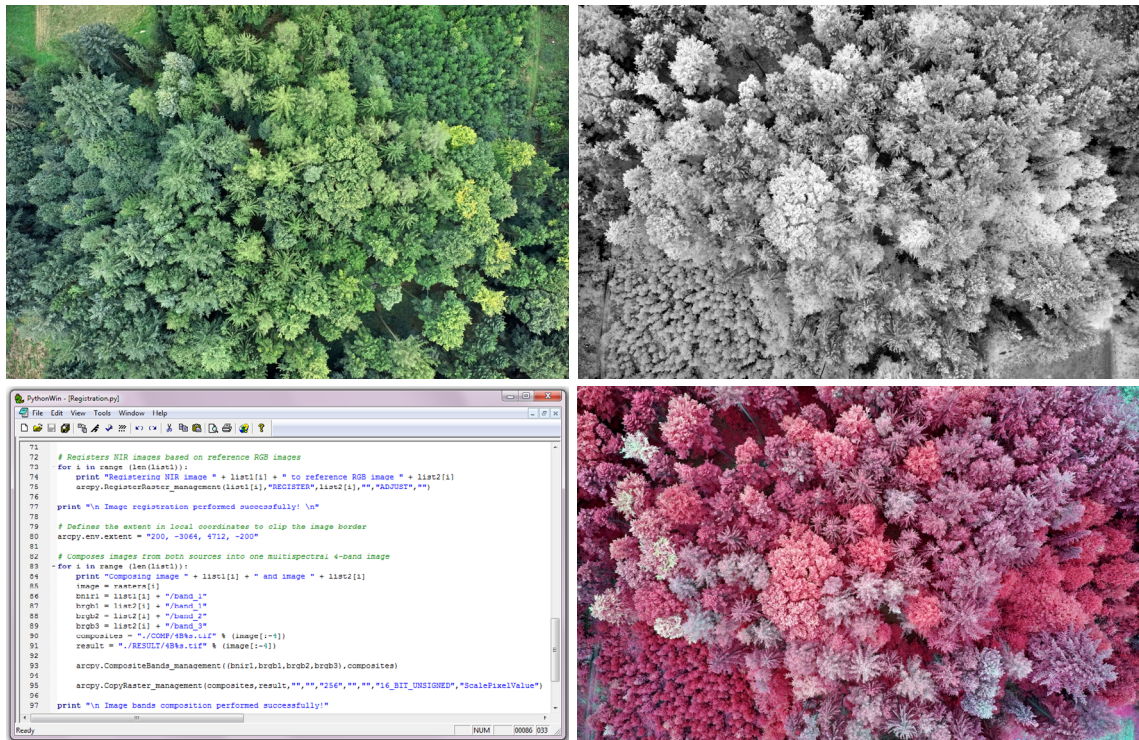


*Fig. 39. Example of automated image registration procedure. Inputs are images from both cameras mounted on the UAV: RGB image (top left) and NIR image (top right). After processing by the python script (bottom left) are the images rotated, registered, clipped and composited into a 4-band multispectral image (displayed as spectrozonal image - bottom right).*

#### 4.6.2. Photogrammetric Image Processing

The multispectral images as results of the automated image registration were prepared for further processing. For this purpose a specialized photogrammetric software Agisoft PhotoScan Professional Edition version 1.0.4. build 1847 (64bit) was utilized (see 4.5.2. Software chapter). The data from each of the 12 flights were processed separately. The workflow of image processing in the Agisoft PhotoScan software was following:

First of all the multispectral images were imported to Agisoft PhotoScan (Fig. 40.). In the Camera Calibration settings the appropriate lens focal length in millimetres was stated and the images were aligned by the “Align Photos” tool.

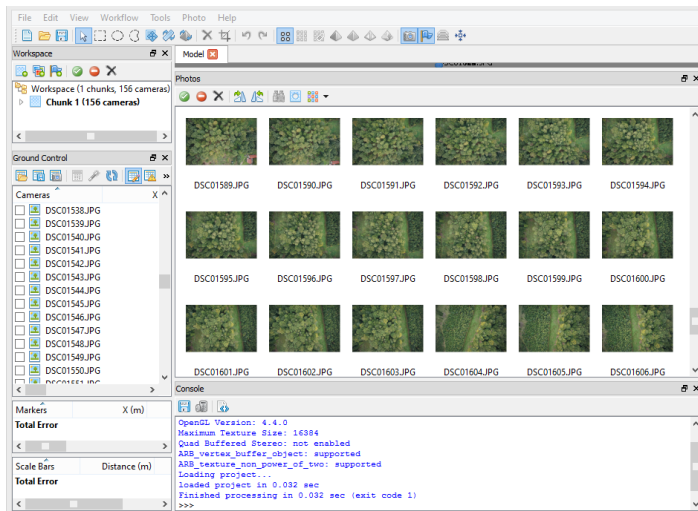


Fig. 40. Registered multispectral images (displayed in RGB) imported into Agisoft PhotoScan software.

During the photo alignment process PhotoScan found the camera position and orientation for each photo and built a sparse point cloud model. The alignment process was each time performed using *High* (i.e. maximal) Accuracy and *Generic Pair* preselection settings with the Point limit of default 40 000 feature points.

According to Agisoft PhotoScan User Manual (2014) at High accuracy setting the software works with original photos as they are without any image reduction. That helps to obtain more accurate camera position estimates. Concerning the Pair preselection a significant portion of the time period needed for the alignment process of large photo sets is spent on matching of detected features across the photos. Image pair preselection option may speed up this process due to selection of a subset of image pairs to be matched. In the Generic preselection mode the overlapping pairs of photos are selected by matching photos using lower accuracy settings first. The Point limit number indicates upper limit of feature points on every image to be taken into account during current processing stage.

When all the images were aligned and the sparse point cloud was created (Fig. 41.), this point cloud was visually assessed. The amount of points in the sparse cloud was usually several hundreds of thousands (specifically between 100 000 and 700 000 based on the flight area and image count). When any error points laying obviously out of the main point cloud were discovered, those points were manually selected and deleted (usually only few up to few tens of points).



Fig. 41. Sparse point cloud as a result of image alignment in Agisoft PhotoScan.

To improve the accuracy of the sparse point cloud the procedure of filtering points based on a specific criterion was performed. The “Gradual Selection” tool using the “Reprojection Error” was utilized for this purpose. As states the Agisoft PhotoScan User Manual (2014) it may be useful to find out where the points with high reprojection error are located within the sparse cloud, or remove points representing high amount of noise. Point cloud filtering helps to select such points, which usually are supposed to be removed. High reprojection error usually indicates poor localization accuracy of the corresponding point projections at the point matching step. It is also typical for false matches. Removing such points can improve accuracy of the subsequent optimization step.

The maximal value of Reprojection error was checked and usually few hundreds of points with highest values were selected (being usually about 0,1 % of total point amount in the sparse point cloud). Those points were then deleted. The overall reprojection error of the sparse point cloud was decreased in this way.

At this point a \*.CSV file containing geodetically measured positions of Ground Control Points (GCPs) was imported into PhotoScan. The precise localization of each GCP marker had to be done manually. All single images where any GCP marker was caught by the cameras were opened and zoomed enough to display the centre of the GCP marker. If this centre could be localized (no branches etc. were hiding it) a flag belonging to appropriate GCP from a text file was positioned there (Fig. 42.). In this way all the flags representing individual GCPs were placed to their proper positions on the images. In this way the point cloud dataset was georeferenced.

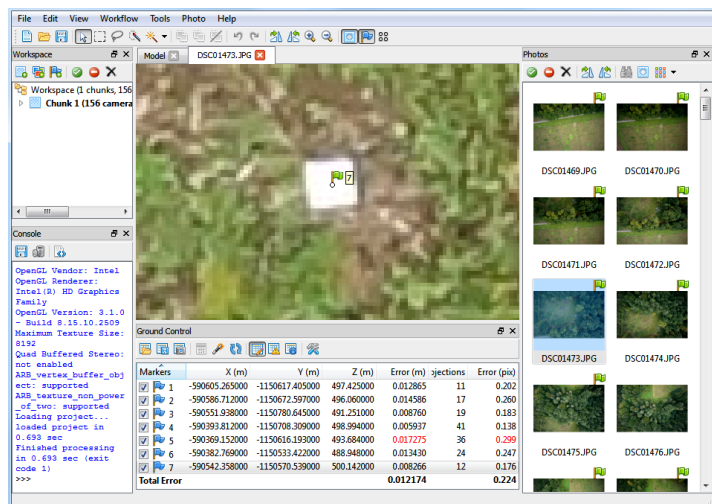


Fig. 42. Placing a Marker in the centre of a Ground Control Point located on a selected photograph.

After georeferencing, an Optimization step could be approached. To achieve higher accuracy in calculating camera external and internal parameters and to correct possible distortion (e.g. “bowl effect” etc.) optimization procedure should be run. This step is especially recommended if the ground control point coordinates are known almost precisely - within several centimetres accuracy

(marker based optimization procedure) (Agisoft PhotoScan Tutorial, 2014). During georeferencing the model is linearly transformed using 7 parameter similarity transformation (3 parameters for translation, 3 for rotation and 1 for scaling). Such transformation can compensate only a linear model misalignment. Possible non-linear deformations of the model can be removed by optimizing the estimated point cloud and camera parameters based on the known reference coordinates. During this optimization PhotoScan adjusts estimated point coordinates and camera parameters minimizing the sum of reprojection error and reference coordinate misalignment error (Agisoft PhotoScan User Manual, 2014).

After the accuracy improvement accomplished by the “Optimize” tool the sparse point cloud was almost prepared for dense point cloud construction. To define the region containing points of the sparse point cloud which should be used in the further processing and to crop the needless border points, a Bounding Box had to be modified. The size of the Bounding Box was adjusted manually. The position was fitted accurately parallel to coordinate system axes by running a python script (PS104\_bounding\_box\_to\_coordinate\_system.py provided by the Agisoft Team). This ensured the right positioning of the ground plane and orthogonal correctness of the consequent mesh.



*Fig. 43. A high quality surface representation in the form of the Dense point cloud in Agisoft PhotoScan.*

To create a dense point cloud (Fig. 43., Fig. 46.) a “Build Dense Cloud” tool was utilized. The two reconstruction parameters were set to *High Quality* and *Moderate Depth* filtering. The *High Quality* level as the second highest option after *Ultra High Quality* was preferred for giving satisfactory point density

in several times shorter computational time compared to *Ultra High Quality* level (hours instead of days). The *Moderate* depth filtering mode was preferred as the middle option between *Mild* mode - conserving numerous small details on the foreground even though they can be outliers and *Aggressive* mode sorting out most of the outliers and smaller details. The amount of points in dense point clouds ranged between 20 000 000 and 110 000 000 in the cases of various flights.

After the dense point cloud was created a polygonal Mesh Model (Fig. 44., Fig. 45., Fig. 46.) could be generated based on the dense cloud data. The Mesh was created using the “Build Mesh” tool with parameters set to *Height field* Surface type, *Dense Cloud* as Data Source, *High* (i.e. maximal) Polygon count and *Enabled*



*Fig. 44. A polygonal Mesh Model with a texture obtained from RGB bands of the registered images.*

*Interpolation*. The Height field surface type was always preferred to Arbitrary surface type for its lower memory requirements as well as better results in canopy surface modelling. Whereas Arbitrary surface type is suitable for modelling of



*Fig. 45. Mesh model - a 3D polygonal mesh with texture representing the object surface based on the dense point cloud. Generated and displayed in Agisoft PhotoScan software.*

closed objects such as statues, Height field type should be selected for aerial photography processing (Agisoft PhotoScan User Manual, 2014). It builds “walls” connecting the edges of higher objects (canopy) with the ground in the way orthogonal to the ground plane defined by the position of the Bounding Box. The amount of vertices of Mesh models ranged from 1 500 000 to almost 10 000 000, the amount of faces in the model then ranged between 3 000 000 to 19 500 000.

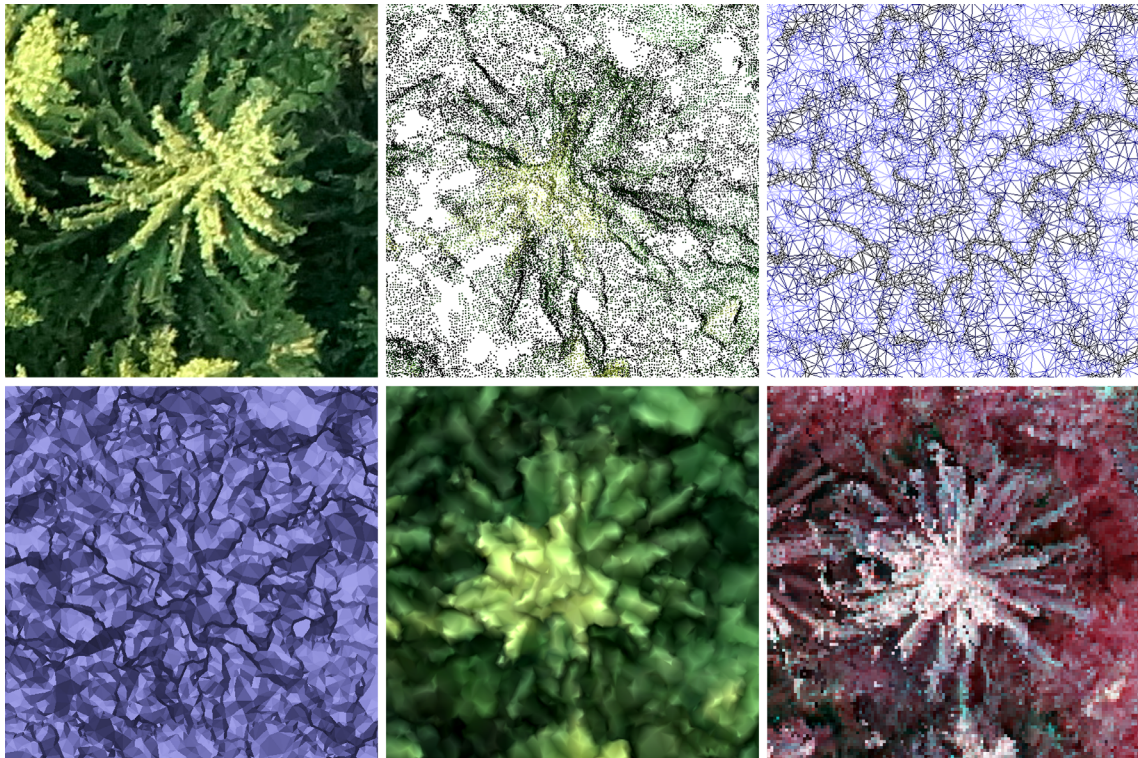


*Fig. 46. Data processing shown on a particular conifer tree example: 1) Conifer captured by an RGB camera mounted on an UAV (top-left). 2) The same tree after automated image registration and photogrammetric image processing shown in the form of a Dense point cloud (top-middle); 3) a Mesh model displayed as a wireframe (top-right); 4) a shaded TIN model (bottom-left); 5) a shaded mesh model with a texture (bottom-middle); 6) and a true orthophoto exported as a 4-band multispectral image (shown as a false colour image) (bottom-right). Representations 2) to 6) were created in Agisoft PhotoScan software.*

The described workflow was performed for each of the twelve datasets. When both the Dense Point Cloud and the Mesh Model were created in each case, the desired processing results could be exported from PhotoScan. Figure 46. depicts some of the parts of the workflow, including the input image, several intermediate data as well as one of the outputs. Together three different kinds of outputs were exported. One was a true orthophoto in the form of 4-band multispectral image containing Near-Infrared, Red, Green and Blue bands (Fig. 46. and Fig. 47.).

The orthophoto was exported using *Planar* Projection type, *Top XY* Projection plane and *Mosaic* Blending mode as a GeoTIFF image. The maximal effective spatial resolution offered by the software was usually between 2 and 4 centimetres, nevertheless the resolution of 7 by 7 centimetres was chosen for the export as being the right compromise between the file size and offered detail.

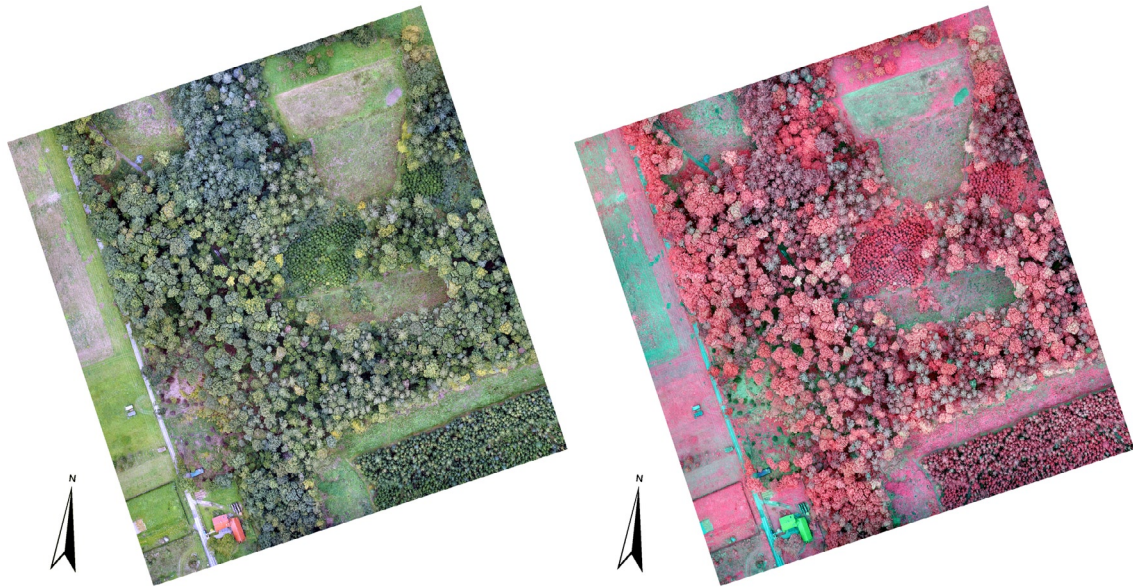


Fig. 47. A true orthophoto as an output of image processing in Agisoft PhotoScan software. One 4-band GeoTIFF image with 7 by 7 cm spatial resolution displayed as a true colour image (left) and as a false colour spectrozonal image (right).

The second type of output was a Digital Elevation Model (DEM). The DEM was also exported using *Planar* Projection type and *Top XY* Projection plane as a GeoTIFF file. The spatial resolution of exported DEMs was 15 by 15 centimetres. The last kind of processing output was the Dense Point Cloud. It was exported without any adjustments as the ASPRS LAS file. All the data were exported in the Czech national S-JTSK Křovák EastNorth Coordinate System.

#### 4.6.3. Auxiliary data

The photogrammetric processing of the UAV data provided all demanded 2D and 3D representations of the forest stands as such. The only type of data which could not be successfully extracted from the UAV-borne imagery was a reliable representation of the terrain below the stands. The examined forest stands were too dense to retrieve the Digital Terrain Model (DTM) with a required accuracy from the point cloud. Therefore a complementary DTM was utilized. Particularly a Digital Terrain Model of the Czech Republic of the 4<sup>th</sup> generation (DTM 4G) and of the 5<sup>th</sup> generation (DTM 5G) were utilized (Fig. 48.).

The DTM 4G represents a picture of natural or by human activity modified terrain surface in digital form as heights of discrete points in a regular grid (5 x 5 m) with coordinates X, Y, H, where H means the altitude in the Baltic Vertical Datum - After Adjustment with total standard error of 0.3 m of height in the bare terrain and 1 m in forested terrain. The DTM 5G represents natural or by human activity modified terrain surface in digital form as heights of discrete points in irregular triangle network (TIN) with X, Y, H coordinates, where H means the altitude in the Baltic Vertical Datum - After Adjustment with total standard error of 0.18 m of height in the bare terrain and 0.3 m in forested terrain. The models are based on the data acquired by altimetry airborne laser scanning of the Czech Republic territory accomplished between years 2009 and 2013 by the State Administration of Land Surveying and Cadastre (ČÚZK, 2016).

These data sources have several significant advantages. First of all they are the latest and most accurate digital terrain representations provided for the country so far. The DTM 4G covers area of the whole Czech Republic, DTM 5G covers already majority of the country (including the area of interest of this work) and it should cover the territory of the whole Czech Republic by the end of the year 2016. At the same time the data can be accessed and for smaller areas also downloaded via the ArcGIS Online service.

The DTMs were downloaded for all research areas. The DTM 4G was downloaded in the 5 x 5 m grid, the spatial resolution of the 5G model was adapted to the terrain conditions. Specifically the resolution of 0.5 x 0.5 m was used for the flat areas with the average slope below 20 degrees and the resolution of 0.2 x 0.2 m was applied for the areas with the average slope over 20 degrees.

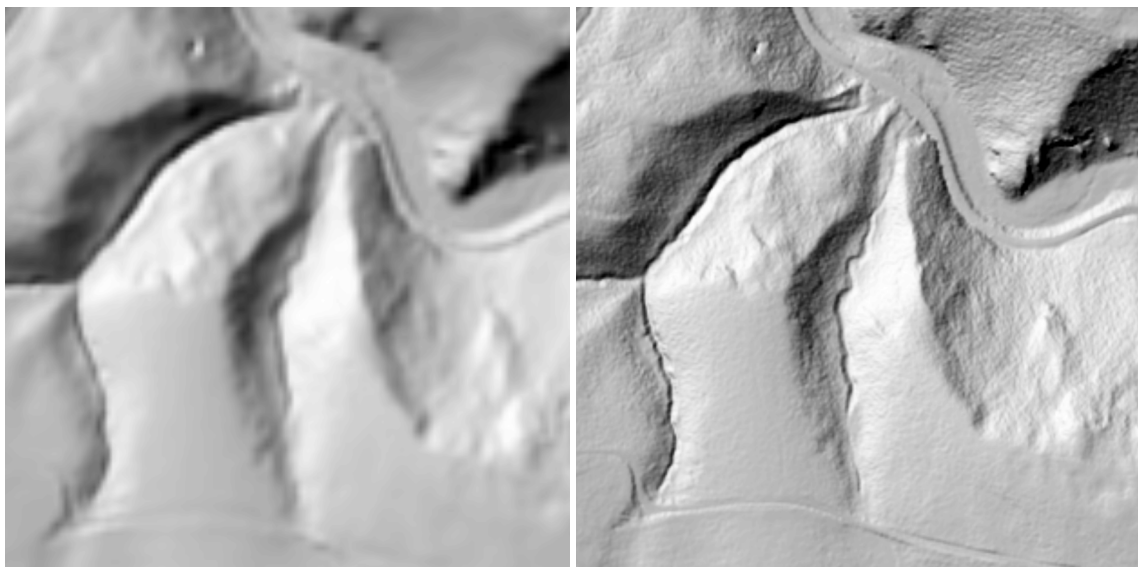


*Fig. 48. The auxiliary Digital Terrain Models DTM 4G (left) and DTM 5G (right) from ArcGIS Online service of State Administration of Land Surveying and Cadastre (ČÚZK, 2016).*



## **4.7. UAV Forest Explorer Software Tool Development**

### **4.7.1. General Description of the UAV Forest Explorer**

The main core of this work was programming of a novel software tool (or an application) for UAV data analysis. The objective of such tool is to identify individual trees in forest stands and extract their heights just based on the remote sensing data, using the principles of Inverse Watershed Segmentation (IWS). The original program, which has been developed within the framework of this work, is named “*UAV Forest Explorer*” and is designed as a unique custom tool running under the ArcGIS® for Desktop Advanced software by Esri®.

The version of ArcGIS enabling to run the tool is 10.0 or later (the tool was tested mainly on version 10.2). The tool was programmed in the Python programming language using the PythonWin IDE and is running on Python version 2.7. One of the program ideas is the universality (within the bounds of possibility of the chosen approach), so that the basic installation of the Python should be sufficient and no external modules, libraries or packages have to be imported or installed. Concerning the hardware, any computer capable of running ArcGIS 10 and its Geoprocessing tools should be able to run the UAV Forest Explorer.

The application is created as an individual \*.tbx file including the source code (python script). Since the source script is imported to the tool, loading the script from an external \*.py file is not needed. The whole source script can be seen in Appendix 2. The tool can be simply added into the ArcGIS Toolbox (e.g. pasted into ArcCatalog to My Toolboxes) and used like any other ArcGIS tool. The program contains a detailed Help, which can be displayed in its graphical user interface (GUI). The help is also provided as a User Guide in the form of a separate \*.PDF file called “User Guide for the UAV Forest Explorer Tool”, which is also a part of this work as an Appendix 3. According to those sources, also an uninitiated user should be able to use the tool properly.

The tool is working with several kinds of data from different sources. Particularly with UAV-borne remote sensing data, with one kind of auxiliary data and optionally also with the ground-truth data. The required remote sensing data should consist of a point cloud derived from the photogrammetrically processed

images of the forest stand gained by the means of an UAV. Such point cloud should provide the elevation information on the forest canopy surface.

The auxiliary data then should represent the elevation of the terrain below the forest stand of interest. In a very sparse stands such data could be hypothetically derived also from the UAV-based point cloud, but in most cases an additional source is needed.

Optionally also the ground truth data can be provided to compare the calculated tree counts and heights with the field-measured data. Basically the tool can be used in two ways. In one way, when the field-measurement data are not provided, the tool automatically processes the remote sensing data, performs IWS calculations, identifies trees in the examined area and delineates their crowns. The results then can be evaluated mainly visually.

In the other way, i.e. when the ground truth data are provided by the user in the demanded form, the tool performs all the previous processes as well, but makes also some additional computations. It takes the field measurements data and compares them with the results of its own trees identification process. Especially it compares the counts and heights of the automatically identified trees with the corresponding values of field-measured trees.

The tool executes series of mathematical and statistical calculations for this purpose, working on the basis of the Individual Tree Approach (ITA) as well as of the Area-Based Approach (ABA). The exact outputs of this comparisons resulting from each combination of the tool settings are then stored also in a tabular form. The results of tens or hundreds of iterations (settings combinations) can be then seen together and assessed by the user easily in this way.

Besides the possibility to use the field measurements data, the tool offers also some other facultative options. For instance to progressively reduce the number of iterations, when excluding those combinations of settings giving the less valuable results; to refine the cell size of the DTM, if being too coarse; to specify the area of interest to delimit the extent of calculations; to provide layer files, which then can be applied on the demanded feature classes created by the tool; or to choose to automatically delete the working datasets, if preserving them is not necessary.

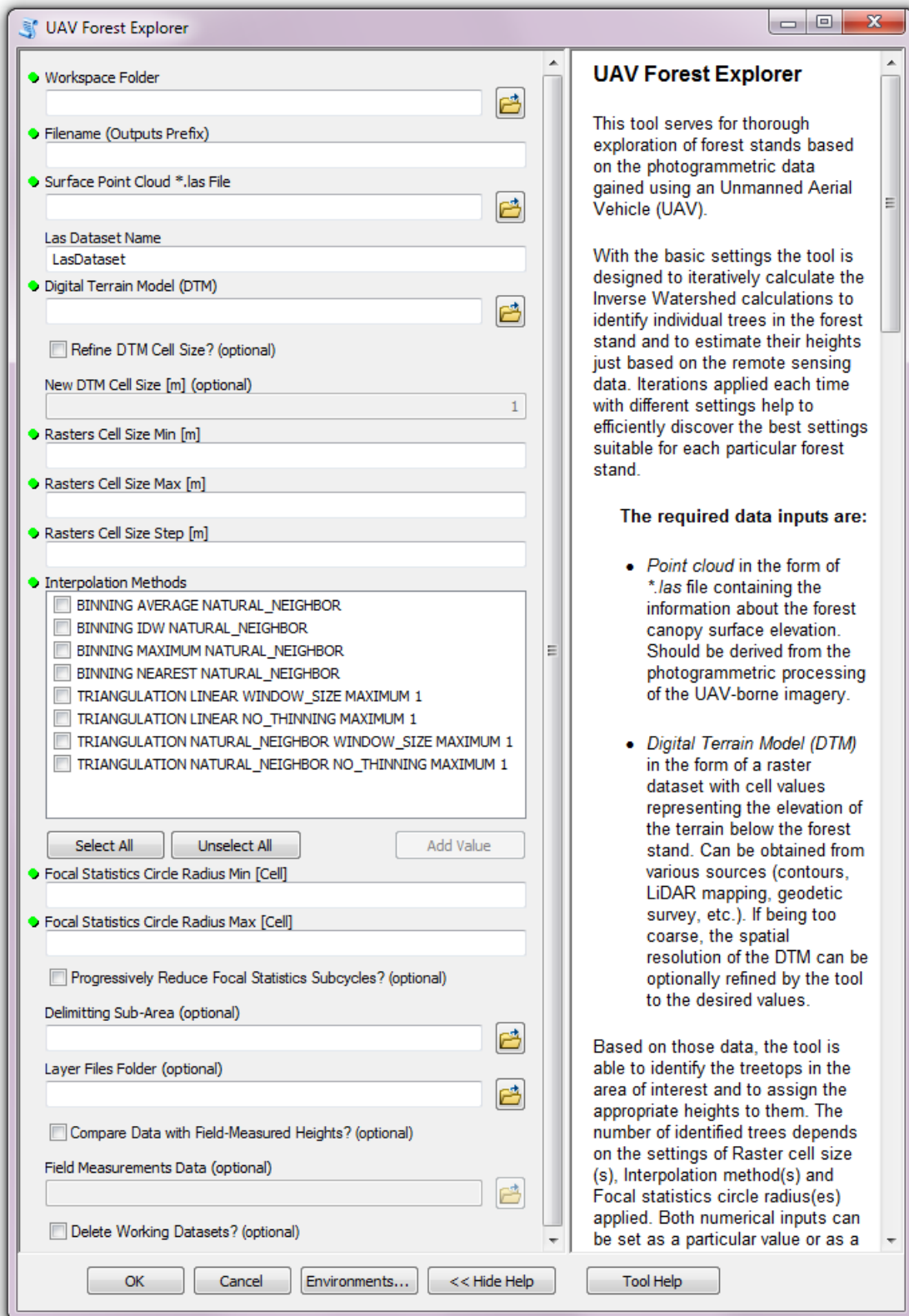


Fig. 49. The graphical user interface of the UAV Forest Explorer. The main window contains fields for required fundamental inputs (marked with green dots) as well as for optional inputs and choices. Some of the fields become active only when a proper checkbox is checked. Besides the fields for initial settings also the tool Help can be seen on the right side of the window.

### 4.7.2. User-Defined Entries and Input Data for Initial Settings

To run the tool, user needs to define series of entries and input data sources at first. Some of these entries are required and some of them are optional. All these inputs of the initial settings are described generally in this chapter, one by one in the same order, as they are sorted in the tool's GUI (Fig. 49.):

- *Workspace Folder:*

Defines a path to an existing folder on a computer hard drive where all the outputs created during a particular tool run will be stored. Since the tool is programmed to overwrite outputs, even if there are some data in the folder, which were created by the tool previously, this should not cause an error and the tool should run successfully.

- *Filename (Outputs Prefix)*

A user-defined filename which will be given as a prefix to the outputs created by the tool in a particular run. The uniquely given filenames enable to differentiate the outputs from multiple tool runs even if more of them are stored in the same Workspace Folder. The filename can be derived for instance from the geographical name of the locality or from the characteristic properties of the forest stand being explored, etc. Subsequently values of all the main settings defined by the user (spatial resolution of rasters, interpolation methods, focal statistics circle radiuses) are in a specific way (e.g. abbreviated) projected into the names of the data outputs, after this prefix. This ensures that if any change is done in the settings, the tool produces new datasets in the next run with new names which encompass these altered settings. In this way, when the same Workspace Folder and Filename are used in different tool runs, all the outputs created with even slightly different settings will produce unique data files which can be easily distinguishable according to their names.

- *Surface Point Cloud \*.las File*

A path to a point cloud stored in the form of a \*.las data file. The point cloud should be acquired by the photogrammetric processing of the UAV-based imagery. The point cloud should contain points representing the elevation of the canopy of the forest stand which is being investigated. The quality of this data file affects the quality of outputs created by the tool.

- *Las Dataset Name*

The name of the Las Dataset created by the tool from the Surface Point Cloud \*.las file. The default name is “LasDataset”. This name can be optionally changed for instance in order to distinguish different Las Datasets from more tool runs saved in one Workspace Folder, which would be overwritten otherwise. The Las Datasets created from the same \*.las file can differ mainly in the potential presence of constraints, which can be defined by providing an optional *Delimitting Sub-Area* by the user (described later).

- *Digital Terrain Model (DTM)*

The path to the Digital Terrain Model of the area of interest. This raster dataset file should comprise the elevation information of the terrain below the investigated forest stand. This dataset can be obtained from various sources, for instance from contours, from LiDAR mapping, geodetic survey, etc. The accuracy of this data file affects the accuracy of outputs created by the tool.

- *Refine DTM Cell Size? (optional)*

This option enables to refine the spatial resolution of the DTM, if it is too coarse. In steep areas, large raster cells of terrain model (e.g. 5 x 5 m of the 4G model by ČÚZK, or similar) may subsequently cause significant inaccuracies in estimation of the height of trees. To mitigate such effect, a new DTM can be created with reduced cell sizes. If this option is checked, following field becomes active to set the new value of the spatial resolution of the DTM.

- *New DTM Cell Size [m] (optional)*

The value of the spatial resolution of the altered DTM after the refinement. This field is active only when the previous checkbox (*Refine DTM Cell Size?*) is checked. The default value is “1 m”, but any value can be given. Only when the DTM, which the user has available, has a poor spatial resolution, and the area of interest is situated in the steep or curved terrain, this option is meaningful to be used.

- *Rasters Cell Size Min [m]*

The value of the minimal spatial resolution of the raster files created by the tool within the Inverse Watershed Segmentations. If a variety of raster cell sizes is to be tested within a single tool run, this value defines the smallest raster resolution which the produced rasters will have.

- *Rasters Cell Size Max [m]*

The value of the maximal spatial resolution of the raster files created by the tool within the Inverse Watershed Segmentations. If only one cell size is desired to be applied, the given value should be the same as the value of the *Rasters Cell Size Min*. If a variety of raster cell sizes is to be tested within a single tool run, this value defines the largest resolution of rasters which will be produced.

- *Rasters Cell Size Step [m]*

If a range of Raster Cell Size values is set in the two previous fields, more than one spatial resolution is to be tested within a single tool run. The *Rasters Cell Size Step* enables to define the step by which the new rasters will be graded. This field therefore defines a value of the raster spatial resolution, which can be iteratively added to the value of *Rasters Cell Size Min*, until the value of the *Rasters Cell Size Max* is reached.

- *Interpolation Methods*

Selectable Interpolation Methods which can be applied by the tool during the Inverse Watershed Segmentations. One up to eight of these methods is to be applied to create a Digital Surface Model (DSM) from the *Surface Point Cloud \*.las File*.

- *Focal Statistics Circle Radius Min [Cell]*

A minimal value standing for a number of raster cells used as a circle radius for calculating the local maxima in the Focal Statistics tool. This serves for smoothing the Canopy Height Model (CHM, a model gained by subtracting the DTM from the DSM) to get rid of the unwanted peaks, which could have remained in the model e.g. from the noise in the point cloud data. The bigger is this value, the larger is the generalization effect.

- *Focal Statistics Circle Radius Max [Cell]*

A maximal value standing for a number of raster cells used as a circle radius for calculating the local maxima in the Focal Statistics tool in order to smooth the CHM. If only one value for the Circle Radius is desired, the value in this field should be the same as the value of *Focal Statistics Circle Radius Min*. If the provided *Max* value is larger than the *Min* value, all the required values in this range are consecutively applied during the tool calculations graded by the step of one cell (1 cell is the obligatory value of the *Focal Statistics Circle Radius Step*).

- *Progressively Reduce Focal Statistics Subcycles? (optional)*

If checked, this option enables to reduce the number of iterations executed by the tool and therefore to decrease the computation time effectively. If ranges of values are set in the *Rasters Cell Size* fields or *Focal Statistics Circle Radius* fields or multiple *Interpolation Methods* are selected, the tool performs a series of cycles within each single run (otherwise only one iteration would be carried out). Since some of the combinations of these settings would produce not demanded results with high probability, this option makes it possible to exclude these combinations from the tool processing.

- *Delimitting Sub-Area (optional)*

An optional polygon feature class usable to define a smaller area for the tool calculations than is the default one. If not provided, the calculations are performed in the area of the whole extent of the *Surface Point Cloud \*.las File* or the *Digital Terrain Model* (the one whose extent is smaller). If provided, the calculations are delimited just to the area of this user-defined polygon, what can save the processing time significantly.

- *Layer Files Folder (optional)*

An optionally provided Folder containing layer files belonging to particular feature classes. The tool produces point and polygon feature classes representing identified trees and their crowns delineations. When many of these feature classes are produced and the user is willing to compare some of them visually, it can be difficult to set the demanded visual properties to each of them (e.g. to make hollow polygons to see the background layer, to set thickness and colour of polygon outlines, size and colour of points, etc.). The user is therefore given the possibility to create his own feature classes with defined properties of both, polygon and point feature classes. When these are saved with appropriate names in a single folder and the path to this folder is provided in this field, the tool automatically uses the properties of these feature classes and applies them to the particular feature classes which it creates. In such case both, original feature classes are produced together with corresponding layer files saved in a separate folder.

- *Compare Data with Field-Measured Heights? (optional)*

An essential option to compare the calculation results with the field-measured ground truth data. If not checked, just general outputs, such as feature classes with

determined tree positions and their calculated heights will be the output of the tool processing. If checked, and if the ground-truth data are provided in the next field, these outputs are compared with the field measurements automatically and thorough statistical calculations are performed.

- *Field Measurements Data (optional)*

A path to a point feature class representing the ground-truth data. Such data should contain field-measured positions and heights of trees in the particular area of interest. Each point in such feature class is considered to be a tree meeting the measurement conditions (see Chapter “4.3.2 Measurements of the trees” to check the measurement conditions used in this work). Therefore no surplus points should be contained. In the attribute table of the feature class a field for unique identification numbers should be called “*ID*” and also a field called “*Height*” should be present. In this field the appropriate heights of trees in metres, measured e.g. by hypsometer, should be recorded. When such feature class is correctly provided, the tool compares the counts and heights of field-measured and calculated trees and executes appropriate statistical computations. The computations are performed on the basis of Area-Based Approach as well as on the basis of Individual Tree Approach. As a result, separate tabular outputs are created. The accuracy of the ground truth data affects the accuracy of the comparison results. This field is active only when the previous checkbox (*Compare Data with Field-Measured Heights?*) is checked.

- *Delete Working Datasets? (optional)*

An option to delete unessential datasets produced during the tool processing. The tool creates series of raster files and feature classes during the Inverse Watershed Segmentations. Many of these datasets are just intermediate data necessary for the processing as such, when one dataset produced by some sub-process serves as an input for another sub-process, and the like. These datasets can be used for instance for the manual control, that the tool was working according to the user’s expectations, but do not have to be always all necessarily kept saved. Since some of these datasets can require a huge storage space on a hard drive (mainly when a large area is processed or many iterations are performed), it can be convenient to choose this option and to let the tool automatically and continually delete these data already within the tool run. The main tool outputs and results are not affected and can be deleted only manually. When not checked, all the datasets created by the tool are preserved in the Workspace Folder.



### 4.7.3. Processing Principles and Tool Outputs

#### 4.7.3.1. Identification of Trees and Computation of their Height

To understand how the UAV Forest Explorer tool is working, the processing background and computation principles are described in this chapter thoroughly. The tool, which is designed to work with remote sensing data, specifically with the photogrammetrically processed images gained by the means of the UAV, can be used in a variety of ways. With the basic settings, it is designed to identify individual trees in the forest stand and to estimate their height using the Inverse Watershed Segmentation principles.

The tool can be run each time either once with a demanded user-defined settings, or when more different settings need to be tested, the tool can run in an iterative mode and can produce a series of outputs at once. These iterations applied each time with different values help to efficiently discover the best settings suitable for each particular forest stand.

Optionally, when the field measurements data are available, the statistical comparison with these ground truth data can be done by the tool, either on the individual tree crown basis, or on the basis of the area-based approach. The tool will be described step by step in the following text, in the similar order as its parts are sorted in the source python script (See Appendix 2).

First of all, several necessary modules need to be imported by the tool to be used during the processing. To provide maximal versatility, only modules contained in the basic python package are used in this program, so that no external modules or libraries have to be downloaded or imported. Namely modules such as *arcpy*, *os*, *numpy*, *decimal* and *arcpy.sa* are imported. The last one stands for a Spatial Analyst extension, which license is automatically checked out in the beginning of each run.

In the beginning of a run the tool also defines the saving options which enable to overwrite outputs with already existing names. Then the *S-JTSK Krovak EastNorth Coordinate System* is defined as a default coordinate system for all the outputs produced by the tool.

Afterwards two new file geodatabases are created in the user-defined Workspace Folder. These geodatabases serve for saving of different kinds of results:

- *WorkingData.gdb* - a file geodatabase for storage of working raster files and feature classes created mainly during Inverse Watershed Segmentations.
- *IdentifiedTrees.gdb* - file geodatabase for storage of point and polygon feature classes representing the automatically identified treetops and appropriate delineations of the tree crowns.

All geodatabases made by the tool are created only if they are not already present in the Workspace Folder. If they were created earlier, all new outputs are subsequently stored in these existing geodatabases. This ensures that datasets contained in these geodatabases would not be overwritten by mistake, if the tool is run more times and each time directed to save outputs into an identical Workspace Folder.

If the user defined an optional path to the *Layer Files Folder* in the settings, the tool also creates a folder in the Workspace Folder. This new folder called "*LayerFiles*" then serves as a storage place for the layer files. These layer files are created for all point and polygon feature classes which are stored in the *IdentifiedTrees* geodatabase.

In the next step the tool creates a Las Dataset from the user-defined \*.las file, using the "Create LAS Dataset" tool. In the case that the user has provided an optional *Delimitting Sub-Area*, this dataset can contain constraints derived from this feature class and all other tool outputs are then also limited by the extent of this demarcation. Otherwise the Las Dataset with no constraints is created and the extent of the tool outputs is not altered.

If the user chose to *Refine DTM Cell Size* and defined the *New DTM Cell Size* in the initial settings, the tool performs several processes to fulfil this request. First of all a new file geodatabase called "*RefinedDTM.gdb*" is created in the Workspace Folder to accommodate the appropriate outputs. Subsequently the "Raster to Point" conversion tool is utilized to create a point feature class from the original DTM. In this feature class all points are situated in the middle of the original raster cells and contain the appropriate elevation information.

Afterwards a "Spline" tool is applied to interpolate a new DTM with the demanded cell size from these points. The advantage is that the newly created raster surface passes exactly through the input points, so that the original elevation

information is not altered. The new DTM with the demanded spatial resolution is then used in all subsequent computations instead of the original DTM with coarse spatial resolution.

The described process enables in a sort of way to improve the quality of the particular input dataset. Especially in steep terrain this option should enable to reduce the influence of errors caused by the fact, that the raster cells of the DTM are too large and the differences between digital number (DN) values of neighbouring pixels are too big. For instance if the user would have only a 4G DTM (Digital Elevation Model of the 4<sup>th</sup> generation from the ČÚZK) available, which has the spatial resolution of 5 x 5 m, the difference in elevation of adjacent raster cells can reach up to several metres in very steep areas easily. Using the DTM cell size refinement the spatial resolution of the converted DTM can be set to for instance 1 m or less. The elevation differences between neighbouring raster cells can then be reduced to sub-metre values efficiently. An example of the DTM refinement process can be seen in Figure 50.

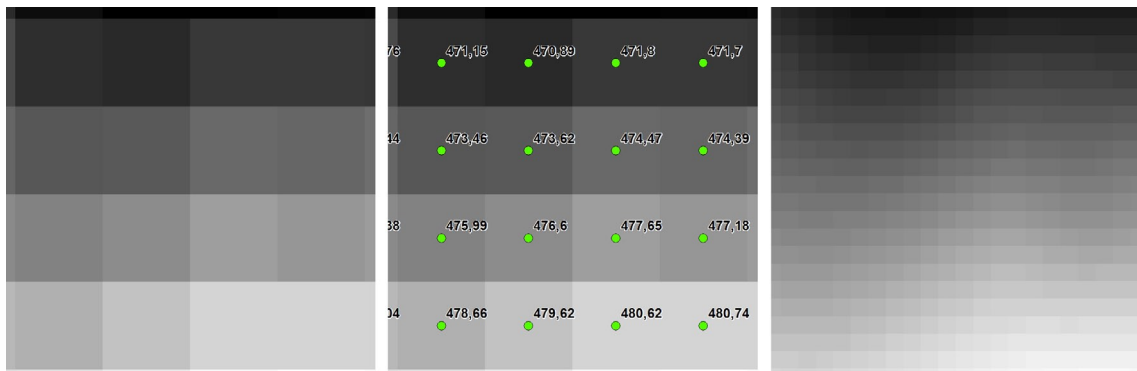


*Fig. 50. An example of automated DTM cell size refinement. The 5 x 5 m pixels of the DTM 4G from ČÚZK (left), the same raster converted to points with displayed elevation attribute (middle) and a new DTM with a 1 x 1 m cell size created from these points using the Spline interpolation (right).*

As the next step the tool sets the inner variables based on the user-defined parameters of the *Rasters Cell Size Min*, *Rasters Cell Size Max*, *Rasters Cell Size Step*, *Interpolation Methods*, *Focal Statistics Circle Radius Min* and *Focal Statistics Circle Radius Max*. The tool also checks if the given entries are logically correct and if not, it warns the user via the Warning Messages displayed in the Progress Dialog Box (i.e. the window continuously showing the progress messages, which is visible only if the tool is running in the Foreground - i.e. when the Background Processing is disabled in the Geoprocessing Options in ArcGIS).

The tool for instance checks if the provided value of *Rasters Cell Size Min* is not larger than the value of *Rasters Cell Size Max*. Also, in case that the *Rasters Cell Size Min* was set to “0” by the user, its value is automatically changed to the value of *Rasters Cell Size Step*, since rasters with 0 m resolution cannot be created. In the case that the user has set the value of *Rasters Cell Size Step* to “0”, it is automatically changed to the value of 0.1 metre. The tool warns the user also in the case when the value of *Focal Statistics Circle Radius Min* is larger than the value of *Focal Statistics Circle Radius Max* and the settings has to be corrected by the user. An example of a Warning Message can be seen in Figure 51.

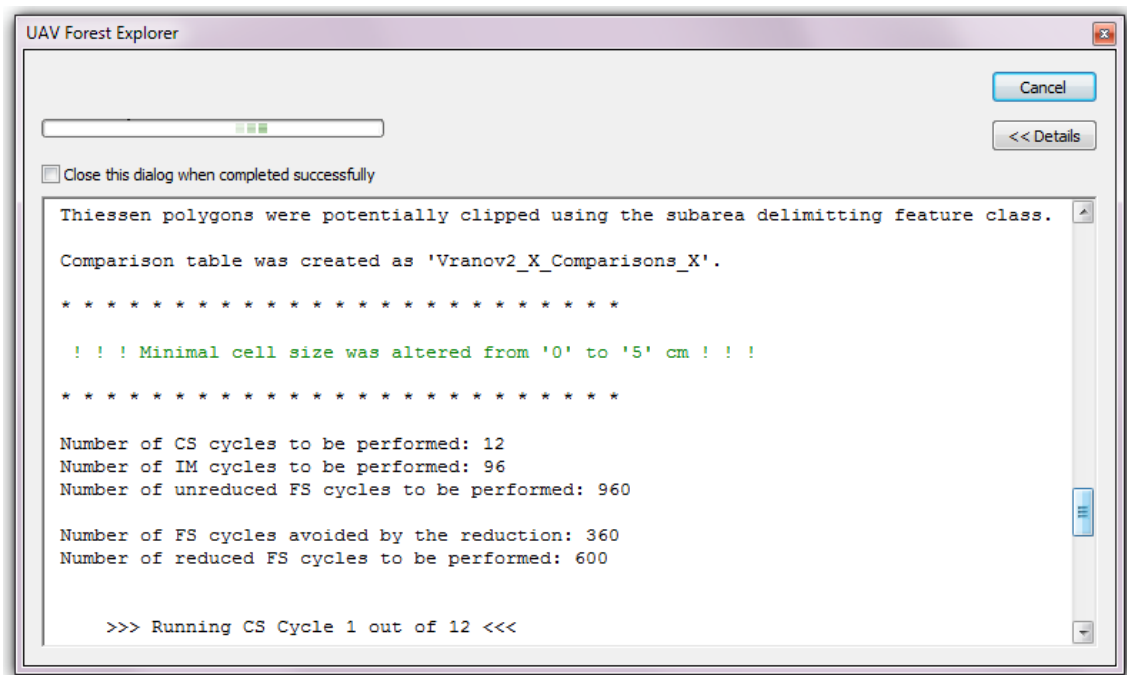


Fig. 51. One of potential Warning Messages (green text) which can be displayed in a Progress Dialog Box when the user-defined initial settings was not correct. Particularly the value of *Rasters Cell Size Min* was set to 0 m and it had to be replaced by the value of *Rasters Cell Size Step*, which was 0.05 m in this case.

In the case that the field measurements data were provided by the user, the tool performs a series of processes to prepare the data for consequent calculations. These processes are to be explained later on in this chapter. The basic processing principles without the ground truth data taken into account are described for now.

At this point the core processing part of the tool together with its related primary principles are to be characterized. For better understanding a broader description is provided first.

The tool offers an array of settings enabling to influence the form and accuracy of the final outputs. Since finding of the settings giving the most appropriate results (the counts of trees and their estimated heights the most corresponding to reality) can be often difficult, the tool offers a relatively simple solution. The elementary parameter inputs such as spatial resolution of the rasters, interpolation methods or the size of the circle radius used for the raster smoothing, can be set not only as a single values, but also as multiple values or ranges.

In other words, the number of identified trees and the values of their calculated heights depend on the settings of *Rasters Cell Size(s)*, *Interpolation Method(s)* and *Focal Statistics Circle Radius(es)*. Both numerical inputs can be set as a particular value or as a range of values. Then, between one to eight interpolation methods can be selected. If only one of each values/methods is set, only one calculation is executed during a single tool run. If the ranges of values are defined or multiple interpolation methods are selected, the tool runs iteratively until all the required combinations are carried out. In such case, tens or hundreds of iterations can be calculated during a single tool run easily. The presence of the user/operator is required only for the initial settings, the tool is working fully autonomously for the rest of the processing time.

This makes the tool very powerful and allows to efficiently perform various possible combinations of settings, which do not have to be tested separately. In this way a computing power of a PC can be utilized primarily, instead of the operator's time and effort, which can be hereby markedly saved. The tool then provides a series of outputs which can be mutually compared and the ones best fitting to reality can be selected.

Principally, the tool is executing Inverse Watershed Segmentation (IWS-based) calculations to identify trees in the remote sensing data and to estimate their heights. If various combinations of settings are to be tested, these calculations are working on the basis of three inner cycles (or loops), to accomplish the required iterations. The cycles can be described as follows:

- *Cell Size (CS) cycle* which encompasses all further Inverse Watershed Segmentation calculations and performs the required processes for each desired raster cell size. The number of CS cycles depends on the values of *Rasters Cell Size Min*, *Rasters Cell Size Max* and *Rasters Cell Size Step* defined by the user. In principle, the specific cell size employed in each CS cycle is applied as a spatial resolution of all rasters created within the particular Inverse Watershed Segmentation.

- *Interpolation Method (IM) cycle* which is calculated for each particular cell size (that means that IM loop is whole enclosed within the CS loop). It creates a Digital Surface Model from the point cloud \*.las file using required user-defined *Interpolation Method(s)*. Subsequently a Canopy Height Model is created by subtracting the DTM from the DSM.
- *Focal Statistics (FS) cycle* which is calculated for each particular *Cell Size* and each particular *Interpolation Method* (that means that FS loop is whole enclosed within the IM loop). It smooths the CHM and calculates the maximum of its cells in the defined neighbourhood. Subsequently it executes all the further processes required to accomplish the Inverse Watershed Segmentations. If the field survey data are provided in the initial settings, most of the relevant processes and statistical calculations are also performed within the FS cycle.

Each of these cycles has a built-in counter enabling the user to control the number of iterations performed during the tool run. The counts of the already executed loops are continuously displayed in the Progress Dialog Box. The user can be therefore constantly aware of the progress and knows how many iterations of each particular cycle (CS, IM or FS cycle) have already been carried out. Since the tool counts in advance also the overall number of these cycles to be performed within the whole tool run, it continuously shows the number of remaining cycles as well. User then knows at any time the amount of processes already done as well as the number of iterations which are to be carried out yet.

If the option to *Progressively Reduce Focal Statistics Subcycles* was selected by the user, the tool appropriately adjusts the number of the cycles to be performed. In such case also the counters are adjusted, to keep the values, provided by them, correct. The tool also shows the user, how many cycles will be carried out after the reduction and how many cycles will be avoided thanks to the reduction.

The Inverse Watershed Segmentation (IWS) calculations, which represent an important part of the tool processing, are incorporated within the described cycles. The IWS calculations basically apply series of mathematical, hydrological, spatial analysis, data management and conversion tools to process and analyze the input data with the objective to identify the trees in them. It initially inverts the

CHM, so that the model, which originally is formed by the peaks of the tree crowns, looks like a terrain full of pits, instead.

This inversion is important, since the subsequently employed hydrological instruments are capable of finding the lowest locally enclosed areas, from which the water would not be able to flow to any direction. These local minima of this negative model are then treated as the local maxima of the positive model - it is as the apexes of the trees. The height of these trees is then simply ascertained as the height of the CHM in the particular position of each treetop. The inverted (negative) model is also subdivided into an amount of the micro-watersheds, which in essence delineate the boundaries of the individual tree crowns.

When progressively describing the tool, mainly based on the structure of the source script, the contents of the individual cycles is to be described at this point. Since the cycles include also all the Inverse Watershed Segmentation calculations, these are also depicted thoroughly in the following text. As already mentioned, the *Cell Size cycle* incorporates both two other cycles and therefore embraces most of the remaining steps and processes performed by the tool. The CS loop is iterating when the actual cell size is smaller than the given value of *Rasters Cell Size Max*. The actual cell size begins on the value of the *Rasters Cell Size Min*. The actual cell size is updated so, that it is enlarged by the value of the *Rasters Cell Size Step* at the end of each CS cycle. In this way all the required spatial resolutions are applied on the produced rasters, until the value of *Rasters Cell Size Max* is reached.

Several parameters are then determined in the beginning of the CS cycle, especially these parameters containing the value of actual cell size e.g. for application in the outputs names, etc. To distinguish the individual tool outputs created based on different settings, some representation or abbreviation of the specific settings is given to the name of the outputs each time. In this case the actual cell size in centimetres is used in the output names just after the user-defined *Filename*.

As the next step the *Interpolation Method cycle* begins. The for loop ensures, that the tool iterates until all the *Interpolation Methods* set by the user are applied. Since the whole IM cycle is enclosed within the CS cycle, each such interpolation method is applied for each actual cell size.

Together one up to eight *Interpolation Methods* can be selected by the user in the initial settings. These methods are subsequently used for the conversion of the previously created Las Dataset into the form of a continuous raster surface. The "LAS Dataset to Raster" tool is used for this purpose and the Digital Surface

Model is the result of the process. The tool offers a variety of Interpolation Types which can be used to produce the demanded raster files. These types are divided into two groups differing in the applied methods, which are described based on the ArcGIS LAS Dataset to Raster tool Help in the following text:

1) “BINNING”, when cell values are obtained using the points that fall in the extent of the cell, with the exception of cells that do not contain points in their extent. Binning method can be specified using the options in two drop-down lists. Based on the logic and empirical experience only the most meaningful computation types and options were applied in this work and only these are described:

a) “Cell Assignment Type” – Method used to define the value for any cell that contains points within its extent. Particularly these Types were made available in the UAV Forest Explorer Tool:

- “AVERAGE” – Assigns the average value of all points in the cell.
- “IDW” – Uses Inverse Distance Weighted interpolation to assign cell value.
- “MAXIMUM” – Assigns the maximum value found in the points within cell.
- “NEAREST” – Uses Nearest Neighbour assignment to determine cell value.

b) “Void Fill Method” – The interpolation method used to define values for cells that do not have points within their extent. From the four available methods, only one following method was chosen to be used in the UAV Forest Explorer Tool, to simplify the processing:

- “NATURAL\_NEIGHBOR” – Uses natural neighbour interpolation to determine the cell value.

2) “TRIANGULATION” – Cell values are obtained by interpolating measurements from a triangulated representation of the LAS dataset. Triangulation method can be also specified using several options in the drop-down lists. Again only meaningful options and combinations were applied in this work and these are also described:

a) “Interpolation Method” – The interpolation method that defines cell values (both two methods were made available):

- “LINEAR” – Uses linear interpolation against the triangulated LAS dataset surface to determine cell value.
- “NATURAL\_NEIGHBOR” – Uses natural neighbour interpolation to determine cell value.



b) “Point Thinning Type” – Determines if LAS data points are thinned (both two types were made available):

- “NO\_THINNING” – LAS points will not be thinned.
- “WINDOW\_SIZE” – LAS points will be thinned by identifying the point that satisfies the selection criteria within the area defined by the window size. This option makes the following two options (c, d) available:

c) “Point Selection Method” – Selection method used for thinning LAS data points when using WINDOW\_SIZE thinning (from three options only one was made available):

- MAXIMUM – The point with the highest value in each window size is maintained.

d) “Resolution” – A numeric value that defines the area of the window size used for thinning points:

- The value of “1 metre” was applied in this option by default.

Concerning other options available in the LAS Dataset to Raster tool, following settings were applied:

- “ELEVATION” for the “Value Field”.
- “FLOAT” for the “Output Data Type”.
- “CELLSIZE” for the “Sampling Type”.
- actual cell size for the “Sampling Value”.

Together eight interpolation methods as the combinations of the described options and settings can be used in the UAV Forest Explorer tool. The names of the particular methods (as the result of the specific settings combinations) are displayed also in the GUI of the tool. For the purposes of naming of the tool outputs, especially to distinguish which output was created using which particular interpolation method, the abbreviations of the method names are made by the tool. These abbreviations are then used in the output names just after the cell size, which stands after the user-defined *Filename*. Following abbreviations are used in the tool outputs for particular interpolation methods:

- “BA” for “BINNING” with “AVERAGE” Cell Assignment Type and “NATURAL\_NEIGHBOR” Void Fill Method,

- *“BI”* for *“BINNING”* with *“IDW”* Cell Assignment Type and *“NATURAL\_NEIGHBOR”* Void Fill Method,
- *“BM”* for *“BINNING”* with *“MAXIMUM”* Cell Assignment Type and *“NATURAL\_NEIGHBOR”* Void Fill Method,
- *“BN”* for *“BINNING”* with *“NEAREST”* Cell Assignment Type and *“NATURAL\_NEIGHBOR”* Void Fill Method,
- *“TLW”* for *“TRIANGULATION”* with *“LINEAR”* Interpolation Method, *“WINDOW\_SIZE”* Point Thinning Type, *“MAXIMUM”* Point Selection Method and *“1 m”* Resolution,
- *“TLN”* for *“TRIANGULATION”* with *“LINEAR”* Interpolation Method and *“NO\_THINNING”* Point Thinning Type,
- *“TNW”* for *“TRIANGULATION”* with *“NATURAL\_NEIGHBOR”* Interpolation Method, *“WINDOW\_SIZE”* Point Thinning Type, *“MAXIMUM”* Point Selection Method and *“1 m”* Resolution,
- *“TNN”* for *“TRIANGULATION”* with *“NATURAL\_NEIGHBOR”* Interpolation Method and *“NO\_THINNING”* Point Thinning Type.

The Interpolation Methods displayed in the GUI of the UAV Forest Explorer are stated exactly in the form, which is required to be accepted by the sub-process performed by the utilized LAS Dataset to Raster tool. An attentive user can notice, that some of the method names do not directly correspond to the options described in the previous paragraphs. Particularly names of two interpolation methods are suspicious: *“TRIANGULATION LINEAR NO\_THINNING MAXIMUM 1”* and *“TRIANGULATION NATURAL\_NEIGHBOR NO\_THINNING MAXIMUM 1”*.

The question is, why in both cases the *“MAXIMUM”* Point Selection Method and *“1 m”* Resolution are stated, when in the case of using *“NO\_THINNING”* Point Thinning Type, normally no Point Selection Method and no Resolution are applicable. The answer is, that it is because of a bug in the LAS Dataset to Raster tool appearing when this tool is used via python scripting. The tool simply requires to senselessly fill in the interpolation methods in this way, and otherwise is not able to execute the required computation. Unfortunately, even though informed, ESRI does not seem to care about debugging the tool or at least about correcting the erroneous tool Help.

Finally, when this IWS calculation sub-process is done, a new DSM is created from the Las Dataset file. Both, the source LAS Dataset as well as the final DSM raster can be seen in Figure 52.

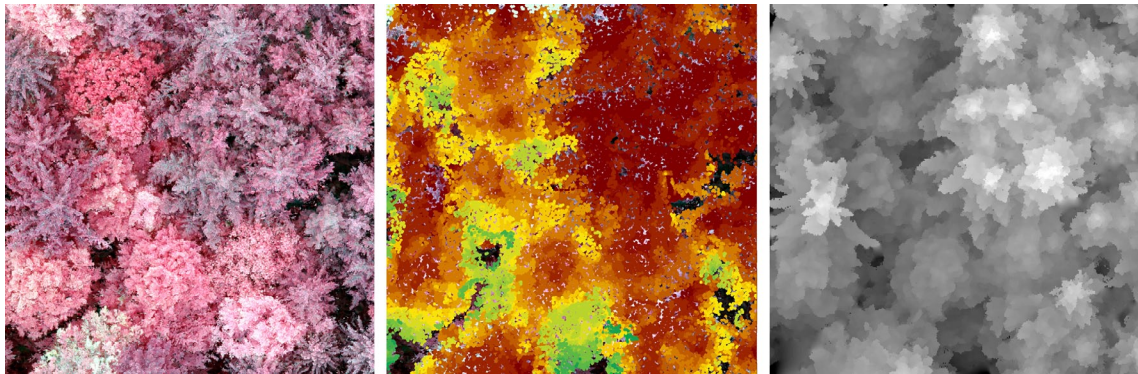


*Fig. 52. Visualization of a DSM creation. A particular forest of interest displayed on a colour-infrared image (left), LAS Dataset created from a photogrammetrically obtained point cloud (middle) and the final Digital Surface Model with 0.1 x 0.1 m cell size created by the UAV Forest Explorer using the LAS Dataset to Raster tool (right).*

When the DSM with the demanded spatial resolution is produced, the Normalized Digital Surface Model (NDSM) is to be created in the following step. It is simply done by subtracting the DTM from the DSM using the mathematical “Minus” function. Whereas DTM represents the elevation of terrain and DSM the elevation of objects, both as a height above sea level, NDSM represents the elevation of particular objects just in the form of height above the ground. Since only data covering forest stands are utilized in this work and only height of trees is examined, the term Canopy Height Model is used for this specific kind of NDSM.

All elevation values used in this work are in metres. All the three raster datasets (DTM, DSM and CHM) can be seen in Figure 53. Similarly as the DSM and as most of the following working outputs of IWS calculations also the CHM is stored in the *WorkingData.gdb*.

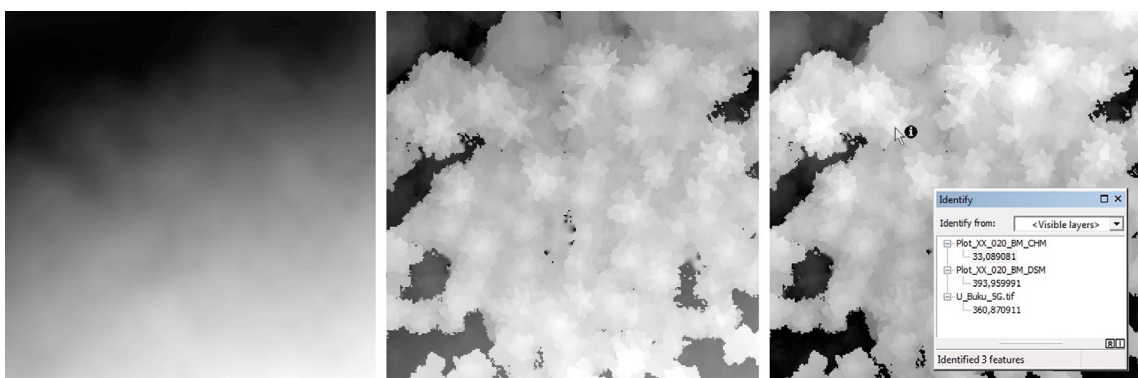


*Fig. 53. Visualization of a CHM creation. A Digital Terrain Model (particularly a 5G DTM from ČÚZK) representing the elevation of a bare ground (left), Digital Surface Model representing the elevation of the canopy surface (middle) and a similarly looking Canopy Height Model representing the height of the canopy surface above the ground (right). The particular elevation information of all three rasters in the position of a selected pixel (arrow with "i") are displayed in metres in the Identify window on the right image. The cell size of all three rasters is 0.2 x 0.2 m.*

At the point when both, DSM and CHM rasters are created, the last tool cycle is ready to begin its loop. This loop belongs to the *Focal Statistics (FS) cycle* and incorporates the rest of the IWS calculations and most of the other remaining computations. The loop iterates until all the required values of *Focal Statistics Circle Radius*, defined by the user in the initial settings, are applied.

Similarly like in the case of the previous two loops, if only one setting is to be tested, the loop runs only once. And much alike in the case of the CS cycle, the actual value of the circle radius begins on the value of *Focal Statistics Circle Radius Min*. Also, when a range of values was set by the user in the appropriate fields in the tool's GUI, the actual value of circle radius is updated at the end of each FS cycle in the way, that 1 cell (the obligatory value for *Focal Statistics Circle Radius Step*) is added. This is done until all required circle radius values are utilized. If more than one *Interpolation Method* was selected for the computations, this series of FS cycles is calculated for each of them.

To summarize the logic of the cycles working within the UAV Forest Explorer tool, it can be described as follows. Let's consider a case when multiple settings are tested within a single tool run, that means that range of values were defined by the user for *Rasters Cell Size Min* and *Max* and *Focal Statistics Circle Radius Min* and *Max* and also multiple *Interpolation Methods* were selected in the initial settings.

Since the FS cycle is whole encapsulated within the IM cycle, all the FS cycles are calculated for each Interpolation Method. Similarly, because of the fact, that IM cycle is encapsulated within the CS cycle, all IM cycles are calculated for each CS cycle. The total number of FS cycles calculated by the tool can be therefore derived by the multiplication of the numbers of all three cycles. That means that the number of basic CS cycles multiplied by the number of selected interpolation methods and multiplied by the number of basic FS cycles gives the total number of iterations carried out by the tool within a particular run.

A summary information about the particular cycle being performed is provided by the tool in the form of a Message shown in the Progress Dialog Box in the beginning of each FS cycle. This enables the user to be continually informed about the progress of computations. These information contain the following: A name of a file just being processed, which is subsequently contained in the names of most of the tool outputs created within a particular iteration. This unique and distinct

name is composed of a user-defined *Filename*, an actual *Cell Size* in centimetres, an abbreviation of the utilized *Interpolation Method* and an abbreviation of “FS” followed by a whole number standing for the value of currently applied circle radius.

Then the number of actually processed CS cycle is written together with the overall number of CS cycles to be calculated within the tool run. In the same way the numbers of actually running IM cycle and FS cycle are written together with the numbers of these cycles to be computed in total. Subsequently a number of actual FS sub-cycle is written together with the overall count of these sub-cycles to be performed. The FS sub-cycles are simply the FS cycles calculated for a single interpolation method.

The next provided information are the value of actual spatial resolution applied on all rasters created within the particular iteration; value of actual *Focal Statistics Circle Radius* and an abbreviation of the utilized *Interpolation Method*. Concerning the Messages, the tool then normally continues to inform the user via Progress Dialog Box, by successive writing the messages when each specific sub-process is finished or another information should be written. The Dialog Box showing the information written in the beginning of a particular FS cycle is shown in Figure 54.

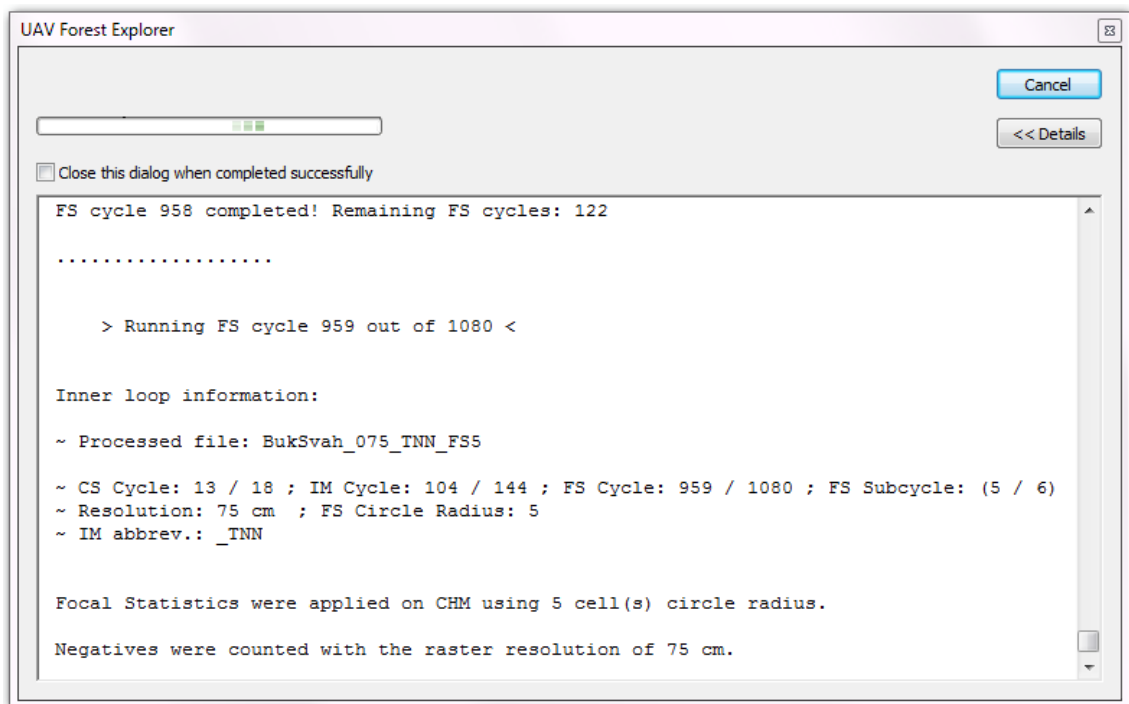
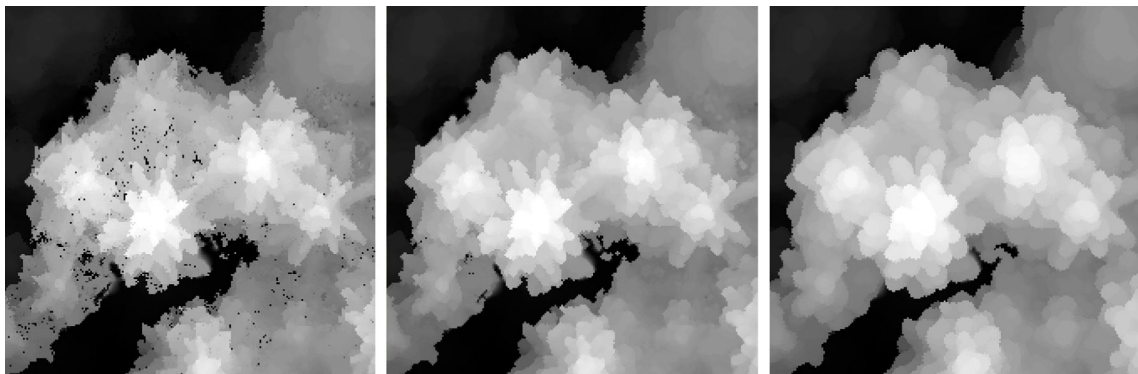


Fig. 54. A Progress Dialog Box showing the Messages containing information about a specific FS cycle (Inner loop information).

The next step of the IWS calculation is the employment of the Focal Statistics as such. The raster file, on which the “Focal Statistics” tool is applied, is the Canopy Height Model. From the Neighbourhood options just the “Circle” neighbourhood is utilized with the Radius in “Cell” units, which is supposed to be provided by the user as the *Focal Statistics Circle Radius* value (particularly as a range from *Min* to *Max* values). The Statistic Type is set to “MAXIMUM” to ensure that the local maxima will be accentuated in the CHM. This way the CHM is smoothed when keeping the original local maxima values unchanged (only surrounding lower values are altered).

Since the “Focal Statistics” tool calculates for each input cell location a statistic of the values within a specified neighbourhood around it, as stated in the tool Help, the radius of the circle which defines this neighbourhood, can significantly influence the result. Basically, the larger is the radius, the more cells are taken into the statistical calculation and the bigger is the smoothing effect. The smoothing is welcome, especially because it can reduce the unwanted roughness of the original CHM caused by the influence of the noise from the source point cloud data. Also potential gaps present in the CHM can be filled by application of this sub-process. An effect of the Focal Statistics can be seen in Figure 55.



*Fig. 55. An example of the smoothing effect of Focal Statistics when accentuating the local maxima. The original CHM with some visible gaps (left), the same raster file after application of Focal Statistics with 1 Cell Circle Radius (middle) and 3 Cells Circle Radius (right). Spatial resolution of all three rasters is 0.1 x 0.1 m.*

The Inverse Watershed Segmentation calculation continues by inverting the smoothed CHM. This inversion, necessary for application of further hydrological and related tools, is done by multiplying the smoothed CHM by the value of “-1”. This step virtually turns the model upside down and the peaks of treetops of the original model, become the pits or depressions in the new, negative model. Both, the CHM smoothed by the Focal Statistics and the negative of this model can be seen in Figure 56.

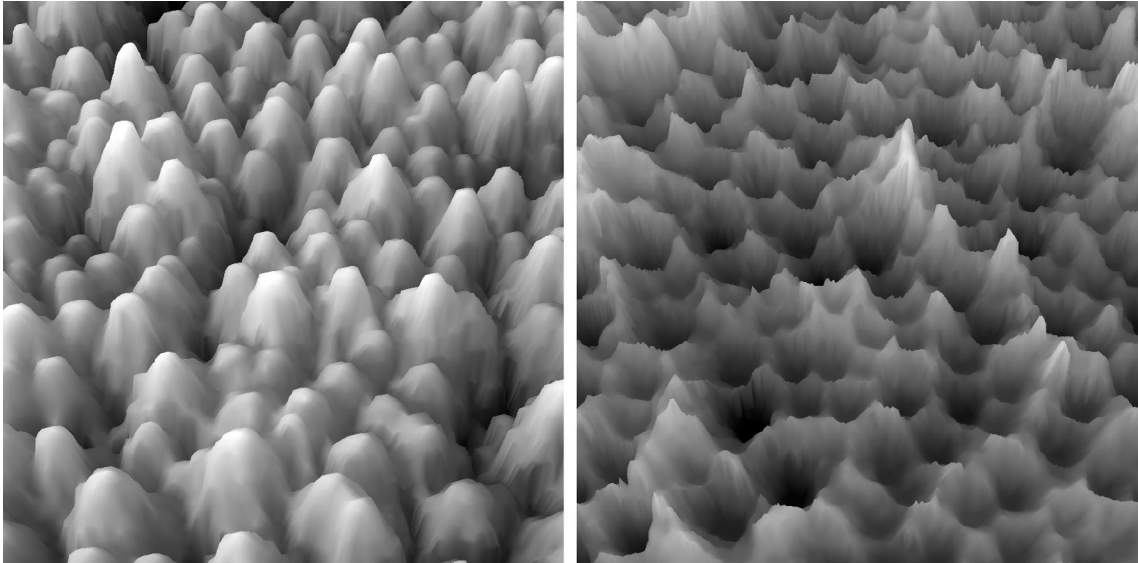


*Fig. 56. Peaks of treetops of the Canopy Height Model after Focal Statistics smoothing (left) and depressions visible on a negative of this model (right). Shown on an example of young coniferous forest stand. Images obtained using ArcScene 10.2.*

When a negative of the smoothed CHM raster is created, the places of tree apexes resemble pits dug in the terrain, in this inverted model. In the real conditions, water poured on such surface would probably remain mainly at the bottoms of these deepened areas. This principle is utilized in the logic of the Inverse Watershed Segmentation and enables to detect the potential tree apexes as the areas without any outflow. That is also why several hydrological instruments are used within the IWS calculations.

First of them is the generation of a “Flow Direction” raster using the tool of the same name. According to the tool Help, it creates a raster of flow direction from each cell to its steepest downslope neighbour. The output of the “Flow Direction” tool is an integer raster whose values range from 1 to 255. The tool can facilitate detection of sinks in an elevation model. A sink is, in an ArcGIS terminology, a cell or set of spatially connected cells whose flow direction cannot be assigned one of the eight valid values in a flow direction raster. This can occur when all neighbouring cells are higher than the processing cell.

The created flow direction raster then serves as an input into another hydrological tool which is called “Flow Length”. As stated in the tool Help, it calculates the upstream or downstream distance, or weighted distance, along the flow path for each cell. In the “Downstream” mode, in which it was applied in the UAV Forest Explorer, it calculates the downslope distance along the flow path, from each cell to a sink or outlet on the edge of the raster. The further is the cell from a sink, the higher value it gets. The cells of sinks then receive a value of “0”.

The flow length raster is reclassified subsequently using the “Reclassify” tool in order to extract only the demanded values belonging to areas of sinks. To reach this aim, all pixels having the DN value of “0” receive a new value of “1”, all other pixels then receive a value of “NoData” during the reclassification. Only locations of presumable presence of tree apexes then remain in the dataset.

The reclassified raster is then converted to polygons in the next step. That is done using the “Raster to Polygon” conversion tool with an option to “No Simplify” the polygons, which preserves the exact cell edges. This newly created polygon feature class is then directly used as an input to the “Feature To Point” tool. This tool is employed to gain the centroids of all polygons from this layer. Each point in the output feature class is then located at the centre of gravity (centroid) of the input polygon. In this way, all potential locations of treetops are converted to points efficiently.

An example of all four layers, a flow direction raster, a flow length raster, a reclassified raster with sinks converted to polygons as well as the centroids of these polygons, are depicted in the Figure 57.

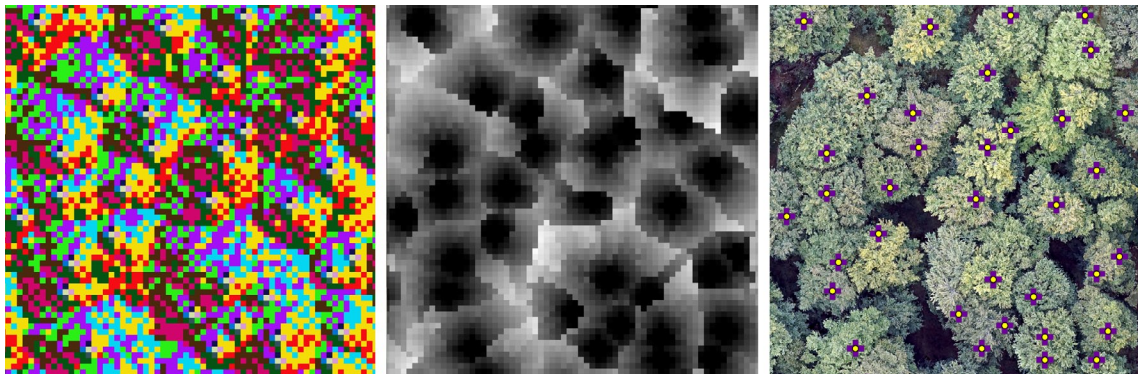


*Fig. 57. An example of hydrological instruments applied on a pre-processed CHM of a broadleaf forest. A Flow Direction raster displayed on the left and a Flow Length raster in the middle. The extracted sink areas displayed in the form of polygons (dark violet crosses) and their centroids displayed above them as yellow points on the right image (RGB orthophoto). The cell size of raster outputs is 0.7 x 0.7 m.*

These obtained points represent the positions of all trees identified in the analysed dataset. To assign them also an attribute of height, another step must be done. Therefore the tool “Extract Values to Points” is called by the UAV Forest Explorer. This tool extracts the DN values of raster cells to the appropriate points and stores them into an attribute table of a new point feature class. The raster, utilized to extract the values from, is the CHM after the application of the Focal Statistics (the original values of local maxima are maintained after Focal Statistics



smoothing). The new point feature class then contains all the original points representing the trees identified under the specific settings, when each of them contains also the appropriate height derived from the remote sensing data. These height values are stored in the attribute table in the “RASTERVALU” field. The feature class is saved in the “IdentifiedTrees.gdb” file geodatabase and contains the text “\_CrownTops” at the end of the file name. The points representing identified trees with their heights are displayed on Figure 58.

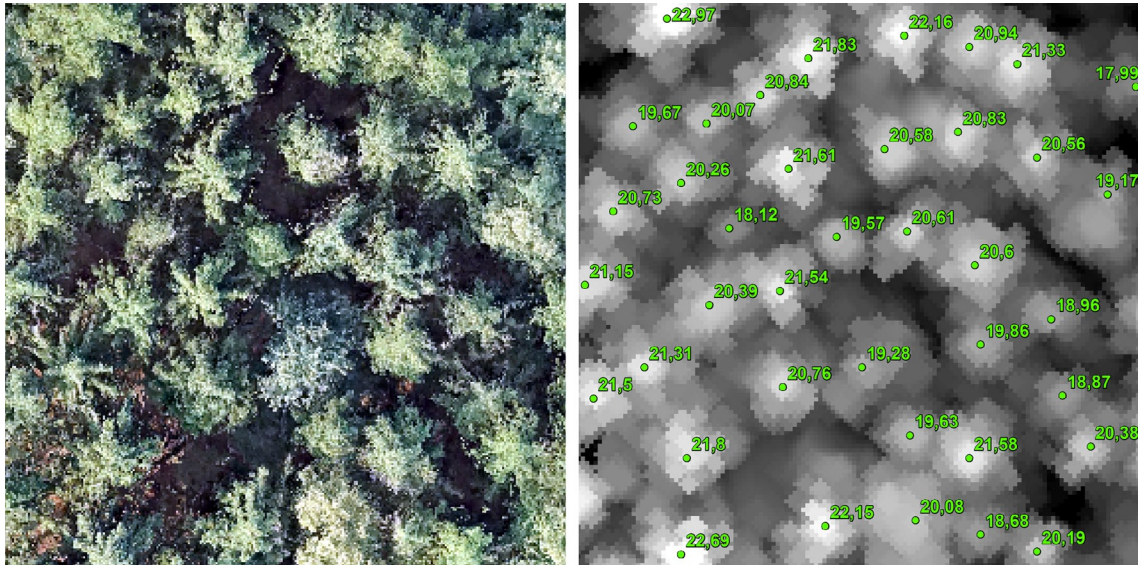


*Fig. 58. An example of the results of automatic trees identification performed by the UAV Forest Explorer. An RGB image of the examined forest with 0.07 x 0.07 m cell size (left). A smoothed CHM with 0.15 x 0.15 m cell size displayed with points representing the automatically identified trees (right). The adjoining numbers are the heights of these trees derived from the remote sensing data.*

When the trees are identified and their positions and calculated heights are stored on a proper place, it is time to distinguish the borderlines between individual tree crowns as well. Another hydrologic tool is utilized for this purpose, particularly a “Basin” tool. This instrument, uses the flow direction raster as an input dataset and creates a raster delimiting all drainage basins. As stated in the tool Help, the drainage basins are delineated within the analysis window by identifying ridge lines between basins. The input flow direction raster is analyzed to find all sets of connected cells that belong to the same drainage basin. The drainage basins are created by locating the pour points at sinks, then identifying the contributing area above each pour point. This results in a raster of drainage basins.

These basins are a good representation of the tree crowns, since each basin surrounds one identified tree apex. The borderlines of the basins can then serve

as individual tree crowns delineations. Therefore the basin raster is subsequently converted to a polygon feature class using the “Raster to Polygon” tool. An option to “Simplify polygons” is applied which enables to smooth polygons into simpler shapes. The smoothing is done in such a way that the polygons contain a minimum number of segments while remaining as close as possible the original raster cell edges, as states the tool Help. The resulting polygon feature class is then stored in the “IdentifiedTrees.gdb” file geodatabase and its name contains the text “\_Crowns” in the end. The drainage basins raster together with the polygonal representation of basins can be seen in Figure 59.

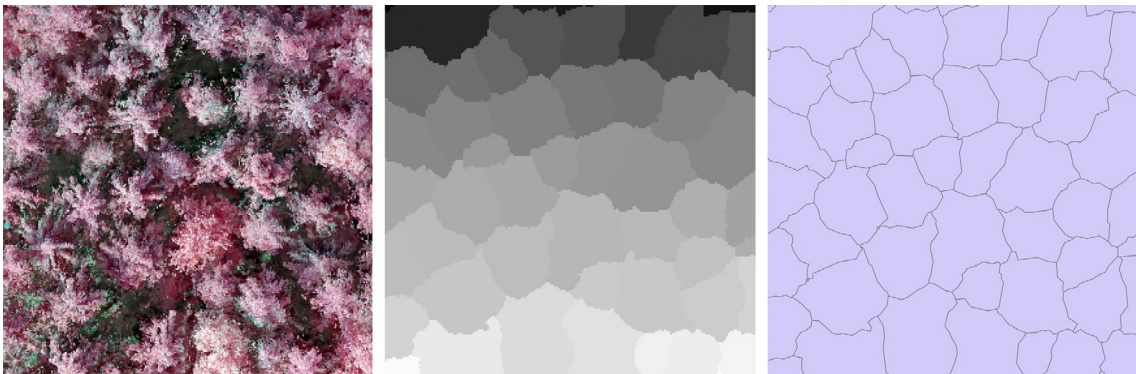


*Fig. 59. A CIR image of the forest stand of interest (left) and a drainage basins raster created using hydrological instruments (middle). This raster converted to a polygon feature class (right) then serves for individual tree crowns delineation.*

At this point the Inverse Watershed Segmentation process as such is completed. All demanded primary outputs are created, since the tree apexes are identified, the tree heights are estimated and the tree crowns are delineated. These results are stored in the “IdentifiedTrees.gdb” file geodatabase in the form of one point and one polygon feature class.

For each particular combination of initial settings the UAV Forest Explorer tool creates one pair of these feature classes. When many such combinations are to be tested, easily tens or hundreds of these feature classes can be produced within a single tool run. It can be highly demanding for the user if he decides to compare some of these outputs visually. For this reason, the option to provide the layer files with required properties is given by the tool, as described earlier. These sample layer files should be stored in a user-defined *Layer Files Folder* and should meet specific conditions concerning their names. Particularly the layer file intended for the polygon feature class has to be named “*Polygon\_layer\_file.lyr*” and the layer file intended for point feature class has to be called “*Point\_layer\_file.lyr*”.

If these sample layer files are provided correctly, the tool automatically uses their properties and applies them on the appropriate feature classes. It results in the creation of new layer files, one for each feature class, which have the same visual properties as the sample layer files. These new layer files are stored in the “*LayerFiles*” folder which is automatically created by the tool in the Workspace Folder.

The method of layer files creation is based on the following operations. First of all a new feature layer is produced using the “Make Feature Layer” tool. The feature layer is temporary and is created based on the input polygon feature class of delineated crowns. Subsequently the tool “Apply Symbology From Layer” is called. This tool applies the demanded visual style of the “*Polygon\_layer\_file.lyr*” on the particular feature layer. The “Save To Layer File” tool is then used to save this updated feature layer as a layer file with the required name. This file is stored in the “*LayerFiles*” folder and contains the “*\_Crowns\_lyr*” text in the end of the file name.

Similar procedure is carried out also with the point feature layer representing identified tree apexes. The layer file “*Point\_layer\_file.lyr*” is utilized to gain the symbology from and the newly created layer file contains the text “*\_CrownTops\_lyr*” in the end of the file name.

The tool is programmed in the way, that when the *Layer Files Folder* is defined by the user, it has to contain both sample layer files, i.e. one for polygon and one for point feature layer, otherwise the process of symbology application cannot be performed correctly. User can either utilize the default sample layer files provided with the UAV Forest Explorer, or can create his own layer files with any kind of properties, in case of need.

In this way the relevant outputs of the IWS calculations, i.e. polygon and point feature classes, are stored in the “IdentifiedTrees.gdb” file geodatabase and corresponding layer files are stored in the “*LayerFiles*” folder. Both kinds of data files represent the same feature classes, with the advantage, that the layer files are already adjusted, based on the user demands, to facilitate the visual comparison between individual files. Both, original feature classes with default visual properties as well as layer files with demanded visual style can be seen on Figure 60.

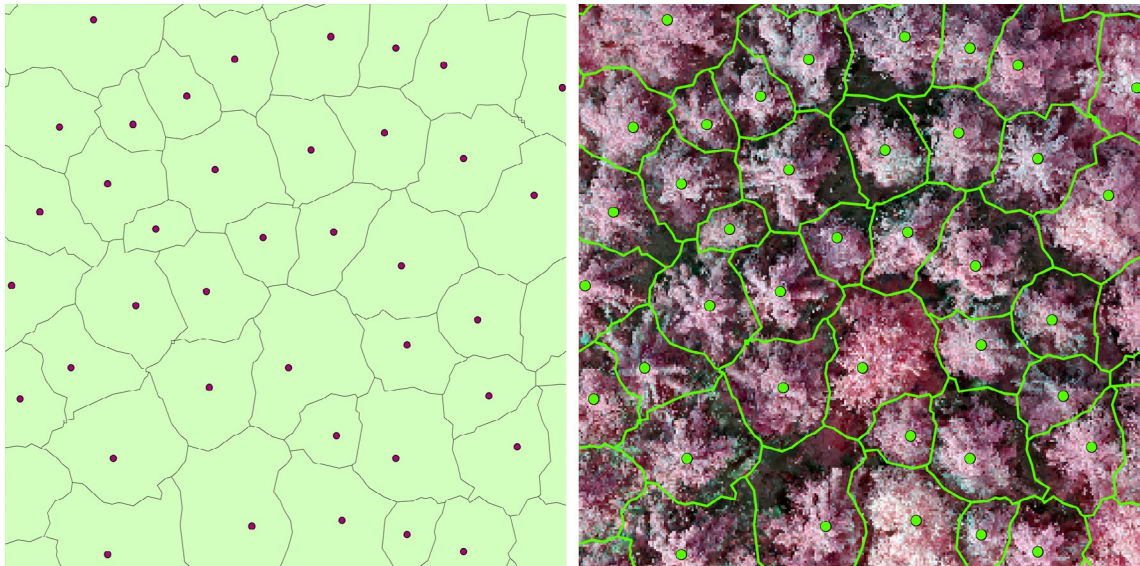


Fig. 60. Point feature class for tree apices and polygon feature class for crowns delineation as a result of the automatic identification of trees (left). The same feature classes displayed as layer files with demanded visual properties (right).

#### 4.7.3.2. Comparison with Field Measurements Data

When the IWS calculations are completed, two possible situations can come to pass afterwards. On the one hand, the Focal Statistics circle can finish and either a new iteration begins, or the tool performs the remaining final processes and leads to the end of the whole run. On the other hand the tool can execute another series of processes. To carry out these additional calculations, one condition has to be met, and it is the fact, that the field measurements ground truth data have to be provided by the user in the initial settings of the UAV Forest Explorer. That means, that the option *Compare Data with Field-Measured Heights?* has to be checked and in the field called *Field Measurements Data* a required feature class has to be provided.

As described earlier, this feature class has to be of point type and all the points it contains should represent the exact tree positions. In its attribute table two fields have to be present, field called “*ID*” containing unique identifier for each record and field called “*Height*” containing the measured height of each tree in metres. When these requirements are fulfilled, the tool automatically performs comparison of these field-measured data with the data acquired during the IWS calculations. That means, that the counts of trees and their heights are put to statistical testing. The synoptic outputs then enable the user

to compare the results of various settings relatively easily and to choose the most convenient ones.

To understand the principles of these procedures, one part of the tool's constituents, which precedes all the IWS cycles, has to be described first. These steps have to be carried out before the start of loops, since they are to be done only once and are not meant to iterate. First such step is the creation of a new file geodatabase in a Workspace Folder. Its name is "*Comparisons.gdb*" and it is intended as a storage place for the comparison results. Also this geodatabase is created only if it does not exist yet. Similarly a new folder is created. This folder is named "*Tables*" and is meant to accommodate the tabular results of comparisons in the Excel format.

In the next step the tool potentially trims the extent of the ground truth data. This happens, only in the case, that the *Delimitting Sub-Area* is provided by the user in the initial settings, and this area is smaller than the area of field measurement data. The trimming is done using the "Clip" analysis tool and the resulting feature class is called "*FMtreesClipped*". This file is actually created each time the sub-area is provided, but if its extent is not smaller than the extent of the ground truth data, it is in essence a copy of the field measurement dataset.

Another ensuing step is the delineation of the space around the individual field-measured trees. This is important to fulfil the demands of the Individual Tree Approach and gives the basis for the tree pairing (within the meaning of pairing field-measured and calculated trees). Specifically Thiessen Polygons were chosen as the most suitable means to reach this goal. To gain them, the "Create Thiessen Polygons" tool is called by the UAV Forest Explorer.

As stated in the tool Help, this tool is used to divide the area covered by the point input features into Thiessen or proximal zones. These zones represent full areas where any location within the zone is closer to its associated input point than to any other input point. Thiessen polygons are created in the way, that all points are triangulated into a triangulated irregular network (TIN) that meets the Delaunay criterion. The perpendicular bisectors for each triangle edge are generated, forming the edges of the Thiessen polygons. The location at which the bisectors intersect determine the locations of the Thiessen polygon vertices. The outside boundary of the output Thiessen polygon feature class is the extent of the point input features plus an additional 10 %.

Based on this workflow, whole area of interest is divided by Thiessen polygons, when each of them surrounds one input point representing the field-measured tree position. The newly created Thiessen polygons feature class contains the user-defined *Filename* in its name followed by the “*Thiessens*” text.

Since the Thiessen polygons feature class has a rectangular shape, which extends beyond the usually circular area of field measurements, it has to be trimmed in some way as well. For this purpose another tool is called, which is named “Minimum Bounding Geometry”. As says its Help, it creates a feature class containing polygons which represent a specified minimum bounding geometry enclosing each input feature or each group of input features. The “CONVEX\_HULL” option was utilized, which creates the smallest convex polygon enclosing an input feature. The point feature class of field measurements data was used as the input feature. The output feature class is then comprised of one polygon the borders of which are going exactly thorough the outer points of the input feature class (Fig. 61.). The output feature class then contains the “*Bounding*” text after the *Filename* in its name.

To extend the area of the newly created polygon a little bit, a “Buffer” tool is utilized. The buffer distance is set to 1 metre. This distance should ensure, that also tree apexes identified slightly further from the plot centre, than are the positions of the boundary measured trees, will be taken into consideration in the further tree pairing. Therefore also apexes of trees trunks of which are slightly leaning out of the plot, will be accepted. The name of the output feature class contains the text of “*BoundingBuffer*” after the *Filename*.

The last step of the Thiessen polygons extent adjustment, is the clipping of the *Thiessens* feature class. The ordinary “Clip” tool is utilized and the *BoundingBuffer* feature class is used to define the clipping extent. This makes the outer borders of Thiessen polygons to better follow the distribution of the source points. The output feature class, bearing “*ThiessensClip*” in its name, then does not contain any redundant corner areas and is prepared for the further calculations. The process of Thiessen polygons creation and trimming can be seen on Figure 61. Potentially, if the *Delimitting Sub-Area* is provided by the user, also the Thiessen polygons are clipped by this area. The output then contains the text “*ThiessensClipSub*” in its name.

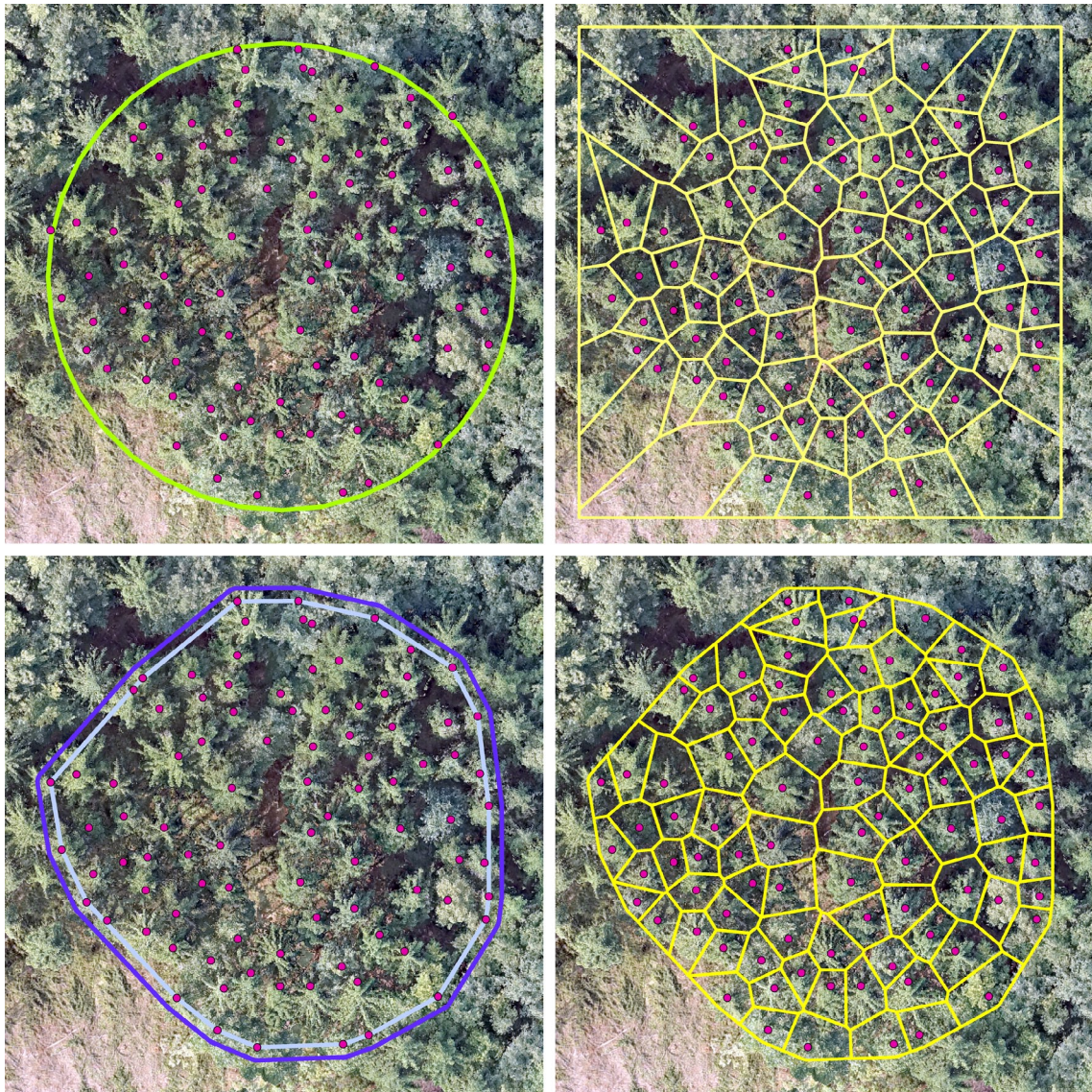


*Fig. 61. The process of Thiessen polygons creation and trimming. The field-measured trees in an examined forest stand are displayed as purple points. The green circle represents the area of the circular study plot of 1000 m<sup>2</sup> size (top left). The yellow polygons are the Thiessen polygons created around the trees (top right). The smallest convex polygon enclosing the field-measured trees is displayed as the light blue polygon together with its 1-metre Buffer polygon displayed in dark blue (bottom left). The last image shows the final Thiessen polygons clipped by this buffered polygon (bottom right).*

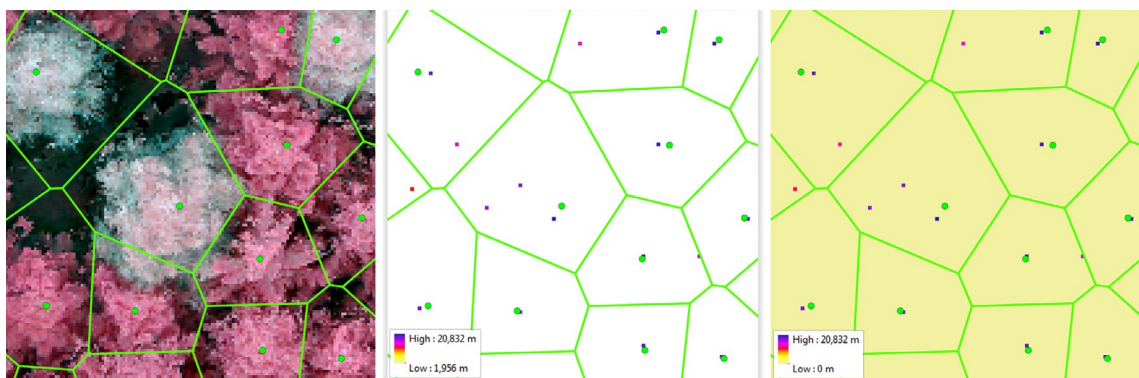
In the next step an important file is created in the *Comparisons.gdb* file geodatabase. It is a table and its name is “*X\_Comparisons\_X*” (The *X* letters are used mainly to put the table at the end of all the files stored in the geodatabase and to accentuate it visually. This should make this file easier findable for the user, if too many files are stored in the geodatabase). This table is meant to contain all the numerical results of the mathematical and statistical comparisons of the particular quantities of the field-measured and automatically identified trees. The

table is subsequently filled with 21 fields (i.e. columns) with appropriate names to accommodate the demanded values. The names of these fields are to be provided later on in this text.

The part of the preparation for comparison procedures which precedes the IWS cycles ends at this point. The remaining comparison calculations encapsulated in the FS cycle will be described in the following text.

First of all, the point feature class representing the treetops identified automatically by the tool, is clipped by the area of the field measurements data. The *BoundingBuffer* polygon is utilized for this purpose using the “Clip” tool. The output point feature class is stored in the *Comparisons.gdb* and contains the text “*Identified*” at the end of the name. This ensures that only the relevant trees, identified just within the exact extent of the study plot, will be employed in the further calculations.

Subsequently, the cell size of the newly created rasters is temporarily set to the value of 0.1 m. This fixed cell size is important for some of the consequent calculations, since some too large cell sizes could cause unwanted results. In the next step the identified treetops are converted to raster format using the “Feature to Raster” conversion tool. The “*RASTERVALU*” field is defined as the source of values to be applied to the raster cells. The appropriate cells of the output raster file lying in the positions of the original points then contain the corresponding height values. All the other cells receive the NoData value.



*Fig. 62. Conversion of point feature class of identified trees to raster datasets shown on a randomly selected result of automatic identification of trees. Thiessen polygons (green polygons) and field-measured trees (green points) are displayed on all images. A CIR image of a forest (left), identified trees converted to raster cells including NoData - white areas (middle), and the corresponding dataset with NoData substituted with Null values - yellow areas (right).*



Since for some following calculations these NoData values are not the most convenient, they are replaced by the Null values in the ensuing step. The “Con” tool is applied to do this task using the IsNull condition. The Con tool performs a conditional if/else evaluation on each of the input cells of an input raster. Both, the original raster containing NoData values as well as the new output raster containing Null values instead (both can be seen in Figure 62.), are to be utilized in the further calculations.

When the rasters containing the heights of identified trees are prepared, the required values can be extracted and demanded calculations can be performed. These calculations are intended to fulfil the requirements of the Area-Based Approach, but also of the Individual Tree Approach.

First of all the appropriate values are extracted within the scope of the ITA. The “Zonal Statistics as Table” tool is called for this purpose. This tool summarizes the values of a raster within the zones of another dataset and reports the results to a table. The tool is used twice, once with the raster containing NoData values as the “Input value raster”, once with the raster containing Null values as the “Input value raster”. In both cases the *ThiessensClip* polygon feature class is provided as the “Input feature zone data”. Since the ID numbers of the Thiessen polygons feature class correspond to the ID numbers of the field-measured trees, the “ID” field is used as the “Zone field” each time.

Also in both cases the “DATA” choice is applied in the “Ignore NoData” option, meaning that within any particular zone, only cells that have a value in the input Value raster will be used in determining the output value for that zone. NoData cells in the Value raster will be ignored in the statistic calculation, as says the tool Help. The “Statistical type” is then set to “ALL” meaning that all the available statistics can be calculated, containing the “COUNT” for count of cells within the zone, “MIN” for minimal cell value, “MAX” for maximal cell value, “RANGE” for difference between minimal and maximal cell values, “MEAN” for the average of all cells in the particular zone, “STD” for the standard deviation of the cells and “SUM” for the total value of all the cells belonging to a single zone.

These computations result in the creation of two tables in the *Comparisons* file geodatabase. The table the name of which ends with “*ZonalStatsCounts*” contains the zonal statistics calculated from the raster with NoData values, the table the name of which ends with “*ZonalStatsFull*” then contains the zonal statistics

calculated from the raster with Null values. In both cases, each line of records in the created table contains the statistical information about the cells situated within one zone of the “Input feature zone data”, i.e. within the individual Thiessen polygon. Since each one Thiessen polygon literally belongs to (and envelopes) one of the field-measured trees, these statistics are calculated for each such tree. This enables for instance to count the number of trees identified in the surroundings of each field-measured tree as well as to know the heights of smallest or tallest one of them, besides the other ascertained information. Particular values can then be used in the consequent ITA-based computations.

The “Zonal Statistics as Table” tool is applied also to fulfil the requirements of the ABA. In this case only the raster with NoData values is used as the “Input value raster”. Then the *BoundingBuffer* is utilized as the “Input feature zone data” constituting one large single zone. The “ORIG\_FID” field is then defined as the “Zone field”. Otherwise all the settings is the same as in the previous case, using the “DATA” option and calculating “ALL” available statistics. The output table then receives the “*ZonalStatsUnpaired*” text for the end of its name. This table contains only one line of records encompassing the overall statistics calculated for all the identified trees situated within the area of field measurements. The count of these trees, their minimal or maximal height and other values are to be found in there and are prepared for the later use.

Then comes the time to interconnect the field measurement data with the corresponding results of the zonal statistics. First of all a copy of the field measurements point feature class is created and saved in the *Comparisons* file geodatabase. The “Feature Class to Feature Class” conversion tool is called to do this job when preserving all the properties of the original dataset. The resulting feature class contains the “*Joined*” text in its name.

Consequently, the table containing the zonal statistics based on ITA, that means calculated from the raster file without NoData using Thiessen polygons, is attached to the attribute table of this *Joined* feature class. The “Join Field” tool is utilized for this purpose. The join is performed based on the “ID” fields of both tables, since the values in these fields represent the unique identifiers which correspond to each other between the two tables. After this process, the *Joined* table contains all the original values, including the heights of trees measured in the field, but also all the values resulting from the zonal statistics calculations.

That means that in this table are then present both, the counts and heights of the field-measured trees, together with the counts and heights of the automatically identified trees, besides other values.

In the ensuing step this *Joined* table is further adjusted and extended. Since some calculations are to be carried out within this table, some of its fields have to be specified and some have to be added using the “Add Field” tool. The names of these fields are following:

“Height” for field-measured (FM) heights (existing field).

“MAX” for calculated heights (existing field).

“Diff” for their difference (added field).

“Abs\_Diff” for absolute value of that difference (added field).

“Diff\_sq2” for the square of that difference (added field).

“No\_Max” for unidentified trees (added field).

“Height\_2” for FM heights of matched trees (added field).

“MAX\_2” for calculated heights of matched trees (added field).

“Diff\_2” for their difference (added field).

Consequently the “UpdateCursor” tool is applied to calculate demanded values in the newly added fields. The first calculation gives the value of 1 to the “No\_Max” field if the value in the “MAX” field is 0, it means that no tree was identified in the particular Thiessen polygon. All other rows then receive the 0 value. This enables to distinguish rows with and without any identified trees.

In the next step the tool calculates the difference between measured height (“Height” field) and the maximal calculated height (“MAX” field) for each zone and stores the results in the “Diff” field. In the case that more than one tree is identified in the extent of one Thiessen polygon, only the tallest one is taken into consideration (is paired or matched with the FM tree). This approach helps to avoid the influence of the falsely identified trees (the right tree apex should be the tallest one in the zone). Subsequently an absolute value of this calculated difference is counted and saved in the “Abs\_Diff” field and the second power of the difference is also counted and the result is saved in the “Diff\_sq2” field.

In the forthcoming step the calculations are carried out only for the zones containing any identified trees, it means for the zones where the field-measured and identified trees can be paired (matched). For such lines in the table, the height

values are copied into the new fields, particularly the value from the “Height” field is copied to the “Height\_2” field and the value from the “MAX” field is copied to the “MAX\_2” field. Afterwards the difference of the values in these fields is counted and the result is saved in the “Diff\_2” field. This enables to calculate only the particular difference between the field-measured and tallest identified tree in a zone, whereas in the “Diff” field the values are counted even in the case that no tree was identified in the zone (it means such calculated value is equal to the value in the “Height” field). These calculations are necessary for the ensuing computations.

In the following part the tool performs required mathematical and statistical calculations focusing on the paired trees. First of all the NumPy arrays are made from the “Height” field and the “MAX” field using the “FeatureClassToNumPyArray”. As says the instrument Help, Numerical Python (NumPy) is a fundamental package for scientific computing in Python, including support for a powerful N-dimensional array object. NumPy provides an avenue to perform complex mathematical operations and is part of the ArcGIS software installation. Table and feature classes can be converted to and from NumPy arrays using functions in the data access (arcpy.da) module.

The number of field-measured trees is then counted as the length (number of records) of the array made from the “Height” field. The number of identified trees falling into the Thiessen polygons (and thus being considered for the comparisons) is then counted as the sum of values in another array. This array is created from the “COUNT” field of the *ZonalStatsCounts* table.

The number of unmatched trees, i.e. the field-measured trees having no identified tree in their surroundings (in the corresponding Thiessen polygon) is then counted as the sum of values in an array made from the “No\_Max” field in the *Identified* feature class table. Then the number of matched trees, i.e. field-measured trees paired with some identified tree present in their Thiessen polygon, is calculated as the difference between the number of field-measured trees and number of unmatched trees. Afterwards also the percentage of matched trees out of the number of all field-measured trees is counted.

The important value for later results assessment is the number of redundant trees. Redundant are considered the identified trees, which were not paired with any field-measured tree. It is counted simply as the difference between the number of identified trees and the number of matched trees.

Subsequently the tool calculates the Mean Absolute Error (MAE) as an average of absolute value differences between field-measured and calculated tree heights. MAE measures how far predicted values are away from observed values. It is calculated using the equation

$$MAE = \frac{1}{n} \sum_{i=1}^n |e_i|$$

where  $n$  is the number of observations and  $|e_i|$  is the absolute value of the residual, calculated as

$$|e_i| = |y_i - y'_i|$$

where  $y_i$  is the predicted value and  $y'_i$  is the observed value. The sum divided by the number of observations then gives the final equation

$$MAE = \frac{1}{n} \sum_{i=1}^n |y_i - y'_i|$$

The mean absolute error is on same scale of data being measured. To calculate the MAE within the UAV Forest Explorer a new array is created. This array comes from the “Abs\_Diff” field in the *Joined* table, which contains the absolute values of differences between the heights of field-measured and matching identified trees counted for each record. Then a sum of the values in this array is calculated and divided by the number of observations (i.e. by the number of records in the array). The result, similarly as the resulting values of most of the following calculations is then rounded to three decimal places.

As the next statistics the Root Mean Square Error (RMSE) is calculated from the differences between field-measured and calculated tree heights. The RMSE is a quadratic scoring rule which measures the average magnitude of the error. The differences between forecast (predicted values) and corresponding observed values are each squared and then averaged over the sample. Finally, the square root of the average is taken. As the square root of the variance of the residuals, RMSE can be interpreted as the standard deviation of the unexplained variance, and has the useful property of being in the same units as the response variable.

Since the errors are squared before they are averaged, the RMSE gives a relatively high weight to large errors. This means the RMSE is most useful when large errors are particularly undesirable (Meloun & Militký 2004, Song et al., 2015). The RMSE is calculated according the following equation

$$RMSE = \sqrt{\frac{1}{n} \sum_{i=1}^n (y_i - y'_i)^2}$$

where  $n$  is the number of observations,  $y_i$  is the predicted value and  $y'_i$  is the observed value.

To calculate RMSE in the UAV Forest Explorer a new array is created. This time the “Diff\_sq2” field from the *Joined* table is used. This field contains the calculated squares of the residuals, i.e. of the differences between measured and calculated heights of paired trees. Similarly like in the previous case, the sum of the values in this array is divided by the number of records in it. Afterwards the square root of this value is taken and the result is rounded to three decimal places.

To quantify the linear correlation between the measured and calculated tree heights another statistics is used. Particularly it is the Pearson’s Correlation Coefficient (or the Pearson Product-Moment Correlation Coefficient), which is usually denoted by the letter  $r$  when applied to a sample. It is basically a numerical measure of the strength and direction of linear relationships between pairs of continuous random variables. In other words it is a quantity that gives the quality of a least squares fitting of the predicted data to the original data.

It, can take a range of values from -1 to +1 where the value  $r = 1$  means a perfect positive correlation and the value  $r = -1$  means a perfect negative correlation. A value of 0 indicates that there is no association between the two variables. It is independent of the units of measurement (Meloun & Militký, 2004 and 2006; Drápela, 2000 and 2002; Litschmannová, 2012; Blašková et al., 2009). The coefficient is computed as the ratio of covariance between the variables to the product of their standard deviations, as can be seen in the following equations according to Drápela, 2002 and Litschmannová, 2012

$$r_{y_1y_2} = r_{y_2y_1} = \frac{cov_{y_1y_2}}{S_{y_1} \cdot S_{y_2}}$$

where  $cov_{y_1y_2}$  is the covariance, which is calculated as

$$cov_{y_1y_2} = \frac{1}{n-1} \sum_{i=1}^n (y_{1i} - \bar{y}_1) \cdot (y_{2i} - \bar{y}_2)$$

where  $n$  is the number of observations,  $y_1, y_2$  are the continuous random variables and  $\bar{y}_1$  and  $\bar{y}_2$  are mean values calculated as

$$\bar{y}_1 = \frac{1}{n} \sum_{i=1}^n y_{1i} \quad , \quad \bar{y}_2 = \frac{1}{n} \sum_{i=1}^n y_{2i}$$

Correlation coefficient is thus a standardized (normalized) covariance. The equation then looks as follows

$$r_{y_1y_2} = \frac{1}{n-1} \sum_{i=1}^n \frac{(y_{1i} - \bar{y}_1)}{\hat{S}_{y_1}} \cdot \frac{(y_{2i} - \bar{y}_2)}{\hat{S}_{y_2}}$$

where  $\hat{S}_{y_i}$  for  $i = 1, 2$  is a point estimate of standard derivation according to the following relation

$$\hat{S}_{y_i}^2 = \frac{\sum_{j=1}^n (y_{ij} - \bar{y}_i)^2}{n-1}$$

That together gives the following complete equation

$$r_{y_1y_2} = \frac{\sum_{i=1}^n (y_{1i} - \bar{y}_1) \cdot (y_{2i} - \bar{y}_2)}{\sqrt{\sum_{i=1}^n (y_{1i} - \bar{y}_1)^2 \cdot \sum_{i=1}^n (y_{2i} - \bar{y}_2)^2}}$$

To incorporate the calculation of the Pearson's Correlation Coefficient into the UAV Forest Explorer, the "CorrCoef" command is called out of the NumPy package. Two arrays are provided as the inputs to the command, particularly arrays previously made from the "Height" field and from the "MAX" field of the *Joined* table. The resulting value of the coefficient is then rounded to three decimal places.

When the Pearson's Correlation Coefficient is calculated, there should be performed also a significance test which enables to decide whether, based upon the processed sample, there is a sufficient evidence to suggest that linear correlation is present in the population.

For this purpose the null hypothesis is to be tested against the alternative hypothesis. The null hypothesis says that there is no linear correlation in the population ( $H_0 : \rho = 0$ ), whereas the alternative hypothesis says there is linear correlation ( $H_1 : \rho \neq 0$ ). The t-test is used to establish if the correlation coefficient is significantly different from zero, and, hence that there is evidence of an association between the two variables. The significance of the correlation coefficient is tested using the following equations (Bedáňová & Večerek, 2007; Drápela, 2002)

$$t = \frac{|r|}{s_r}$$

where  $r$  is the calculated Pearson's Correlation Coefficient and  $s_r$  is the standard error of the correlation coefficient, which is calculated as

$$s_r = \sqrt{\frac{1 - r^2}{n - 2}}$$

where  $n$  is sample size (i.e. number of observations) and  $n - 2$  are degrees of freedom of the Student's t-distribution. When implemented to the first equation the result is following

$$t = \frac{|r| \sqrt{n - 2}}{\sqrt{1 - r^2}}$$



This mathematical equation is implemented also in the UAV Forest Explorer to count the significance of the ascertained correlation coefficient. The calculated test criterion  $t$  is then compared with the critical values of the t-statistic for significance level  $\alpha = 0.05$  (i.e. for 95% confidence interval) for the two-tailed test. Simplified t-table with relevant critical values corresponding to particular degrees of freedom was inserted to the source script for this purpose.

The significance of the  $r$  value is then evaluated as follows. If the calculated  $t$  value is smaller than the corresponding critical value, the null hypothesis cannot be rejected and the counted correlation coefficient is considered to be statistically insignificant. On the contrary, if the  $t$  value is larger than the appropriate critical value, the null hypothesis is rejected and the alternative hypothesis, saying that  $r$  is sufficiently different from zero, is accepted. In this case the calculated correlation coefficient is considered statistically significant. This is how the calculated value of the Pearson's Correlation Coefficient is evaluated and according to the described workflow receives either the label "Yes" for being statistically significant or "No" for being statistically insignificant.

Amongst the other statistics, also the Coefficient of Determination (R-squared) is calculated, as an important output of regression analysis, being a measure of how well the regression line represents the data. It is interpreted as the proportion of the variance in the dependent variable that is predictable from the independent variable. The Coefficient of Determination (denoted by  $r^2$  or  $R^2$ ) is the square of the correlation ( $r$ ) and expresses the strength of the linear association between predicted  $y$  scores and original  $y$  scores; thus, it ranges from 0 to 1.

An  $R^2$  of 0 means that the dependent variable cannot be predicted from the independent variable. An  $R^2$  of 1 means the dependent variable can be predicted without error from the independent variable and indicates that the model explains all the variability of the response data around its mean. Since  $R^2$  represents the percentage of the response variable variation that is explained by a linear regression model, its value of 0.65, for example, means that 65 % of the dependent variable is predicted by the independent variable. Since the Coefficient of Determination is the ratio of the explained variation to the total variation, it can be calculated as follows (Drápela, 2002; Meloun & Militký, 2006)

$$R^2 = \frac{S_{y_2'}^2}{S_{y_2}^2}$$

where  $S_{y_2'}^2$  is the variance explained by the regression model, i.e. variability of the regression model points around the mean. It is also called the regression (or explained) sum of squares and is calculated in the following way

$$S_{y_2'}^2 = \frac{\sum_{i=1}^n (y_{2i}' - \bar{y}_2)^2}{n}$$

and  $S_{y_2}^2$  is the total variance (total sum of squares) of the experimental points around the average, calculated as

$$S_{y_2}^2 = \frac{\sum_{i=1}^n (y_{2i} - \bar{y}_2)^2}{n}$$

where in both cases  $n$  is the number of observations,  $y_{2i}'$  is the regression model value for the  $i$  observation,  $y_{2i}$  is the original data value for the  $i$  observation, and  $\bar{y}_2$  is the mean of the observed data. The Coefficient of Determination can be expressed also using the sum of squares of residuals (also called the residual sum of squares), as follows

$$R^2 = 1 - \frac{S_{y_1 y_2}^2}{S_{y_2}^2}$$

where  $S_{y_1 y_2}^2$  is the sum of squared errors  $e$ , which is calculated in the following way

$$S_{y_1 y_2}^2 = \frac{\sum_{i=1}^n (y_{2i} - y_{2i}')^2}{n} = \frac{\sum_{i=1}^n e_i^2}{n}$$

The  $R^2$  can be then calculated in both ways, as shown here

$$R^2 = \frac{S_{y_2'}^2}{S_{y_2}^2} = 1 - \frac{S_{y_1 y_2}^2}{S_{y_2}^2}$$

In the UAV Forest Explorer the Coefficient of Determination is calculated as the second power of the Pearson's Correlation Coefficient. The resulting value is then rounded to three decimal places.

Up to this point, the performed calculations were usually taking all the records in the processed tables into account. This means, that records for matched trees, together with records for field-measured trees which were not paired with any identified tree, were utilized in the calculations. That results in the fact, that the larger is the number of field-measured trees without any matching tree, the more are the calculated statistics influenced by the error originating in the records of these trees. To facilitate evaluation of the proper values without this influence, the subsequent calculations within the UAV Forest Explorer are focused on processing only the records of paired trees.

First of such calculations is an ascertainment of the difference in heights of field-measured trees and tallest identified trees matched to them within their zones. As described before, the fields "Height\_2", "MAX\_2" and "Diff\_2" contain only the values for paired trees. The last field contains the value of difference of the two previous fields ("Diff\_2" = "Height\_2" - "MAX\_2"). The record lines of the zones where the trees were not paired, contain "<Null>" values.

To utilize these fields in the demanded statistical calculations, NumPy arrays are created from all of them. Subsequently a sum of values in the array made from "Diff\_2" field is created and divided by the number of records in it. This gives the mean difference between the heights of field-measured and identified trees which were matched to them. Since this difference is counted without raising to a power or without putting to absolute values, the resulting value gives also the information about the tendency of the identified trees to be on average taller (negative value) or smaller (positive value) than the field-measured trees.

In the next step the Pearson's Correlation Coefficient is calculated for the paired trees only. The arrays made from the "Height\_2" field and "MAX\_2" field are utilized for this purpose. Again the "CorrCoef" command from the NumPy package is called to calculate the coefficient properly. Consequently the Coefficient of Determination is ascertained for paired trees. It is calculated as the second power of the just gained Correlation Coefficient.

Then the average height of field-measured trees (paired and unpaired together) is computed. The sum of values in the array made from "Height" field is created and then divided by the number of field-measured trees. The same array is then utilized to calculate also the Standard Deviation of the field-measured heights.

Standard Deviation determines the spread of scores within a set of data. According to Drápela (2000) and Meloun & Militký (2006) Standard Deviation is statistic used as a measure of the dispersion or variation in a frequency distribution, equal to the square root of the arithmetic mean of the squares of deviations of the observed values from their mean. Contrary to variance, which squares the units, the advantage of Standard Deviation, is that it preserves the units of the spread keeping them the same as the original data units. Standard deviation is calculated as the square root of the variance. The formula of the variance of a sample is following

$$s^2 = \frac{1}{n-1} \sum_{i=1}^n (y_i - \bar{y})^2$$

where  $n$  is the sample size (number of elements in the sample),  $y_i$  is the  $i^{th}$  element from the sample and  $\bar{y}$  is the sample mean. After the root extraction, the equation for the Standard Deviation of a sample looks as follows

$$s = \sqrt{s^2} = \sqrt{\frac{1}{n-1} \sum_{i=1}^n (y_i - \bar{y})^2} = \sqrt{\left( \frac{1}{n-1} \sum_{i=1}^n y_i^2 \right) - \frac{1}{n} \left( \sum_{i=1}^n y_i \right)^2}$$

In the environment of the UAV Forest Explorer the Standard Deviation is calculated utilizing the “STD” command from the NumPy package using the mentioned array. At this point the calculations based on the Individual Tree Approach are completed. Subsequent calculations are then performed within the scope of the Area-Based Approach, which means regardless of the pairing of trees. For this purpose the “*ZonalStatsUnpaired*” table is used, since it contains the summary statistics calculated for all trees identified within the area of field measurements. First of all the value from the “MEAN” field is utilized, as it represents the average height of identified trees. Then the value in the “STD” field is used for the Standard Deviation of calculated heights of these identified trees.

In the next step the difference between the counts of identified and field-measured trees is calculated. This value is important, since it says how close the number of automatically identified trees is to the number of field-measured trees. The positive value means that there were identified more trees than were

measured in the field, negative value says that the tool identified less trees than were measured in the area of interest. The closer the values is to zero, the better is the result of the particular tool run concerning the number of identified trees.

Subsequently also the difference between the average heights of identified and field-measured trees is calculated. The mean height of field-measured trees is subtracted from the mean height of trees identified within the *BoundingBox*. The positive value means that the average height of identified trees is larger than the average height of field-measured trees, and vice versa. In this case the values close to zero stand for the potentially right results concerning the height of automatically identified trees within the ABA. Also this output value, similarly as the values resulting from previous computations, is rounded to three decimal places.

At this point all the calculations performed within the particular FS cycle are completed. All the appropriate computed values ascertained during this cycle are to be filled into the “*X\_Comparisons\_X*” table in the next step. The “InsertRow” command within the “InsertCursor” instrument is used to add a new row in the table and to fill the proper values into the activated fields. All 21 previously created fields are utilized in this step. The names of these fields and the content they stand for is following:

“FileName” for the name of the processed file created within individual settings.

“Measured” for the number of field-measured (FM) trees.

“Identified” for the number of trees identified within Thiessen polygons.

“Unmatched” for the number of FM trees without any matching identified tree.

“Matched” for the number of FM trees matched with (i.e. paired to) identified trees.

“Matched\_Pct” for the percentage of matched trees from all FM trees.

“Redundant” for the number of redundantly identified trees (not matched).

“\_MAE\_” for the Mean Absolute Error for FM and counted heights.

“\_RMSE\_” for the Root Mean Square Error for FM and counted heights.

“Corr\_Coef” for the Pearson’s Correlation Coefficient for FM and counted heights.

“R\_squared” for the Coefficient of Determination for FM and counted heights.

“Stat\_Sig\_R” for the Statistical Significance of the Pearson’s Correlation Coefficient.

“Mean\_Diff\_MT” for the Mean Difference between average values of FM and counted heights for Matched Trees (MT) only.

“Corr\_Coef\_MT” for the Pearson’s Correlation Coefficient for Matched Trees only.

“R\_squared\_MT” for the Coefficient of Determination for Matched Trees only.

“Mean\_FM\_Ht” for the Mean height of FM trees.

“SD\_FM\_Ht” for the Standard Deviation of heights of FM trees.

“Mean\_IT\_Ht” for the Mean height of Identified Trees (IT).

“SD\_IT\_Ht” for the Standard Deviation of heights of identified trees.

“Count\_Diff” for the Difference between count of identified and FM trees.

“Height\_Diff” for the Difference between mean height of identified and FM trees.

At this moment the *X\_Comparisons\_X* table is updated, since new row was added and filled with appropriate values. Each such row contains values calculated under the specific settings of the UAV Forest Explorer. Just one row can be added within a single FS cycle. The number of rows in the table basically corresponds to the number of combinations of the various tool settings, that means to the number of iterations (and particularly sum of individual FS cycles) carried out within the tool run.

At the end of the FS cycle the due cycle counters are updated. Then, either the following FS cycle begins, or the particular series of FS subcycles ends (subcycles denote FS cycles performed within a single IM cycle). Since the whole FS cycle is enclosed within the IM cycle, the tool processing gets again to the IM cycle, when the last FS subcycle is finished. Here only one more operation can be executed, namely partial deleting of the working datasets.

If the option to *Delete Working Datasets?* was checked by the user in the initial settings of the UAV Forest Explorer, the tool does not delete the data all at once at the end of the run, but it deletes the data continuously, just at the end of each IM cycle. The tool at first lists separately all the feature classes and rasters which were stored in the *WorkingData.gdb* file geodatabase during the IM cycle. Then it applies the “Delete” command to remove them permanently. The geodatabase is then empty and is ready to accommodate the new datasets created within the subsequent IM cycle, if there is any. In the case that the *Delete Working Datasets?* option was not selected by the user, all the datasets saved in the *WorkingData* geodatabase remain stored there.

As the last step within the IM cycle, the appropriate cycle counters are updated. Then, either the particular loop continues and another IM cycle begins, or if no more Interpolation Methods should be applied within the actual CS cycle, the loop is finished. Because the whole IM cycle is enclosed within the CS cycle, the tool processing gets into the CS cycle again. Here are also the appropriate cycle counters updated. Before the end of the CS cycle, one more process can be

performed. When the option to *Progressively Reduce Focal Statistics Subcycles?* is checked in the initial settings, the tool adjusts the proper variables to fulfil this requirement.

When large number of various combinations is to be tested based on the user-defined settings, that means that plenty of iterations should be calculated, the reduction of the FS cycles can be welcome. Usually not all combinations of Cell Size values and FS Circle Radius values are really meaningful and therefore desired. Especially the combinations of large Cell Sizes and large FS Circle Radiuses can be found inessential (such combinations generally lead to identifying too few trees). Since processing of these combinations consumes standard computing power and time, but leads to inapplicable results, it can be highly useful to avoid them. This option therefore gives the possibility to reduce the number of redundant FS cycles and thus to significantly decrease the computation time.

Technically it works in the way, that when the reduction option is checked, the tool progressively reduces the value of *Focal Statistics Circle Radius Max* for the cycles with largest Cell Sizes. When the particular conditions are met, its value is reduced by 1 cell at the end of each Cell Size cycle. At the same time the value can never be reduced below 1 cell. It is ensured by the fact, that the reduction begins only in such CS cycle, when the number of remaining CS cycles is smaller than the number of FS subcycles (number of FS subcycles is the difference between *FS Circle Radius Max* and *FS Circle Radius Min* defined by the user, that means it is the original number of FS cycles to be carried out within each IM cycle).

In other words, when the tool processing reaches the point, that the number of CS cycles, which remain to be done until the end of the tool run, is smaller than the original number of the FS subcycles, the value of *FS Circle Radius Max* is reduced by one cell. It means that in the subsequent CS cycle the number of FS cycles performed within each IM cycle is of 1 value smaller than in the previous CS cycle. In the same manner the value of *FS Circle Radius Max* can be reduced within each CS cycle potentially up to the value of 1 cell applied within the last CS cycle.

In the case that the number of CS cycles, meant to be executed based on the initial settings, is from the beginning smaller than the number of FS subcycles, the reduction begins already at the end of the first CS cycle (and is manifested within the IM cycles of the second CS cycle). In such case also the value of smallest *FS Circle Radius Max* is larger than 1 cell. For example when 4 CS cycles are to be carried out and 10 FS subcycles are demanded to be calculated, the actual number of FS subcycles performed within the IM cycles of the last CS cycle is 7.

The final number of FS cycles reduced by application of this option within the whole tool run then depends also on the number of IM cycles executed within each CS cycle. If there are for instance all 8 interpolation methods demanded to be applied, 8 IM cycles are carried out within each CS cycle. If there was no reduction demanded in the previous example, 10 FS subcycles would be performed within each IM cycle. That leads into executing  $4 \times 8 \times 10$  cycles, which is together 320 FS cycles.

If the cycles reduction option was checked, the number of performed cycles is following: 8 x 10 cycles in the first CS cycle, 8 x 9 cycles in the second CS cycle, 8 x 8 cycles in the third CS cycle and 8 x 7 FS cycles in the fourth CS cycle. That makes together 272 FS cycles, which means that 48 cycles were avoided thanks to the reduction in this case. More examples for better understanding the principles of the FS subcycles reduction are provided in the Appendix 3 - User Guide for the UAV Forest Explorer.

After the potential variables and counters adjustment in the scope of the described reduction option, the CS cycle reaches its end. Then either the next CS cycle starts from the beginning, or if no more CS cycles are to be carried out and all iterations are finished, the tool processing gets out of all of the loops.

Subsequently the counts of all executed iterations within different cycles are recapitulated. The tool puts the numbers of performed CS, IM and FS cycles into the messages shown in the Progress Dialog Box and compares them with the predicted values. The actual total numbers and predicted numbers should correspond to each other. If some difference appears by chance, it can be caused most likely by rounding of certain values of Cell Sizes, since python manages some integers and float numbers in a specific way. Nevertheless in an overwhelming majority of cases the corresponding values should match precisely. If the reduction option was utilized, the tool also writes out the number of potential FS cycles to be performed without reduction and the actual number of FS cycles avoided thanks to the reduction.

In the ensuing step the tool exports the *X\_Comparisons\_X* table to an \*.xls format. This can be done only if the tool calculations results were compared with the ground truth data and the table thus exists. The "TableToExcel" conversion tool is applied for this purpose. The name of the exported table is "*Comparisons.xls*" and it is saved in the *Tables* folder. From here it can be easily accessed using e.g. Microsoft Office Excel software.



The very last process potentially executed within the UAV Forest Explorer is the deletion of the *WorkingData.gdb* file geodatabase. This can be done only if the *Delete Working Datasets?* option was applied in the initial settings. Since the data stored in the geodatabase were deleted continuously in such case, now only the empty geodatabase is to be removed. The “Delete” command is used to do this job and the whole geodatabase is erased from the Workspace Folder.

At this point the whole run of the UAV Forest Explorer is completed and the tool finishes its processing.

#### **4.7.4. Specific Workflow Applied in this Study**

##### **4.7.4.1. Running the Tool**

The particular settings and procedures utilized in this work are described in this chapter. The tool was used to process the data from the twenty examined study plots, to identify trees in them and to compare the results with the field-measurements data. Concerning the initial settings and data inputs, the applied entries were following.

As a *Workspace Folder* usually a newly created folder, named according to the study plot under investigation, was utilized. Also the *Filename* corresponded to the particular study plot and reflected the locality it was situated in, or the typical properties of the studied forest stand (for instance the prevailing species, the characteristics of the terrain, etc.), so that the certain plot could be easily recognised according to that name. When applying the ground truth data, the filename also contained some abbreviation to specify, if all field-measured trees were processed, or the data without suppressed trees were utilized.

As a *Surface Point Cloud \*.las File* a point cloud created from the photogrammetric processing of the UAV-based images in the Agisoft Photoscan software (See chapter 4.6.2. Photogrammetric Image Processing for more information) was utilized each time. The \*.las file was prepared to cover just the area of interest, to avoid having uselessly large datasets. For the *Las Dataset Name* usually the default “*LasDataset*” designation was maintained, if no experiments with the Las Dataset creation were carried out.

For the *Digital Terrain Model (DTM)* field a Digital Terrain Model of the

Czech Republic of the 5<sup>th</sup> generation (DTM 5G) was provided each time (the DTM is described in the chapter 4.6.3. Auxiliary data). As also described earlier, the spatial resolution of the utilized DTM was 0.2 x 0.2 and 0.5 x 0.5 metres, depending on the terrain conditions. When the UAV Forest Explorer tool was in its early stage of the development, the DTM of the 5<sup>th</sup> generation was not available for the area of Training Forest Enterprise Masaryk Forest Křtiny yet. Therefore the tool was tested on the model of the 4<sup>th</sup> generation (DTM 4G), with 5 x 5 m spatial resolution, which was available that time.

The option to *Refine DTM Cell Size* to a new finer value was therefore utilized only within testing of the tool during its development, but not during the full operation, when the DTM 5G with sufficient spatial resolution was employed on every of the twenty processed study plots. Nevertheless this option is still meaningful for working on areas where no such detailed DTM is available.

Concerning the settings for the limitations of the tool cycles, i.e. setting of the *Rasters Cell Sizes*, *Interpolation Methods* and *Focal Statistics Circle Radiuses*, the tool was usually applied in a two-phase way as follows.

1) First of all, when a new forest stand was taken for processing, just a basic calculations were used to find the most suitable range of Cell Size values for the particular area. The *Rasters Cell Size Min* was usually set to 0.1 m, *Rasters Cell Size Max* approximately to 1.5 m for mainly coniferous forests and around 2.0 m for mainly broadleaf forests, and *Rasters Cell Size Step* was set to 0.1 m. Then only one *Interpolation Method* (usually Binning with Average cell assignment type) was selected. *Focal Statistics Circle Radius Min* and *Max* values were then coincidentally set to the value of 1 cell, to ensure that only one FS subcycle will be applied. Then a path to a folder containing sample layer files was given in the *Layer Files Folder* field. The field-measurements data were not necessarily provided. The *Delete Working Datasets?* option was not checked, to maintain the working rasters and feature classes, for the case of any inspection needs.

With these settings the tool was run and performed usually between 15 to 20 iterations (based on the applied CS values range) graded by 10 centimetres of the rasters spatial resolution. Then usually the resulting layer files were evaluated visually and compared between each other. The main goal of such assessment was to find the upper limit of the applied Cell Size values, which are still meaningful for the particular forest stand.

2) Based on the previously executed primary investigation, the maximal relevant value of the Cell Sizes was found out. Then the full operation of the tool could be started. The Workspace Folder and Filename were potentially adjusted for the new run, the point cloud file and DTM dataset were provided the same as before. The limiting values defining the tool cycles were then set in the following way. The *Rasters Cell Size Min* was usually set to 0.05 m, *Rasters Cell Size Max* was set for instance the value of 1.0 m (based on the particular ascertainment from the basic run), and the *Rasters Cell Size Step* was each time set to 0.05 m.

Then all 8 *Interpolation Methods* were selected. The *Focal Statistics Circle Radius Min* was ordinarily set to 1 cell and *Focal Statistics Circle Radius Max* was usually set to the value of 10 cells. The option to *Progressively Reduce Focal Statistics Subcycles* was selected, to decrease the computing time. Then usually a square polygon surrounding the area of the certain study plot was provided as the *Delimitting Sub-Area*. The *Layer Files* were normally not applied in this second full run. On the contrary the option to *Compare Data with Field-Measured Heights* was employed and the *Field Measurements Data* were provided for the particular study plot in the required form. The last option - to *Delete Working Datasets* was also utilized in the vast majority of cases. The full operation run was then started with these initial settings.

The settings applied on the different forest stands varied mainly in the range of Cell Size values (particularly in the used *Max* value). The other entries were usually applied similarly on all the twenty study plots. Based specifically on this described settings of the full operation run, the tool performed just 1240 iterations. Together 360 FS cycles were avoided thanks to the reduction (otherwise 1600 iterations were to be performed).

The tool was applied on each of the twenty study plots twice, and in some cases even three times. The first run was carried out using the field-measurements data with no adjustments, that means with all the trees meeting the elemental conditions, which were measured in the field. Nevertheless these data often contained also thicker understorey and suppressed main-storey trees, which could not be detected by the tool. The reason was the simple fact, that their apexes did not penetrate sufficiently into the canopy layer and were overshadowed by taller trees. Since the crowns of these trees did not constitute a fully-fledged part of the canopy, they could not be represented in the photogrammetrically acquired point cloud or in the subsequent DSM either.

For this reason, the second run of the tool was each time executed using the field-measurements data without the understory and suppressed trees. The trees to be excluded were selected mainly based on the histogram of the field-measured height data (Figure 63.) in the combination with the visual assessment of the DSM (the one created in the Agisoft PhotoScan software from the dense point cloud data) and RGB/CIR true orthophoto images of the forest stand. For this reason a copy of the point feature class representing the field-measurement data was created and from this layer the selected trees were removed. Such feature class was then provided as a ground truth in the second run of the tool at each plot.

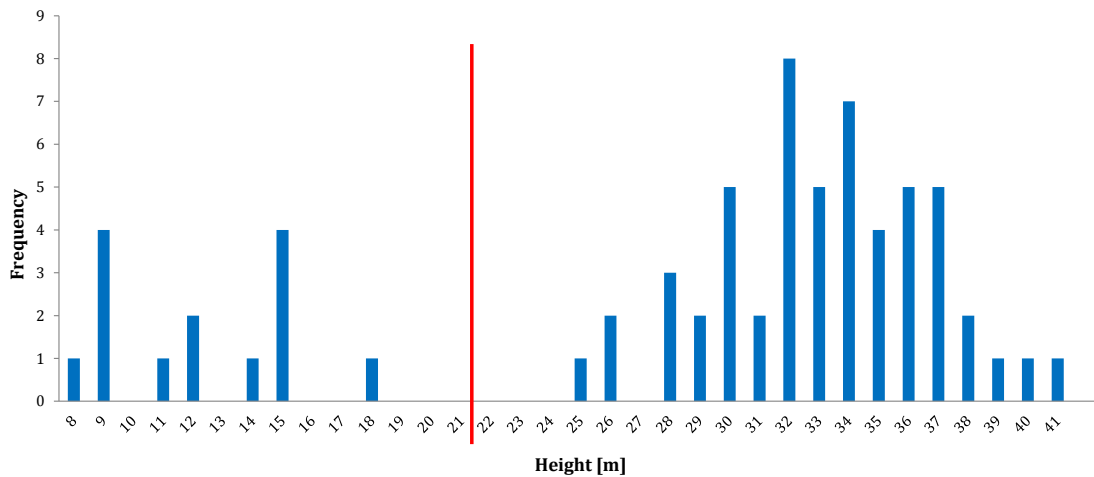


*Fig. 63. Histogram of field-measured height values in a particular study plot. The red line shows the obvious division between the understory and suppressed trees (left) and the trees forming the main canopy (right).*

On several plots even a third run of the tool was executed. It was on the plots, where a significant portion of the present tree species constituted mature pines (in our case between 90 and 100 years old). These trees are typical for their often tendency to have highly leaning or kind of twisted trunks. That causes, that the field-measured position of the trunk base often does not correspond to the position of the tree apex. Particularly three study plots were affected by this characteristic behaviour. On these plots the direction and rate of leaning of each tree was recorded during the field measurements.

Then during the data processing, another copy of the field-measurements data was created (of the version already without suppressed trees). In this

dataset a manual modification of positions of the concerned trees was carried out, based on the leaning notes from the field investigation and based on the detailed inspection of the orthophoto images and DSM of the forest stand (Figure 64.). Then, the third run of the tool was executed using this modified feature class as the field-measurements data in the case of the three particular study plots. This enabled to find out, if such modification has any influence on the results of the trees identification and heights assessment process.

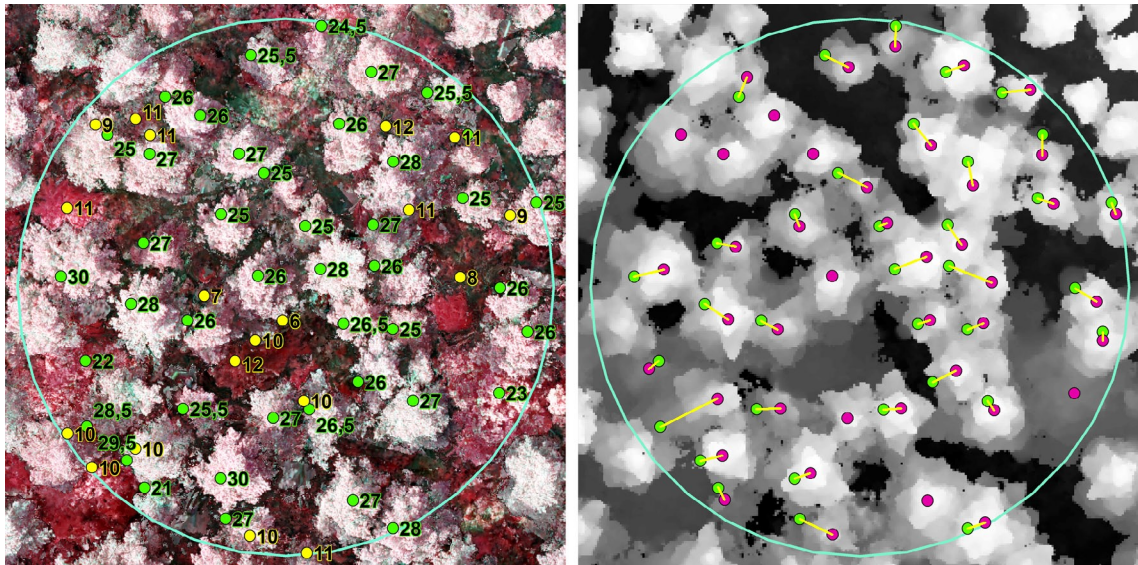


*Fig. 64. The process of tree positions modification. Above the CIR image on the left are shown the original positions and heights of field-measured trees. Green points represent the main-storey trees, yellow points the suppressed and understorey trees. Above the DSM on the right image can be seen the same main-storey trees (green points) and these trees after the modification, placed on the proper positions of tree apexes (purple points). The yellow lines show the links between corresponding trees. Where the line is missing the position of the tree was not modified.*

Based on the described workflow, the tool was run twice on 17 study plots and three times on 3 study plots. That makes together 43 runs. When the average number of iterations performed within one tool run was around 900 (the value varied depending on the applied *Rasters Cell Size Max* value), the total number of iterations carried out within this work was close to 40 000.

The tool within these runs created series of outputs stored mainly in the *IdentifiedTrees.gdb* and *Comparisons.gdb* file geodatabases and also in the *Tables* folders. Concerning these results, predominantly the *...Comparisons.xls* table was further deeply examined, since it contained together all the important characteristics of the trees identified within each single iteration.

#### 4.7.4.2. Assessing the Tool Outputs

The overall results of each tool run stored in the *Comparisons.xls* table were further thoroughly studied in the Microsoft Excel software. As already explained, for each of the twenty plots more than one tool run was performed. That resulted in the creation of 2 Comparisons tables for 17 study plots and creation of 3 Comparisons tables for 3 study plots. The most suitable results meeting particular conditions were searched for each plot and then stored in separate “Best Results” tables. These resulting 43 tables can be seen in Appendix 4. The tables have slightly adjusted names of some columns compared to the original Comparisons tables, but the selected records contain the same values as the source tables. The logic used to select the best results, or in other words used to find the settings giving the results with most satisfactory specific values is described in the following text.

The records in the Comparisons tables were assessed both, on the ITA basis and also on the ABA basis. In both cases the fundamental quantity taken into account was the difference between count of identified and count of FM trees. This value calculated for each iteration was stored in the “Count\_Diff” field. The value was important for ABA as well as the ITA method since results giving very low errors or showing high correlation between calculated and field-measured heights would be meaningless, if the number of automatically identified trees would be just a little portion, or on the contrary would be several times higher, than the number of FM trees.

Concerning the ITA method, the results were divided into two groups based on the count difference for that reason. The first group was for the best results the count difference of which was in the range of -5 to +5 trees. This category was called “Smaller Range”. The second group called “Larger Range” then contained also results the count difference of which could be larger. The range varied in the case of tables resulting from the tool runs where all FM trees were utilized as the ground truth and in the case where reduced number (and also reduced number and modified positions) were applied as the ground truth during the tool run.

In the first case the Larger Range was with count difference between -30 % and +10 % of FM trees provided in the particular run. In the second case the lower limit of the range was also -30 % of the FM trees and the upper limit was +1.5 multiple of the difference between all FM trees measured on the plot and the reduced number of FM trees used in the specific run.

So for example if 80 trees were physically measured in the selected plot and 20 of them were found to be suppressed or understory trees and were removed from the ground truth data for the second tool run, the ranges used for outputs assessment were following: Smaller Range was from -5 to +5 trees of Count Difference, Larger Range was from -24 to +8 trees of Count Difference for all FM trees as the ground truth and from -24 to +30 trees of Count Difference for the reduced FM trees as the ground truth.

These ranges enabled to assess the outputs from two points of view. The first one evaluating only those results which maximally correspond with the number of identified trees to the number of FM trees (Smaller Range), the second one taking into account also the outputs with much less identified trees than is the number of corresponding FM trees (Larger Range). In the second case, if very good results appeared with up to 30 % less trees compared to the original ground truth dataset, it can suggest that a lot of trees in the area are suppressed and therefore cannot be detected by the tool.

The upper limits then give some tolerance to accept also results with slightly higher amount of identified trees. In the case of results from the runs with reduced number of FM trees the lower range of -30 % allows to incorporate also results indicating that even more trees could be removed from the ground truth data, and the upper limit of +1.5 multiple of the number of reduced FM trees then encompasses also the results calculated with number of identified trees similar to the number of FM trees before the reduction, also giving some tolerance.

Concerning the ABA the specific ranges used for outputs evaluation will be described later. At this point, the process of the most appropriate results selection is described, beginning with the ITA method. Since it may look complicated to process the large Comparisons tables efficiently, the applied workflow of assessing all the 43 tables is described in the following text.

The first aim was to find records with lowest number of FM trees which were not paired with any identified tree in each iteration, and at the same time with lowest number of excessively identified trees. For this purpose all the data in the processed table were sorted according to the “Unmatched” field first, and the records in this column were gradually coloured according to the particular demands. Similarly were treated also records in the “Redundant” field. They were also sorted ascending and gradually coloured. Both columns were then visually assessed, utilizing the applied colours as a support, and the records with lowest values together in both of them were highlighted.

In the next step all the records in the table were sorted ascending according to the “RMSE” field and the highlighted records with lowest values of RMSE were also coloured. Then the table was sorted descending according to the “Corr\_Coef” field and from the highlighted records those with the highest correlation coefficient were marked with a selected colour.

Subsequently from these preselected records meeting the described requirements, one compromise “the most ideal” record was selected. This record was selected as having the relatively lowest numbers of unmatched and redundant trees, lowest value of RMSE and highest value of correlation coefficient at the same time. Then this record was copied into the new Best Results table (see Appendix 4). Since the lowest possible numbers of unmatched and redundant trees were preselected, also the count difference between field-measured and identified trees stored in the “Count\_Diff” field was preferably as low as possible. Therefore the chosen record was stored in the new table into the Smaller Range section. The combination of both parameters, based on which the record was mainly selected, was given in the “Best Parameter” field as the “RMSE & R”.

In the next steps the other parameters in the scope of the Smaller Range were evaluated and sufficient records were selected. From the records with Count Difference in the range of  $\pm 5$  trees the one with smallest RMSE was chosen and copied into the appropriate field in the new table. Similarly also the record with the highest value of correlation coefficient was selected and put to the table in the line with “R” for the “Best Parameter”. All these described parameters were searched for only between the records whose correlation coefficient was statistically significant, if possible. That means that they contained “Yes” in the field “Stat\_Sig\_R”. If no such records were found to be relevant, the records with statistically insignificant R had to be chosen in some cases.

The last assessed parameter in the scope of the Smaller Range was the correlation coefficient calculated only for the matched trees. Therefore the records in the table were sorted descending according to the “Corr\_Coef\_MT” field and the one with highest value (and still only up to  $\pm 5$  trees of the Count Difference) was chosen and copied to the “R for MT” field standing in the “Best Parameter” section.

In a similar manner also the demanded parameters for the purposes of the Larger Range were searched. In this case the records with lowest RMSE, then highest correlation coefficient and then those with highest correlation coefficient for matched trees only, were selected and stored in the proper part of



the appropriate Best Results table. These records could be sometimes the same as the results in the Smaller Range, but often were these records different, since the range of Count Difference was much larger in this case, as described earlier. This enabled to evaluate also the results more varying in the number of identified trees and to subsequently allow to judge if the Larger Range enabled to find better results than the highly limiting Smaller Range.

Together 7 most satisfactory records were selected from each Comparisons table based on the ITA method, particularly 4 meeting the conditions of the Smaller Range and 3 suitable for the Larger Range. Subsequently the best results concerning the ABA were searched for. Also in this case the fundamental parameter was the Count Difference, since also now only the records with number of identified trees maximally corresponding to the number of field-measured trees were demanded. Therefore in the first stage only records with the difference of 0 trees were preselected, if such records were available.

The second parameter used for assessing the results was the difference between average height of FM trees and average height of appropriate identified trees. Therefore from the preselected records the one with lowest value in the "Height\_Diff" field was chosen. Such record was then copied into the Best Results table in the line having the "Count Diff (0)" stated as the Best Parameter.

If no record having zero Count Difference was present in the investigated Comparisons table, the record with lowest value of this difference was selected. If more records had zero or another smallest Count Difference and some of them had similar Height Difference, the one with smallest Standard Deviation of heights of identified trees (with lowest value in the "SD\_IT\_Ht" field) was chosen.

For the second most suitable result in the scope of ABA the acceptable Count Difference was enlarged from 0 to the range of  $\pm 1$  tree. Now in this range again the record with lowest Height Difference was searched. The best result was also copied in the appropriate table to the row having "Count Diff ( $\pm 1$ )" in the Best Parameter field. Both these described selected records were giving the information about the difference of average heights between FM and identified trees when the difference in their counts was minimal.

To give the information from the opposite point of view, it means to find what is the Count Difference when the Height Difference is the lowest, another selection was performed. For this purpose the record with the smallest Height Difference from all records in the table was chosen and copied into the Best Results table in

the line bearing "Height\_Diff" in the Best Parameter field. The Count Difference in such records can reach sometimes very extreme values.

The last parameter used to find the required records within the Comparisons tables was the Standard Deviation of heights of identified trees. The range of records suitable for selection had to fulfil the condition of having maximally  $\pm 1$  tree of Count Difference, if possible. Then the record with lowest value in the "SD\_IT\_Ht" field was located between these records and copied into the Best Results table into the row with corresponding name.

Together 4 records were selected from each Comparisons table in the scope of ABA and with the 7 records acquired in the scope of the ITA altogether 11 records were chosen as the most appropriate and stored in each Best Results table. The described process was applied on all 43 Comparisons tables gained during the previous UAV Forest Explorer runs. The resulting Best Results tables were then differentiated based on the numbers of study plots and also based on the form of the ground truth data provided for the calculations (All FM trees / Reduced number of FM trees / Reduced number of FM trees with modified positions). All these tables can be seen as Appendix 4.

## 5. Results

As the workflow in this study consisted of two fundamental parts, i.e. collecting of the field measurements ground truth data and collecting and processing of the data from the UAV, the results are also divided into such two groups, respectively.

### 5.1. Results of the Field Measurements

As described thoroughly in the chapter 4.3. Forest Stands Measurements, together 20 study plots in different forest stands and with diverse terrain and growing conditions was established and explored in detail within this study. The sizes of these circular study plots varied between 1000 m<sup>2</sup> and 3300 m<sup>2</sup>. Differing were also the counts of trees present at each study plot.

#### 5.1.1. Counts of Field-Measured Trees

Together 1446 trees was measured during the field measurements. All these trees were meeting the required conditions (explained in chapter 4.2. Specification of Study Plots). The number of trees present in individual study plots ranged between 60 and 110 trees. The relationship between the particular numbers of these field-measured trees, the diameter of each study plot and the age of the forests stand can be concluded from the Table 3. containing all these three parameters. The values combined into a single diagram are then visualized in the Figure 65.

*Table 3. Combination of the age of examined forest stands (in the year 2014), the diameter of each study plot and the number of trees being measured at each plot.*

<b>Plot Number</b>	<b>I.</b>	<b>II.</b>	<b>III.</b>	<b>IV.</b>	<b>V.</b>	<b>VI.</b>	<b>VII.</b>	<b>VIII.</b>	<b>IX.</b>	<b>X.</b>
<b>Stand Age [years]</b>	61	61	102	102	70	76	99	92	92	47
<b>Plot Diameter [m]</b>	35.68	35.68	40.68	40.68	35.68	35.68	64.82	43.70	43.70	35.68
<b>Number of Trees</b>	93	98	64	64	72	79	60	68	71	92
<b>Plot Number</b>	<b>XI.</b>	<b>XII.</b>	<b>XIII.</b>	<b>XIV.</b>	<b>XV.</b>	<b>XVI.</b>	<b>XVII.</b>	<b>XVIII.</b>	<b>XIX.</b>	<b>XX.</b>
<b>Stand Age [years]</b>	125	141	90	90	100	31	31	71	36	110
<b>Plot Diameter [m]</b>	50.46	43.70	39.09	39.09	39.09	35.68	35.68	42.22	35.68	40.68
<b>Number of Trees</b>	60	60	62	67	61	66	110	63	74	62

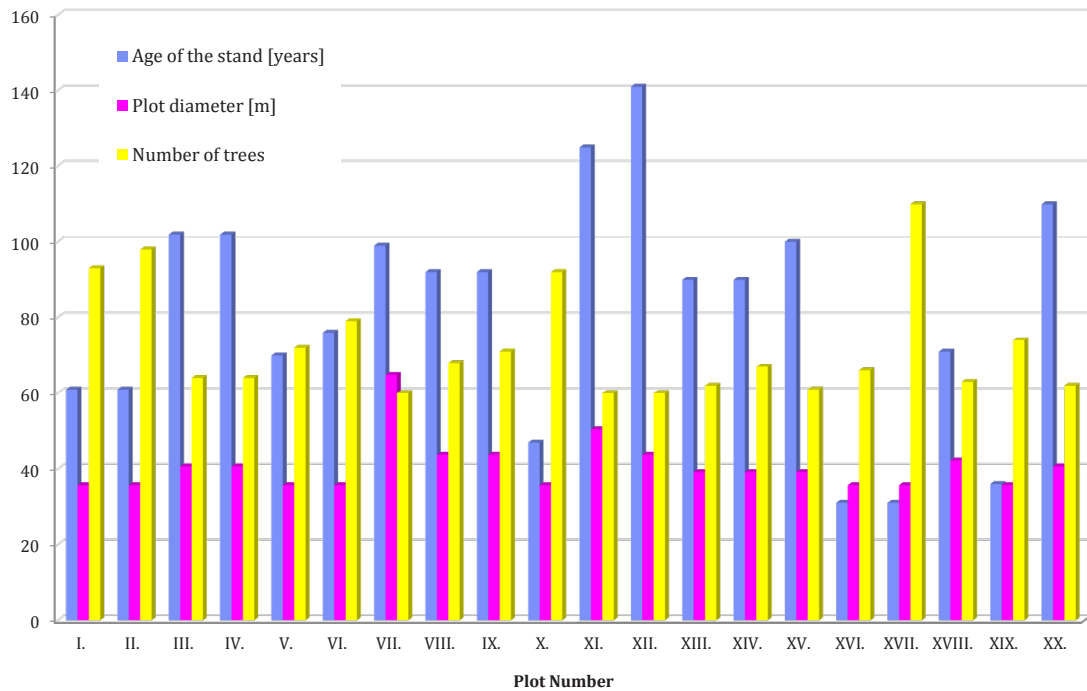


Fig. 65. Diagram showing the combination of the age of the investigated forest stands, the diameter of the study plots and the number of field-measured trees present at each study plot.

### 5.1.2. Forest Stands Composition

Different kinds of information about the trees within the study plots were gathered during the thorough field measurements. One of them was the data about the composition of the forest stands. The information about all the various tree species which were recorded at each plot is summed in the following tables and graphs.

The first table (Table 4.) contains the summarization of broadleaf and coniferous trees present on the 20 study plots together with the abbreviation of the prevailing type. When at least 75 % of trees in a study plot were broadleaf, they received letter “B”, similarly plots with more than 75 % of conifers received the abbreviation “C”, the remaining study plots were then marked with letter “M” standing for mixed forest.

As is clear from the table, from the total number of 1446 trees measured during the field measurements 684 trees were broadleaf and 762 trees were coniferous. The distribution of broadleaf and coniferous trees in particular study plots is visualised in the Figure 66.

Table 4. Summarized amount of broadleaf and coniferous trees at each study plot. The last column contains the abbreviations of prevailing trees, where B stands for Broadleaf, C for Coniferous and M for Mixed forest stand.

Plot Number	Number of Trees			Prevailing Trees
	Broadleaf	Coniferous	Total	
I.	92	1	93	B
II.	88	10	98	B
III.	63	1	64	B
IV.	49	15	64	B
V.	71	1	72	B
VI.	37	42	79	M
VII.	60	0	60	B
VIII.	15	53	68	C
IX.	8	63	71	C
X.	20	72	92	C
XI.	60	0	60	B
XII.	56	4	60	B
XIII.	20	42	62	M
XIV.	15	52	67	C
XV.	6	55	61	C
XVI.	0	66	66	C
XVII.	3	107	110	C
XVIII.	2	61	63	C
XIX.	19	55	74	M
XX.	0	62	62	C
<b>Sum:</b>	<b>684</b>	<b>762</b>	<b>1446</b>	<b>8B/9C/3M</b>

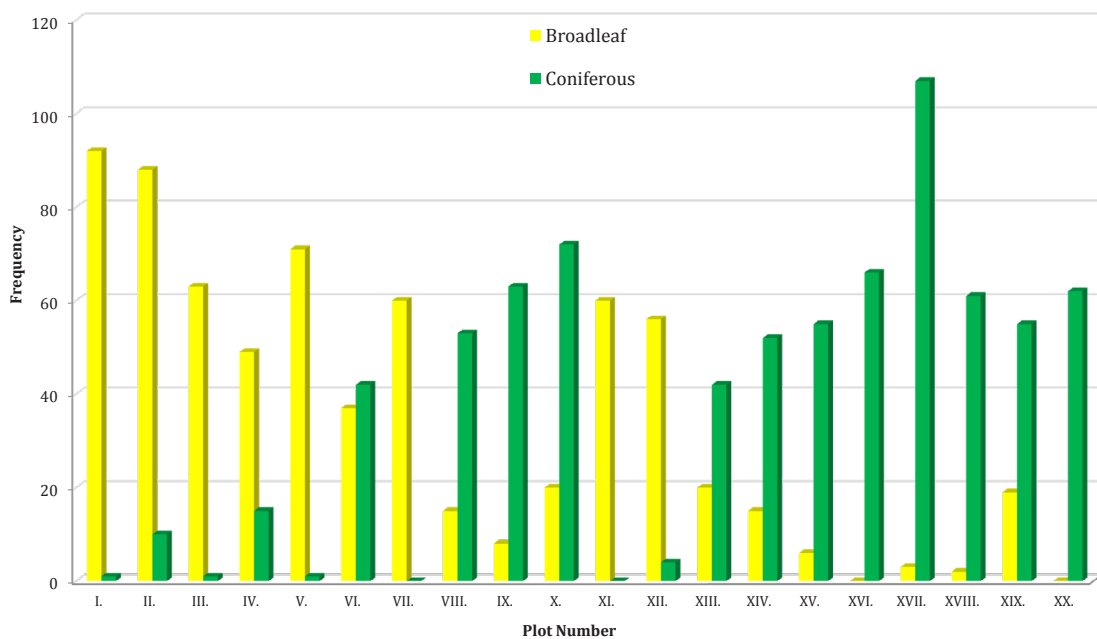


Fig. 66. The visual representations of broadleaf and coniferous trees measured at each of the 20 examined study plots.

Together 16 different tree species were found on the study plots during the field measurements. Their numerical representations can be seen in Figure 67.

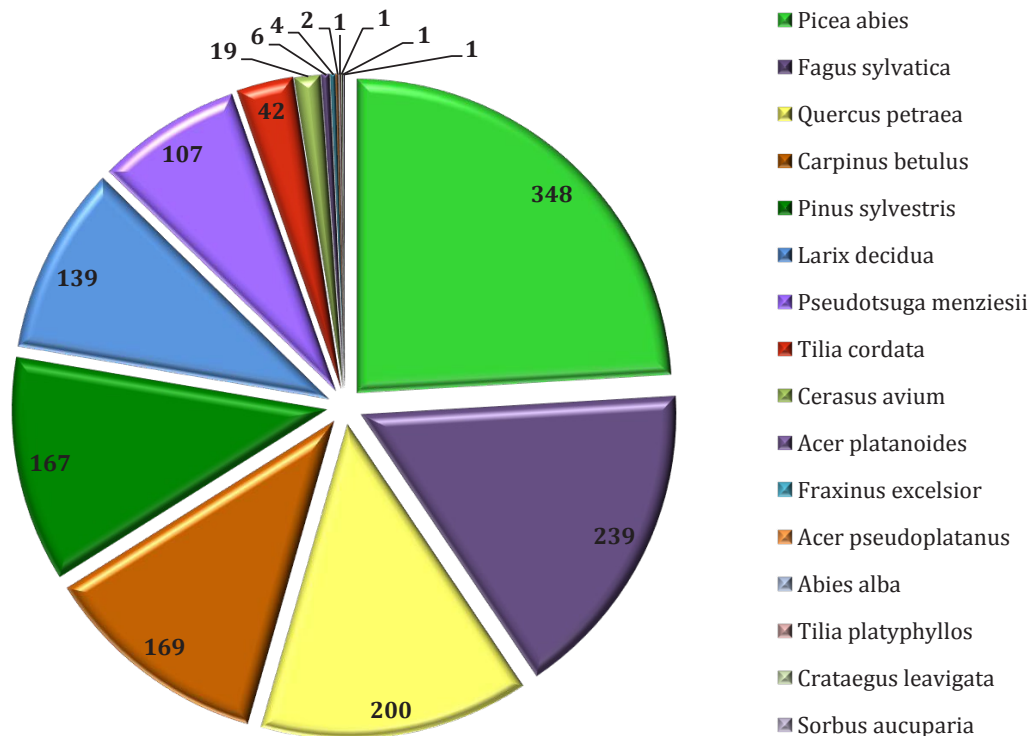


Fig. 67. Representation of individual tree species summarized for all the 20 study plots. The species are arranged clockwise according to their count in the descending order.

The most individuals were represented by Norway spruce (*Picea abies*) with 348 trees, the second most abundant species was European beech (*Fagus sylvatica*) with 239 pieces, the third was then sessile oak (*Quercus petraea*) represented by 200 trees. The following species were European hornbeam (*Carpinus betulus*) with 169 representatives, Scotch pine (*Pinus sylvestris*) with 167 trees, European larch (*Larix decidua*) with 139 individuals, followed by Douglas fir (*Pseudotsuga menziesii*) with 107 measured trees.

Another nine species were represented with less than 100 trees, particularly it were small-leaved linden (*Tilia cordata*) with 42 trees, wild cherry tree (*Cerasus avium*) with 19 individuals, Norway maple (*Acer platanoides*) with 6 representatives, common ash (*Fraxinus excelsior*) with together 4 trees or Scottish maple (*Acer pseudoplatanus*) with just two found individuals. The last four species were then represented each only by one single tree: European fir (*Abies alba*), large-leaved linden (*Tilia platyphyllos*), European hawthorn (*Crataegus leavigata*) and rowan tree (*Sorbus aucuparia*). The particular distribution of all the 1446 trees amongst the individual study plots can be seen in the Table 5.

Table 5. The overall numbers of individual tree species found at particular study plots. The species are arranged in descending order from left to right according to their count. All the data were gained during the field measurements.

Tree species Plot Number	<i>Picea abies</i>	<i>Fagus sylvatica</i>	<i>Quercus petraea</i>	<i>Carpinus betulus</i>	<i>Pinus sylvestris</i>	<i>Larix decidua</i>	<i>Pseudotsuga menziesii</i>	<i>Tilia cordata</i>	<i>Cerasus avium</i>	<i>Acer platanoides</i>	<i>Fraxinus excelsior</i>	<i>Acer pseudoplatanus</i>	<i>Abies alba</i>	<i>Tilia platyphyllos</i>	<i>Crataegus leavigata</i>	<i>Sorbus aucuparia</i>
I.	0	16	52	22	0	1	0	1	0	0	0	0	0	1	0	0
II.	0	25	17	41	2	8	0	2	0	3	0	0	0	0	0	0
III.	0	15	7	40	1	0	0	1	0	0	0	0	0	0	0	0
IV.	0	16	22	10	6	5	3	0	0	0	0	0	1	0	1	0
V.	0	10	13	47	0	1	0	1	0	0	0	0	0	0	0	0
VI.	0	2	0	0	1	41	0	35	0	0	0	0	0	0	0	0
VII.	0	60	0	0	0	0	0	0	0	0	0	0	0	0	0	0
VIII.	9	10	1	1	1	1	42	0	0	0	0	2	0	0	0	1
IX.	35	8	0	0	1	27	0	0	0	0	0	0	0	0	0	0
X.	72	15	3	2	0	0	0	0	0	0	0	0	0	0	0	0
XI.	0	56	0	0	0	0	0	0	0	1	3	0	0	0	0	0
XII.	0	0	56	0	0	4	0	0	0	0	0	0	0	0	0	0
XIII.	1	0	2	2	41	0	0	0	15	1	0	0	0	0	0	0
XIV.	0	0	9	0	52	0	0	0	4	1	1	0	0	0	0	0
XV.	32	1	0	4	23	0	0	1	0	0	0	0	0	0	0	0
XVI.	0	0	0	0	0	4	62	0	0	0	0	0	0	0	0	0
XVII.	93	1	2	0	0	14	0	0	0	0	0	0	0	0	0	0
XVIII.	52	2	0	0	1	8	0	0	0	0	0	0	0	0	0	0
XIX.	0	2	16	0	32	23	0	1	0	0	0	0	0	0	0	0
XX.	54	0	0	0	6	2	0	0	0	0	0	0	0	0	0	0
Sum	348	239	200	169	167	139	107	42	19	6	4	2	1	1	1	1

### 5.1.3. Field-Measured Height of Trees

For each of the 1446 trees the height was measured using the digital hypsometer. The average height of all trees measured within each of the 20 study plots can be seen in the Figure 68. The distribution of height values of individual trees present at each plot can be seen in the Figure 69.

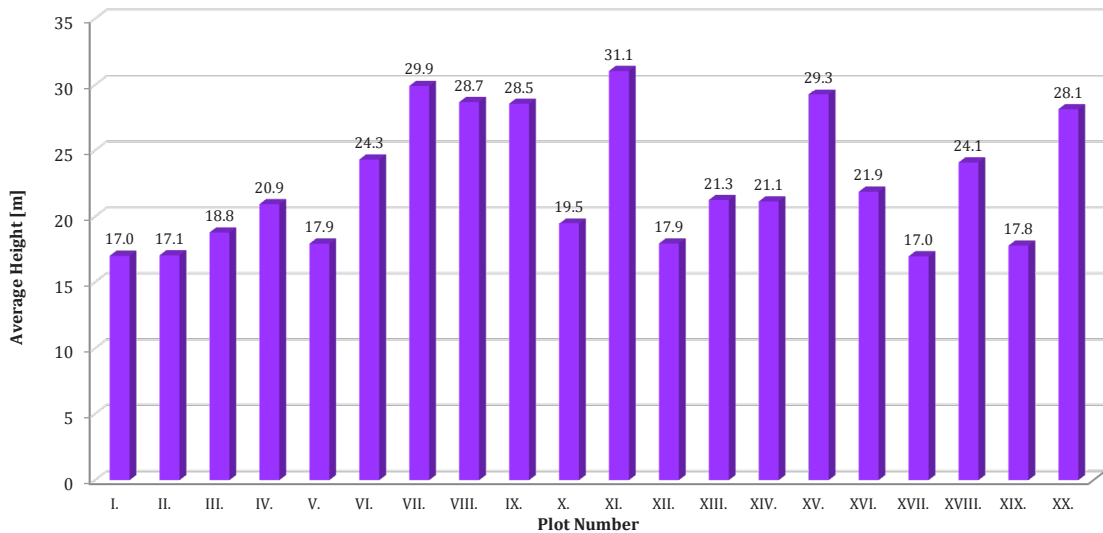


Fig. 68. The average field-measured height of trees within each study plot.

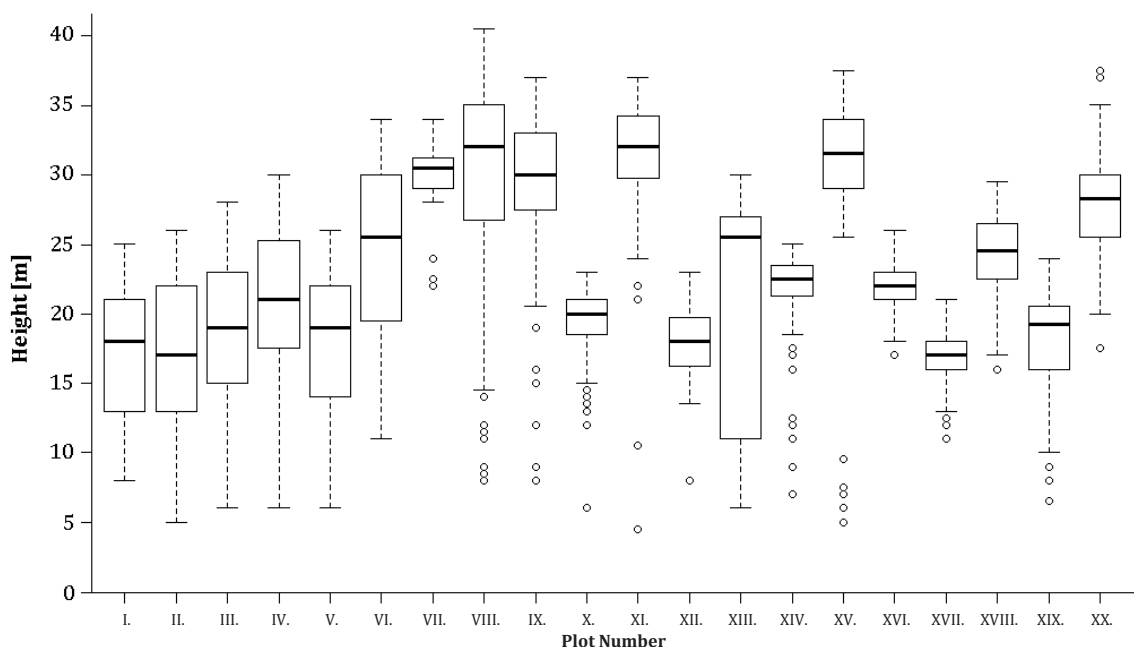


Fig. 69. The box and whiskers plots showing the distribution of field-measured height of trees on particular study plots. The bottom and the top of the boxes represent the first and third quartile of the values respectively, and hence the boxes contain 50 % of the values. The inner line then stands for the median. The whiskers then represent the 1.5 multiple of the interquartiles of the lower and upper quartiles and the circles then show the outliers.



Figure 70. shows the Standard Deviation of FM height of trees at each plot.

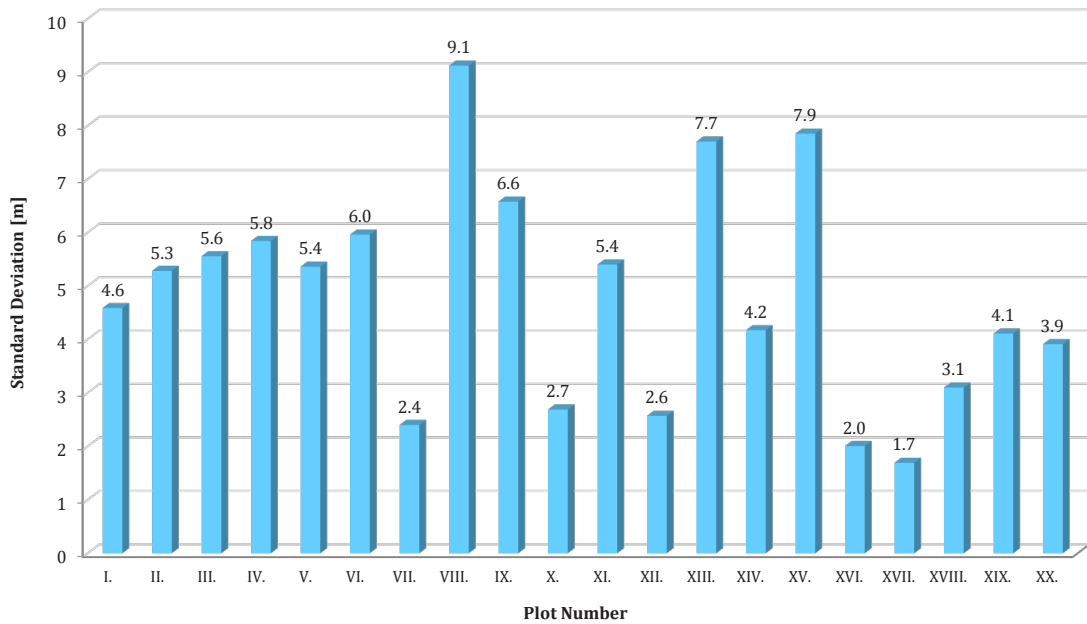


Fig. 70. The Standard Deviations of field-measured height of trees within each study plot.

Since the height of each tree was measured at least twice from different positions and sometimes even five or seven times (see chapter 4.3.2 Measurements of the trees) the acquired values had each time a particular range. The mean range was calculated as an average of the differences between maximal and minimal height values measured for each tree in a particular plot. The resulting values can be seen in Figure 71.

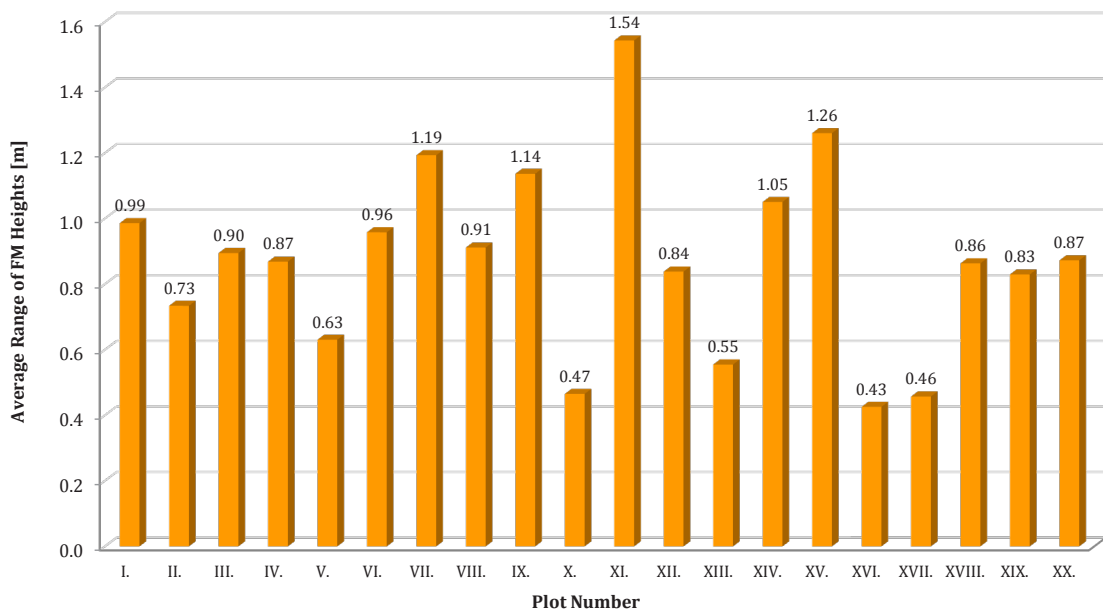


Fig. 71. The average range of field-measured heights of trees within each study plot.

## **5.2. Results of the UAV Forest Explorer Runs**

As described in the chapter 4.7.4.2. Assessing the Tool Outputs, the statistics calculated within each iteration of UAV Forest Explorer runs, which were comparing the properties of field-measured and automatically identified trees, were used for selection of the best results for each study plot. These results, which at the same time represent the most suitable settings applicable for each explored forest stand, were then saved in the Best Results tables and can be seen in Appendix 4. The acquired results are described in the following chapters.

### **5.2.1. Individual Tree Approach Results**

Generally the statistics were calculated both, for the Individual Tree Approach and for the Area-Based Approach. Between the statistics calculated in the scope of ITA were mainly the Mean Absolute Error (MAE) and Root Mean Square Error (RMSE) of calculated and FM heights, Pearson's Correlation Coefficient (R) of these heights together with its Statistical Significance (Stat. Sig. R), Coefficient of Determination ( $R^2$ ), Mean Difference between average heights of FM and counted heights for matched trees only (Mean Diff. MT), Pearson's Correlation Coefficient calculated for matched trees only (R (MT)) and corresponding Coefficient of Determination ( $R^2$  (MT)). Between the important calculated quantities belonged also the number of identified trees vs. the number of FM trees, number of matched or also unmatched trees or the number of redundantly identified trees.

From all these statistics, just selected representatives were utilized for choosing the best results. Mainly it was the RMSE, R and its statistical significance, R for matched trees and the counts of identified vs. field-measured trees. Only the results best fitting the requirements considering the definitions of Smaller Range and Larger Range of Count Differences (see chapter 4.7.4.2. Assessing the Tool Outputs), were selected as the most suitable ones. The best results, which are summed up in the following chapters are differentiated both, on the basis of the provided ground truth data (All FM trees / Reduced number of FM trees / Modified positions of FM trees) as well as the described ranges (Smaller Range / Larger Range).

### 5.2.1.1. Root Mean Square Error (RMSE)

The best results in each category concerning the lowest values of the RMSE of the field-measured and calculated tree heights are summarized in the following table (Table 6.) and diagrams (Figure 72. and Figure 73.).

*Table 6. The lowest values of RMSE of the field-measured and calculated tree heights for particular study plots. The table is divided based on the form of field-measurements data (All FM Trees / Reduced Number of FM Trees) and based on the defined ranges of Count Difference (Smaller Range / Larger Range). Also the average values calculated for each category and for each study plot are contained.*

RMSE	All FM Trees		Reduced FM Trees		Average
	Smaller Range	Larger Range	Smaller Range	Larger Range	
I.	10.194	9.489	10.194	7.939	9.454
II.	9.883	9.806	7.858	5.500	8.262
III.	11.846	11.565	10.615	10.125	11.038
IV.	10.302	10.302	11.161	5.703	9.367
V.	9.741	9.741	10.013	8.425	9.480
VI.	13.734	14.276	11.107	2.053	10.293
VII.	11.061	11.061	9.720	9.720	10.391
VIII.	12.806	12.806	12.964	11.990	12.642
IX.	9.865	9.599	7.389	5.070	7.981
X.	4.037	4.037	3.419	3.295	3.697
XI.	16.024	16.024	16.229	16.229	16.127
XII.	8.671	8.458	8.576	8.576	8.570
XIII.	9.989	9.989	10.819	8.651	9.862
XIV.	7.130	6.373	5.870	5.255	6.157
XV.	15.790	14.654	14.230	14.114	14.697
XVI.	3.094	3.094	0.438	0.395	1.755
XVII.	3.672	3.373	2.298	2.290	2.908
XVIII.	8.416	8.416	4.171	4.115	6.280
XIX.	6.137	6.137	2.475	2.474	4.306
XX.	12.559	12.559	10.983	9.623	11.431
<b>Average</b>	9.748	9.588	8.526	7.077	8.735

The following diagrams visualise the data from Table 6. and enable to easily recognize the differences between various categories on individual study plots.

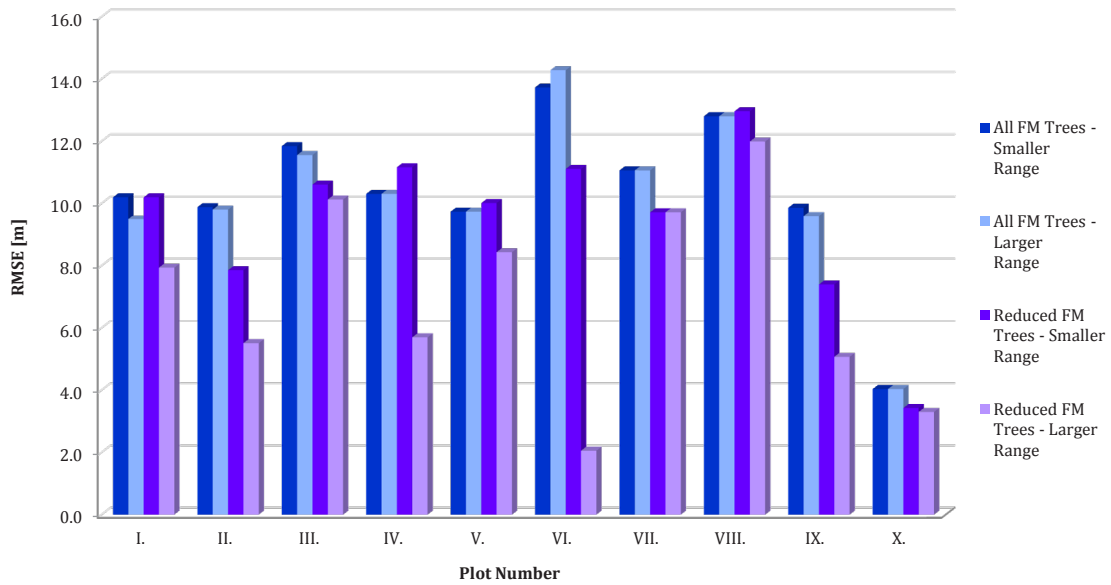


Fig. 72. The lowest values of RMSE of the field-measured and calculated tree heights divided based on the defined categories. Diagram represents data from study plots I. to X.

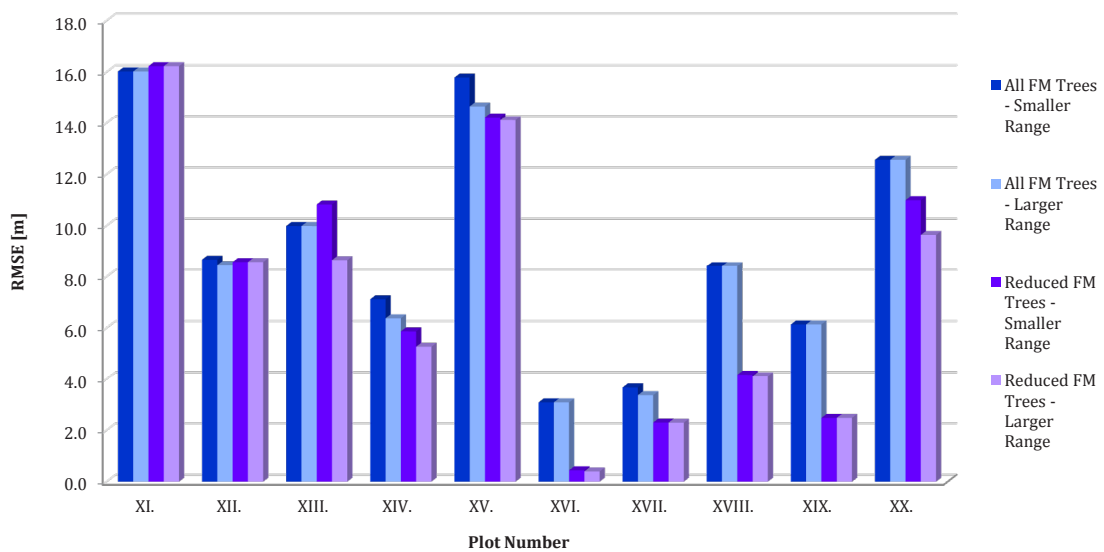


Fig. 73. The lowest values of RMSE of the field-measured and calculated tree heights divided based on the defined categories. Diagram represents data from study plots XI. to XX.

As described earlier, in the case of three study plots not only two, but three tool runs were applied to process the data. The first and second run were classically comparing the automatically identified trees with all field-measured trees and with reduced number of FM trees, respectively. The third run was then utilizing the reduced number of FM trees after the manual modification of tree positions (see chapter 4.7.4.1. Running the Tool).

This process was performed only on plots with prevailing representation of Scotch pine (*Pinus sylvestris*) in the species composition, particularly on plots XIII., XIV. and XV. The plot number XIX., which also contained relevant portion of Scotch pines was not included in this process, since the forest stand was relatively young (only 36 years contrary to 90 - 100 years in the case of the concerned three plots) and the trees were not significantly leaning yet. The effect of the tree positions modification can be evaluated based on Table 7. and Figure 74.

Table 7. The lowest values of RMSE of the field-measured and calculated heights for three study plots, where also the ground truth data with modified positions of trees were provided.

RMSE	All FM trees		Reduced Trees		Modified Trees		Average
	Smaller Range	Larger Range	Smaller Range	Larger Range	Smaller Range	Larger Range	
<b>XIII.</b>	9.989	9.989	10.819	8.651	4.965	1.048	7.577
<b>XIV.</b>	7.130	6.373	5.870	5.255	3.909	0.999	4.923
<b>XV.</b>	15.790	14.654	14.230	14.114	9.152	8.439	12.730
<b>Average</b>	10.970	10.339	10.306	9.340	6.009	3.495	8.410

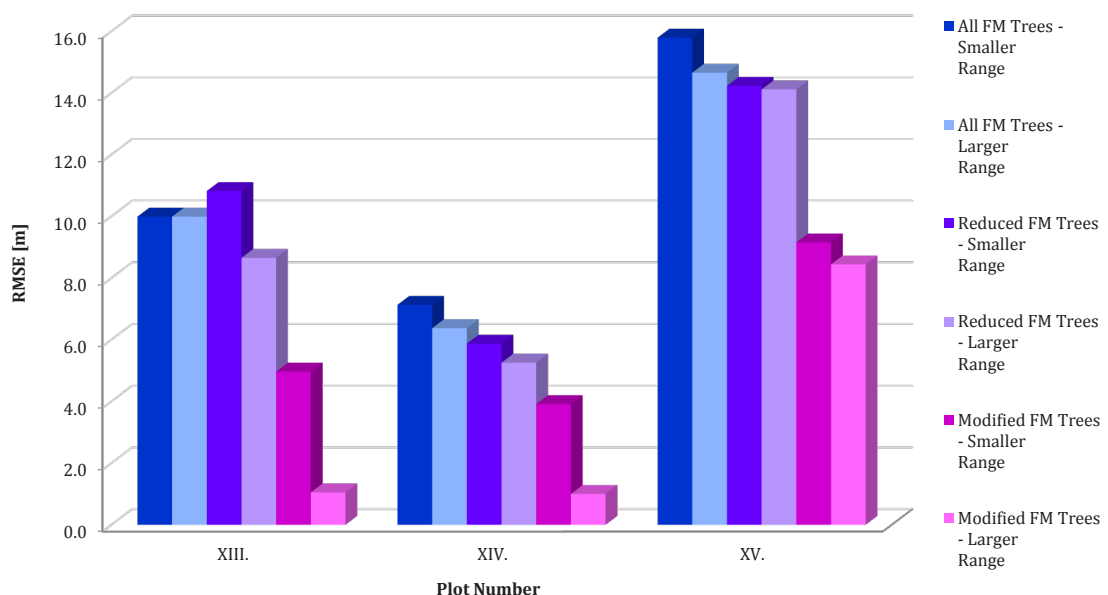


Fig. 74. The lowest values of RMSE of the field-measured and calculated tree heights. Diagram represents data from study plots XIII., XIV. and XV. where the ground truth data with Modified positions of FM trees were processed.

### 5.2.1.2. Pearson's Correlation Coefficient (R)

The best results in each category concerning the highest values of the Pearson's Correlation Coefficient counted for the field-measured and calculated tree heights are summarized in the following table (Table 8.) and depicted in the diagrams (Figure 75. and Figure 76.).

*Table 8. The highest values of the Pearson's Correlation Coefficient of the field-measured and calculated tree heights for particular study plots. The table is divided based on the form of field-measurements data (All FM Trees / Reduced Number of FM Trees) and based on the defined ranges of Count Difference (Smaller Range / Larger Range).*

R	All FM Trees		Reduced FM Trees		Average
	Smaller Range	Larger Range	Smaller Range	Larger Range	
I.	0.117	0.131	0.059	0.172	0.120
II.	0.414	0.516	0.792	0.798	0.630
III.	0.259	0.326	0.253	0.271	0.277
IV.	0.543	0.555	0.478	0.478	0.514
V.	0.519	0.559	0.505	0.511	0.524
VI.	0.150	0.340	0.448	0.559	0.374
VII.	0.657	0.657	0.436	0.521	0.568
VIII.	0.603	0.632	0.533	0.564	0.583
IX.	0.697	0.726	0.632	0.699	0.689
X.	0.800	0.812	0.671	0.694	0.744
XI.	0.360	0.360	0.292	0.355	0.342
XII.	0.434	0.487	0.373	0.387	0.420
XIII.	0.560	0.612	0.494	0.494	0.540
XIV.	0.608	0.608	0.516	0.572	0.576
XV.	0.323	0.470	0.609	0.638	0.510
XVI.	0.752	0.767	0.969	0.969	0.864
XVII.	0.756	0.801	0.628	0.689	0.719
XVIII.	0.745	0.867	0.469	0.577	0.665
XIX.	0.708	0.783	0.644	0.644	0.695
XX.	0.544	0.663	0.450	0.549	0.552
<b>Average</b>	0.527	0.584	0.513	0.557	0.545

The following diagrams are then depicting the data from Table 8. and enable to easily assess the differences between various categories on particular study plots.

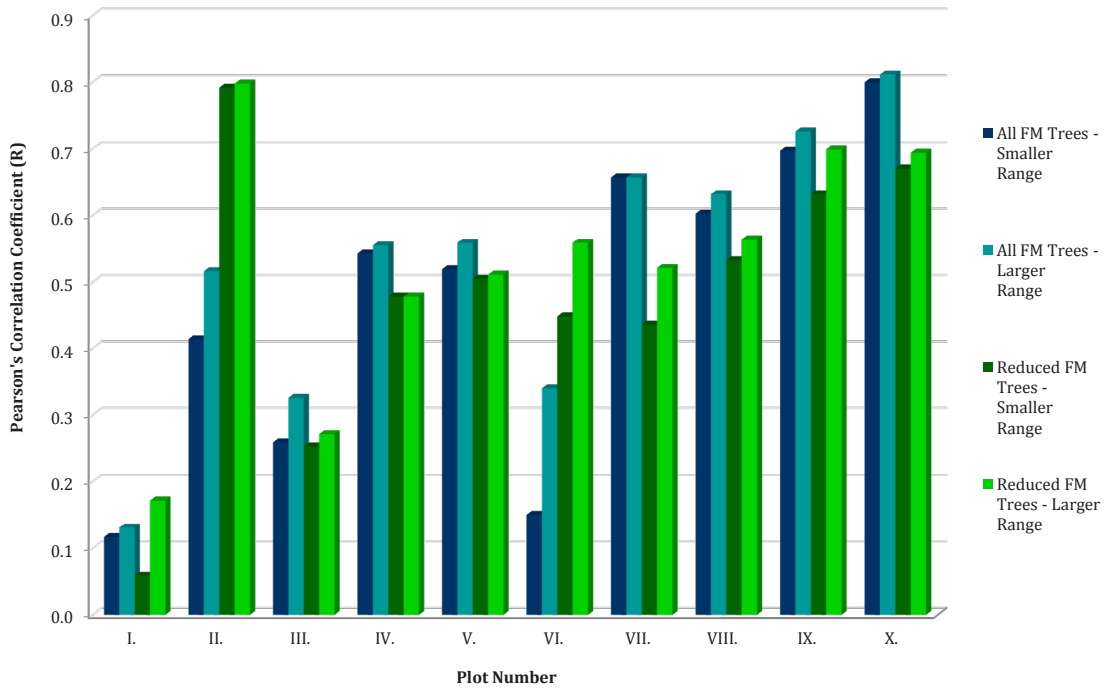


Fig. 75. The highest values of the Pearson's Correlation Coefficient computed for the field-measured and calculated tree heights for particular study plots divided based on the defined categories. Diagram represents data from study plots I. to X.

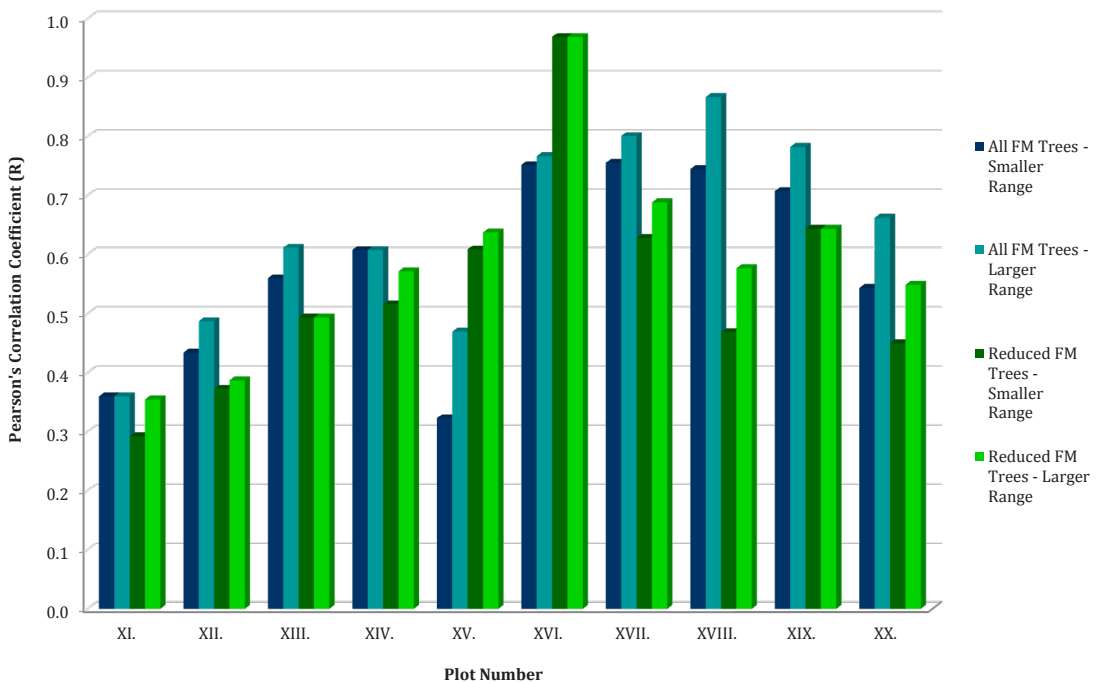


Fig. 76. The highest values of the Pearson's Correlation Coefficient computed for the field-measured and calculated tree heights for particular study plots divided based on the defined categories. Diagram represents data from study plots XI. to XX.

As described in the previous chapter, in the case of three study plots with prevailing Scotch pine (*Pinus sylvestris*) in the species composition, particularly plots number XIII., XIV. and XV. there were three tool runs of the UAV Forest Explorer applied. The third run was each time performed using the reduced number of field-measured trees with modified positions as the ground truth (explained in the chapter 4.7.4.1. Running the Tool). The effect of the tree positions modification can be evaluated based on Table 9. and Figure 77.

Table 9. The highest values of the Pearson's Correlation Coefficient of the field-measured and calculated tree heights for particular study plots, where also the ground truth data with modified positions of trees were provided.

R	All FM trees		Reduced Trees		Modified Trees		Average
Plot Number	Smaller Range	Larger Range	Smaller Range	Larger Range	Smaller Range	Larger Range	
XIII.	0.560	0.612	0.494	0.494	0.758	0.862	0.630
XIV.	0.608	0.608	0.516	0.572	0.671	0.850	0.638
XV.	0.323	0.470	0.609	0.638	0.804	0.804	0.608
<b>Average</b>	0.497	0.563	0.540	0.568	0.744	0.839	0.625

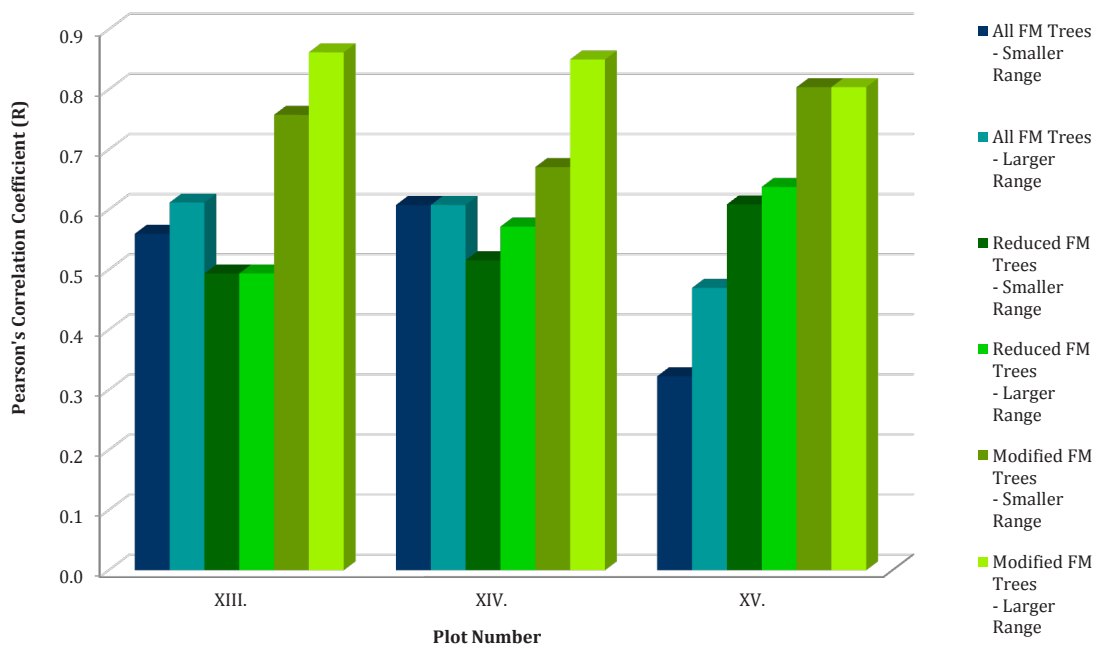


Fig. 77. The highest values of the Pearson's Correlation Coefficient computed for the field-measured and calculated tree heights for particular study plots. Diagram represents data from study plots XIII., XIV. and XV. where the ground truth data with Modified positions of FM trees were processed.



### 5.2.1.3. Pearson's Correlation Coefficient (R) for Matched Trees Only

The Pearson's Correlation Coefficient for the field-measured and calculated tree heights, which was calculated only for the Matched Trees, was also utilized for the results assessment (see chapter 4.7.4.2. Assessing the Tool Outputs). The best results in each category regarding this quantity are summarized in the following table (Table 10.)

*Table 10. The highest values of the Pearson's Correlation Coefficient of the field-measured and calculated tree heights counted for Matched Trees only. The table is divided based on the form of field-measurements data (All FM Trees / Reduced Number of FM Trees / Modified Positions of Reduced FM Trees) and based on the defined ranges of Count Difference (Smaller Range / Larger Range).*

R for MT	All FM Trees		Reduced FM Trees		Modified FM Trees		Average
	Smaller Range	Larger Range	Smaller Range	Larger Range	Smaller Range	Larger Range	
I.	0.165	0.275	0.422	0.458			0.330
II.	0.551	0.587	0.595	0.679			0.603
III.	0.082	0.144	0.130	0.243			0.150
IV.	0.652	0.658	0.877	0.920			0.777
V.	0.422	0.521	0.487	0.500			0.483
VI.	0.572	0.643	0.703	0.703			0.655
VII.	0.527	0.598	0.538	0.538			0.550
VIII.	0.757	0.827	0.900	0.903			0.847
IX.	0.644	0.688	0.950	0.951			0.808
X.	0.958	0.967	0.971	0.972			0.967
XI.	0.506	0.605	0.556	0.662			0.582
XII.	0.714	0.714	0.606	0.606			0.660
XIII.	0.482	0.482	0.808	0.808	0.847	0.890	0.720
XIV.	0.586	0.586	0.879	0.879	0.888	0.895	0.786
XV.	0.614	0.623	0.817	0.824	0.902	0.902	0.780
XVI.	0.978	0.978	0.971	0.973			0.975
XVII.	0.951	0.959	0.962	0.962			0.959
XVIII.	0.953	0.972	0.983	0.986			0.974
XIX.	0.769	0.915	0.960	0.960			0.901
XX.	0.856	0.873	0.968	0.970			0.917
<b>Average</b>	0.637	0.681	0.754	0.775	0.879	0.896	0.724

### 5.2.1.4. Mean Difference of Heights for Matched Trees Only

This subchapter contains the summarisation of best results regarding the Mean Difference between average values of field-measured and counted heights for Matched Trees (MT) only. Since results with this value closest to zero contain more or less unsuitable values of other quantities, those results were not preferred.

Instead, the average of all the values in “Mean Diff (MT)” field in the ITA part of each Best Results table was calculated. That means that this average was each time counted from 7 values (4 from Smaller Range and 3 from Larger Range) from the best results matching the previously described requirements. The diagram depicting these average values calculated for each plot and each version of ground truth data can be seen as the Figure 78.

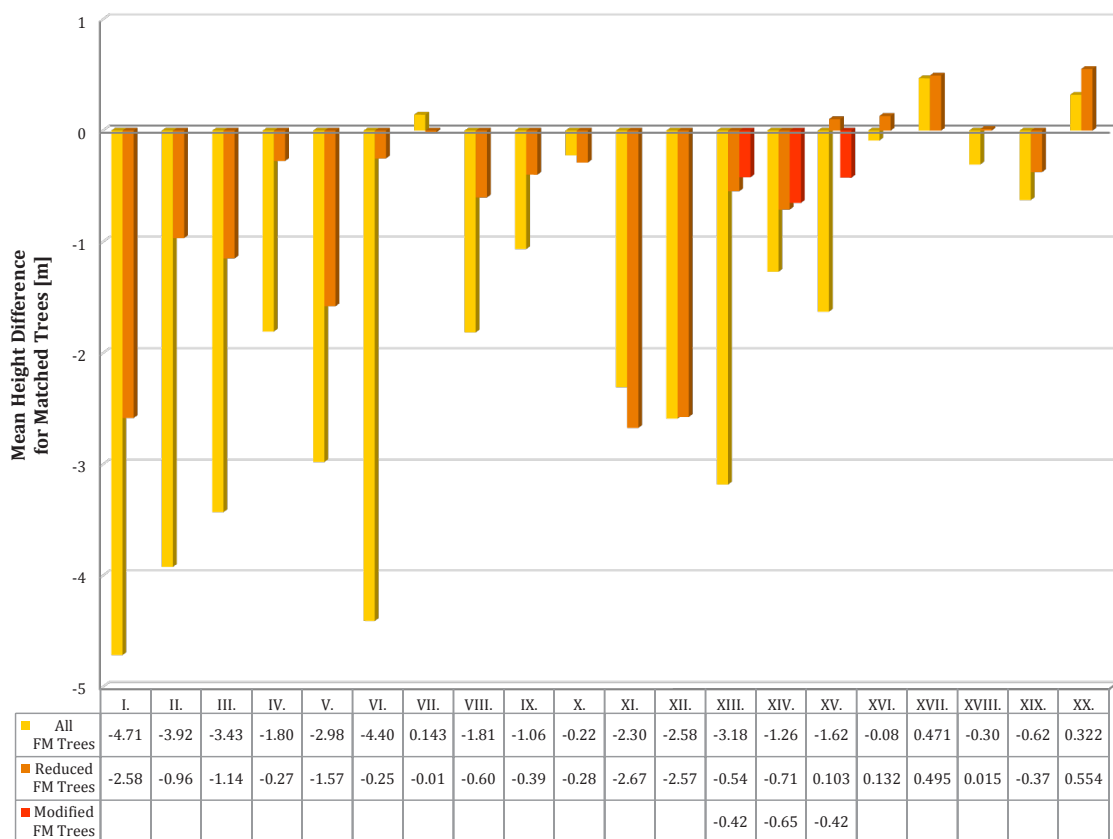


Fig. 78. The average values of the Mean Difference between average values of FM and calculated heights for Matched Trees. Counted from all values in the ITA section of the Best Results tables. The diagram contains data gained using different ground truth data (All FM Trees / Reduced Number of FM Trees / Modified Positions of Reduced FM Trees).

### **5.2.1.5. Suitable CS, IM and FS Settings of the Tool within the ITA**

The basic settings of the UAV Forest Explorer leading to the demanded results are described in this chapter. The Cell Size, Interpolation Method and Focal Statistics Circle Radius belong to these settings. To summarize the frequencies and distributions of the selected settings applied for processing the data and resulting in the most satisfactory outputs, two approaches were used.

First of all just the results meeting the requirements of both, the lowest Root Mean Square Error and highest Pearson's Correlation Coefficient at one time (tagged as "RMSE & R" in the Best Results table) were utilized for assessing the most suitable settings. These results, being a compromise for both these main quantities and keeping the lowest Count Difference between the FM and identified trees at the same time, can be considered the representatives of the relatively most appropriate settings for each particular forest stand being explored. Therefore the CS, IM and FS values from the "RMSE & R" field were picked up from the Best Results of the each tool run.

The second approach works with less limitation and accepts all the results in the whole ITA group. Therefore both, Smaller and Larger Range were utilized for this purpose. That gives together 7 results being used for the settings extraction regarding the outputs from each of the 43 tool runs. The summarisation of the ascertainment regarding the most suitable settings based on the described approach can be seen in the following tables and diagrams.

Table 11. contains Cell Size values, Interpolation Methods and Focal Statistics circle radius values extracted just from the results meeting the lowest RMSE and highest R requirements. The CS, IM and FS values used for calculation of the demanded outputs were selected for each study plot and for each kind of the ground truth data (All FM trees / Reduced number of FM trees / Modified positions of the reduced FM trees).

Tables 12. to 14. then contain summarized frequencies of CS, IM and FS values extracted from all the 301 results ( $43 * 7$ ) of the ITA group. Namely Table 12. sums the representations of the Cell Size values, Table 13. contains frequencies of particular Interpolation Methods and Table 14. then shows summed counts of the Focal Statistics Circle Radiuses extracted from these results.

Table 11. The Cell Size, Interpolation Method and Focal Statistics circle radius values selected as the best results meeting the "RMSE & R" conditions for each study plot. The table is divided based on the form of field-measurements data.

Plot Number	All FM Trees			Reduced FM Trees			Modified FM Trees		
	CS	IM	FS	CS	IM	FS	CS	IM	FS
I.	20	TNN	2	40	BI	1			
II.	25	BM	1	10	BA	5			
III.	25	BI	2	45	BN	1			
IV.	10	BI	5	55	TNN	1			
V.	15	BA	3	15	TNN	4			
VI.	10	TNW	3	15	BI	5			
VII.	25	BA	4	30	TLN	4			
VIII.	25	BA	2	45	TNN	1			
IX.	15	BN	4	10	TNW	7			
X.	30	TLW	1	35	TLW	1			
XI.	70	BA	1	65	TLN	1			
XII.	15	BI	6	10	TLN	8			
XIII.	35	TNW	1	60	TLN	1	60	TNN	1
XIV.	45	TNN	1	50	TLW	1	60	TLN	1
XV.	35	TNN	1	35	BI	1	40	TLN	1
XVI.	10	BN	5	40	BN	1			
XVII.	25	TNW	1	25	TNW	1			
XVIII.	10	TNW	5	65	BA	1			
XIX.	30	TLN	1	10	TNW	5			
XX.	20	BA	3	35	TNN	2			

Table 12. The Cell Size values applied for the tool runs leading to the best results concerning the ITA. The table sums the frequencies from all the 301 ITA best results.

CS	5	10	15	20	25	30	35	40	45	50	55	60	65	70	75	80	85 - 95	100
Frequency	12	56	36	27	28	26	32	23	19	5	9	8	7	7	3	2	0	1

Table 13. The Interpolation Methods applied for the tool runs leading to the best results concerning the ITA. The table sums the frequencies from all the 301 ITA best results.

IM	BA	BI	BM	BN	TLN	TLW	TNN	TNW
Frequency	46	48	21	34	40	22	49	41

Table 14. The Focal Statistics circle radiuses applied for the tool runs leading to the best results concerning the ITA. The table sums the frequencies from all the 301 ITA best results.

FS	1	2	3	4	5	6	7	8	9	10
Frequency	132	32	29	35	27	19	13	6	6	2

Figure 79. contains the selected Cell Size values representing the Best Results meeting only the “RMSE & R” category demands, extracted for each plot. Figure 80. then depicts the overall frequency of particular CS values in the scope of the whole ITA category.

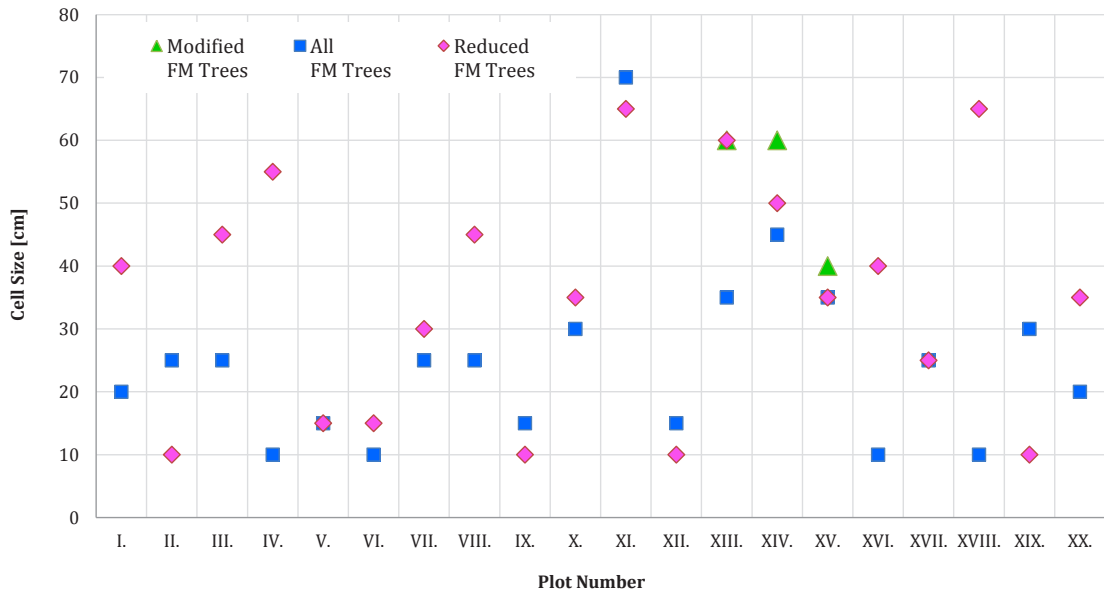


Fig. 79. The selected Cell Size values representing the Best Results meeting the condition of lowest RMSE and highest R at the same time for each study plot. The diagram shows values gained using different ground truth data.

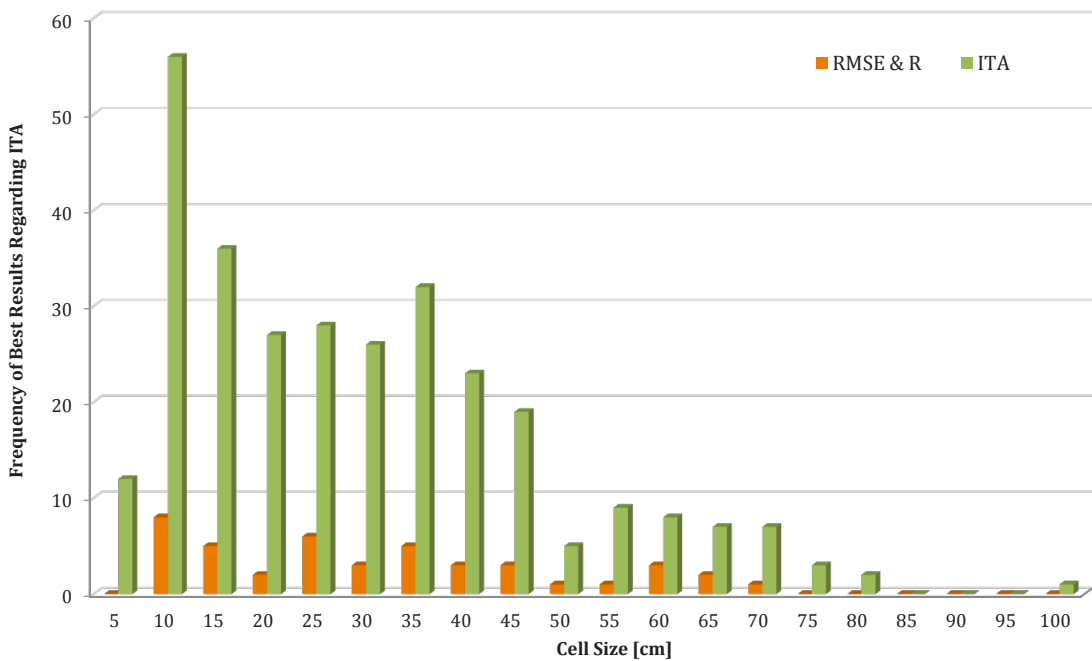


Fig. 80. The frequencies of Cell Size values representing the Best Results in the scope of the “RMSE & R” group (43 results) and in the scope of all the 301 ITA results.

The frequency of specific Interpolation Methods and Focal Statistics Circle Radius values applied in the case of the Best Results, meeting the conditions of the “RMSE & R” category as well as of the whole ITA group, are displayed in the Figure 81. and Figure 82. respectively.

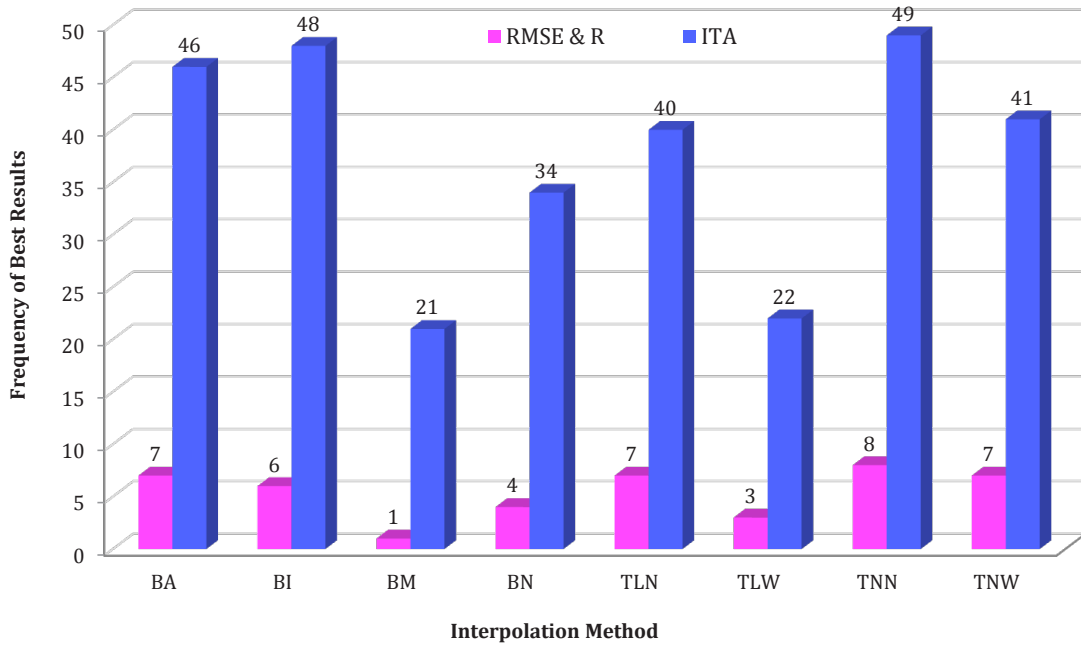


Fig. 81. The frequency of Interpolation Methods representing the Best Results in the scope of the "RMSE & R" group (43 results) and in the scope of all the 301 ITA results.

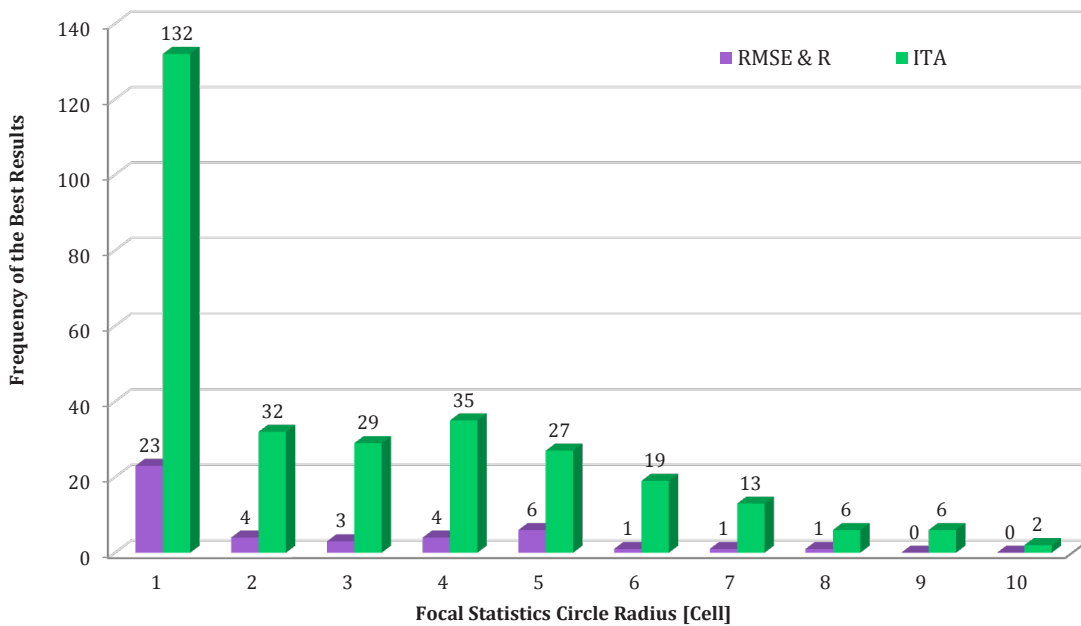


Fig. 82. The frequency of Focal Statistics Circle Radiuses representing the Best Results in the scope of the "RMSE & R" group (43 results) and in the scope of all the 301 ITA results.

Since the relationship between CS and FS values can provide much more information than these values as such, the frequency and distribution of their combinations were also ascertained. Visualisations including the trends are shown as the Figure 83. for the results from the "RMSE & R" category and as the Figure 84. for the results encompassing the whole ITA outputs group. The diagrams were 'jittered' to better show the frequencies of particular combinations of values.

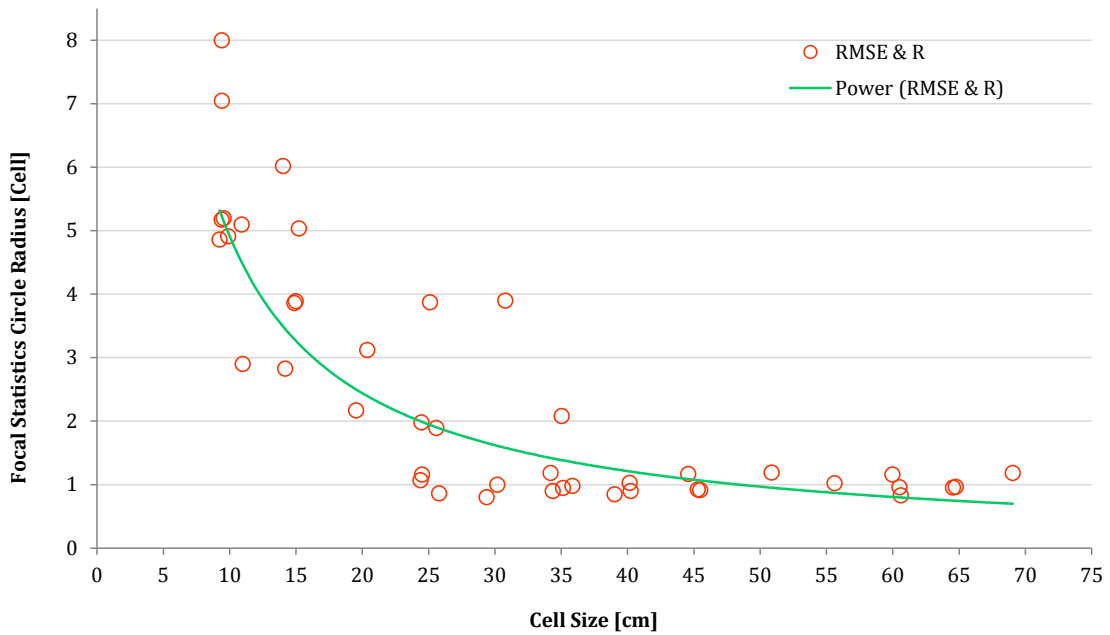


Fig. 83. The combinations of CS and FS values used for acquisition of the Best Results in the "RMSE & R" category. The green line is the trend of data counted as the power regression.

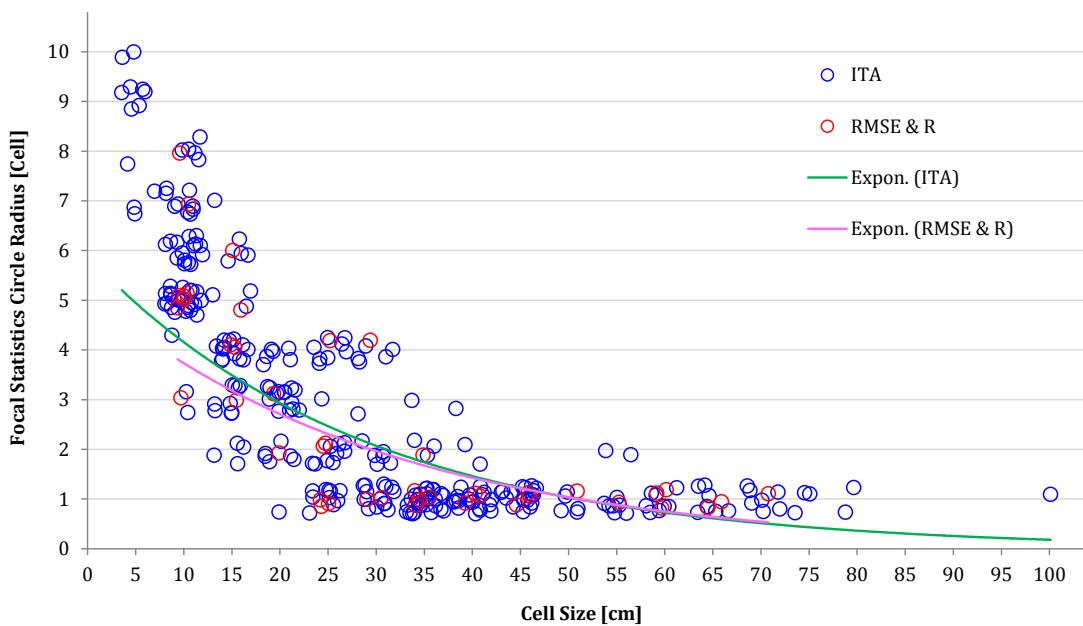


Fig. 84. The combinations of CS and FS values from the "RMSE & R" category and from the ITA group. The lines represent the trend of data calculated as the exponential regression.

## 5.2.2. Area-Based Approach Results

### 5.2.2.1. Count Difference, Height Difference and Standard Deviation

The statistics calculated in the scope of the ABA were mainly the mean height of identified trees, standard deviation of heights of identified trees, the difference between the count of identified and FM trees and the difference between the mean height of identified and FM trees. These values could be compared also with the mean height of FM trees and with the standard deviation of heights of the FM trees. As described earlier, the Best Results regarding the ABA were selected mainly based on the lowest Count Difference (either 0 and  $\pm 1$  tree if possible) and lowest Height Difference at the same time, on the lowest Height Difference only and on the lowest Standard Deviation in the  $\pm 1$  tree Count Difference range. The values of the lowest Height Difference of the selected results with the Count Difference of 0 and  $\pm 1$  tree can be seen in the Table 15.

*Table 15. The lowest values of the Height Difference as the difference between mean height of identified and FM trees in metres. The values are extracted from the Best Results with Count Difference of 0 trees and from the range of  $\pm 1$  tree of Count Difference.*

Height Diff. [m]	Count Difference (0 trees)				Count Difference ( $\pm 1$ tree)			
	Plot Number	All FM Trees	Reduced FM Trees	Modified FM Trees	Average	All FM Trees	Reduced FM Trees	Modified FM Trees
I.	4.644	2.445		3.545	4.620	2.445		3.533
II.	5.091	1.600		3.346	5.091	1.498		3.295
III.	4.480	1.544		3.012	4.502	1.106		2.804
IV.	3.353	-0.028		1.663	3.353	-0.028		1.663
V.	4.812	2.381		3.597	4.716	2.353		3.535
VI.	4.543	-0.025		2.259	4.499	-0.036		2.232
VII.	0.065	0.001		0.033	-0.100	0.004		-0.048
VIII.	3.894	0.765		2.330	3.894	0.236		2.065
IX.	2.582	0.349		1.466	2.156	0.349		1.253
X.	-0.460	0.378		-0.041	-0.460	-0.033		-0.247
XI.	2.462	2.437		2.450	0.785	1.432		1.109
XII.	2.112	2.926		2.519	1.961	0.581		1.271
XIII.	2.890	0.115	-0.092	0.971	2.890	-0.052	-0.040	0.933
XIV.	1.959	0.563	-0.343	0.726	1.029	0.303	0.031	0.454
XV.	2.921	-0.059	1.018	1.293	2.921	0.224	1.027	1.391
XVI.	0.011	-0.013		-0.001	0.090	0.015		0.053
XVII.	-0.342	-0.493		-0.418	-0.364	-0.505		-0.435
XVIII.	0.041	0.010		0.026	0.041	0.030		0.036
XIX.	1.535	-0.059		0.738	1.465	-0.073		0.696
XX.	-0.275	-0.369		-0.322	0.046	0.135		0.091
<b>Average</b>	2.316	0.723	0.194	1.427	2.157	0.499	0.339	1.259



Since the values of Height Difference are significantly close to each other in the two groups of the Count Difference (0 trees and  $\pm 1$  tree range), only values from the second group are visualised in the Figure 85.

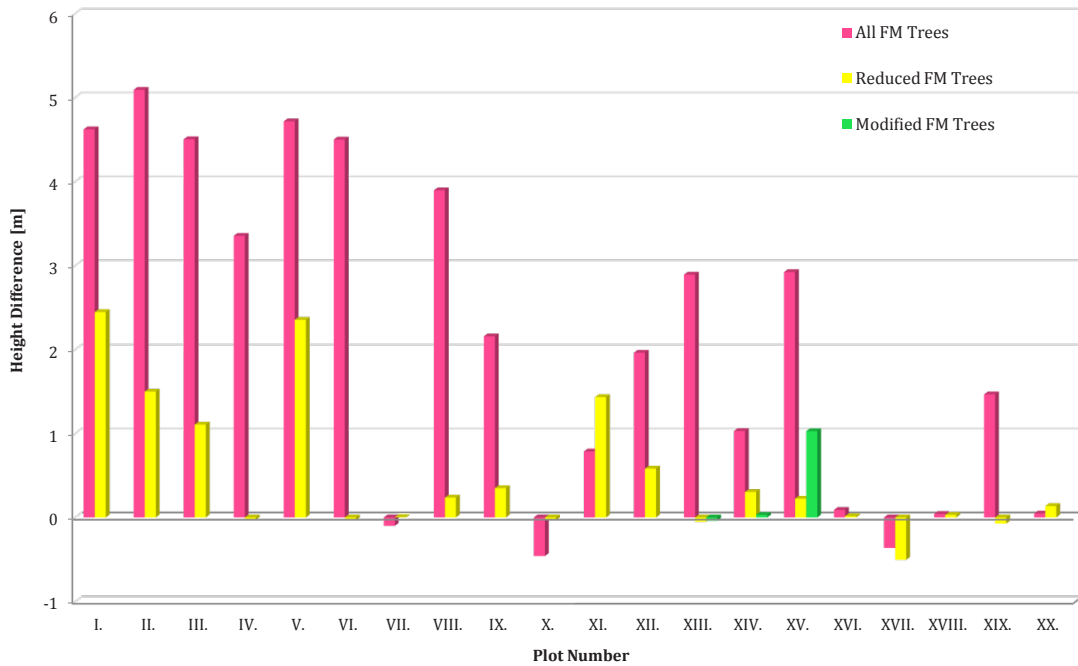


Fig. 85. The lowest values of the Height Difference as the difference in metres between average height of identified trees and FM trees. From results with  $\pm 1$  tree Count Difference.

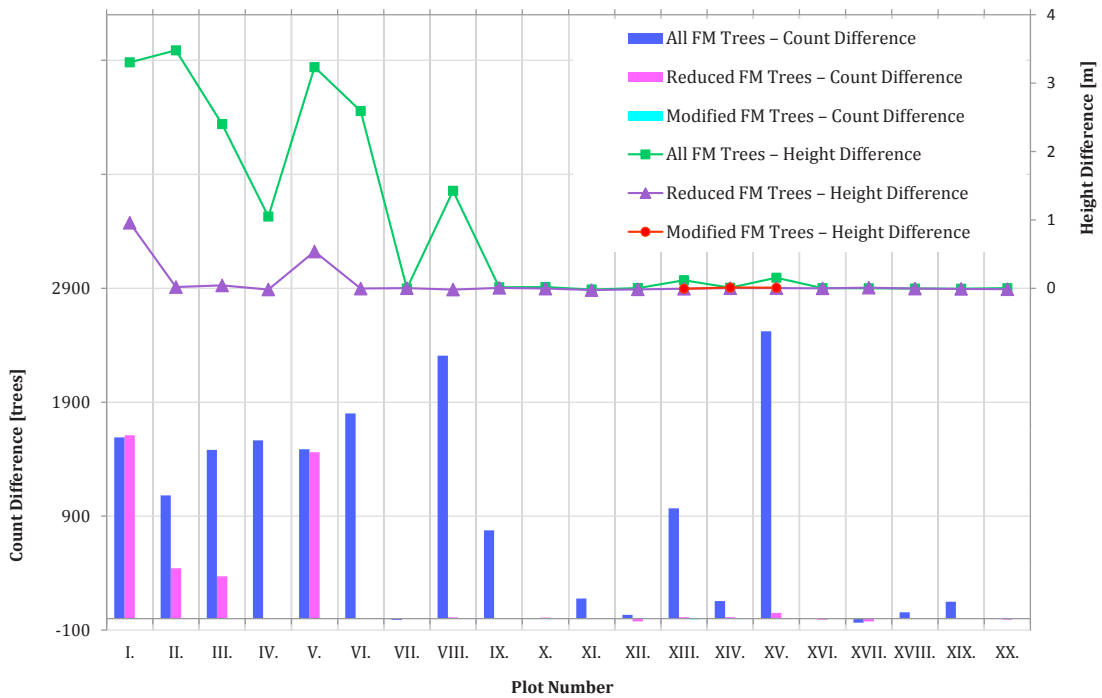


Fig. 86. The combined diagram showing the values of Height Difference (upper part and right axis) and Count Difference (lower part and left axis) for each study plot and each FM data. Created from Best Results with the lowest Height Difference from all the tool outputs.

The diagram in Figure 86. contains the data extracted from the results meeting the condition of the absolutely lowest Height Difference from all the results created by the UAV Forest Explorer within each specific run. The diagram contains the combination of both, the Height Difference values (line chart) and the Count Difference values (bar chart) resulting from the appropriate tool outputs, which were selected as the Best results.

Values come from each study plot using all three types of ground truth data (All FM trees / Reduced number of FM trees / Modified positions of the reduced FM trees). The particular values of the source data used for the visualisation are then present in the Table 16.

*Table 16. The values of the Count Difference [trees] and Height Difference [metres] gained from the Best Results meeting the condition of the lowest value of Height Difference from all the tool outputs. Values gained for each study plot and for each kind of field-measurements data.*

Min. HD	All FM Trees		Reduced FM Trees		Modified FM Trees	
	Count Difference	Height Difference	Count Difference	Height Difference	Count Difference	Height Difference
<b>I.</b>	1591	3.305	1610	0.958		
<b>II.</b>	1083	3.480	443	0.018		
<b>III.</b>	1481	2.402	372	0.041		
<b>IV.</b>	1565	1.049	1	-0.018		
<b>V.</b>	1488	3.234	1461	0.537		
<b>VI.</b>	1801	2.592		-0.005		
<b>VII.</b>	-10	-0.003	0	0.001		
<b>VIII.</b>	2308	1.425	12	-0.019		
<b>IX.</b>	775	0.014		0.006		
<b>X.</b>	4	0.019	9	-0.005		
<b>XI.</b>	177	-0.018	3	-0.027		
<b>XII.</b>	35	0.003	-23	-0.015		
<b>XIII.</b>	969	0.118	13	-0.007	-5	-0.006
<b>XIV.</b>	155	0.008	13	0.001	-3	0.010
<b>XV.</b>	2523	0.154	51	0.003	1	0.007
<b>XVI.</b>	1	0.002	-9	-0.001		
<b>XVII.</b>	-35	0.000	-23	0.009		
<b>XVIII.</b>	56	-0.004	1	-0.005		
<b>XIX.</b>	149	-0.007		-0.009		
<b>XX.</b>	7	0.001	-9	-0.014		
<b>Average</b>	806	0.889	196	0.072	-2	0.004

The last assessed quantity concerning the Best Results from the UAV Forest Explorer outputs from the 20 study plots, is the Standard Deviation of the height values of the automatically identified trees. As described earlier, the lowest values of the Standard Deviation were extracted only from the results whose Count Difference was in the range of  $\pm 1$  tree.

The Table 17. contains the particular values of the Standard Deviation together with corresponding values of Height Difference acquired within the same tool iterations leading to the demanded Best Results. Data were extracted from the outputs from all study plots using all three kinds of ground truth data (All FM trees / Reduced number of FM trees / Modified positions of the reduced FM trees).

*Table 17. The values of the Count Difference [trees] and Height Difference [metres] gained from the Best Results meeting the condition of the lowest value of Height Difference from all the tool outputs. Values gained for each study plot and for each kind of FM data.*

Min. SD	All FM Trees		Reduced FM Trees		Modified FM Trees	
	SD of Height of IT	Height Difference	SD of Height of IT	Height Difference	SD of Height of IT	Height Difference
I.	1.179	4.657	1.109	2.553		
II.	1.508	5.165	1.463	1.773		
III.	1.387	4.785	1.475	1.719		
IV.	2.556	3.353	2.487	0.271		
V.	1.388	4.997	1.224	2.381		
VI.	2.632	4.543	1.982	0.049		
VII.	1.076	0.648	1.026	-0.270		
VIII.	3.700	4.503	2.778	0.765		
IX.	2.487	2.156	2.243	0.294		
X.	1.668	0.785	1.509	-0.033		
XI.	4.571	3.058	4.624	2.917		
XII.	3.058	2.508	3.097	2.793		
XIII.	3.709	4.453	1.256	0.891	1.224	0.654
XIV.	1.855	1.029	1.236	0.991	1.217	0.945
XV.	2.255	3.123	2.195	0.696	2.158	1.327
XVI.	1.772	0.011	1.553	-0.385		
XVII.	1.562	-0.342	1.349	-0.493		
XVIII.	2.731	0.041	1.678	-0.342		
XIX.	1.791	1.988	1.354	0.176		
XX.	5.252	-2.535	2.827	0.135		
<b>Average</b>	<b>2.407</b>	<b>2.446</b>	<b>1.923</b>	<b>0.844</b>	<b>1.533</b>	<b>0.975</b>

The lowest values of Standard Deviation from Table 17. are visualised in the combined diagram in the Figure 87. The line chart represents the values of Height Difference and the bar chart the values of Standard Deviation (both in m).

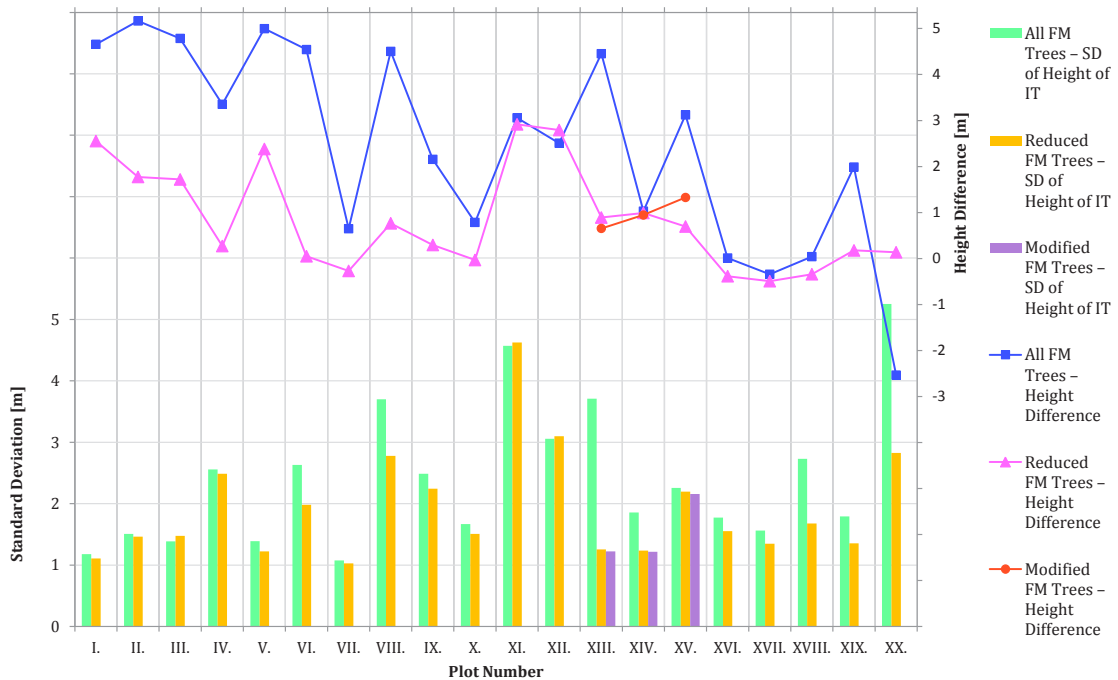


Fig. 87. The combined diagram showing the values of Height Difference (upper part and right axis) and Standard Deviation values (lower part and left axis) for each study plot and each FM data. Created from Best Results with  $\pm 1$  tree of Count Difference.

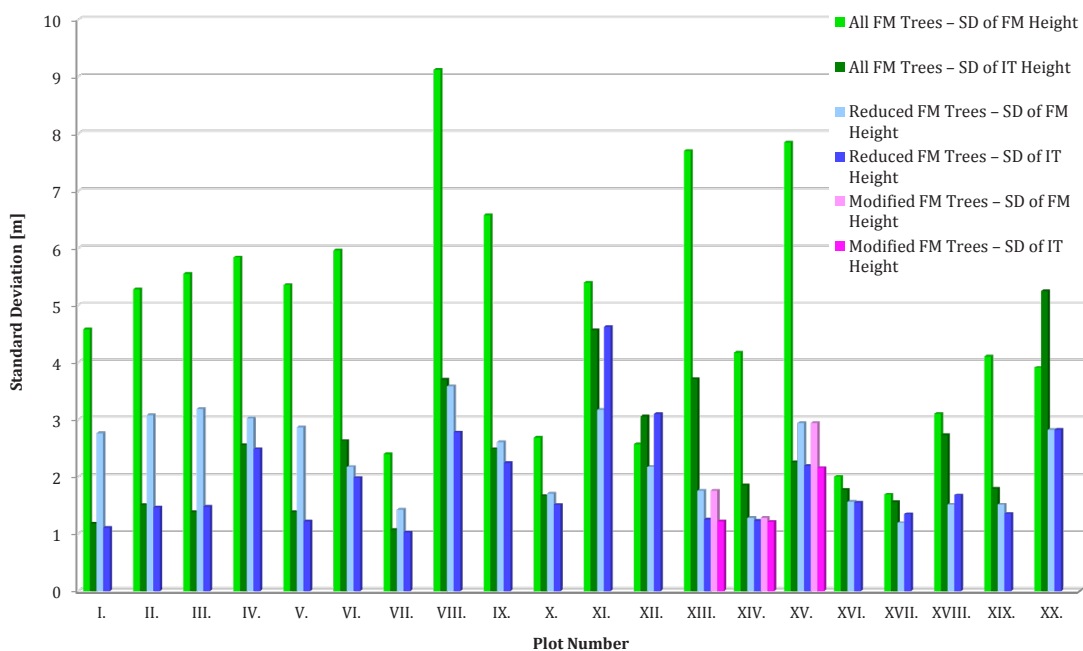


Fig. 88. The comparison of Standard Deviation of height values of field-measured trees and of identified trees (the lowest SD from results with Count Difference of  $\pm 1$  tree).

The diagram in Figure 88. is then showing the comparison of Standard Deviations counted for the final height values of FM trees at each plot and for the calculated height values of identified trees - lowest within the results with Count Difference of  $\pm 1$  tree. The source values are then stored in the Table 18.

*Table 18. The values of the Standard Deviation of Height values of field measured trees and of identified trees within the results with Count Difference of  $\pm 1$  tree.*

SD of FM/IT	All FM Trees		Reduced FM Trees		Modified FM Trees	
	SD of FM Height	SD of IT Height	SD of FM Height	SD of IT Height	SD of FM Height	SD of IT Height
I.	4.586	1.179	2.759	1.109		
II.	5.281	1.508	3.075	1.463		
III.	5.556	1.387	3.187	1.475		
IV.	5.841	2.556	3.025	2.487		
V.	5.360	1.388	2.867	1.224		
VI.	5.960	2.632	2.176	1.982		
VII.	2.398	1.076	1.426	1.026		
VIII.	9.122	3.700	3.581	2.778		
IX.	6.577	2.487	2.605	2.243		
X.	2.688	1.668	1.709	1.509		
XI.	5.400	4.571	3.174	4.624		
XII.	2.569	3.058	2.173	3.097		
XIII.	7.701	3.709	1.757	1.256	1.757	1.224
XIV.	4.172	1.855	1.281	1.236	1.281	1.217
XV.	7.850	2.255	2.936	2.195	2.936	2.158
XVI.	2.005	1.772	1.567	1.553		
XVII.	1.690	1.562	1.194	1.349		
XVIII.	3.099	2.731	1.512	1.678		
XIX.	4.109	1.791	1.512	1.354		
XX.	3.910	5.252	2.826	2.827		
<b>Average</b>	4.794	2.407	2.317	1.923	1.991	1.533

#### 5.2.2.2. Suitable CS, IM and FS Settings of the Tool within the ABA

This part is devoted to an assessment of the initial settings of the UAV Forest explorer which led to the Best Results regarding the ABA. Also now all three types of settings, that means Cell Size, Interpolation Method and Focal Statistics Circle Radius, are evaluated. Each Best Results table contains four rows, each representing the most appropriate result meeting various requirements. Between these requirements belong lowest value of Height Difference from outputs with Count Difference of 0 trees, lowest

value of Height Difference from outputs with Count Difference of  $\pm 1$  tree, lowest value of Height Difference from all the outputs and lowest value of Standard Deviation of height values of identified trees from outputs with Count Difference of  $\pm 1$  tree.

Since the third mentioned kind of results i.e. lowest value of Height Difference from all the outputs, is rather of an informative character, then being a Best Result in the proper meaning, this type of results was not utilized in the settings assessment.

From the remaining three types of results either only one, or all of them were processed. The results having the lowest Height Difference and meeting the condition of having the Count Difference of zero trees can be considered the most convenient from all the outputs. The settings from this type of results should therefore provide the information of the most suitable way how to process the data of the specific explored forest stands regarding the Area-Based Approach. These settings were therefore selected and arranged in the Table 19.

*Table 19. The Cell Size, Interpolation Method and Focal Statistics circle radius values selected as the Best Results for each study plot. The source results were meeting the condition of the lowest Height Difference and the 0 trees of Count Difference (if possible).*

Plot Number	All FM Trees			Reduced FM Trees			Modified FM Trees		
	CS	IM	FS	CS	IM	FS	CS	IM	FS
I.	20	TNN	2	35	BI	1			
II.	10	BN	4	25	BA	2			
III.	35	BM	1	45	BM	1			
IV.	40	BN	1	45	TNN	1			
V.	10	BA	5	15	TNN	4			
VI.	10	TNW	3	30	BA	2			
VII.	45	BA	2	35	TNN	3			
VIII.	40	TNN	1	30	TNN	2			
IX.	15	BI	4	40	BN	2			
X.	35	BA	1	10	TLN	5			
XI.	20	BA	5	30	TNN	3			
XII.	60	TLN	1	50	TNW	1			
XIII.	40	BI	1	50	TNN	1	20	BI	4
XIV.	10	TNN	6	45	TLW	1	55	BI	1
XV.	10	TNN	5	35	BA	1	25	TNW	2
XVI.	15	BA	4	45	TLW	1			
XVII.	5	TNW	7	10	TLN	4			
XVIII.	35	BI	1	20	TNN	4			
XIX.	30	TLN	1	45	TLW	1			
XX.	15	TNN	4	45	BM	1			

The summarized frequencies of CS, IM and FS values extracted from the 129 results (43 \* 3) of the reduced ABA group (without the described category) are arranged in the Tables 20. to 22. and visualised in the Figures 89. to 91. Namely representations of the Cell Size values are shown in Table 20. and Figure 89., frequencies of particular Interpolation Methods are contained in Table 21. and Figure 90. and summed counts of the Focal Statistics Circle Radiuses extracted from these results are to be seen in Table 22. and Figure 91.

Table 20. The frequency of Cell Sizes representing the Best Results within ABA.

CS	5	10	15	20	25	30	35	40	45	50	55	60	65	70
Frequency	6	19	17	9	14	11	16	12	16	4	1	1	1	2

Table 21. The frequency of Interpolation Methods representing the Best Results within ABA.

IM	BA	BI	BM	BN	TLN	TLW	TNN	TNW
Frequency	24	22	11	11	19	8	23	11

Table 22. The frequency of Focal Statistics Circle Radius values representing the Best Results within ABA.

FS	1	2	3	4	5	6	7	8	9	10
Frequency	48	26	11	19	8	4	8	2	2	1

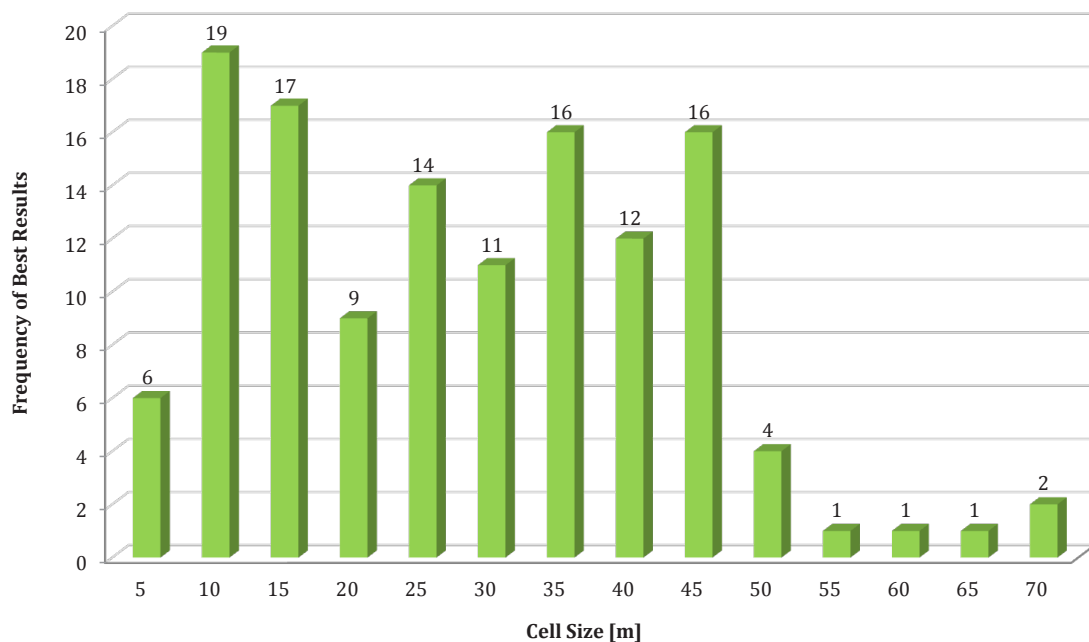


Fig. 89. The Cell Size values applied for the tool runs leading to the best results concerning the ABA. The diagram sums the frequencies from the 129 ABA best results.

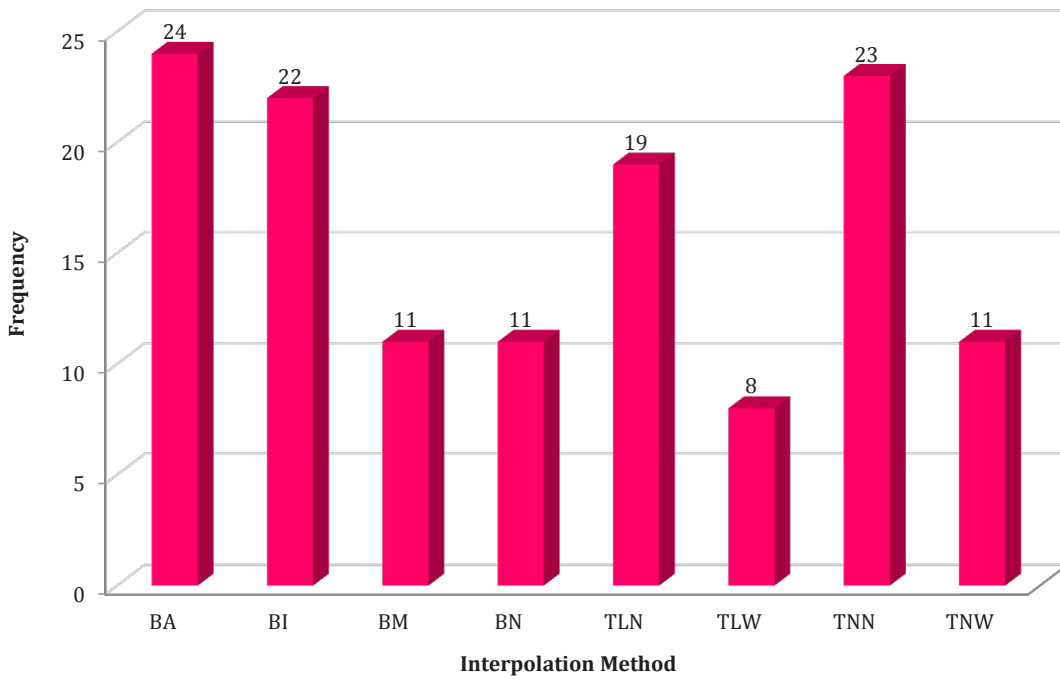


Fig. 90. The Interpolation Methods applied for the tool runs leading to the best results concerning the ABA. The diagram sums the frequencies from the 129 ABA best results.

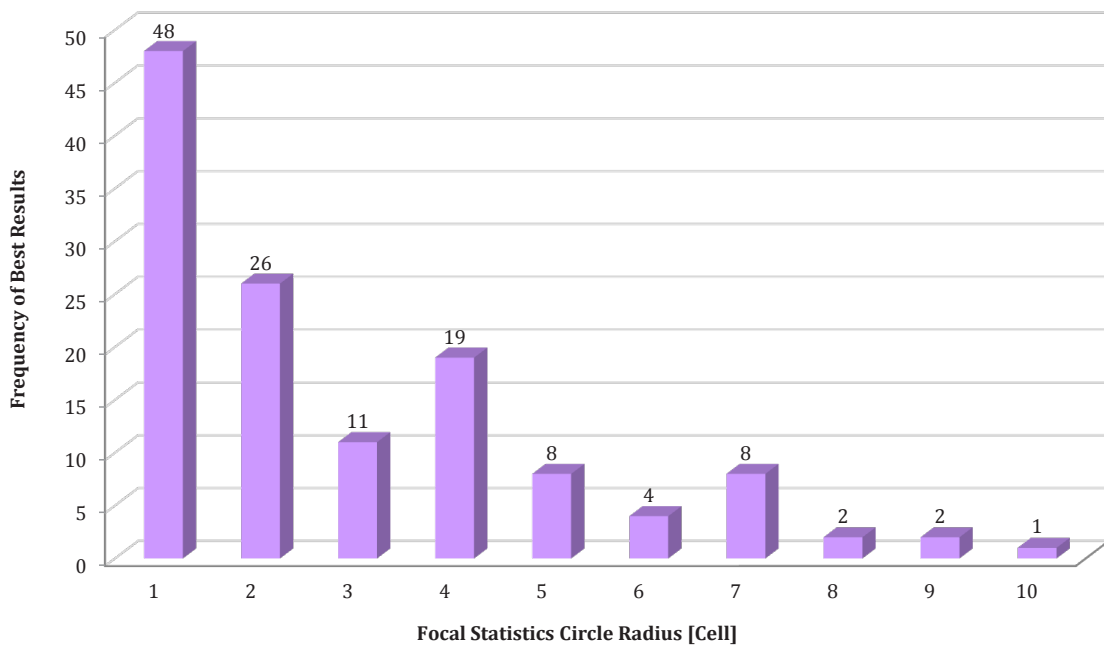
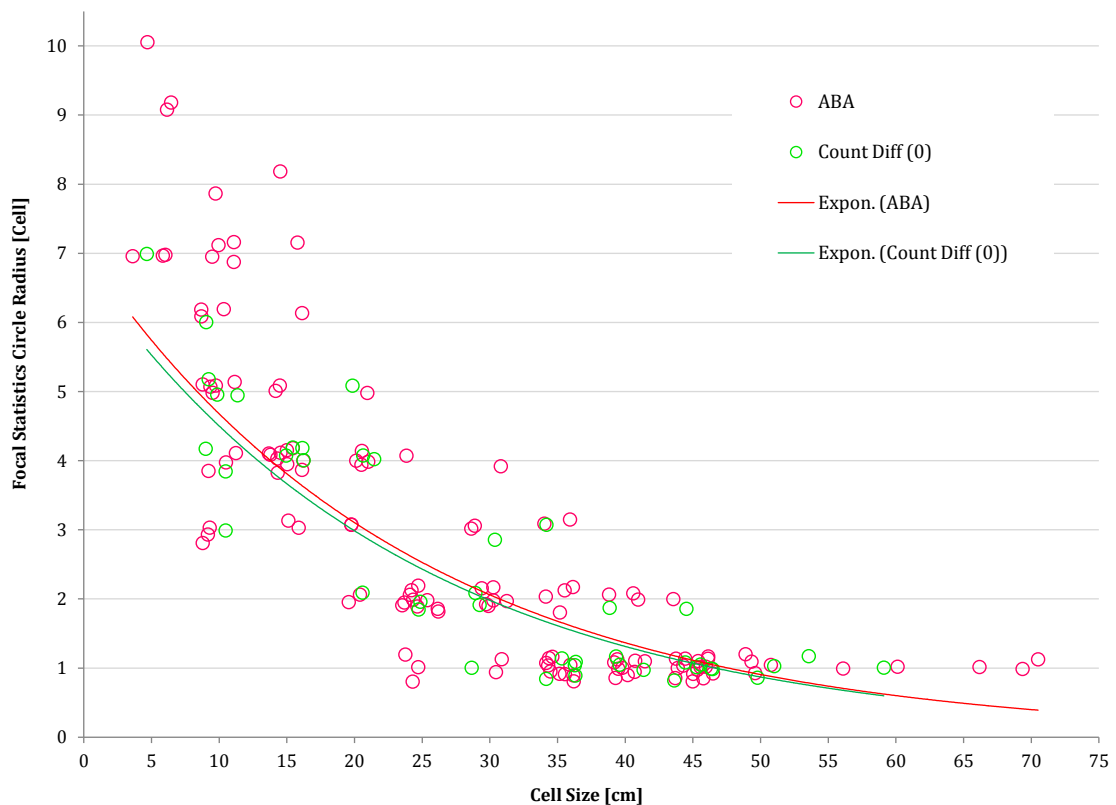


Fig. 91. The Focal Statistics Circle Radius values applied for the tool runs leading to the best results concerning the ABA. The diagram sums the frequencies from the 129 ABA best results.



Also now the relationship between CS and FS values was examined. The combinations of these values leading to the Best Results within ABA are depicted in the Figure 92. Both types of results were used in this case, i.e. 1) only these meeting the condition of the lowest Height Difference within the results with Count Difference of 0 trees, and 2) also all the cumulative 129 results within the whole ABA group.

Also in this case the data in the diagram were purposely 'jittered' by adding some random noise to reveal also the numerous overlapping values. This enables to better visualise the distribution and frequencies of particular combinations of CS and FS values.



*Fig. 92. The combinations of CS and FS values from the ABA group. Includes both, the data only from Best Results with Count Difference of 0 trees (43 results), but also the data from the whole ABA group after reduction (129 results). The lines represent the trend of data calculated as the exponential regression.*

## **5.3. Interpretation of Results**

In this chapter the results are examined, summarized, and some important relationships between various kinds of results are described.

### **5.3.1. Interpretation of DTM Processing Results**

As described in the chapter 4.2. Specification of Study Plots, some terrain conditions and characteristics were derived by the analysis of the DTM 5G from the ČÚZK. Concerning the average slope of the terrain at each plot, the lowest value of  $1.1^\circ$  was at plot number VIII. Another 11 plots had the average slope between 2 and 5 degrees, 4 plots between 5 and 10 degrees. One plot reached the value of  $12^\circ$  and remaining three plots had all slope larger than  $20^\circ$ . Particularly plot XII. had average slope of  $23.3^\circ$ , plot XI. reached the value of  $25.1^\circ$  and the steepest terrain was at plot number XX. with the average value of slope being  $28.5^\circ$ .

The rate of curvature values gained as the difference between maximal and minimal curvature counted for each plot was lowest at plots number I. and VII. reaching the value of only 0.4. Another six plots had the value still lower than 1 and 7 plots reached values between 1 and 2. More uneven terrain was at plot number III. with the value of 4.3 or plot IX. with value of 6.8. Even more rough terrain then could be found at plots XII. and XX., both with the curvature rate of 7. The most curved terrain was then at plot number XI.

It is worthy of notice, that the last four mentioned study plots (IX., XI., XII. and XX.) are also those with highest values of the slope. These four plots with steepest slopes therefore can also be considered generally having the most curved terrain conditions from all the twenty study plots.

### **5.3.2. Interpretation of Field Measurements Results**

#### **5.3.2.1. Counts of Trees and Species Composition**

Concerning the counts of trees present at particular study plots, their relations to ages of forest stands and to plot sizes are clarified. Therefore the logic of setting the plot sizes should be reminded first. The minimal required plot size was  $1000 \text{ m}^2$  (diameter 35.68 m) and the minimal demanded count of trees was 60. That means that if the  $1000 \text{ m}^2$  plot contained at least 60 trees, the size was

kept. If not enough trees were present in such plot, its size was enlarged (to up to 3300 m<sup>2</sup> which is 64.82 m diameter).

The minimal number of 60 trees was measured at only 3 study plots. At 9 study plots the count of trees ranged between 61 and 70 trees, at 4 plots between 71 and 80 trees and from the remaining plots 3 had the count of trees between 91 and 100 and one plot reached the maximum of 110 trees. The age of forest stands ranged between 31 and 141 years.

The plots with lowest numbers of trees (between 60 and 70) were mostly those with oldest trees (between 90 and 141 years) with two exceptions. One exception was a plot with 63 trees which were 71 years old (plot XVIII.) and another exception was plot XVI. with 66 trees, which were only 31 years old. This is interesting, since this is one of the two youngest forest stands which were examined and the second forest plot of the same age contained the maximal count of together 110 trees (both with 1000 m<sup>2</sup> plot size). The significant difference between the tree density of both forest stands originates in their composition, when the first mentioned plot consisted mainly of Douglas fir trees with larger spacing, and the second plot mainly of Norway spruce trees which were much closer to each other.

Concerning the age, the three oldest forest stands were following: plot XX. with mainly Norway spruce trees which were 110 years old (plot size was 1300 m<sup>2</sup>), plot XI. with mainly European beech trees, which were 125 years old (with plot size of 2000 m<sup>2</sup>), and plot XII. with mainly sessile oak trees, which were 141 years old (with plot size 1500 m<sup>2</sup>).

The second oldest forest stand (plot XI.) was at the same time the one with second largest study plot (2000 m<sup>2</sup>). Interesting is, that the forest stand with largest plot size was also composed of European beech trees (plot VII.) but these were 26 years younger (99 years old). The spacing between these trees was so large, that the plot size had to be enlarged to 3300 m<sup>2</sup> to reach the required minimum of 60 trees.

Regarding the forest stands composition, 8 study plots were broadleaf, i.e. with more than 75 % of broad-leaved trees (and from them 2 plots were fully broadleaf without any admixture), 9 study plots were coniferous (also 2 plots were fully coniferous) and 3 plots consisted of mixed deciduous and coniferous trees. From the particular tree species the most abundant was Norway spruce comprising over 24 % of all the trees present at the study plots. The second European beech then constituted 16.5 % and third sessile oak almost 14 % of the trees. Important

were also European hornbeam representing 11.7 %, Scotch pine 11.5 %, European larch 9.6 % or Douglas fir 7.4 % of all trees. The remaining nine species comprised less than 3 % of the trees.

Only one study plot had only one-species tree composition. It was plot VII. with 100 % of European beech trees. All other plots contained at least two species in their composition. The lowest portions of the admixture were at the plot XVI. with almost 94 % of Douglas fir, plot XI. with 93.3 % of European beech, plot XII. with 93.3 % of sessile oak, plot XX. with 87 % of Norway spruce, plot XVII. with 84.5 % of Norway spruce, plot XVIII. with 82.5 % of Norway spruce, plot X. with 78.3 % of Norway spruce or plot XIV. with 77.6 % of Scotch pine. At the remaining study plots the prevailing tree species constituted less than 75 % of the composition of the present trees.

On the other hand the study plots with the most complex species composition were plot number VIII. with together 9 different tree species, plot IV. with 8 tree species, plot II. with 7 species, or plots I. and XIII. each having 6 tree species present. Together 5 plots then contained 5 tree species, another 5 plots contained 4 species, 2 plots had 3 species present, 2 plots contained 2 species and 1 plot was constituted by one species only.

### **5.3.2.2. Height of Trees**

The field-measured height of trees can be summarized from different points of view. Concerning the average height of trees counted from all the trees present at each study plot, the lowest values began at 17 metres (plots I., II. and XVII.). Also plots III., V., X., XII. and XIX. had the average height lower than 20 metres. Plots IV., VI., XIII., XIV., XVI. and XVIII. then had the average height between 20 and 25 metres. Plots VII., VIII., IX., XV., and XX. then reached the average height of 25 up to 30 metres. The tallest trees from all the study plots were then measured in the plot number XI., since their average height reached the value of 31.1 metres. The average height of all the 1446 was then 22.6 metres.

The distribution of the height values ascertained at each study plot (meaning only one final value for each tree) can be deduced from the box-plots shown in the Figure 69. The diagram shows, that plots with highest dispersion of core values (i.e. with largest difference between first and third quartiles) were mainly plots I. to VI., VIII. and XIII. From these plots 5 forest stands have the prevailing trees broadleaf, two are mixed and only one is mainly coniferous. The age of these forest stands then ranged between 61 and 102 years.

On the other hand the plots with the most cumulated height values were plots VII., X., XIV., XVI. or XVII. From these plots only one consisted of broadleaved trees and 4 of coniferous trees. The age of the concerned trees then ranged between 31 and 99 years. The forest stands with the largest numbers of detected lower-values outliers are then at following plots: VIII., IX., X., XI., XIV. or XV.

Regarding the Standard Deviation of the field-measured height values (also taking into account only the one final value for each tree), the largest values were counted for plots VIII., XV. and XIII. (between 7 and 9 metres). In the case of 12 plots the SD varied between 3 and 7 metres, the lowest values of SD were then at plots number XVII., XVI., VII., XII., and X., ranging between 1.7 and 2.7 metres. The average value of SD for all the 20 study plots was then 4.8 metres.

The last assessed quantity concerning the field-measured heights of trees is the range of height values counted as the difference between maximal and minimal height acquired by the measuring person for each particular tree. The mean of these ranges counted for each study plot gives the idea of the variability and also accuracy of the field-measured height values. The largest average range reaching the value of more than 1.5 m comes from the plot number XI. This is a plot with mainly European beech trees being 125 years old, with second steepest slope and with highest rate of curvature from all the study plots. This plot also contains the tallest trees from all examined forest stands.

The second place then took number XV. with the average range of FM height values of almost 1.3 m. This forest stand with large portion of Scotch pine trees was 100 years old. The third highest value of the average range (1.2 m) then comes from the plot VII. This is the only one single-species forest stand, consisting of only European beech trees, being 99 years old. This plot also keeps the primacy in the size of the study plot (the one with 3300 m<sup>2</sup> area).

In the case of both European beech forest stands (plots VII. and XI.) the high values of the average range can be explained by the fact, that it is often quite difficult for the measuring person to see the real apex of the tall broadleaved tree with large-sized crown. In addition, when the tree crowns are closely adjacent to each other, it is often even impossible to reach the demanded distance from the tree to ensure the proper measuring conditions. The reason for the high range value in the case of plot XV. probably comes from the presence of relatively old Scotch pine trees. Their trunks were often curled and leaning and therefore it was also not easy for the measuring person to find the proper position and to ensure the highest accuracy of measurements.

Contrariwise, the lowest values of the average range of FM height values reached plots X., XVI. and XVII. with values between 0.4 and 0.5 metres. All three these forest stands were coniferous and relatively young. Forest in the plot X. was 47 years old and composed of Norway spruce. The terrain with almost 9° slope was the sixth steepest from all plots. Forest stand in the plot XVI. then consisted of Douglas fir being only 31 years old, situated on flat terrain. The study plot XVII. then contained mainly Norway spruce trees also only 31 years old. The terrain with slope of more than 9° was the fifth steepest. From these facts can be deduced, that young coniferous forest stands, even being on steeper terrain, offer good conditions for manual measurements of height of trees. The mean value of average range of height values counted for all the twenty study plots was then 0.87 m.

### **5.3.3. Interpretation of UAV Forest Explorer Results**

#### **5.3.3.1. Individual Tree Approach Results**

The various results regarding the statistical comparisons of the tool outputs with the field-measurements data are described in this chapter. Since the Best Results were acquired for three different types of FM data (using all FM trees, reduced number of FM trees without suppressed and undergrowth trees and in three cases also using reduced number of FM trees with manually modified positions), also the statistics were evaluated separately for these three groups. The following abbreviations will be used in this text for the described groups: AFM for All FM trees, RFM for Reduced number of FM trees and MFM for Modified positions of FM trees.

Another division was then based on the ranges of Count Difference values, as giving the important information about the difference between identified and field-measured trees. Also this division (Smaller Range (SR) and Larger Range (LR)) was applied for evaluation of the required statistics. Since also the combinations of these described divisions are important, the results are often described as belonging to AFM-SR, AFM-LR, RFM-SR, RFM-LR, MFM-SR or MFM-LR.

### 5.3.3.1.1. Root Mean Square Error

The first assessed quantity was the RMSE counted from the measured heights of FM trees versus the counted heights of identified trees. Its value was ranging between 0.4 (plot XVI.) and 16.2 (plot XI.) metres within all the divisions and all the study plots, with the average value of 8.5 m (including also the MFM group). From the average values of RMSE calculated for all the six combinations of groups (see Table 6. and 7.) for all the twenty study plots the differences between various groups can be clearly observed.

Generally the larger values of RMSE were gained on average in the AFM group (mean RMSE 9.7 m) compared to RFM group (mean RMSE 7.8 m) and in the SR group (mean RMSE 8.9 m) compared to LR group (mean RMSE 8.0 m). The descending tendency can be deduced from average values of RMSE from particular groups: AFM-SR: 9.7 m, AFM-LR: 9.6 m, RFM-SR: 8.5 m and RFM-LR: 7.1 m.

In the next part the average values of RMSE through all the groups are assessed for the specific study plots. The brackets adjacent to plot numbers contain brief characteristics to provide fast overview about the plots. Namely they contain the abbreviation of prevailing kind of species (B/C/M), the slope of the terrain in degrees and the curvature rate ascertained for the particular plots.

The three plots with largest values of RMSE were then following: Plot XI. (B, 25.1°, 13.8) with average RMSE of 16.1 m, plot XV. (C, 6.8°, 1.3) with the value of 14.7 m and plot VIII. (C, 1.1°, 1.3) with mean RMSE of 12.6 m. On the contrary the three plots with lowest average values of RMSE were plot XVI. (C, 4.3°, 0.5) with the value of 1.8 m, plot XVII. (C, 9.1°, 0.8) with average RMSE of 2.9 m and plot X. (C, 8.7°, 1.4) with the mean value of 3.7 m.

The largest difference between values from different groups concerning one study plot can be found in the case of plot number VI. (M, 3.7°, 0.6) when the RMSE value of 14.3 m (in the AFM-LR group) jumps down to only 2.1 m (in the RFM-LR group). Just to explain, why in some cases like here the value of RMSE is higher in the LR group than in the SR group (here 14.3 m vs. 13.7 m within the AFM group), the reason is simple. The priority when searching for the Best Results like RMSE or R was besides other things also the statistical significance of the Pearson's Correlation Coefficient. Since in the case of some study plots like plot VI. there were no statistically significant R values within the Smaller Range, the results

regardless this significance were picked up. Since in the case of Larger Range also some results with statistically significant R appeared, those were preferred, and even though having worse values of the main parameters, they were picked up for the Best Results.

The last assessment of the RMSE values is focused on the study plots, where also FM data with modified positions of trees were utilized (plots XIII., XIV. and XV.). The benefit of the positions of FM trees modification is obvious from the acquired data. When the average value of RMSE from the AFM group is 10.6 m, and the average RMSE in the RFM group is 9.8 m, the average value counted from data in the MFM group is less than half - only 4.8 m. Then in the scope of Smaller Range the average value for AFM data is almost 11 m, for the RFM data it is 10.3 m and for the MFM group only 6.0 m. Similarly comparing data from the Larger Range group, the average from the AFM data is 10.3 m, from the RFM data 9.3 m and from the MFM data only 3.5 m.

When looking at particular values, it is also apparent, that with exclusion of plot XVI. having the lowest values of RMSE, the plots XIV. and XIII. with ground truth data after modification are reaching the next lowest values within the Larger Range (only 0.99 m and 1.05 m respectively). That means that even though the examined plots with high portion of leaning Scotch pines had below-average values of RMSE concerning the AFM and RFM groups, the values from data after the modification dropped down to one of the best values from all study plots.

#### **5.3.3.1.2. Pearson's Correlation Coefficient**

The next evaluated statistics was the Pearson's Correlation Coefficient (R). The values of R ranged between 0.97 (plot XVI.) and 0.06 (plot I.) within all the study plots and various kinds of ground truth data, and the average value was 0.56 (including the FMF group). Contrary to the RMSE, in this case the differences between various divisions were much less significant and the mean values varied more or less around the overall average. Particularly the average of the AFM group was 0.56 and of the RFM group 0.54, the mean of SR group values was 0.54 and of the LR group 0.59. The specific combinations of groups then had following average values: AFM-SR: 0.53, AFM-LR: 0.58, RFM-SR: 0.51 and RFM-LR: 0.56.

When assessing the average values of R across all the division groups for single study plots, the 3 plots with highest values are following: Plot XVI. (C, 4.3°,



0.5) with mean R value of 0.86, plot X. (C, 8.7°, 1.4) with the value of 0.74 and plot XVII. (C, 9.1°, 0.8) with average R value of 0.72. The plots with lowest values of Correlation Coefficient were then following: Plot number I. (B, 3.6°, 0.4) with the R value of 0.12, plot III. (B, 3.8°, 4.3) with value of 0.28 and plot XI. (B, 25.1°, 13.8) with R reaching only 0.34. The largest difference between R values from various groups within single plots can be then found in plot number VI. (M, 3.7°, 0.6) with the highest value of 0.56 in the RFM-LR group and smallest R value of 0.15 in the AFM-SR group.

Evaluating the three forest plots where the modified FM data were utilized, (plots XIII., XIV. and XV.), the differences between particular groups are more obvious. The average value of R within AFM group came out 0.53, within RFM group similarly 0.55, but within MFM group raised to 0.79. Concerning the Smaller Range the average R value within AFM group was 0.50, within RFM group 0.54 and within MFM group 0.74. Then when assessing the Larger Range the mean value within AFM group was 0.56, within RFM group 0.57 and within MFM group even 0.84. The largest difference within a single plot between the specific divisions can be observed at plot XV., where the R raised from the value of 0.32 in the AFM-SR group to the value of 0.80 in the MFM-SR group (difference of 0.48).

All these data show, that even though the differences between all FM trees and reduced number of FM trees used as the ground truth were rather negligible, the effect of forest positions modification raised the R values significantly.

#### **5.3.3.1.3. Pearson's Correlation Coefficient for Matched Trees Only**

The values of Correlation Coefficient calculated only for the Matched Trees give better information about matching the calculated height values to the field-measured heights. Contrary to R described in the previous chapter, this value is not influenced by the FM trees which were not paired with any of the identified trees.

The values of R for MT then ranged between 0.99 (plot XVIII.) and 0.08 (plot III.) and the average value for all the division groups was 0.72. The differences between various groups were more significant in this case. The average of the AFM group was 0.66, of the RFM group 0.77, and of the MFM group even 0.89. The mean of SR group values was then 0.71 and of the LR group 0.74. The specific combinations of groups then had following average values: AFM-SR: 0.64, AFM-LR: 0.68, RFM-SR: 0.75, RFM-LR: 0.78, MFM-SR: 0.88 and MFM-LR: 0.90.

The 3 plots with largest average values of R for MT across the division groups were then following: XVI. (C, 4.3°, 0.5) with the mean value of 0.98, plot XVIII. (C, 6.8°, 1.1) with the value of 0.97 and plot X. (C, 8.7°, 1.4) also reaching the value of 0.97. In the contrary the study plots with lowest values of average R for MT were these: plot III. (B, 3.8°, 4.3) reaching the average value of only 0.15, plot I. (B, 3.6°, 0.4) with the value of 0.33 and plot V. (B, 4.5°, 0.5) with the mean value of 0.48. The largest difference between R values (calculated for matched trees only) from various groups within single plots then comes from the plot XIII. (M, 4.2°, 0.6) with the highest value of 0.81 in the RFM-LR group and lowest value of 0.48 in the AFM-SR group.

When assessing the three study plots with the MFM group of values, the most significant differences are not between this group and the RFM group, like in the previous case, but already between RFM group and the AFM group. The average value of R for MT is 0.56 within the AFM group, then 0.84 within RFM group and 0.89 for the MFM group. Regarding the Smaller Range the average value of R for MT within AFM group was 0.56, within RFM group 0.84 and within MFM group 0.88. Then when evaluating the Larger Range the mean value within AFM group was also 0.56, within RFM group also 0.84 and within MFM group then 0.90. The largest difference within a single plot between the specific divisions was then found at plot XIII., where the R for MT raised from the value of 0.48 in the AFM-LR group to the value of 0.89 in the MFM-LR group (difference of 0.41).

#### **5.3.3.1.4. Mean Difference of Heights for Matched Trees Only**

The Mean Difference of Heights for Matched Trees was counted as the averaged difference between the field-measured height of matched trees and the calculated height of these trees. That means, that if the resulting value was negative, the calculated heights were on average higher, than the measured heights, and vice versa. From the summarised results from all plots it is obvious, that in most of the cases the resulting values were negative.

Together 14 plots showed negative values for both AFM and RFM groups, one plot for AFM and MFM group, three plots had negligible difference from zero and only two plots showed positive values of the difference. The average mean difference for all plots and all types of ground truth data was -1.2 m. The average value for AFM group then was -1.8 m, for RFM group -0.7 m and for the MFM group

-0.5 m. The largest negative difference was present in the plot I. (B, 3.6°, 0.4) in the AFM group with the value of -4.7 m, largest positive difference was present in the plot XX. (C, 28.5°, 7.0) reaching the value of +0.6 m in the RFM group.

The three plots with largest mean difference across the division groups were following: plot I. (B, 3.6°, 0.4) with the average value of -3.6 m, plot XII. (B, 23.3°, 7.0) with the value of -2.6 m and plot XI. (B, 25.1°, 13.8) with the average value of -2.5 m. The plots with the average mean difference across the division groups closest to zero were then following: plot XVI. (C, 4.3°, 0.5) with the mean difference of only 0.02 m, plot VII. (B, 2.0°, 0.4) with the value of 0.06 m and plot XVIII. (C, 6.8°, 1.1) having the average difference of -0.15 m. The plots with the positive values of the mean difference across the divisions were these: plot XVII. (C, 9.1°, 0.8) with the mean value of +0.5 m and plot XX. (C, 28.5°, 7.0) with the average value of +0.4 m.

The largest contrast between the mean difference values from various division groups within the single plots could be found in the case of plot VI. (M, 3.7°, 0.6), having the value in the AFM group -4.4 m and in the RFM group only -0.3 m (difference of 4.2 m). The drop of the mean difference between AFM and RFM groups could be observed in most of the study plots. On average the difference between these two groups was 1,1 m. Only in the case of two study plots, particularly plot X. (C, 8.7°, 1.4) and XI. (B, 25.1°, 13.8) the negative difference slightly raised in the RFM group compared to the AFM group.

#### **5.3.3.1.5. Suitable CS, IM and FS Settings of the Tool within the ITA**

The initial settings of the UAV Forest Explorer which led to reaching of the Best Results within the ITA method, are described in this chapter. When assessing the Cell Sizes separately and only for the Best Results from the “RMSE & R” category, some facts can be deduced. For instance in the case of 12 study plots the CS value within AFM group was lower, than in the RFM group, in 3 cases the values were the same and in 5 cases the value within AFM group was higher than the value on the RFM group.

The average CS value of AFM group within the “RMSE & R” category then was 24.8 cm, and of the RFM group on average just 10 cm higher, i.e. 34.8 cm. When assessing all the 301 Best Results of the ITA group, the average CS value

within the AFM section was 24.4 cm and within the RFM section of 8.5 cm higher, exactly 32.9 cm. These data manifest the general inclination to larger Cell Sizes when using the FM data with reduced number of trees.

Concerning the CS values from the occurrence point of view, the most frequent value within the 301 Best Results was Cell Size of 10 cm appearing 56 times. The second place belonged to CS of 15 cm appearing 36 times and third place to CS of 35 cm which was used 32 times to reach some of the Best Results. All of the values between 5 and 45 cm appeared more than 10 times (with lowest frequency of CS 5 appearing only 12 times). The frequencies of Cell Sizes of 50 cm and larger then varied between 1 and 9 with the second largest CS value of 80 cm (used 2 times) and the only once appearing largest CS value of 100 cm.

When evaluating the frequencies of Interpolation Methods utilized for reaching the Best Results within the whole ITA group, it is obvious, that some of the methods were less favoured than the others. Particularly methods as BM (Binning with 'Maximum' Cell Assignment) and TLW (Triangulation with 'Linear' IM and 'Window\_Size' Point Thinning Type) were used only around 20 times each. The method BN (Binning with 'Nearest' Cell Assignment Type) was then used 34 times and all the other 5 Interpolation Methods (BA, BI, TLN, TNN and TNW) were applied similarly between 40 and 50 times.

When assessing separately the values of Focal Statistics Circle Radiuses used for reaching the Best Results within ITA, the most abundant value was 1 Cell with the frequency of 132. The second most often utilized value of 4 Cells was appearing only 35 times. The other values of FS 2 - 3 Cells and 5 - 10 Cells then appeared between 32 and 2 times with descending tendency from 2 to 10.

Since the appearance of FS and also CS values separately does not provide enough information, the combinations of both values were assessed as well. From the diagrams in Figures 83. and 84. is apparent, that according to the expectations the combinations of smallest CS values and smallest FS values or large CS values and large FS values generally did not appear in the Best Results. For the Cell Size of 5 cm the most frequent FS values vary around 9 cells, for CS 10 is most often FS value 5 and 6, CS of 15 cm was appearing in combination with values of FS around 4 Cells, CS 20 then liked FS values around 3 to be paired with, CS 25 and 30 often appeared with FS value of 2 Cells and CS values of 35 cm and larger were then most often utilized in the combination with FS value of 1 Cell.

### 5.3.3.2. Area-Based Approach Results

#### 5.3.3.2.1. Count Difference, Height Difference and Standard Deviation

Within the Area-Based Approach the results with lowest Height Difference (HD), Count Difference (CD) and Standard Deviation (SD) of height values of identified trees were searched and exported as the Best Results. Regarding the four groups of results (one for the results with lowest Height Difference and with the Count Difference equal to 0 (CD0), another with Count Difference of maximally  $\pm 1$  (CD1), the third for outputs with lowest Height Difference at all and the last one for smallest Standard Deviation within the group of Count Difference of  $\pm 1$ ), the outputs can be summarized as follows.

First of all the first two groups were assessed. Within the group with the lowest Count Difference (if possible equal to zero) the Height Difference values ranged between -0.5 m in plot XVII. (C, 9.1°, 0.8) and 5.1 m in plot II. (B, 3.1°, 1.3) across all the kinds of ground truth data. The average Height Difference for this group then was 1.43 m. The differences between the two division groups were obvious. The mean Height Difference within the AFM group was 2.3 m, within the RFM group then 0.7 m.

The three plots with largest averaged Height Difference values within the CD0 group across the types of ground truth data, were plot V. (B, 4.5°, 0.5) reaching the value of 3.6 m, plot I. (B, 3.6°, 0.4) with the value of 3.5 m and plot II. (B, 3.1°, 1.3) reaching the value of 3.3 m. In the contrary, the three plots with the Height Difference values closest to zero were following: plot XVI. (C, 4.3°, 0.5) with the smallest mean value of only 0.001 m, plot XVIII. (C, 6.8°, 1.1) with the value of 0.03 m and plot VII. (B, 2.0°, 0.4) also with the value of 0.03 m. The largest difference between the AFM and RFM groups within single study plots then appeared in plot VI. (M, 3.7°, 0.6), having the AFM value 4.54 m and RFM value only -0.03 m (the difference is 4.51 m).

When assessing the three plots using the modified ground truth data, the largest difference is apparent still between values from AFM group (average HD of 2.6 m) and RFM group (average HD of 0.2 m), since the average value of MFM group is also almost 0.2 m.

As the second basic group of Best Results the one with Count Difference of  $\pm 1$  tree was evaluated. The values in this group ranged between -0.51 m in the case of plot XVII. (C, 9.1°, 0.8) and 5.09 m in the case of plot II. (B, 3.1°, 1.3) across

the types of ground truth data. The average Height Difference for this group then was 1.26 m (a bit less compared to 1.43 m of CD0 group). The differences between the two division groups were even more obvious in this case. The mean Height Difference within the AFM group was 2.2 m, within the RFM group then 0.5 m.

The 3 plots with largest mean value of HD within this group through both main kinds of ground truth data were the same as in the case of CD0 group, i.e. plots V, I. and II., with the only difference, that plot V. now had of 0.1 m smaller average value (3.5 m vs. 3.6 m). The three plots with the HD value closest to zero were also the same, but values different in this case and were following: plot XVIII. (C, 6.8°, 1.1) with the average HD value of 0.04 m, plot VII. (B, 2.0°, 0.4) having the value of -0.05 and plot XVI. (C, 4.3°, 0.5) reaching the value of 0.05 m. The largest difference between the AFM and RFM groups within single study plots then appeared again in plot VI., now with values of 4.50 m (AFM) and -0.04 m (RFM).

When assessing the three plots using the modified ground truth data, the largest difference the average values of HD for different groups were following: 2.28 m for AFM group, 0.16 m for RFM group and bit larger 0.34 for MFM group.

As the next evaluated group, the one containing values of absolutely lowest Height Difference from all the results from each tool run, was processed. The results with lowest HD were characteristic with sometimes unusually extreme values of Count Difference and therefore generally should not be considered being suitable for application.

Assessing these results based on the kinds of ground truth data shows significant differences between various groups. The average value of HD within the AFM group was 0.89 m and within the RFM group less than twelve times smaller, only 0.07 m. In the AFM group 7 plots had the smallest HD value larger than 1 m, particularly plots I. - VI. and VIII. with the average HD of 2.5 m. The remaining 13 plots than had the average HD of 0.02 m only.

This shows that the named 7 plots did not reach satisfactory values of Height Difference in any of the tool iterations and the calculated heights were always overestimated against the ground truth. This could be caused by the presence of many understorey trees in these plots. When using the Reduced ground truth data without the suppressed trees, the average Height Differences dropped down to few-centimetre values (except plots I. and V. still having the values in tens of centimetres).

Concerning the Count Difference, its average value was 806 trees within the AFM group, and more than four times smaller, particularly 196 trees in the RFM group. In the AFM group together 10 plots had the Count Difference of more than 500 trees. Again these were plots I. - VI., and VIII., then IX., XIII. and XV. The remaining ten plots had the value between 1 and 177 trees. In the RFM group then only four plots showed significantly large values, particularly plots I. - III. and V. had values of CD between 370 and 1610 trees. The remaining 16 plots had the average value of only 2.3 trees. But the relevance of these CD values is limited, since they varied a lot between the results with low HD values from each tool run.

When evaluating the three plots using the Modified ground truth data, the average smallest HD was 0.093 m within the AFM group, -0.001 m within the RFM group and 0.004 m within the MFM group. The average CD values were then following: 1216 within AFM group, 26 within RFM group and -2 within MFM group. The improving tendency is therefore obvious not only in the direction from the AFM group towards the RFM group, but also towards the MFM group.

The last assessed group within ABA then was the one with lowest Standard Deviation of height values of identified trees with the results with Count Difference of maximally  $\pm 1$  tree. Also now the values of the examined quantity were assessed together with the values of the Height Difference. The values of SD varied through the two basic kinds of ground truth data from 1.03 m at plot VII. (B, 2.0°, 0.4) to 5.25 m at plot XX. (C, 28.5°, 7.0) and the values of HD varied between -2.53 m at plot XX. (C, 28.5°, 7.0) and 5.17 m at plot II. (B, 3.1°, 1.3).

Concerning the particular kinds of ground truth data, also in this case the differences between the values in the two groups were noticeable. The average SD within the AFM group was 2.4 m, within the RFM group then 1.9 m. The average value of HD was then 2.5 m within AFM group and almost three times smaller, i.e. 0.84 m within the RFM group. Regarding the three plots using the MFM data the average SD then dropped from the value of 2.6 m within the AFM group to the value of 1.6 m within the RFM group and to the value of 1.5 m in the MFM group.

The three plots with lowest SD averaged across both main ground truth classes were then following: plot VII. (B, 2.0°, 0.4) with the average SD value of 1.05 m, plot I. (B, 3.6°, 0.4) with the value of 1.14 m and plot V. (B, 4.5°, 0.5) with the average SD of 1.31 m. The three plots with highest average SD (from the described Best Results with lowest SD within the CD1 group) were then following: plot XI. (B, 25.1°, 13.8) with the value of 4.60 m, plot XX. (C, 28.5°, 7.0) reaching the value of 4.04 m and plot VIII. (C, 1.1°, 1.3) with the average SD of 3.24 m.

Interesting is then comparison of Standard Deviations of heights of FM trees (counted only from the final height values of all trees within each study plot) and of Standard Deviations of the height values of identified trees calculated by the tool within the CD1 group. The SD values of heights of FM trees then ranged between 1.2 m in the plot XVII. (C, 9.1°, 0.8) and 9.1 m in the plot VIII. (C, 1.1°, 1.3).

Regarding the ground truth data types, the average value of SD for FM heights within AFM group was 4.8 m and within RFM group 2.3 m. Corresponding values of SD for IT heights were 2.4 m within AFM group and 1.9 m within RFM group. The three plots utilizing modified FM data then showed classical tendency when having following values: mean SD of FM heights within AFM group was 6.6 m, within RFM and MFM groups then 2.0 m. The average SD of IT heights was 2.6 m within AFM group, 1.6 m within RFM group and 1.5 m within MFM group.

#### **5.3.3.2.2. Suitable CS, IM and FS Settings of the Tool within the ABA**

The last assessment of the ABA results was then related to the initial settings of the UAV Forest Explorer which enabled to reach the particular Best Results. The results were evaluated based on two approaches. First only the results meeting the condition of lowest HD within the group with Count Difference of 0 trees were utilized (that gives 43 results) and then all the meaningful results within the ABA group were used - that means without the results with absolutely lowest HD values (that gives together 129 results).

In the first group, i.e. in the one within CD0 group, the summarization of the applied settings is following. The average CS value within the AFM group was 25.0 cm, in the RFM group then almost 10 cm larger, i.e. 34.3 cm. In the larger group of all the 129 results the average CS was 23.6 cm within the AFM group and 29.3 cm within the RFM group. So, similarly like in the ITA results also now the data show the logical inclination to larger CS values when using reduced number of FM trees.

Concerning the Interpolation Methods, the most often utilized methods within the 129 ABA Best Results were methods BA, BI, TLN and TNN, each applied between 15 and 20 times. The remaining interpolation methods (BM, BN, TLW and TNW) were then utilized between 8 and 11 times. The largest difference in the relative frequencies compared to ITA group then noticed methods BN and TNW having largest slump in the case of ABA.



The Focal Statistics Circle Radius values most often used to reach some of the 129 Best Results within ABA were then following: again the leader was FS value of 1 Cell utilized 48 times, followed by FS 2 (used 26 times) and FS 4 (used 19 times). The last FS value exceeding the threshold of 10 applications was the value of 3 Cells. The remaining FS values (5 to 10) were applied 8 times and less. When evaluating the important combinations of CS and FS values, the trend is obviously similar to the one of the combinations within ITA group. The only significant difference is in the maximal utilized CS value (in the combination with FS value of 1 Cell), now being only 70 cm (compared to 100 cm in the ITA case). Therefore it can be in a simplified way concluded, that the most often utilized combinations of CS and FS values are generally independent on the utilized assessment method (ITA vs. ABA).

## 5.4. Summarization of Results

The Table 23. contains summarized results from all the main categories regarding the terrain conditions (slope and curvature), field measurements (SD and Range of FM heights), and both - ITA method (RMSE, R, R for MT, Mean Difference for MT) and ABA method (HD within CD0 and CD1, SD of heights of IT in CD1) of UAV Forest Explorer runs. Particularly three study plots with lowest values and three study plots with highest values for each of the subcategories were picked up and arranged into the table. Then the study plots with relatively positive and negative primacies were summed up.

The summarized results can be described as follows. The study plot with the maximum of positive primacies (together 7 out of 10 possible) was plot number XVI. (C, 4.3°, 0.5) composed of Douglas firs being 31 years old. Even though this plot did not hold any primacy concerning the slope and curvature of terrain, it was one of the three plots with smallest Standard Deviation of field-measured heights, smallest range of FM heights, smallest RMSE, largest R, largest R for Matched Trees, smallest Mean Difference for Matched Trees and smallest HD within Count Difference of 0 and  $\pm 1$  tree.

The plot with second largest number of positive primacies (together 6) was then plot number VII. (B, 2.0°, 0.4) consisting of European beech trees 99 years

old. This plot gained the primacies already within the terrain conditions group, when having one of the flattest terrain with marginal curvature.

Concerning the field measurements it was one of the three plots with lowest SD of FM heights, but at the same time one of the three plots with largest range of FM heights as a negative primacy. The remaining primacies were only positive, particularly having one of the smallest Mean Differences for MT, smallest HD within CD0 and CD1 and smallest SD of heights of identified trees. As such this was the only plot having both possible primacies within ABA (having smallest both HD and SD). Since it was also the only plot having both primacies concerning the terrain conditions, some relationship between them and the other satisfactory results can be deduced.

The next study plots with largest number of positive primacies were plot X. (C, 8.7°, 1.4) composed of Norway spruces being 47 years old, plot XVII. (C, 9.1°, 0.8) composed also of Norway spruces, in this case being 31 years old (both having 4 positive primacies) and plot XVIII. (C, 6.8°, 1.1) consisting also of mainly Norway spruces being 71 years old. This plot then had together 3 positive primacies.

The plots with largest numbers of negative primacies were then following: Plot XI. (B, 25.1°, 13.8) composed of European beech trees being 125 years old having 7 negative primacies. This plot was the one with second steepest terrain and highest value of curvature rate. It had also primacy in having one of the largest ranges of FM heights. Then it was one of the three plots with largest RMSE, lowest R, largest Mean Difference for MT or largest SD of heights of identified trees. In the case of this plot a connexion between rough terrain conditions and not very satisfactory results of the field measurements and the tool computations can be deduced.

The plot with second highest number of negative primacies (together 6) was plot number I. (B, 3.6°, 0.4) consisting of various broadleaved trees (mainly sessile oaks, European hornbeams and European beeches) being 61 years old. This plot kept primacies in smallest R, smallest R for MT, largest Mean Difference for MT and largest HD within CD0 and CD1 groups. The remaining plots had 3 or less negative primacies.

Table 23. Summarization of results regarding study plots. 3 plots with smallest and 3 plots with largest values concerning each category are arranged in the table.

Plot Number	Terrain Conditions				Field Measurements				Individual Tree Approach								Area-Based Approach				Sums	
	Mildest Slope	Steepest Slope	Smallest Curvature Rate	Largest Curvature Rate	Smallest SD of FM Heights	Largest SD of FM Heights	Smallest Range of FM Heights	Largest Range of FM Heights	Smallest RMSE	Largest RMSE	Largest R	Smallest R	Largest R for Matched Trees	Smallest R for Matched Trees	Smallest Mean Difference for MT	Largest Mean Difference for MT	Smallest HD within CD0 and CD1	Largest HD within CD0 and CD1	Smallest SD of IT Heights in CD1	Largest SD of IT Heights in CD1	Sum of Positive Records	Sum of Negative Records
I.			X									X		X		X		X	X		2	4
II.																	X				0	1
III.											X		X								0	2
IV.	X																				1	0
V.													X				X	X			1	2
VI.																					0	0
VII.	X		X		X		X							X		X		X			6	1
VIII.	X				X				X										X		1	3
IX.																					0	0
X.						X		X		X		X									4	0
XI.		X		X			X		X		X				X				X		0	7
XII.		X		X											X						0	3
XIII.					X																0	1
XIV.																					0	0
XV.					X		X		X												0	3
XVI.					X		X		X		X		X		X		X				7	0
XVII.					X		X		X		X										4	0
XVIII.												X		X		X					3	0
XIX.			X																		1	0
XX.		X		X															X		0	3

## 6. Discussion

First of all it should be mentioned, that the developed UAV Forest Explorer tool was tested mainly on ArcGIS version 10.2. During all the approximately 40 000 iterations performed within this work, it proved to be 100% reliable and the tool performed well even during e.g. night-long calculations. Nevertheless, during some testing on version 10.3 there were observed some abnormalities causing crashing of the program a few times. The cause was not revealed within the scope of this work, therefore on versions else than 10.2, some instability may be observed. Since during the tool development several bugs were discovered in ArcGIS tools when applied for python scripting, it is possible that also this incompatibility between two ArcGIS versions can be caused by some bug in Esri products.

One disadvantage of the presented approach can be seen in the necessity to provide auxiliary raster data, representing the terrain below the examined forest stand. This may be an obstacle in areas, where no such datasets are available. But this is a general problem of photogrammetric processing of the aerial image data of densely forested areas. Some researchers already outlined the possibility to use also photogrammetrically derived DTMs gained from the UAV-based imagery, with promising results (Dandois & Ellis, 2013). When using the leaf-off season SfM-derived DTM in a broadleaf forest, the accuracy of tree height assessment was comparable to the accuracy gained when using LiDAR-derived DTM. The results using leaf-on season DTM were then less satisfying. Such approach and testing in coniferous stands should be a subject of further studies. In this work, only LiDAR-derived DTMs were utilized for their facile availability for the research areas. It should be also noted, that the accuracy and spatial resolution of the provided DMT influences the acquired accuracy of the calculated height of trees.

The accuracy of tree height assessment is a large topic for discussion. It should be emphasized, that the tool can provide only as accurate results, as accurate are the data provided as a ground truth measured in the field. Therefore the precision of field measurements directly influences all the further processing. Many different participating variables may suffer by some error or may be biased. Even though the height of trees was measured by a high-quality laser hypsometer, the difference in height values acquired for one tree from two or more positions, could be significant. Especially in the case of leaning trees the range of such values could reach up to several metres.

Difficult was also measurement of broadleaf trees in stands with closed canopy, where was not easy to see the apexes of the trees and to target them from at least two positions. Not surprisingly the highest range values were reached in such plot, furthermore situated on a steep curved terrain (plot XI.). The fact, that this plot collected also the highest cumulative grade concerning the number of negative quantities in the final comparison of study plots (Table R21.), indicates that the rough conditions, causing the difficulties in the field measurements, can be projected also in the accuracy of further data processing. For this assumption speaks also the plot with opposite primacy, i.e. with most of the positive quantities (plot XVI.). This coniferous forest stand situated on a flat terrain, had the smallest range of field measurement heights from all the twenty study plots.

Another element seemingly decreasing the accuracy of the field measurements was also the rounding of the final height value with a half-meter precision. It was, however a logical approach, taking the typical range of acquired values into consideration. Since all such and similar drawbacks are generally a common attribute of the field measurements of height of trees, it can be presumed, that utilization of data affected by these effects for processing within the tool, had similar impact, as would have only manual measurement of all the trees of interest.

Regarding the identification of individual trees and their counts, also several aspects could influence the final accuracy. Besides some rather rare tree abnormalities, such as double trunks or dead/broken-off treetops, it were also the more frequent leaning trunks. Since the position of trees was measured 1.3 m above the ground in the middle of the trunks (using the horizontal offset made by the total station), the real position of apex of leaning trees in a horizontal plane was often somewhere else. In the most obvious cases of old pine stands (plots XIII., XIV. and XV.) it was proved, that manual correction of the treetops based on the own remote sensing data, can highly improve the accuracy of results.

The success rate of matching the identified trees with corresponding field-measured trees could be influenced also by the chosen approach of creating Thiessen polygons, or by making a 1-m buffer around the convex hull surrounding the FM trees (what could potentially exclude trees with apexes leaning more than 1 m out of the plot). Nevertheless, these methods were chosen as giving very satisfactory results in most of the cases.

The general deficiency, that some suppressed and undergrowth trees cannot be discerned in the image-based remote sensing data, was tried to be circumvented in two ways. One was the utilization of a copy of field-measurements data with removed suppressed trees according to the histogram evaluation. Since all the tool calculations were processed also on all such datasets, it was obvious from the results, that the reduction contributed to decrease of the RMSE of heights in most of the plots. However, in the case of correlation coefficient, the trend was similar, when its value also decreased in most of the cases, what speaks rather against the reduction. The effect of reduction is therefore more or less disputable.

The second way was usage of Larger Range during the outputs assessment. This enabled to take into account also results with larger Count Difference, between the counts of identified and field-measured trees, than was the range of only  $\pm 5$  trees in the case of Smaller Range. The range was enlarged mainly into the negative direction, which means that the results with up to 30 % less identified trees, than are the reference trees, could be chosen as the best results. The final results show, that both RMSE and R values were improved by this step in most of the plots. This is partly logical, since it is generally easier to find more suitable values in the larger range of available results, partly it can indicate, that another numbers of suppressed trees could be removed from the reference data. Another approach for their selection could be chosen. Preferably all the trees could be classified as belonging to either dominant or suppressed tree layer, e.g. according to the Kraft's classification, already during the field surveys (e.g., Assmann, 1970).

The influence of suppressed trees can be observed also from the resulting values of Mean Difference of heights for matched trees. In most of the plots this value was negative for both, all and reduced FM trees used as reference data. That shows, that the height values of identified trees were often larger, than height values of corresponding FM trees. On the one hand this can indicate a general underestimation bias of field measurements data. On the other hand it can be explicated, that there was some portion of false matches, when a suppressed tree was paired with some taller identified tree in its neighbourhood. The highest negative Mean Difference values were reached in broadleaf forest stands, what can be explained by false matches caused by the typical crown shape of deciduous trees, where multiple apexes can appear and some nearby suppressed tree could be easily paired with such out-centric apex. Since only the highest identified tree

within each Thiessen polygon could be paired with FM tree, the false matches were caused probably mainly due to leaning trees in the case of coniferous forest stands.

Regarding the overall accuracy of the height assessment results from the UAV Forest Explorer from all the study plots, following assumptions can be made. The average RMSE from all plots was 8.73 m, ranging between 0.40 m (plot XVI.) and 16.23 m (plot XI.). In the literature dealing with the same approach (use of UAV-based imagery and SfM software) can be often found better results. Such results range between 0.2 m (Díaz-Varela et al., 2015) and 10.9 m (Dandois & Ellis, 2013) with the average value being around 2.5 m. The average value of  $R^2$  at all the study plots was 0.30 ranging between 0.01 (plot I.) and 0.94 (plot XVI.). In the available studies the value of  $R^2$  ranged between 0.07 (Díaz-Varela et al., 2015) and 0.95 (Puliti et al., 2015) with the average value around 0,65. Also these values do on average seem to be better, than those reached in this work.

The reason why in this work were not reached such satisfactory results as in the available literature, can be very simple. The main constraint on the selection of the Best Results in this work was the Count Difference, i.e. the difference between counts of identified and field-measured trees, either within the individual tree approach, or area-based approach. This is an important variable, since it would be easy to find results with lowest RMSE or highest  $R^2$ , without regard to the numbers of actually identified trees. In such cases, numbers of identified trees can easily manifold exceed the numbers of FM trees, or vice versa. It is no doubt, that such results are not very useful for a seriously meant height assessment. In spite of this fact, some authors seem to ignore to uncover how many trees they used for their height assessment (Lisein et al., 2013), or compared only few trees at each plot (Dandois & Ellis, 2013). The works showing their success rate of trees identification, then did not reach very good results, even though their authors identified the trees purely manually (Wallace et al., 2016; Sperlich et al., 2014).

As one of the largest advantages of the UAV Forest Explorer tool, can be considered the fact, that it makes it easy to select just such results, which do differ in the Count Difference only within demanded limits. When the settings leading to these results are subsequently applied on the whole forest stand, it can be expected, that the gained values highly correspond with not only heights, but also counts of the actually present trees in the explored forest stand. The serviceability of such results is then very high and can compete the area-wide manual inventory.

Between the remaining issues to be discussed, belongs the methodological improvement which could test the accuracy of the selected settings, when applied on the whole forest stand far beyond the area of field measurements. In further research some reference study plots could be established, so that two or more of them would be present in selected larger forest stands. Then it would be possible to assess suitability of the best results from one study plot, when applied on the corresponding study plot. Also, if differing, some average settings from both study plots could be selected for the final application. But future implementation of such approach would require more manpower and time for the field measurements.

Further it can be discussed, if time and economical efficiency of the UAV Forest Explorer could be assessed. For such assessment the records of time consumption of individual steps of the workflow, such as field measurements, UAV campaigns or photogrammetric processing of the data as well as processing within the own tool, would be needed. Since such data were not collected in a suitable form, it cannot be responsibly stated, e.g. what is the threshold area of forest stand, from which it is worthwhile to apply the methodology and software presented in this work. Such time-demands data collection and economical efficiency calculation, could be for sure a subject of further research.

Another interesting topic is the possible calculation of other dendrometrical parameters. Many authors use remote sensing data to calculate and derive e.g. density and volume of trunks, stocking, biomass volume, carbon stocks, stand productivity, etc. (e.g. Borgefors et al., 1999; van Leeuwen & Nieuwenhuis, 2010). However, only the height of trees, being generally a fundamental quantity for all such calculations, was assessed in this work. Extension to deal with derivations of other parameters would need to be a subject of other studies.

The last thing to be discussed is the potentiality of the UAV Forest Explorer to process also LiDAR data. Based on the high similarity of the data resulting from the SfM software and of the data acquired during the aerial laser scanning missions (both point clouds in \*.las format) it can be assumed, that also the LiDAR data could be used as a Surface Point Cloud input for the tool. Nevertheless, such trials were out of the scope of this work and can be a subject of further investigations.

Finally it should be emphasized, that the methods and novel software tool described in this work are fully in accordance with the actual trends in precision forestry in developed countries and have high potential to improve the accuracy and operability of forest inventories and to support efficient forest management. Hopefully such technology will soon contribute to advancement of forest praxis.



## 7. Conclusion

All the aims of this work were successfully accomplished. Primarily a brand new software application for assessing the height of trees, based on the remote sensing data, was developed and programmed. This application, which was called “UAV Forest Explorer”, was designed as a novel custom tool running within the ArcGIS for Desktop software. The source data to be processed by the application, were images from two digital cameras (RGB and NIR) mounted on an Unmanned Aerial Vehicle, particularly a hexacopter DJI Spreading Wings S800.

To acquire such images, a series of 20 circular study plots was established in the Training Forest Enterprise Masaryk Forest Křtiny belonging to Mendel university in Brno. Different study plots were chosen to represent various kinds of forest stands concerning their ages, species compositions, densities of trees or terrain conditions. All the forest stands containing these study plots were then orthogonally photographed by the means of UAS. To accurately georeference the data, the ground control points were measured using geodetic GNSS devices.

All the images were then photogrammetrically processed within Agisoft PhotoScan software and the image-based 3D point clouds, ready for Canopy Height Models formation, were created for each study plot. Alongside the source code of the application was progressively developed and the whole script was programmed in the PythonWin software. The graphical user interface of the custom tool was then designed in ArcMap software. The tool was projected to work with the described point cloud data representing the canopy surface and with auxiliary raster data representing the terrain under the examined forest stands.

The Inverse Watershed Segmentation principles incorporated within the tool then enabled to identify the individual trees in the provided data and to calculate their height. The tool was designed in the way to optionally iterate to produce a series of results differing from each other due to various user-defined settings of the IWS applied on the processed data. The settings producing the results best fitting to the real numbers and heights of the examined trees were then sought. The most appropriate results regarding the numbers of identified trees could be assessed already visually, simply using the orthophoto images.

To assess the height values of identified trees, the reference ground truth data were needed. For this purpose, all the 20 study plots were visited with necessary equipment and the required properties of almost 1500 trees were thoroughly

manually measured. First of all the height of each tree with DBH larger than 7 cm was measured using the laser hypsometer. The species of trees, morphological abnormalities or health conditions were also recorded. Then the exact position of the middle of each tree trunk was measured using total stations.

The data acquired during the field measurements then could be provided in the initial settings of the UAV Forest Explorer as the ground truth. In such case the tool automatically compared the outputs of its own calculations, i.e. identifications of trees and estimation of their height, with the provided field-measurements data. It performed a series of mathematical and statistical calculations comparing the processed datasets using area-based approach as well as individual tree approach.

The results of such comparison then provided values such as Mean Absolute Error, Root Mean Square Error, Pearson's Correlation Coefficient and its statistical significance, Coefficient of Determination, but also the numbers of matched trees or redundantly identified trees, within the scope of ITA. For the ABA were then relevant values such as Height Difference between average height of field-measured and identified trees, Standard Deviation of these heights and Count Difference between numbers of measured and automatically identified trees.

Because each of the numerous iterations (hundreds for each study plot) raising from the ranges of user-defined inputs produced its own cumulative statistics, these were synoptically exported in a tabular form as one of the final outputs of the tool. The settings, which led to the results the most fitting to the particular field measurements, then could be easily found. These results were finally described in detail and the study plots were graded concerning the smallest and largest values of the examined variables within the scope of each approach.

The tool proved to be fully applicable for height assessment of various types of forest stands. Since usually only little portions of the forest stands are meant to be used for the field measurements of the tree heights and positions, the discovered most suitable settings then can be applied on the full extent of these particular stands. Because not only the difference between the heights, but also the difference between the counts of measured and identified trees should be minimal, using the selected settings, this should guarantee, that the results will be calculated with highest available accuracy and will maximally fit to each particularly examined forest stand. The effort and time consumption of such endeavour are then to be a fraction compared to potential manual measurements of all such trees.

## 8. Souhrn

Všech cílů vytyčených v této práci bylo úspěšně dosaženo. Především byl vyvinut a naprogramován zcela nový softwarový nástroj pro hodnocení výšky stromů na základě dat dálkového průzkumu Země. Tato aplikace, jež byla nazvána „UAV Forest Explorer“, byla navržena jako nový uživatelský nástroj fungující v rámci programu ArcGIS for Desktop. Zdrojovými daty určenými ke zpracování tímto nástrojem byly snímky ze dvou fotoaparátů (RGB a NIR) připevněných k bezpilotnímu prostředku, konkrétně hexakoptéře DJI Spreading Wings S800.

K získání takovýchto snímků bylo na území Školního lesního podniku Masarykův les Křtiny, patřícímu Mendelově univerzitě v Brně, založeno dvacet kruhových výzkumných ploch. Výzkumné plochy byly volené tak, aby reprezentovaly nejrůznější typy lesních porostů vzhledem k jejich věku, druhové skladbě, zakmenění, či terénním podmínkám. Všechny lesní porosty, v nichž se tyto zkusné plochy nacházely, byly poté ortogonálně nasnímány pomocí bezpilotního systému. Pro potřeby georeferencování získaných dat byly zaměřeny vlíčovací body pomocí geodetických GNSS zařízení.

Všechny snímky byly následně fotogrammetricky zpracovány v programu Agisoft PhotoScan a pro každou zkusnou plochu bylo vytvořeno 3D mračno bodů, následně využité k tvorbě výškového modelu korunového zápoje. Souběžně byl vyvíjen návrh aplikace, jejíž zdrojový kód byl postupně naprogramován v softwaru PythonWin. Grafické uživatelské prostředí vlastního nástroje bylo vytvořeno v programu ArcMap. Nástroj byl navržen k práci s popsány mračny bodů, reprezentujícími povrch korun, a s pomocnými rastrovými daty, která charakterizují terén pod zkoumanými lesními porosty.

Principy segmentace inverzních povodí obsažené v nástroji poté umožnily identifikovat v poskytnutých datech jednotlivé stromy a určit jejich výšku. Nástroj byl navržen tak, aby mohl volitelně provést mnoho opakování a vytvořit tak řadu výstupů. Ty se od sebe liší na základě různých vstupních uživatelských nastavení, jež jsou na zpracovávaná data aplikována. Následně byla hledána nastavení vedoucí k výsledkům, které nejlépe odpovídaly reálným počtům stromů a jejich výškám.

K zjištění přesnosti vypočtených výšek stromů bylo zapotřebí referenčních dat pozemního šetření. Za tímto účelem bylo všech 20 výzkumných ploch navštíveno s nezbytným vybavením a byly zde důkladně manuálně změřeny všechny požadované vlastnosti téměř 1500 stromů. Nejprve byla pomocí

laserového výškoměru změřena výška všech stromů s výčetní tloušťkou větší než 7 cm. Dále byly zaznamenány druhy stromů, v některých případech i jejich morfologické abnormality či zdravotní stav. Následně byla změřena přesná poloha středu každého kmene pomocí totální stanice.

Data získaná při pozemních měřeních poté mohla být použita v základním nastavení UAV Forest Exploreru jako referenční data. V takovém případě nástroj automaticky porovnal výstupy vlastních výpočtů, tedy identifikace stromů a odhadu jejich výšky, s poskytnutými daty pozemních měření. Nástroj provedl sérii matematických a statistických výpočtů pro porovnání zpracovávaných dat jak za použití plošného přístupu, tak přístupu po jednotlivých stromech.

Výsledky porovnání na úrovni jednotlivých stromů poté poskytly hodnoty jako je střední absolutní chyba, odmocnina ze střední kvadratické chyby, Pearsonův korelační koeficient a jeho statistická významnost, koeficient determinace, ale také počty spárovaných nebo nadbytečně identifikovaných stromů. Pro plošný přístup byly pak důležité hodnoty jako rozdíl výšek mezi průměrnou výškou změřených a identifikovaných stromů, směrodatná odchylka těchto výšek, či rozdíl mezi počtem změřených a identifikovaných stromů.

Každá z početných iterací (řádově stovky pro každou plochu), vycházejících z rozmezí uživatelských vstupů, vytvořila vlastní souhrnné statistiky. Ty byly jako jeden z finálních výstupů nástroje exportovány ve formě přehledné tabulky. Poté mohla být snadno nalezena taková vstupní nastavení, která vedla k výsledkům nejlépe odpovídajícím patřičným pozemním měřením. Tyto výsledky byly následně podrobně popsány a výzkumné plochy byly zhodnoceny z hlediska nejnižších a nejvyšších hodnot zkoumaných veličin v rámci každého z přístupů.

Nástroj se osvědčil jako plně použitelný pro hodnocení výšek stromů v různých typech lesních porostů. Jelikož při pozemních měřeních výšky a polohy stromů by mělo stačit využít jen malou reprezentativní část lesních porostů, zjištěná nejlepší nastavení nástroje pro danou plochu poté mohou být aplikována na území celého daného porostu. Poněvadž při použití zvoleného nastavení by neměly být minimální jen rozdíly ve výškách, ale také v počtech identifikovaných a měřených stromů, mělo by být zaručeno, že výsledky budou vždy vypočítány s nejvyšší možnou přesností a budou maximálně odpovídat každému konkrétně zkoumanému lesnímu porostu. Časové i fyzické nároky takového snažení by tak měly být pouze zlomkem ve srovnání s případným ručním měřením všech stromů.

## 9. References

- Agisoft PhotoScan Tutorial (Intermediate level): Orthophoto and DEM generation with Agisoft PhotoScan Pro 1.0.0 (with Ground Control Points), 2014, PDF document, downloadable at [<http://www.agisoft.com/>]
- Agisoft PhotoScan User Manual: Professional Edition, Version 1.0, 2014, PDF document, downloadable at [<http://www.agisoft.com/downloads/user-manuals/>]
- Ahmad, A., 2008, Digital photogrammetry: an experience of processing aerial photograph of UTM acquired using digital camera. Final Thesis, Faculty of Geoinformation Science & Engineering, Universiti Teknologi Malaysia.
- Amoda, N., Kulkarni, R. K., 2013, Image Segmentation and Detection using Watershed Transform and Region Based Image Retrieval, 2(2), 89–94. doi.org/10.1.1.24.5229
- Andersen, H.-E., 2009, Using airborne light detection and ranging (lidar) to characterize forest stand condition on the Kenai peninsula of Alaska. *Western Journal of Applied Forestry*, 24, 95-102.
- Andersen, H.-E., Reutebuch, S. E., McGaughey, R. J., 2006, A rigorous assessment of tree height measurements obtained using airborne lidar and conventional field methods. *Canadian Journal of Remote Sensing*.
- Anderson, E. S., Thompson, J. A., Crouse, D. A., Austin, R. E., 2006, Horizontal resolution and data density effects on remotely sensed lidar-based DEM. *Geoderma*, 132, 06-415. *Journal of Remote Sensing*. 32(5), 355-366. DOI: 10.5589/m06-030.
- Anderson, K., Gaston, K. J., 2013, Lightweight unmanned aerial vehicles will revolutionize spatial ecology. *Front. Ecol. Environ.* 11, doi:10.1890/120150.
- Anttila P., 1998, On the accuracy of tree-wise attributes obtained by analytical stereoplotter and aerial images. MSc thesis, University of Joensuu, Faculty of Forestry, Joensuu, 36 p.
- ArcMap Help, 2016, Environmental Systems Research Institute (Esri), ArcGIS for Desktop, ArcMap Help, Accessible at [<http://desktop.arcgis.com/en/arcmap/>]. Cited in July 2016.
- Asner, G. P., 2009, Tropical forest carbon assessment: Integrating satellite and airborne mapping approaches. *Environmental Research Letters*, 4, 034009.
- ASPRS - The American Society for Photogrammetry & Remote Sensing, 2012, 5410 Grosvenor Lane, Suite 210, Bethesda, Maryland 20814-2160, Accessible at [<https://www.asprs.org/>]. Cited in August 2012.
- Assmann, E., 1970, *The principles of forest yield study: studies in the organic production, structure, increment and yield of forest stands*. Pergamon Press, Oxford.
- Avery, T. E., Burkhart, H., 2011, *Forest Measurements*, 5<sup>th</sup> edition McGraw-Hill, NY.
- Banin, L., Feldpausch, T. R., Phillips, O. L., Baker, T. R., Lloyd, J., Affum-Baffoe, K. et al., 2012, What controls tropical forest architecture? testing environmental, structural and floristic drivers. *Global Ecology and Biogeography*, 21, 1179–1190.
- Balenović, I., Marjanović, H., Benko, M., 2010, The use of aerial photographs in forest management in Croatia. *Forest lists*. 134 (11-12): 623-631

- Balenović, I., Seletković, A., Pernar, R., Jazbec, A., 2015, Estimation of the mean tree height of forest stands by photogrammetric measurement using digital aerial images of high spatial resolution. *Annals of Forest Research*, 58(1). DOI: 10.15287/afr.2015.300. ISSN 20652445.
- Balenović, I., Seletković, A., Pernar, R., Marjanović, H., Vuletić, D., Paladinić, E., Kolić J., Benko, M., 2011, Digital Photogrammetry – State of the Art and Potential for Application in Forest Management in Croatia. *South-east European forestry* 2(2), 81-93, DOI: 10.15177/seeфор.11-09. ISSN 18476481.
- Baltsavias, E., Gruen, A., Eisenbeiss, H., Zhang, L., Waser, L. T., 2008, High-quality image matching and automated generation of three-dimensional tree models. *International Journal of Remote Sensing*, 29, 1243–1259.
- Baumann, P. R., 2014, History of remote sensing, Aerial photography. State University of New York, College at Oneonta
- Bedáňová, I., Večeřek, V., 2007, *Základy statistiky pro studující veterinární medicíny a farmacie*, Veterinární a farmaceutická univerzita Brno, skriptum.
- Belaid, L. J., Mourou, W., 2009, Image segmentation: A watershed transformation algorithm. *Image Analysis and Stereology*, 28(2), 93–102.
- Bendig, J., Bolten, A., Bareth, G., 2012, Introducing a low-cost mini-UAV for thermal- and multispectral-imaging, *International Archives of the Photogrammetry, Remote Sensing and Spatial Information Sciences*, XXXIX-B1, pp. 345-349.
- Benko, M., Balenović, I., 2011, Past, present and future of application of remote sensing methods in Croatian forest inventory. *Sumarski List* 135:272–281
- Beucher, S., 1990, *Segmentation d'image et Morphologie mathématique*. The Doctoral Thesis, Ecole Nationale Supérieure des Mines de Paris.
- Beucher, S., 1992, The Watershed transformation applied to image segmentation, *Scanning Microscopy International*, suppl. 6, pp. 299-314.
- Beucher, S., Lantuejoul, C., 1979, Use of watersheds in contour detection, *International Workshop on Image Processing, Realtime Edge and Motion Detection/Estimation*, Rennes, France.
- Blaaha, M., Eisenbeiß, H., Grimm, D., Limpach, P., 2011, Direct georeferencing of UAVs. *International Archives of the Photogrammetry, Remote Sensing and Spatial Information Sciences*, Vol. XXXVIII-1/C22 UAV-g 2011, Conference on Unmanned Aerial Vehicle in Geomatics, Zurich, Switzerland.
- Blašková, V., 2009, *Statistika I*, Brno: Mendelova zemědělská a lesnická univerzita v Brně, ISBN 978-80-7375-286-6.
- Blozan, W., 2006, Tree measuring guidelines of the eastern native tree society. *Bulletin of the Eastern Native Tree Society*, 1, 3–10.
- Bohlin, J., Wallerman, J., Fransson, J. E. S., 2012a, Forest variable estimation using photogrammetric matching of digital aerial images in combination with a high-resolution DEM. *Scandinavian Journal of Forest Research*, 27, 692–699.
- Bohlin, J., Wallermann, J., Olsson, H. Fransson, J. E. S., 2012b, Species-specific forest variable estimation using non-parametric modelling of multi-spectral photogrammetric point cloud data. *International Archives of the Photogrammetry, Remote Sensing and Spatial Information Sciences*, ISPRS Congress, XXXIX, Part B8, pp. 387.

- Böhm, B. et al., 2010, Application of drone-based air images - mosaicking, equalization and data analysis. Final report of the collaborative research project. University of Jena, Institute of Geography, Department of Geoinformatics, Hydrology and Modelling, Jena, Germany.
- Borgefors, G., Brandtberg, T., Walter, F., 1999, Forest Parameter Extraction from Airborne Sensors, IAPRS, Vol. 32, Part 3-2W5, "Automatic Extraction of GIS Objects from Digital Imagery", München, Sept. 8-10, pp 151 – 158.
- Bragg, D. C., 2007, An improved tree height measurement technique tested on mature southern pines. *Southern Journal of Applied Forestry*, 32, 38–43.
- Brandtberg, T., Warner, T. A., Landenberger, R. E., McGraw, J. B., 2003, Detection and analysis of individual leaf-off tree crowns in small footprint, high density lidar data from the eastern deciduous forest in North America. *Remote Sensing of Environment*, 85: 290–303.
- Breidenbach, J., Astrup, R., 2014, The Semi-Individual Tree Crown Approach. *Forestry Applications of Airborne Laser Scanning*, DOI:10.1007/978-94-017-8663-8\_6
- Breidenbach, J., Næsset, E., Lien, V., Gobakken, T., Solberg, S., 2010, Prediction of species specific forest inventory attributes using a nonparametric semi-individual tree crown approach based on fused airborne laser scanning and multispectral data. *Remote Sensing Environment*, 114, 911–924.
- Campbell, J., 2008, *Introduction to remote sensing*. New York: The Guilford Press.
- Carson, W. W., Andersen, H.-E., Reutebuch, S. E., McGaughey, R. J., 2004, LiDAR applications in forestry: An overview. *ASPRS Annual Conference Proceedings*.
- Casbeer, D., Beard, R., McLain, T., Li, S., Mehra, R., 2005, Forest fire monitoring with multiple small UAVs, in *Proceedings of 2005 American Control Conference*.
- CENIA, 2015, Web Map Service of INSPIRE national geoportal of Czech Environmental Information Agency. Accessible at [<http://geoportal.gov.cz/>]
- Chave, J., 2005, *Measuring tree height for tropical forest trees - A field manual*. Lab. Evolution et Diversité Biologique, Université Paul Sabatier, Toulouse, France.
- Chave, J., Andalo, C., Brown, S., Cairns, M. A., Chambers, J. Q., Eamus, D. et al., 2005, Tree allometry and improved estimation of carbon stocks and balance in tropical forests. *Oecologia*, 145, 87–99.
- Chen, Q., Baldocchi, D., Gong, P., Kelly, M., 2006, Isolating individual trees in a savanna woodland using small footprint lidar data. *Photogrammetry Engineering and Remote Sensing*, 72:923–932
- Cheng, G., Han, J., 2016, A Survey on Object Detection in Optical Remote Sensing Images. *ISPRS Journal of Photogrammetry and Remote Sensing*, 117, 11–28.
- Ciceli, T., 2004, *The use of digital cameras in terrestrial photogrammetry*. Master's thesis, Faculty of Geodesy, University of Zagreb, p 92.
- Clark, D. A., Clark, D. B., 2001, Getting to the canopy: tree height growth in a Neotropical rain forest. *Ecology*, 82, 1460–1472.
- Córcoles, J. I., Ortega, J. F., Hernández, D., Moreno, M. A., 2013, Use of digital photography from unmanned aerial vehicles for estimation of leaf area index in onion (*Allium cepa* L.), *European Journal of Agronomy*, Volume 45, pp. 96-104.

- Corona, P., Fattorini, L., 2008, Area-based lidar-assisted estimation of forest standing volume. *Canadian Journal of Forest Research*, 38, 2911–2916.
- Cramer, M., 2005, Digital airborne cameras - status and future. In: Heipke C, Jacobsen K, Gerke M (eds) *High resolution earth imaging for geospatial information*. ISPRS, Hanover, p 1-8
- CTFS - Centre for Tropical Forest Science, 2007, *Crown traits* – BCI.
- Culvenor, D.S., 2002, TIDA: an algorithm for the delineation of tree crowns in high spatial resolution remotely sensed imagery. *Computing Geoscience* 28, 33–44.
- ČÚZK, 2015, Web Map Service of State Administration of Land Surveying and Cadastre. Accessible at [<http://geoportal.cuzk.cz/>]
- ČÚZK, 2016, Digital Terrain Model of the Czech Republic of the 5th generation (DMR 5G), State Administration of Land Surveying and Cadastre. Accessible at [<http://geoportal.cuzk.cz/>]. Cited in April 2016.
- Dandois, J. P., Ellis, E. C., 2010, Remote sensing of vegetation structure using computer vision. *Remote Sensing*, 2, 1157–1176.
- Dandois, J. P., Ellis, E. C., 2013, High spatial resolution three-dimensional mapping of vegetation spectral dynamics using computer vision. *Remote Sensing of Environment*, 136(August), 259–276. doi.org/10.1016/j.rse.2013.04.005
- Dey, D., Mummert, L., Sukthankar, R., 2012, Classification of plant structures from uncalibrated image sequences. *Applications of Computer Vision (WACV), 2012 IEEE Workshop on* (pp. 329–336).
- Díaz-Varela, R., de la Rosa, R., León, L., Zarco-Tejada, P., 2015, High-Resolution Airborne UAV Imagery to Assess Olive Tree Crown Parameters Using 3D Photo Reconstruction: Application in Breeding Trials. *Remote Sensing*, 7, 4213–4232.
- DJI, 2015, DJI Spreading Wings S800 Specification, Da-Jiang Innovations Science and Technology Co., Ltd. Accessible at [<http://www.dji.com/product/spreading-wings-s800/spec>]. Cited in May 2015.
- DJI, 2015b, DJI PC Ground Station Specification, Da-Jiang Innovations Science and Technology Co., Ltd.,. Accessible at [<http://www.dji.com/product/pc-ground-station/spec>]. Cited in May 2015.
- Drápela, K., 2002, *Statistické metody II: (pro obory lesního, dřevařského a krajinného inženýrství)*, MENDELU Brno. ISBN 80-7157-474-0.
- Drápela, K., Zach, J., 2000, *Statistické metody I: (pro obory lesního dřevařského a krajinného inženýrství)*, MENDELU Brno. ISBN 80-7157-416-3.
- Ecosynth, 2016, 3D tools for ecology. Software suite, Webpage of the company. Accessible at [<http://ecosynth.org/page/about>]. Cited in August 2016.
- Edson, C., Wing, M. G., 2011, Airborne Light Detection and Ranging (LiDAR) for Individual Tree Stem Location, Height, and Biomass Measurements. *Remote Sens.* 3, 2494-2528.
- Eid, T., Gobakken, T., Næsset, E., 2004, Comparing stand inventories for large areas based on photo-interpretation and laser scanning by means of cost-plus-loss analyses. *Scandinavian Journal of Forest Research* 19(6): 512-523. DOI: 10.1080/02827580410019463.



- Erdody, T. L., Moskal, L. M., 2010, Fusion of LiDAR and imagery for estimating forest canopy fuels. *Remote Sensing of Environment*, 114, 725–737.
- Esposito, S., Mura, M., Fallavollita, P., Balsi, M., Chirici, G., Oradini, A., Marchetti, M., 2014, Performance evaluation of lightweight LiDAR for UAV applications. *International Geoscience and Remote Sensing Symposium (IGARSS)*, 792–795.
- Esri, 2016, Environmental Systems Research Institute, Redlands, California, United States. Webpage of the company, Accessible at [<http://www.esri.com/software/arcgis/>]. Cited in July 2016.
- Evans, D. L., Roberts, S. D., Parker, R. C., 2006, LiDAR—A new tool for forest measurements. *Forestry Chronicle*, 62, 211–219.
- FAA, 2013, Federal Aviation Administration, A Integration of Civil Unmanned Aircraft Systems (UAS) in the National Airspace System (NAS) Roadmap. U.S. Department of Transportation. PDF document, downloadable at [[http://www.faa.gov/uas/media/uas\\_roadmap\\_2013.pdf](http://www.faa.gov/uas/media/uas_roadmap_2013.pdf)].
- Feldpausch, T. R., Lloyd, J., Lewis, S. L., Brienen, R. J. W., Gloor, M., Monteagudo Mendoza, A. et al., 2012, Tree height integrated into pantropical forest biomass estimates. *Biogeosciences*, 9, 3381–3403.
- Flewelling, J., 2008, Probability models for individually segmented tree crown images in a sampling context. In: Hill, R.A., Rosette, J. & Suárez, J. (eds.). *Proceedings of SilviLaser 2008: 8th international conference on LiDAR applications in forest assessment and inventory*. September 2008, Edinburgh, UK, pp. 284–294.
- Gatziolis, D., Lienard, J. F., Vogs, A., Strigul, N. S., 2015, 3D tree dimensionality assessment using photogrammetry and small unmanned aerial vehicles. *PLoS ONE*, 10(9), 1–21. doi.org/10.1371/journal.pone.0137765
- Gehrke, S., Morin, K., Downey, M., Boehrer, N., Fuchs, T., 2010, Semi-Global Matching: An Alternative to LiDAR for DSM Generation? In *Proceedings of the 2010 Canadian Geomatics Conference and Symposium of Commission I, ISPRS Convergence in Geomatics—Shaping Canada’s Competitive Landscape*, Calgary, Canada, 15–18.
- Gini, R., Passoni, D., Pinto, L., Sona, G., 2012, Aerial Images from an UAV system: 3D modeling and tree species classification in a park area. *International Archives of the Photogrammetry, Remote Sensing and Spatial Information Sciences*, XXXIX, Part B1, pp. 361–366.
- GISBOX, 2016, GISBOX SRL, Accessible at [[www.gisbox.ro](http://www.gisbox.ro)]. Cited in August 2016.
- Goerndt, M. E., 2010, Comparison and Analysis of Small Area Estimation Methods for Improving Estimates of Selected Forest Attributes. Ph.D. Dissertation, Oregon State University, Corvallis, OR, USA.
- Goerndt, M. E., Monleon, V. J., 2010, Temesgen, H. Relating forest attributes with area- and tree-based light detection and ranging metrics for western Oregon. *Western Journal of Applied Forestry*, 25, 105–111.
- Gonzalez, P., Asner, G. P., Battles, J. J., Lefsky, M. A., Waring, K. M., Palace, M., 2010, Forest carbon densities and uncertainties from LIDAR, QuickBird, and field measurements in California. *Remote Sensing of Environment*, 114, 1561–1575.
- Goodwind, A. N., 2004, Measuring tall tree heights from the ground. *Tasforests*, 15, pp. 85–97.

- Gougeon, F., Leckie, D., Gillis, M., 1992, Individual tree identification from high resolution MEIS images. In: International Forum on Airborne Multispectral Scanning for Forestry and Mapping. Quebec: Petawawa National Forestry Institute, Forestry Canada, pp. 117–128.
- Gougeon, F. A., Moore, T., 1989, Classification individuelle des arbres à partir d'images à haute résolution spatiale (Classification of individual trees from high spatial resolution images), pp. 185–196.
- Grau, V., Mewes, A. U. J., Alcaniz, M., Kikinis, R., Warfield, S. K., 2004, Improved watershed transform for medical image segmentation using prior information. *IEEE Transactions on Medical Imaging*, 23(4), 447–458. doi.org/10.1109/TMI.2004.824224
- Graupner, 2015, Microcomputer Radio Remote Control System Graupner MX-20 HoTT Transmitter and Graupner GR-24 HoTT Receiver Specifications, Graupner/SJ GmbH. Accessible at [<http://www.graupner.de/en/products/1736df13-32af-4183-aa8e-80f31a7f03cb/2/productcategory.aspx>]. Cited in May 2015.
- Gupta, S., Weinacker, H., Koch, B., 2010, Comparative analysis of clustering-based approaches for 3-d single tree detection using airborne fullwave lidar data. *Remote Sensing* 2(4), pp. 968-989.
- Haala, N., 2009, Comeback of digital image matching. *Photogrammetric Week 09*, Wichmann Verlag, Heidelberg, 289–301.
- Haala, N., 2013, The Landscape of Dense Image Matching Algorithms. *EuroSDR Benchmark on Image Matching for DSM Computation*, 29.
- Haala, N., Cramer, M., Weimer, F., and Trittler, M., 2011, Performance test on UAV-based photogrammetric data collection. *Proceedings of the International Archives of the Photogrammetry, Remote Sensing and Spatial Information Sciences*. 38(1/C22): 7–12
- Haala, N., Hastedt, H., Wolf, K., Ressler, C., Baltrusch, S., 2010, Digital photogrammetric camera evaluation – Generation of digital elevation models. *Photogramm Fernerkun*, 2, 99–115.
- Haala, N., Rothermel, M., 2012, Dense multiple stereo matching of highly overlapping UAV imagery. *International Archives of the Photogrammetry, Remote Sensing and Spatial Information Sciences*, XXXIX, Part B1, pp. 387-392.
- Häme, T., 2012, Improvements in forest resource monitoring practices in the Baltic Sea region. BSAG workshop. VTT Technical Research Centre of Finland.
- Hardin, P. J., Jensen, R. R., 2011, Small-scale unmanned aerial vehicles in environmental remote sensing: challenges and opportunities. *GIScience & Remote Sensing*. 48(1): 99–111
- Heipke C., 2001, Digital photogrammetric workstations - a review of the state-of-the-art for topographic applications. *GIM International* 15 (4): 35-37
- van Henten, E. J., Goense, D., Lokhorst, C., 2009, Precision Agriculture '09: Papers Presented at the 7th European Conference on Precision Agriculture, Wageningen, the Netherlands, p. 10–11. 992 p.
- Heurich, M., 2008, Automatic recognition and measurement of single trees based on data from airborne laser scanning over the richly structured natural forests of the Bavarian Forest National Park. *Forest Ecology Management*, 255:2416–2433

- Hillier, A., 2011, Manual for working with ArcGIS 10, University of Pennsylvania, From the Selected Works of Amy Hillier, PDF document, downloadable at [[https://works.bepress.com/amy\\_hillier/24/](https://works.bepress.com/amy_hillier/24/)].
- Hirschmugl, M., Ofner, M., Raggam, J., Schardt, M., 2007, Single tree detection in very high resolution remote sensing data. *Remote Sensing of Environment* 110, 533–544.
- Hirschmüller, H., 2008, Stereo processing by semi-global matching and mutual information. *IEEE Transactions on Pattern Analysis and Machine Intelligence*, 30, 328–341.
- Holl, K. D., Zahawi, R. A., Cole, R. J., Ostertag, R., Cordell, S., 2011, Planting seedlings in tree islands versus plantations as a large-scale tropical forest restoration strategy. *Restoration Ecology*, 19, 470–479.
- Hollaus, M., Briese, Ch., Sotier, B., 2014, High resolution aerial images from UAV for forest applications State-of-the-Art. *Forest Resources & LiDAR*, (2). Interreg Alpine Space project - New technologies for a better mountain forest timber mobilization.
- Holmgren, J., Jonsson, T., 2004, Large Scale Airborne Laser Scanning of Forest Resources in Sweden. *International Archives of Photogrammetry, Remote Sensing and Spatial Information Sciences XXXVI (8/W2)*:157-60.
- Holmgren, J., Persson, Å., 2004, Identifying species of individual trees using airborne laser scanner. *Remote Sens. Environ.* 90, 415–423.
- Honkavaara E., Arbiol R., Markelin L., Martinez L., Cramer M., Bovet S., Chandelier L., et al., 2009, Digital airborne photogrammetry - a new tool for quantitative remote sensing? A state-of-the-art review on radiometric aspects of digital photogrammetric images. *Remote Sensing* 1(3): 577-605. DOI: 10.3390/rs1030577.
- Hoya, 2015, Near-Infrared Filter R72 specification, Special Effect Filters, Hoya Corporation, Kenko Tokina Co., Ltd. Accessible at [<http://www.hoyafilter.com/hoya/products/specialeffectsfilters/r72infrared/>]. Cited in August 2015.
- Hughenoltz, C. H., Whitehead, K., Barchyn, T. E., Brown, O. W., Moorman, B. J., et al., 2013, Geomorphological mapping with a small unmanned aircraft system (sUAS): feature detection and accuracy assessment of a photogrammetrically-derived digital terrain model. *Geomorphology*. 194: 16–24. DOI: 10.1016/j.geomorph.2013.03.023
- Hung, C., Bryson, M., Sukkarieh, S., 2012, Multi-class predictive template for tree crown detection. *Journal of Photogrammetry and Remote Sensing*, 68, 170–183.
- Husch, B., Miller, C., Beers, T., 1972, *Forest Mensuration*. 2th ed. Ronald Press, NY.
- Hyypä, H., Hyypä J., 1999, Comparing the Accuracy of Laser Scanner with Other Optical Remote Sensing Data Sources for Stand Attribute Retrieval. *The Photogrammetric Journal of Finland* 16(2):5-15.
- Hyypä, J., Hyypä, H., Inkinen, M., Engdahl, M., Linko, S., Zhu, Y. H., 2000, Accuracy comparison of various remote sensing data sources in the retrieval of forest stand attributes. *Forest Ecology and Management*, 128(1–2), 109–120. doi.org/10.1016/S0378-1127(99)00278-9
- Hyypä, J., Hyypä, H., Leckie, D., Gougeon, F., Yu, X., Maltamo, M., 2008, Review of methods of small-footprint airborne laser scanning for extracting forest inventory data in boreal forests. *International Journal of Remote Sensing*, 29, 1339–1366.

Hyyppä, J., Hyyppä, H., Litkey, P., Yu, X., Haggren, H., Ronnholm, P., Pyysalo, U., Pitkanen, J., Maltamo, M., 2004, Algorithms and Methods of Airborne Laser Scanning for Forest Measurements. In Proceedings of the ISPRS Working Group VIII/2 "Laser-Scanners for Forest and Landscape Assessment", Freiburg, Germany, 3–6, In IAPRS, Volume 36, pp. 82-89.

Hyyppä, J., Inkinen, M., 1999, Detecting and estimating attributes for single trees using laser scanner. *The Photogrammetric Journal of Finland* 16(2): 27–42.

Introduction to GIS Using ArcGIS Desktop 10, 2012, University of Maryland Libraries, U.S. Government Information, Maps & GIS Services, PDF document, downloadable at [<http://www.lib.umd.edu/>].

Jaakkola, A., Hyyppä, J., Hyyppä, H., Kukko, A., Yu, X., Kaartinen, H., Lethomäki, M. and Lin, Y., 2011, A low-cost multi-sensoral mobile mapping system and its feasibility for tree measurements. *ISPRS Journal of Photogrammetry and Remote Sensing* Vol. 65, pp. 514–522.

Jacobsen K., 2009, Potential of large format digital aerial cameras. *Map World Forum Hyderabad, GIS Development*.

Järnstedt, J., Pekkarinen, A., Tuominen, S., Ginzler, C., Holopainen, M., Viitala, R., 2012, Forest variable estimation using a high-resolution digital surface model. *ISPRS J. Photogrammetry and Remote Sensing*, 74, 78–84.

Joint Doctrine Note 3/10, 2010, Unmanned Aircraft Systems: Terminology, Definitions And Classification. The Development, Concepts and Doctrine Centre. PDF document, downloadable at [<https://www.gov.uk/government/>].

Kaartinen, H., Hyyppä, J., 2008, EuroSDR / ISPRS Commission II Project "Tree Extraction" – Final report. Official publication n:o 53. EuroSDR, 60 p.

Kaartinen, H., Hyyppä, J., Yu, X., Vastaranta, M., Hyyppä, H., Kukko, A., Holopainen, M., Heipke, C., Hirschmugl, M., Morsdorf, F., Næsset, E., Pitkänen, J., Popescu, S., Solberg, S., Wolf, B. M., Wu, J.-C., 2012, An international comparison of individual tree detection and extraction using airborne laser scanning. *Remote Sensing* 4, 950–974.

Kamdi, S., Krishna, R. K., 2011, Image Segmentation and Region Growing Algorithm. *International Journal of Computer Technology and Electronics Engineering*, 2(1), 103–107.

Kant, S., Alavalapati, J., 2014, *Handbook of Forest Resource Economics, Forest Resource Economics and Management*, Faculty of Forestry, University of Toronto, Canada. Routledge, ISBN 9781136253294.

Ke, Y., Quackenbush, L. J., 2011, A review of methods for automatic individual tree crown detection and delineation from passive remote sensing. *International Journal of Remote Sensing*, 32, 4725–4747.

Kim, H., Lee, J., Choi, K., Lee, I., 2012, Determination of exterior orientation parameters through direct geo-referencing in a real-time aerial monitoring system. *International Archives of the Photogrammetry, Remote Sensing and Spatial Information Sciences*, XXXIX-B1, pp. 399-403.

King, D. J., 2000, Airborne remote sensing in forestry: sensors, analysis and applications. *Forest Chron* 76 (6): 25-42

King, D. A., Clark, D. A., 2011, Allometry of emergent tree species from saplings to above-canopy adults in a Costa Rican rain forest. *Journal of Tropical Ecology*, 27.

- Knoth, C., Prinz, T., Loef, P., 2011, Microcopter-Based Color Infrared (CIR) Close Range Remote Sensing as a Subsidiary Tool for Precision Farming. Proceedings of the ISPRS Workshop on Methods for Change Detection and Process Modelling, Cologne, Germany.
- Koch, B., Heyder, U., Weinacker, H., 2006, Detection of individual tree crowns in airborne lidar data. *Photogrammetric Engineering & Remote Sensing* 72(4): 357–363.
- Koo, V. C., Chan, Y. K., Gobi, V., Chua, M. Y., Lim, C. H., Lim, C. S., Sew, B. C., 2012, A new unmanned aerial vehicle synthetic aperture radar for environmental monitoring. *Progress in Electromagnetics Research*, 122, 245–268.
- Korning, J., Thomsen, K., 1994, A new method for measuring tree height in tropical rain forest. *Journal of Vegetation Science*, 5, 139–140.
- Korpela, I., 2004, Individual tree measurements by means of digital aerial photogrammetry. *Silva Fennica Monography* 3, The Finnish Society of Forest Science, The Finnish Forest Research Institute.
- Kovats, M., 1997, A large-scale aerial photographic technique for measuring tree heights on long-term forest installations. *Photogrammetric Engineering and Remote Sensing* 63(6): 741-747.
- Kraus, K., Pfeifer, N., 1998, Determination of terrain models in wooded areas with airborne laser scanner data. *ISPRS J. Photogrammetry*, 53, 193-203.
- Kwak, D.-A. A., Lee, W.-K. K., Lee, J.-H. H., Biging, G. S., Gong, P., 2007, Detection of individual trees and estimation of tree height using LiDAR data. *Journal of Forest Research*, 12, 425–434. doi.org/10.1007/s10310-007-0041-9
- van Laar A., Akça A., 2007, *Forest mensuration*. Springer, Dordrecht, 376 p. DOI: 10.1007/978-1-4020-5991-9.
- Larjavaara, M., Muller-Landau, C. H., 2013, Measuring tree height: a quantitative comparison of two common field methods in a moist tropical forest. *Methods in Ecology and Evolution*. 4(9), 793-801. DOI: 10.1111/2041-210X.12071. ISSN 2041210x.
- Larsen, M., Eriksson, M., Descombes, X., Perrin, G., Brandtberg, T., Gougeon, F. A., 2011, Comparison of six individual tree crown detection algorithms evaluated under varying forest conditions. *Int. J. Remote Sensing*, 32, 5827–5852.
- Larsen, M., Rudemo, M., 1998, Optimizing templates for finding trees in aerial photographs. *Pattern Recognition Letters* 19, 1153–1162.
- Laser Technology, 2004, TruPulse® Laser Series Hardware Specifications fact sheet, Laser Technology, Inc., PDF document, downloadable at [<http://www.lasertech.com/content/Brochures/TruPulse-Criterion-Combo-Brochure.pdf>].
- Leberl, F., Irschara, A., Pock, T., Meixner, P., Gruber, M., Scholz, S., Wiechert, A., 2010, Point Clouds: Lidar versus 3D Vision. *Photogrammetric Engineering & Remote Sensing*, 76(10), 1123–1134. doi.org/0099-1112/10/7610-1123
- Lee A. C., Lucas R. M., 2007, A LiDAR-derived canopy density model for tree stem and crown mapping in Australian forests. *Remote Sensing Environment*. p.493–518
- Lee, H., Slatton, K. C., Roth, B. E., Cropper, W. P., 2010, Adaptive clustering of airborne LiDAR data to segment individual tree crowns in managed pine forests. *International Journal of Remote Sensing*, 31, 117–139.

- van Leeuwen, M., Nieuwenhuis, M., 2010, Retrieval of forest structural parameters using LiDAR remote sensing. *European Journal of Forest Research*, 129(4), 749–770. doi.org/10.1007/s10342-010-0381-4
- Lefsky, M., Keller, M., Pang, Y., de Camargo, P. B., Hunter, M. O., 2007, Revised method for forest canopy height estimation from geoscience laser altimeter system waveforms. *Journal of Applied Remote Sensing*, 1:013537
- Lemmens, M., 2009, Product survey on Digital photogrammetric workstations. *GIM International* 21 (12): 22-25
- Lemmens, M., 2011, Digital Photogrammetric Workstations - Status and Features. *GIM International* 25: 12.
- Lewis, P., Hancock, S., 2007, LiDAR for vegetation applications, UCL, Gower St, UK.
- Li, W., Niu, Z., Gao, S., Huang, N., Chen, H., 2014, Correlating the horizontal and vertical distribution of LiDAR point clouds with components of biomass in a *Picea crassifolia* forest. *Forests*, 5(8), 1910–1930. doi.org/10.3390/f5081910
- Lillesand, T. M., Kiefer, R. W., 1987, *Remote Sensing and Image Interpretation*, 2nd ed., John Wiley and Sons: New York, NY, USA.
- Lim, K., Treitz, P., Wulder, M., St-Onge, B., Flood, M., 2003, Lidar remote sensing of forest structure. *Progress in Physical Geography*, 27, 88-106.
- Lindberg, E., Holmgren, J., Olofsson, K., Olsson, H., Wallerman, J., 2010, Estimation of tree lists from airborne laser scanning by combining single tree and area-based methods. *International Journal of Remote Sensing* 31: 1175–1192.
- Linder W., 2009, *Digital photogrammetry - A practical course*. Springer, Berlin. 220 p. DOI: 10.1007/978-3- 540-92725-9.
- Lisein, J., Pierrot-Deseilligny, M., Bonnet, S., Lejeune, P., 2013, A photogrammetric workflow for the creation of a forest canopy height model from small unmanned aerial system imagery. *Forests*, 4(4), 922–944. doi.org/10.3390/f4040922
- Litschmannová, M., 2012, Úvod do statistiky, Fakulta elektrotechniky a informatiky, Vysoká škola báňská – Technická univerzita Ostrava, Západočeská univerzita v Plzni. Elektronická skripta, interaktivní učební text. PDF document, downloadable at [[http://mi21.vsb.cz/sites/mi21.vsb.cz/files/unit/uvod\\_do\\_statistiky.pdf](http://mi21.vsb.cz/sites/mi21.vsb.cz/files/unit/uvod_do_statistiky.pdf)]
- Lovell, J. L., Jupp, D. L. B., Newnham, G. J., Coops, N. C., Culvenor, D. S., 2005, Simulation study for finding optimal lidar acquisition parameters for forest height retrieval. *Forest Ecology Management*, 214, 398-412.
- Lucas, R. M., Lee, A. C., Bunting, P. J., 2008, Retrieving forest biomass through integration of CASI and lidar data. *Int. J. Remote Sensing*, 29, 1553-1577.
- Machala, M., 2012, Use of eCognition Developer software for forest stands heights assessment. In *Colloquium on Landscape Management*. s. 8--10. ISBN 978-80-7375-612-3.
- Machala, M., Honzová, M., Klimánek, M., 2015, Generating land-cover maps from remotely sensed data: manual vectorization versus object-oriented automation, *Applied GIS*, 11(1), 1-30, ISSN: 1832-5505.
- Machala, M., Honzová, M., Mikita, M., Klimánek, M., 2014, Geoinformation Support of Land Use / Land Cover Mapping. In: Maděra P. et al., *Czech villages in Romanian Banat: landscape, nature, and culture*. 1st edition, 348 p. ISBN 978-80-7375-960-5.

- Machala, M., Janata, P., 2014, Trees Detection and Height Estimation Based on Image Data Gained by Unmanned Aerial Vehicle (UAV). In *SilvaNet-WoodNet*. 1. vyd. Brno: Mendelova univerzita v Brně, 2014, p. 62-63. ISBN 978-80-7509-137-6.
- Machala, M., Zejdová, L., 2014, Forest mapping through Object-based image analysis of multispectral and LiDAR Aerial data. *European Journal of Remote Sensing*, vol. 47, issue 1, 117 - 131. DOI: 10.5721/EuJRS20144708.
- Madani M., 1996, Digital aerial triangulation – the operational comparison. In: *International Archives of Photogrammetry and Remote Sensing*, 31, 490-495.
- Magnusson, M., Fransson, J. E. S., 2005, Evaluation of aerial photo-interpretation for estimation of forest stem volume at stand level. In: Olsson H (ed.) "Operational Tools in Forestry Using Remote Sensing Techniques, 31 May-3 June, 2005, Borås. Swedish Forest Agency, Report 8, Vol C, pp. 102-106.
- Magnusson, M., Fransson, J.E.S., Olsson H., 2007, Aerial photo-interpretation using Z/I DMC images for estimation of forest variables. *Scandinavian Journal of Forest Research* 22(3): 254-266. DOI: 10.1080/02827580701262964.
- Maltamo, M., Bollandsas, O. M., Næsset, E., Gobakken, T., Packalén, P., 2011, Different Plot Selection Strategies for Field Training Data in ALS-Assisted Forest Inventory. *Forestry* 84(1):23-31.
- Maltamo, M., Eerikäinen, K., Packalén, P., Hyypä, J., 2006, Estimation of stem volume using laser scanning-based canopy height metrics. *Forestry*, 79, 217–230.
- Maltamo, M., Eerikäinen, K., Pitkänen, J., Hyypä, J., Vehmas, M., 2004, Estimation of timber volume and stem density based on scanning laser altimetry and expected tree size distribution functions. *Remote Sensing Environment*, 90:319–330.
- Maltamo, M., Naesset, E., Vauhkonen, J., 2014, *Forestry Applications of Airborne Laser Scanning: Concepts and Case Studies, Managing Forest Ecosystems*. Springer Science & Business Media, 464 p., ISBN: 9789401786638
- Matese, A., Toscano, P., Di Gennaro, S.F., Genesio, L., Vaccari, F.P., Primicerio, J., Belli, C., Zaldei, A., Bianconi, R., Gioli, B., 2015, Intercomparison of UAV, Aircraft and Satellite Remote Sensing Platforms for Precision Viticulture. *Remote Sens.* 7, 2971–2990.
- McGaughey, R., 2007, *Fusion/LDV: Software for Lidar Data Analysis and Visualization*, USDA Forest Service, Pacific Northwest Research Station: Portland, OR, USA.
- Mehtätalo, L., 2006, Eliminating the effect of overlapping crowns from aerial inventory estimates. *Canadian Journal of Forest Research* 36: 1649–1660.
- Meloun, M., Militký, J., 2004, *Statistická analýza experimentálních dat*. Vyd. 2., Praha: Academia, ISBN 80-200-1254-0.
- Meloun, M., Militký, J., 2006, *Kompendum statistického zpracování dat: metody a řešené úlohy*. Vyd. 2., Praha: Academia, 2006. ISBN 80-200-1396-2.
- Miller, A., 2014, *Canopy Segmentation using Airborne LiDAR*, Chester F. Carlson Center for Imaging Science, Rochester Institute of Technology
- Mohan, B. K., Kadam, S. U., Rao, E. P., 2003, *Segmentation of High Resolution Imagery*, Geospatial World, Centre of Studies in Resources Engineering.
- NASA Image, 2014, National Aeronautics and Space Administration, Armstrong Fact Sheet: Unmanned Aircraft Systems Integration in the National Airspace System. Accessible at [<https://www.nasa.gov/>]. Accessed in August 2016.

- Næsset, E., 1996, Determination of number of stems in coniferous forest stands by means of aerial photo-interpretation. *Scandinavian Journal of Forest Research* 11(1): 76-84. DOI: 10.1080/02827589609 382914.
- Næsset, E., 2002a, Determination of mean tree height of forest stands by means of digital photogrammetry. *Scandinavian Journal of Forest Research* 17(5): 446-459. DOI: 10.1080/028275802320435469.
- Næsset, E., 2002b, Predicting forest stand characteristics with airborne scanning laser using a practical two-stage procedure and field data. *Remote Sensing Environment*, 80, 88–99.
- Næsset, E., 2007, Airborne laser scanning as a method in operational forest inventory: Status of accuracy assessments accomplished in Scandinavia. *Scandinavian Journal of Forest Research*, 22, 433–442.
- Næsset, E., Gobakken, T., Holmgren, J., Hyyppä, H., Hyyppä, J., Maltamo, M., Nilsson, M., Olsson, H., Persson, Å., Söderman, U., 2004, Laser scanning of forest resources: the Nordic experience. *Scandinavian Journal of Forest Research* 19:482–499.
- Nex, F., Remondino, F., 2014, UAV for 3D mapping applications: A review. *Appl. Geomat.* 6, 1–15.
- Novotný, J., Mikita, T., Machala, M., Homolová, L., 2014, Applications of airborne laser scanning in forestry. In: Zemek et al. *Airborne remote sensing: theory and practice in assessment of terrestrial ecosystems*. Global Change Research Centre AS CR, v.vi. ISBN: 978-80-87902-05-9
- Nyström, M., 2015, 3D point cloud from image matching, Swedish University of Agricultural Sciences, Ljungberglaboratoriet, SLU, Umeå, Sweden.
- Ofner, M., Hirschmugl, M., Raggam, H., Schardt, M., 2006, 3D stereo mapping by means of UltracamD data. In T. Koukal, & W. Schieder (Eds.), *Proceedings of the International Workshop on 3D Remote Sensing in Forestry* (Vienna, Austria).
- One Drone Cloud, 2016, Terra Imaging LLC UAS, UAV Drone Mapping Solutions. Accessible at [<http://www.onedronecloud.com>]. Cited in August 2016.
- Paine, D. P, Kiser, J. D., 2012, *Aerial photography and image interpretation*. Third Edition. John Wiley & Sons, Inc., Hoboken, New Jersey. DOI: 10.1002/9781118110997.
- Persson, Å., Holmgren, J., Söderman, U., 2002, Detecting and measuring individual trees using an airborne laser scanner. *Photogrammetric Engineering & Remote Sensing* 68: 925–932.
- Petrie, G., 1997, Developments in digital photogrammetric systems for topographic mapping applications. *ITC Journal* 2: 121-135
- Petrie, G., Walker, A. S., 2007, Airborne digital imaging technology: a new overview. *Photogrammetry Recordings*, 22 (119): 203-225
- Pfeifer, N., Glira, P., Briese, Ch., 2012, Direct georeferencing with onboard navigation components of light-weight UAV platforms. *International Archives of the Photogrammetry, Remote Sensing and Spatial Information Sciences, ISPRS Congress, Melbourne, Australia, XXXIX, Part B7*, pp. 487 – 492.
- Pitkänen, J., 2001, Individual tree detection in digital aerial images by combining locally adaptive binarization and local maxima methods. *Can. J. For. Res.* 31, 832–844.



- Pitkänen, J., Maltamo, M., Hyyppä, J., Yu, X., 2004, Adaptive methods for individual tree detection on airborne laser based canopy height model. In: Theis, M., Koch, B., Spiecker, H. & Weinacker, H. (eds.). Proceedings of ISPRS working group VIII/2: Laser-Scanners for Forest and Landscape Assessment. pp. 187–191.
- Pitt, D., Pineau, J., 2009, Forest inventory research at the Canadian Wood Fibre Centre: Notes from a research coordination workshop, 3–4 June 2009, Point Claire, QC. *Forestry Chronicle*, 85, 859–869.
- Popescu, S. C., Randolph, H. W., John, A. S., 2004, Fusion of small-footprint lidar and multispectral data to estimate plot-level volume and biomass in deciduous and pine forests in Virginia, USA. *Forest Science*, 50, 551-565.
- Popescu S. C., Wynne R. H., 2004, Seeing the trees in the forest: using lidar and multi-spectral data fusion with local filtering and variable window size for estimating tree height. *Photogrammetry Engineering and Remote Sensing* 70:589–604
- Popescu, S. C., Wynne, R. H., Nelson, R. F., 2002, Estimating plot-level tree heights with lidar: Local filtering with a canopy-height based variable window size. *Computers and Electronics in Agriculture*, Vol. 37, 71–95.
- Popescu, S. C., Wynne, R. H., Nelson R. F., 2003, Measuring individual tree crown diameter with lidar and assessing its influence on estimating forest volume and biomass. *Canadian Journal of Remote Sensing*, 29: 564–577.
- Poso, S., Häme, T., Paananen, Z., 1984, A Method of Estimating the Stand Characteristics of a Forest Compartment Using Satellite Imagery. *Silva Fennica* 18:261-92.
- Puliti, S., Olerka, H., Gobakken, T., Næsset, E., 2015, Inventory of Small Forest Areas Using an Unmanned Aerial System. *Remote Sensing*, 7(8), 9632–9654.
- Reitberger, J., Schnörr, C., Krzystek, P., Stilla, U., 2009, 3D segmentation of single trees exploiting full waveform LIDAR data. *ISPRS J. Photogrammetry and Remote Sensing*, 64, 561–574.
- Rennie, J. C., 1978, Comparison of height-measurement techniques in a dense loblolly pine plantation. *Southern Journal of Applied Forestry*, 3, 146–148.
- Reutebuch, S. E., Andersen, H.-E., McGaughey, R. J., 2005, Light detection and ranging (LIDAR): An emerging tool for multiple resource inventory. *Journal of Forestry*, 103.
- Rieke, M., Foerster, T., Geipel, J., Prinz, T., 2011, High-precision positioning and real-time data processing of UAV-systems. *International Archives of the Photogrammetry, Remote Sensing and Spatial Information Sciences*, XXXVIII-1/C22, pp. 119-124.
- Rosnell, T., Honkavaara, E., 2012, Point cloud generation from aerial image data acquired by a quadrocopter type micro unmanned aerial vehicle and a digital still camera. *Sensors*, 12, 453–480.
- Ruzgienė B., 2007, Comparison between digital photogrammetric systems. *Geodezija ir Kartografija (Geodesy and Cartography)* 33 (3): 75-79
- Sandau R., 2010, *Digital Airborne Camera, Introduction and Technology*. Springer, Dordrecht, 343 p. DOI: 10.1007/978-1-4020-8878-0.
- SanDisc, 2015, SanDisc Extreme PRO SDHC Memory Cards Specification, SanDisk Corporation, SanDisk Storage Solutions. Accessible at [<http://www.sandisk.com/>]. Cited in August 2015.

- Schardt, M., Ziegler, M., Wimmer, A., Wack, R., Data, L. S., 2002, Assessment of forest parameters by means of laser scanning. *International Archives of Photogrammetry Remote Sensing and Spatial Information Sciences*, 34(3/A), 302–309.
- Schenk, T., 2005, Introduction to photogrammetry. Department of Civil and Environmental Engineering and Geodetic Science, The Ohio State University. p. 95.
- Schimmel, D., Keller, M., Berukoff, S., Kao, B., Loescher, H., Powell, H., et al., 2011, NEON Science Infrastructure. *Science Strategy* (pp. 36–38).
- Schlich, W., 1911, *Manual of forestry, volume III: Forest management*. Bradbury, Agnew, and Co., London, UK. 403 p.
- Schreuder, H., Gregoire, T., Wood, G., 1993, *Sampling methods for multiresource forest inventory*. Wiley, New York.
- Schuckman, K., Renslow, M., 2012, *Manual of Airborne Topographic Lidar* College of Earth and Mineral Sciences, The Pennsylvania State University, a courseware module, Accessible at [[https://www.e-education.psu.edu/geog481/l1\\_p3.html](https://www.e-education.psu.edu/geog481/l1_p3.html)]. Cited in August 2012.
- Serra, J., 1982, *Image Analysis and Mathematical Morphology*. New York, N.Y.: Academic Press.
- Shang, X., Chazette, P., Totems, J., Dieudonné, E., Hamonou, E., Duflot, V., Tulet, P., 2016, Tropical forests of Réunion Island classified from airborne full-waveform LiDAR measurements. *Remote Sensing*, 8(1). doi.org/10.3390/rs8010043
- SharpGIS, 2016, SharpGIS. Accessible at [[www.sharpgis.net/](http://www.sharpgis.net/)]. Cited in August 2016
- da Silva, G. F., Curto, R. D. A., Boechat Soares, C.P., Piassi, L. C., 2012b, Evaluation of height measurement methods in natural forests. *Revista Arvore*, 36, 341–348.
- da Silva, G. F., de Oliveira, O. M., Martinelli de Souza, C. A., Boechat Soares, C. P., Lemoss, R., 2012a, Influence of different sources of errors on the measurements of heights of trees. *Cerne*, 18, 397–405.
- Skovsgaard, J. P., Johannsen, V. K., Vanclay, J. K., 1998, Accuracy and precision of two laser dendrometers. *Forestry*, 71, 131–139.
- Soille, P., 1999, *Morphological Image Analysis*, Springer, Berlin, 316 p.
- Solberg, S., Naesset, E., Bollandsas, O. M., 2006, Single tree segmentation using airborne laser scanner data in a structurally heterogeneous spruce forest. *Photogrammetry Engineering and Remote Sensing*, 72, 1369–1378.
- Song, G., Xiaofei, L., Fangming, L., Yanmin, Z., 2015, *Collaborative Computing: Networking, Applications, and Worksharing*. New York, NY: Springer Berlin Heidelberg, 2016. ISBN 9783319289090.
- Sony, 2015, NEX-5R Camera Specification, Sony Corporation, Sony Europe Limited. Accessible at [<http://www.sony.cz/support/cs/>]. Cited in May 2015.
- Spencer, R.D., Hall, R. J., 1988, Canadian large-scale aerial photographic systems (LSP). *Photogrammetric Engineering and Remote Sensing* 54(4): 475-482.
- Sperlich, M., Kattenborn, T., Koch, B., Kattenborn, G., 2014, Potential of Unmanned Aerial Vehicle Based Photogrammetric Point Clouds for Automatic Single Tree Detection. *Gemeinsame Tagung Der DGfK, Der DGPF, Der GfGI Und Des GIN*, 1–6.

- Stephens, R., 2015, A selection of 100 unmanned aerial vehicles (UAVs, remotely piloted aircraft, drones). Ric Stephens Planning and Design.
- St-Onge, B., Vega, C., Fournier, R. A., Hu, Y., 2008, Mapping canopy height using a combination of digital stereo-photogrammetry and lidar. *International Journal of Remote Sensing*, 29, 3343–3364.
- Strîmbu, V. F., Strîmbu, B. M., 2015, A graph-based segmentation algorithm for tree crown extraction using airborne LiDAR data. *ISPRS Journal of photogrammetry and Remote Sensing*, 104, 30–43. doi.org/10.1016/j.isprsjprs.2015.01.018
- Tang, F., Zhang, X., Liu, J., 2007, Segmentation of tree crown model with complex structure from airborne LIDAR data. pp. 67520A-67520A-67529.
- Tao, W., Lei, Y., Mooney, P., 2011, Dense point cloud extraction from UAV captured images in forest area. 2011 IEEE International Conference on Spatial Data Mining and Geographical Knowledge Services. Fuzhou: June 29 2011 - July 1 2011.
- Tarp-Johanssen M. J., 2001, Locating individual trees in even-aged oak stands by digital image processing of aerial photographs. PhD Thesis. Dept. of Mathematics and Physics. RVAU. Copenhagen, Denmark. 158 p.
- Technopedia, 2016, Techopedia™ - The IT Education Site. Accessible at [<http://www.techopedia.com>]. Cited in August 2016.
- TFE Křtiny, 2013, Training Forest Enterprise Masaryk Forest Křtiny characterization, Školní lesní podnik Masarykův les Křtiny. Accessible at [[www.slpkrtiny.cz](http://www.slpkrtiny.cz)]. Cited in April 2015.
- TheUAV, webpage, accessible at [<http://www.theuav.com>]. Cited in August 2016.
- Tompalski, P., Coops, N. C., White, J. C., Wulder, M. A., 2015, Enriching ALS-derived area-based estimates of volume through tree-level downscaling. *Forests*, 6(8).
- TOPCON, 2004, HiPer Pro GNSS receiver, GPS+ RTK system fact sheet, Topcon Positioning Systems, Inc., TOPCON Corporation. PDF document, downloadable at [[topconpositioning.com/sites/default/files/literature/HiPerPro\\_Broch\\_REVB.pdf](http://topconpositioning.com/sites/default/files/literature/HiPerPro_Broch_REVB.pdf)]
- TOPCON, 2006, FC-200 Windows® Field Controller fact sheet, Topcon Positioning Systems, Inc., TOPCON Corporation. PDF document, downloadable at [[topconpositioning.com/sites/default/files/literature/FC200\\_Broch\\_7010\\_0901\\_RevB.pdf](http://topconpositioning.com/sites/default/files/literature/FC200_Broch_7010_0901_RevB.pdf)]
- TOPCON, 2007, GTS-100N Construction Total Station fact sheet, Topcon Positioning Systems, Inc., TOPCON Corporation. PDF document, downloadable at [<http://www.topconpositioning.com/sites/default/files/literature/GTS100NBroch1.pdf>]
- TOPCON, 2008, GPT-9003M Reflectorless Motorised Total Station fact sheet, Topcon Positioning Systems, Inc., TOPCON Corporation. PDF document, downloadable at [<http://www.phoenixse.com/topcon-gpt-9003m-motorised-total-station.html>]
- Tuominen, S., Pitkänen, J., Balazs, A., Korhonen, K. T., Hyvönen, P., Muinonen, E., 2014, NFI plots as complementary reference data in forest inventory based on airborne laser scanning and aerial photography in Finland. *Silva Fennica* 48 (2).
- Turner, D., Lucieer, A., Watson, C., 2012, An automated technique for generating georectified mosaics from ultra-high resolution unmanned aerial vehicle (UAV) imagery, based on structure from motion (SfM) point clouds. *Remote Sens.* 2012, 4, 1392–1410.

- Trimble, 2008, Zephyr Model 2 Antenna Specifications, Trimble Navigation Limited. PDF document, downloadable at [<http://measutronics.com/wp-content/>]
- Trimble, 2011, GeoExplorer 6000 Series GeoXH Handheld Datasheet, Trimble Navigation Limited. PDF document, downloadable at [<http://files-trl.trimble.com/>]
- UHUL, 2003, Inventarizace lesů v České republice 2001-2004, Metodika venkovního sběru dat, Verze : 6.0., Ústav pro hospodářskou úpravu lesů Brandýs nad Labem.
- Vastaranta, M., Holopainen, M., Haapanen, R., Melkas, T., Hyyppä, J., Hyyppä, H., 2009, Comparison Between An Area-Based and Individual Tree Detection Method For Low-Pulse Density ALS-Based Forest Inventory. *International Archives of Photogrammetry, Remote Sensing and Spatial Information Sciences*, XXXVIII, 147–151.
- Vastaranta, M., Holopainen, M., Yu, X., Hyyppä, J., Mäkinen, A., Rasinmäki, J., Melkas, T., Kaartinen, H., Hyyppä, H., 2011, Effects of Individual Tree Detection Error Sources on Forest Management Planning Calculations. *Remote Sensing*, 3, 1614–1626.
- Vauhkonen, J., 2010, Estimating single-tree attributes by airborne laser scanning: methods based on computational geometry of the 3-D point data, Academic Dissertation, University of Eastern Finland, Yliopistokatu, Joensuu.
- Vauhkonen, J., Ene, L., Gupta, S., Heinzl, J., Holmgren, J., Pitkänen, J., Solberg, S., Wang, Y., Weinacker, H., Hauglin, K. M., 2011, Comparative testing of single-tree detection algorithms under different types of forest. *Forestry*, doi:10.1093/forestry/cpr051.
- Vauhkonen, J., Maltamo, M., McRoberts, R. E., Næsset, E., 2014, Introduction to forestry applications of airborne laser scanning. In *Forestry Applications of Airborne Laser Scanning*, Maltamo, M., Næsset, E., Vauhkonen, J., Eds, Springer: Dordrecht, The Netherlands,, pp. 1–16.
- Verhoeven, G., Doneus, M., Briese, C., Vermeulen, F., 2012, Mapping by matching: a computer vision-based approach to fast and accurate georeferencing of archaeological aerial photographs. *Journal of Archaeological Science* 39, 2060–2070.
- VideoDrone, 2016, VideoDrone Finland Oy, Accessible at [<http://videodrone.fi/>].
- Vincent, L., Soille, P., 1991, Watersheds in Digital Spaces: An Efficient Algorithm based on Immersion Simulations, *IEEE Transactions on Pattern Analysis and Machine Intelligence*, Vol. 13, No. 6, pp. 583-589.
- Voigtländer, 2015, Super Wide Heliar Aspherical Lenses Specification, Voigtländer GmbH. Accessible at [<http://voigtlaender.com/>]. Cited in May 2015.
- Wallace, L., Lucieer, A., Malenovský, Z., Turner, D., Vopěnka, P., 2016, Assessment of forest structure using two UAV techniques: A comparison of airborne laser scanning and structure from motion (SfM) point clouds. *Forests*, 7(3), 1–16.
- Wallace, L., Lucieer, A., Watson, C., 2012a, Assessing the feasibility of UAV-based LiDAR for high resolution forest change detection. *International Archives of the Photogrammetry, Remote Sensing and Spatial Information Sciences*, ISPRS Congress, Melbourne, Australia, XXXIX. Part B7, pp. 499 – 504.
- Wallace, L., Lucieer, A., Watson, C., Turner, D., 2012b, Development of a UAV-LiDAR system with application to forest inventory. *Remote Sensing*. 4, 1519–1543.
- Wallace, L., Musk, R., Lucieer, A., 2014, An assessment of the repeatability of automatic forest inventory metrics derived from UAV-borne laser scanning data. *IEEE Transactions on Geoscience Remote Sensing* 52, 7160–7169.

- Wang G., Weng Q., 2013, Remote sensing of natural resources, Remote Sensing Applications Series, Boca Raton: CRC Press, 580 p., ISBN 9781466556935.
- Wang, Y., Weinacker, H., Koch, B., 2008, A lidar point cloud based procedure for vertical canopy structure analysis and 3D single tree modelling in forest. *Sensors* 8: 3938–3951.
- Wannasiri, W., Nagai, M., Honda, K., Santitamont, P., & Miphokasap, P., 2013, Extraction of mangrove biophysical parameters using airborne LiDAR. *Remote Sensing*, 5(4), 1787–1808. doi.org/10.3390/rs5041787
- West, P. W., 2004, Tree and Forest Measurement, School of Environmental Science and Management, Springer Science & Business Media, 167 p., ISBN 3540403906.
- White, J. C., Wulder, M. A., Vastaranta, M., Coops, N. C., Pitt, D., Woods, M., 2013a, The utility of image-based point clouds for forest inventory: A comparison with airborne laser scanning. *Forests*, 4(3), 518–536. doi.org/10.3390/f4030518
- White, J. C., Wulder, M. A., Varhola, A., Vastaranta, M., Coops, N. C., Cook, B. D., Pitt D., Woods, M., 2013b, A best practices guide for generating forest inventory attributes from airborne laser scanning data using an area-based approach. *Forestry Chronicle* (Vol. 89). doi.org/10.5558/tfc2013-132
- Whitehead, K., Hugenholtz, C. H., 2014, Remote sensing of the environment with small unmanned aircraft systems (UASs), part 1: a review of progress and challenges. *Journal of Unmanned Vehicle Systems*, 2(3), 86–102. doi.org/10.1139/juvs-2014-0007
- Whitehead, K., Hugenholtz, C. H., Myshak, S., Brown, O., LeClair, A., Tamminga, A., Eaton, B., 2014, Remote sensing of the environment with small unmanned aircraft systems (UASs), part 2: scientific and commercial applications. *Journal of Unmanned Vehicle Systems*, 2(3), 86–102. doi.org/10.1139/juvs-2014-0007
- Whitehead, K., Moorman, B. J., Hugenholtz, C. H., 2013, Low-cost, on-demand aerial photogrammetry for glaciological measurement. *The Cryosphere*. 7(6): 1879–1884. doi: 10.5194/tc-7-1879-2013
- Williams, M. S., Bechtold, W. A., LaBau, V. J., 1994, Five instruments for measuring tree height: an evaluation. *Southern Journal of Applied Forestry*, 18.
- Wing, M. G., Solmie, D., Kellogg, L., 2004, Comparing digital range finders for forestry applications. *Journal of Forestry*, 102, 16–20.
- Wolf, B.-M., Heipke, C., 2007, Automatic extraction and delineation of single trees from remote sensing data. *Mach. Vis. Appl.* 18, 317–330.
- Woods, M., Pitt, D., Penner, M., Lim, K., Nesbitt, D., Etheridge, D., Treitz, P., 2011, Operational implementation of a LiDAR inventory in boreal Ontario. *The Forestry Chronicle* 87(4):512–528.
- Worley D. P., Landis G. H., 1954, The accuracy of height measurements with parallax instruments on 1:12000 photographs. *Photogrammetric Engineering* 20(1): 823–829.
- Wulder, M. A., Bater, C. W., Coops, N. C., Hilker, T., White, J. C., 2008, The role of LiDAR in sustainable forest management. *Forestry Chronicle*, 84, 807–826.
- Wulder, M., Niemann, K. O., Goodenough, D. G., 2000, Local maximum filtering for the extraction of tree locations and basal area from high spatial resolution imagery. *Remote Sens. Environ.* 73, 103–114.

- Yu, Q., Gong, P., Clinton, N., Biging, N., Kelly, M., Schirokauer, D., 2006, Object-based Detailed Vegetation Classification with Airborne High Spatial Resolution Remote Sensing Imagery. *Photogrammetric Engineering & Remote Sensing*, 72, pp. 799 – 811.
- Yu, X., Hyyppä, J., Vastaranta, M., Holopainen, M., 2011, Predicting Individual Tree Attributes from Airborne Laser Point Clouds Based on Random Forest Technique." *ISPRS Journal of Photogrammetry and Remote Sensing* 66:28-37.
- Zahawi, R. A., Dandois, J. P., Holl, K. D., Nadwodny, D., Reid, J. L., Ellis, E. C., 2015, Using lightweight unmanned aerial vehicles to monitor tropical forest recovery. *Biological Conservation*, 186, 287–295.
- Zarco-Tejada, P.J., Diaz-Varela, R., Angileri, V., Loudjani, P., 2014, Tree height quantification using very high resolution imagery acquired from an unmanned aerial vehicle (UAV) and automatic 3D photo-reconstruction methods. *Eur. J. Agron.* 55, 89–99.
- Zarco-Tejada, P. J., Gonzales-Dugo, V., Berni, J. A. J., 2012, Fluorescence, temperature and narrow-band indices acquired from a UAV platform for water stress detection using a micro-hyperspectral imager and a thermal camera. *Remote Sensing of Environment*, Vol. 117, pp. 322–337.
- Zhang, Y., Xiong, J., Hao, L., 2011, Photogrammetric processing of low-altitude images acquired by unpiloted aerial vehicles. *The Photogrammetric Record*. 26(134): 190–211. DOI: 10.1111/j.1477-9730.2011.00641.x
- Zhao, K., Popescu, S., 2007, Hierarchical Watershed Segmentation of Canopy Height Model for Multi-Scale Forest Inventory. *Intelligence*, (2006), 436–441.
- Zhao K., Popescu S., Nelson R., 2009, LiDAR remote sensing of forest biomass: a scale invariant estimation approach using airborne lasers. *Remote Sensing Environment*, 113:182–196
- Zhen, Z., Quackenbush, L. J., Stehman, S. V., Zhang, L., 2015, Agent-based region growing for individual tree crown delineation from airborne laser scanning (ALS) data. *International Journal of Remote Sensing*, 36, 1965–1993.
- Zhen, Z., Quackenbush, L., Zhang, L., 2016, Trends in Automatic Individual Tree Crown Detection and Delineation - Evolution of LiDAR Data. *Remote Sensing*, 8(4), 333. doi.org/10.3390/rs8040333
- Zitová, B., Flusser, J., 2003, Image registration methods: A survey. *Image and Vision Computing*, 21, 977–1000.

## List of Abbreviations

- ABA – Area-Based Approach
- AFM – All Field-Measured Trees
- BA – Binning with ‘Average’ Cell Assignment Type Interpolation Method
- BI – Binning with ‘IDW’ Cell Assignment Type Interpolation Method
- BM – Binning with ‘Maximum’ Cell Assignment Type Interpolation Method
- BN – Binning with ‘Nearest’ Cell Assignment Type Interpolation Method
- CCD – Charge-Coupled Device
- CD – Count Difference
- ČÚZK – Český Úřad Zeměměřický a Katastrální (The Czech Office for Surveying, Mapping and Cadastre)
- CHM – Canopy Height Model
- CMOS – Complementary Metal-Oxide-Semiconductor
- CPU – Central Processing Unit
- CS – Cell Size
- CSV – Comma-separated values / Character-separated values
- CV – Cross-Validation
- DAC – Digital Aerophotogrammetric Camera
- DBH – Diameter at Breast Height
- Diff – Difference
- DEM – Digital Elevation Model
- DN – Digital Number
- DPW – Digital Photogrammetric Workstation
- DPZ – Dálkový Průzkum Země (Remote Sensing)
- DSLR – Digital Single-Lens Reflex Camera
- DSM – Digital Surface Model
- DTM – Digital Terrain Model
- ESC – Electronic Speed Controller
- EOP – Exterior Orientation Parameter
- FAA – Federal Aviation Administration
- FHSS – Frequency Hopping Spread Spectrum
- FM – Field-Measured
- FMP – Forest Management Plan
- FS – Focal Statistics

GCP – Ground Control Point  
GIS – Geographic Information System  
GNSS – Global Navigation Satellite System  
GPS – Global Positioning System  
GPU – Graphics Processing Unit  
GSD – Ground Sampling Distance  
GUI – Graphical User Interface  
HD – Height Difference  
HRMS – Horizontal Root Mean Square  
Ht – Height  
IDE – Integrated Development Environment  
IDLE – Integrated Development and Learning Environment  
IDW – Inverse Distance Weighted Interpolation Method  
IM – Interpolation Method  
IMU – Inertial Measurement Unit  
INS – Inertial Navigation System  
IOP – Inner Orientation Parameters  
IT – Identified Trees  
ITA – Individual Tree Approach  
IWS – Inverse Watershed Segmentation  
LiDAR – Light Detection And Ranging  
LM – Local Maxima  
LMF – Local Maxima Filtering  
LR – Larger Range  
MAE – Mean Absolute Error  
MFM – Reduced Number of Field-Measured Trees with Modified Positions  
MC – Main flight Controller  
MT – Matched Trees  
NATO – North Atlantic Treaty Organization  
NDSM – Normalized Digital Surface Model  
NIR – Near-Infrared light  
OBIA – Object-Based Image Analysis  
OSD – On-Screen Display  
PC – Personal Computer  
Pct – Percent



PMU – Power Monitoring Unit  
PTT – Point Thinning Type  
R – Pearson’s Correlation Coefficient  
 $R^2$  – Coefficient of Determination  
RAM – Random-Access Memory  
RC – Remote Control  
RFM – Reduced Number of Field-Measured Trees  
RGB – Red, Green, Blue – Additive colour model  
RMSE – Root Mean Square Error  
RPA – Remotely Piloted Aircraft  
RPAS – Remotely Piloted Aircraft System  
RTK – Real Time Kinematic  
SD – Standard Deviation  
SDHC – Secure Digital High Capacity memory card  
SfM – Structure from Motion  
SGM – Semi-Global Matching  
SIFT – Scale-Invariant Feature Transform  
SR – Smaller Range  
Stat Sig – Statistically Significant  
TFE – Training Forest Enterprise of Mendel university in Brno  
TIN – Triangulated Irregular Network  
TLN – Triangulation with ,Linear‘ IM and ,No\_Thinning‘ Point Thinning Type  
TLW – Triangulation with ,Linear‘ IM and ,Window\_Size‘ Point Thinning Type  
TNN – Triangulation with ,Natural Neighbour‘ IM and ,No\_Thinning‘ PTT  
TNW – Triangulation with ,Natural Neighbour‘ IM and ,Window\_Size‘ PTT  
UA – Unmanned Aircraft  
UAV – Unmanned Aerial Vehicle  
UAS – Unmanned Aerial System  
UHS – Ultra High Speed bus  
VRS – Virtual Reference Station  
WMS – Web Map Services

# **List of Appendices**

All appendices are in electronic form present on an attached compact disk.

**Appendix 1 – Automated Image Registration Source Script**

**Appendix 2 – UAV Forest Explorer Source Script**

**Appendix 3 – UAV Forest Explorer User Guide**

**Appendix 4 – Best Results of UAV Forest Explorer Runs**

# Appendix 1

```
1. # * * Registration of Images From Visible and Near-Infrared Spectrum * *
2.
3. """
4. This script enables to register raster images from two cameras from
   Unmanned Aerial Vehicle into single multispectral images.
5.
6. ArcGIS software including Spatial Analyst extension should be
   installed at the computer.
7.
8. The inputs are supposed to be images taken in Near-Infrared (NIR) light
   in one folder and corresponding images taken in visible light (RGB)
   in another folder.
9.
10. The result images are 4-band multispectral TIFF images containing bands
    in this order: 1 - Near-Infrared, 2 - Red, 3 - Green, 4 - Blue.
11.
12.
13. * * * Instructions to properly run the script * * *
14.
15.
16. 1) First of all copy this script and paste it into the folder, where
    following folders are present:
17.
18.     ./NIR - folder containing Near-Infrared images
19.     ./RGB - folder containing RGB images
20.
21. 2) Run the script
22.
23. 3) Check the results in the ./RESULT folder
24.
25. """
26.
27. print "\n Registration of images has begun. \n"
28.
29. # Imports all necessary modules
30. import arcpy
31. import glob
32. import shutil
33. from arcpy import env
34. from arcpy.sa import *
35.
36. # Retrieves the ArcGIS Spatial Analyst extension license
37. arcpy.CheckOutExtension("Spatial")
38.
39. # Creates folders to store intermediate and output image data
40. arcpy.CreateFolder_management(".", "RGBROT")
41. arcpy.CreateFolder_management(".", "COMP")
42. arcpy.CreateFolder_management(".", "RESULT")
43.
44. # Defines folder paths and raster suffixes
45. path1 = "./NIR/"
46. path2 = "./RGB/"
47. path3 = "./RGBROT/"
48. suffix1 = ".JPG"
49. suffix2 = ".TIF"
50.
51. # Defines workspace and lists all Jpeg images
52. arcpy.env.workspace = path2
53. rasters = arcpy.ListRasters("*", "JPG")
54.
```

```

55. # Rotates RGB images by 180°. The center of rotation is defined from
    top-left corner in local coordinates.
56. for raster in rasters:
57.     print "Rotating RGB image " + raster
58.     arcpy.Rotate_management(raster, path3 + raster[:-4] + ".tif", "180",
        "2456 - 1632", "")
59.
60. print "\n Image rotation performed successfully! \n"
61.
62. # Sorts rasters before registration
63. list1 = glob.glob(path1 + '*' + suffix1)
64. list2 = glob.glob(path3 + '*' + suffix2)
65. list1.sort()
66. list2.sort()
67. rasters.sort()
68.
69. # Registers NIR images based on reference RGB images
70. for i in range (len(list1)):
71.     print "Registering NIR image " + list1[i] + " to reference RGB image "
        + list 2[i]
72.     arcpy.RegisterRaster_management(list1[i], "REGISTER", list2[i], "",
        "ADJUST", "")
73.
74. print "\n Image registration performed successfully! \n"
75.
76. # Defines the extent in local coordinates to clip the image border
77. arcpy.env.extent = "200, -3064, 4712, -200"
78.
79. # Composes images from both sources into one multispectral 4-band image
80. for i in range (len(list1)):
81.     print "Composing image " + list1[i] + " and image " + list2[i]
82.     image = rasters[i]
83.     bnir1 = list1[i] + "/band_1"
84.     brgb1 = list2[i] + "/band_1"
85.     brgb2 = list2[i] + "/band_2"
86.     brgb3 = list2[i] + "/band_3"
87.     composites = "./COMP/4B%s.tif" % (image[:-4])
88.     result = "./RESULT/4B%s.tif" % (image[:-4])
89.
90.     arcpy.CompositeBands_management((bnir1,brgb1,brgb2,brgb3), composites)
91.
92.     arcpy.CopyRaster_management(composites, result, "", "", "256", "", "",
        "16_BIT_UNSIGNED", "ScalePixelValue")
93.
94. print "\n Image bands composition performed successfully!"
95.
96. # Deletes folders with intermediate results
97. shutil.rmtree("./RGBROT")
98. shutil.rmtree("./COMP")
99.
100. print "\n Intermediate data were deleted."
101.
102. print "\n All images were successfully registered and outputs are saved
        in the RESULT folder! \n"

```

## Appendix 2

```
1. # * / * / * / * / * / * UAV Forest Explorer * \ * \ * \ * \ * \ *
2.
3. """
4. This script is to be used as a source code for the 'UAV Forest Explorer'
   Tool in ArcGIS ©.
5. The tool requires ArcGIS for Desktop Advanced, version 10.0 or later.
6. The tool is running on the Python version 2.7.
7. This version of the tool is for non-commercial use only!
8. Not to be distributed without the awareness of the author.
9. © Martin Machala 2014 - 2016
10.
11. Basic Description:
12. This tool serves for thorough exploration of forest stands based on the
13. photogrammetric data gained using an Unmanned Aerial Vehicle (UAV).
14.
15. With the basic settings the tool is designed to iteratively calculate the
   Inverse Watershed Segmentation calculations to identify individual trees
16. in the forest stand and to estimate their heights just based on the
   remote sensing data.
17. Iterations applied each time with different settings help to efficiently
   discover the best settings suitable for each particular forest stand.
18.
19. Optionally, the comparison with the field measurements ground truth data
   is available, either on the individual tree crown basis, or on the basis
20. of the area-based approach.
21.
22. For instructions on how to run the tool, check the
   'UAV Forest Explorer User Guide'.
23. """
24.
25. # - - - Importing necessary modules (all should be available in the basic
   Python installation):
26. import arcpy
27. from arcpy import env
28. import os
29. import numpy
30. from decimal import *
31. arcpy.CheckOutExtension(„Spatial“) # Checks out the ArcGIS Spatial Analyst
   extension license.
32. from arcpy.sa import *
33.
34. # - - - Allows to overwrite existing datasets:
35. arcpy.env.overwriteOutput = True
36.
37. # - - - Sets the code for S-JTSK_Krovak_East_North Coordinate System:
38. arcpy.env.outputCoordinateSystem = 102067
39.
40. arcpy.AddMessage(„\nUAV Forest Explorer tool has just begun running.“)
41.
42. # - - - Lists the abbreviations used in the script and tool dialog
   messages:
43. arcpy.AddMessage(„\nAbbreviations used:“)
44. arcpy.AddMessage(„ABA - Area-Based Approach“)
45. arcpy.AddMessage(„CHM - Canopy Height Model“)
46. arcpy.AddMessage(„CS - Cell Size“)
47. arcpy.AddMessage(„DSM - Digital Surface Model“)
48. arcpy.AddMessage(„DTM - Digital Terrain Model“)
49. arcpy.AddMessage(„FM - Field-Measured“)
50. arcpy.AddMessage(„FS - Focal Statistics“)
51. arcpy.AddMessage(„Ht - Height“)
52. arcpy.AddMessage(„IM - Interpolation Method“)
53. arcpy.AddMessage(„IT - Identified Trees“)
```

```

54. arcpy.AddMessage („ITA - Individual Tree Approach“)
55. arcpy.AddMessage („MAE - Mean Absolute Error“)
56. arcpy.AddMessage („MT - Matched Trees“)
57. arcpy.AddMessage („Pct - Percent“)
58. arcpy.AddMessage („RMSE - Root Mean Square Error“)
59. arcpy.AddMessage („SD - Standard Deviation“)
60.
61. # - - - Sets workspace folder to accomodate the output data:
62. wspace = arcpy.GetParameterAsText(0)
63. arcpy.AddMessage („\nWorkspace folder was set to the following location:
   \n'" + wspace + "','"")
64.
65. # The folders and geodatabases created by the tool are made only if they
   do not exist already.
66.
67. # - - - Creates working geodatabase to accomodate the processing data:
68. wbase = „WorkingData.gdb“
69. wdbase = wspace + os.sep + wbase
70.
71. if arcpy.Exists(wdbase):
72.     arcpy.AddMessage („\nNew datasets will be added to an existing
       geodatabase,'" + wbase + "','"")
73.
74. else:
75.     arcpy.CreateFileGDB_management(wspace, wbase)
76.     arcpy.AddMessage („\nNew geodatabase,'" + wbase + "','" was created to
       accomodate new datasets.")
77.
78.
79. # - - - Creates geodatabase to accomodate appropriate results data:
80. rbase = „IdentifiedTrees.gdb“
81. rdbase = wspace + os.sep + rbase
82.
83. if arcpy.Exists(rdbase):
84.     arcpy.AddMessage („\nFinal datasets will be added to an existing
       geodatabase,'" + rbase + "','"")
85.
86. else:
87.     arcpy.CreateFileGDB_management(wspace, rbase)
88.     arcpy.AddMessage („\nNew geodatabase,'" + rbase + "','" was created to
       accomodate final datasets.")
89.
90.
91. # - - - Sets the filename which will be contained in the names of the
   output files:
92. fileNameIn = arcpy.GetParameterAsText(1)
93. fileName = fileNameIn + "_"
94. arcpy.AddMessage („\nGiven prefix for the output file names:,'"
   + fileNameIn + "','"")
95.
96.
97. # - - - Optionally sets specific subset area to delineate the borderline
   for data processing:
98. subAreaIn = arcpy.GetParameterAsText(14)
99.
100. if arcpy.Exists(subAreaIn):
101.     constraints = „'%s' <None> Hard_Clip" % subAreaIn
102.     arcpy.AddMessage („\nSubarea delimitting feature class:,'"
       + subAreaIn + "','"")
103.
104. else:
105.     constraints = ""
106.     arcpy.AddMessage („\nNo delimitting subarea was defined.")
107.
108.
109. # - - - Optionally creates folder to accomodate the final layer files:
110. layerFilesFolder = arcpy.GetParameterAsText(15)

```



```

173.         arcpy.AddMessage(„\nNew DTM datasets will be added to an existing
           geodatabase ,“ + mbase + „\.”)
174.
175.     else:
176.         arcpy.CreateFileGDB_management(wspace, mbase)
177.         arcpy.AddMessage(„\nNew geodatabase ,“ + mbase + „\ was created.”)
178.
179.     # Converts DTM raster to points containing the original elevation
           values:
180.     DTMpoints = mbase + os.sep + fileName + „Orig_DTM_Points”
181.     valueField = „VALUE”
182.     arcpy.RasterToPoint_conversion(DTM, DTMpoints, valueField)
183.     arcpy.AddMessage(„DTM was converted to points.”)
184.
185.     # Creates new DTM raster with defined cell size using Spline
           interpolation method:
186.     refinedDTM = mbase + os.sep + fileName + „Refined_DTM_”
           + str(int(newDTMresolution*100))
187.     env.workspace = mbase
188.     zField = „GRID_CODE”
189.     outSpline = Spline(DTMpoints, zField, newDTMresolution, „REGULARIZED”,
           0.1)
190.     outSpline.save(refinedDTM)
191.     del outSpline
192.
193.     DTM = refinedDTM
194.     arcpy.AddMessage(„Refined version of the DTM was created.”)
195.     arcpy.AddMessage(„\n - New spatial resolution of the DTM is „
           + str(newDTMresolution) + „ m.”)
196.
197. else:
198.     arcpy.AddMessage(„\nDTM resolution was not altered.”)
199.
200.
201. # - - - Sets the rasters Cell Size (CS) variables based on user-defined
           inputs:
202. outCellSizeMinIn = arcpy.GetParameterAsText(7)
203. outCellSizeMin = float(outCellSizeMinIn.replace(„,“,‘.’))
204. arcpy.AddMessage(„\n - Minimal output cell size was set to „
           + str(outCellSizeMin) + „ m.”)
205.
206. outCellSizeMaxIn = arcpy.GetParameterAsText(8)
207. outCellSizeMax = float(outCellSizeMaxIn.replace(„,“,‘.’))
208. arcpy.AddMessage(„ - Maximal output cell size was set to „
           + str(outCellSizeMax) + „ m.”)
209.
210. outCellSizeStepIn = arcpy.GetParameterAsText(9)
211. outCellSizeStep = float(outCellSizeStepIn.replace(„,“,‘.’))
212. arcpy.AddMessage(„ - Cell size Step was set to „ + str(outCellSizeStep)
           + „ m.”)
213.
214.
215. # - - - Sets the Interpolation Method (IM) variables based on user-defined
           inputs:
216. interpolationMethod = arcpy.GetParameterAsText(10)
217. interpolationMethodList = interpolationMethod.split(„;”)
218. interpolationMethods = len(interpolationMethodList)
219. arcpy.AddMessage(„\n - Number of selected Interpolation Methods: „
           + str(interpolationMethods))
220. arcpy.AddMessage(„ - List of selected Interpolation Methods: \n „
           + str(interpolationMethod).replace(„;“,‘\n ’))
221.
222.
223. # - - - Sets the Focal Statistics (FS) variables based on user-defined
           inputs:
224. FScircleRadiusMinIn = arcpy.GetParameterAsText(11)
225. FScircleRadiusMin = int(FScircleRadiusMinIn)

```





```

282.         arcpy.AddMessage(„\nNew folder called „ + tables + „` was created
283.         to accomodate comparison tables.“)
284.
285.     # - - - Clips the field measurement data if the subarea is provided
286.     and is smaller than the field measurements area:
287.     if arcpy.Exists(subAreaIn):
288.         fieldMeasClipped = cdbase + os.sep + fileName + „FMtreesClipped“
289.         arcpy.Clip_analysis(fieldMeasurements, subAreaIn, fieldMeasClipped)
290.         fieldMeasurements = fieldMeasClipped
291.         arcpy.AddMessage(„\nField measurements data were potentially
292.         clipped using the subarea delimitting feature class.“)
293.
294.     else:
295.         arcpy.AddMessage(„\nField measurements data were not clipped.“)
296.
297.     # - - - Creates Thiessen Polygons to make zones around individual
298.     measured trees:
299.     thiessens = cdbase + os.sep + fileName + „Thiessens“
300.
301.     if arcpy.Exists(thiessens):
302.         arcpy.AddMessage(„\nThiessen polygons already exist.“)
303.
304.     else:
305.         arcpy.CreateThiessenPolygons_analysis(fieldMeasurements, thiessens,
306.         „ALL“)
307.         arcpy.AddMessage(„\nThiessen polygons were created based on the
308.         field measured tree positions data.“)
309.
310.     # - - - Creates convex bounding polygon around field-measured trees:
311.     bounding = cdbase + os.sep + fileName + „Bounding“
312.
313.     if arcpy.Exists(bounding):
314.         arcpy.AddMessage(„\nBounding polygon already exists.“)
315.
316.     else:
317.         arcpy.MinimumBoundingGeometry_management(fieldMeasurements,
318.         bounding, „CONVEX_HULL“)
319.         arcpy.AddMessage(„\nBounding polygon was created around field
320.         measured trees.“)
321.
322.     # - - - Creates a buffer around the bounding polygon:
323.     boundBuffer = cdbase + os.sep + fileName + „BoundingBuffer“
324.
325.     if arcpy.Exists(boundBuffer):
326.         arcpy.AddMessage(„\nBuffer of the bounding polygon already
327.         exists.“)
328.
329.     else:
330.         buffDistance = „1 Meters“
331.         arcpy.Buffer_analysis(bounding, boundBuffer, buffDistance)
332.         arcpy.AddMessage(„\nBuffer was created around the bounding
333.         polygon.“)
334.
335.     # - - - Clips Thiessen polygons using the buffered bounding polygon:
336.     thiessenClip = cdbase + os.sep + fileName + „ThiessensClip“
337.
338.     if arcpy.Exists(thiessenClip):
339.         arcpy.AddMessage(„\nClipped thiessen polygons already exist.“)
340.
341.     else:
342.         arcpy.Clip_analysis(thiessens, boundBuffer, thiessenClip)
343.         arcpy.AddMessage(„\nThiessen polygons were clipped using the
344.         buffered bounding polygon.“)

```

```

339.
340.     if arcpy.Exists(subAreaIn):
341.         thiessenClipSub = cdbase + os.sep + fileName +
            „ThiessensClipSub“
342.         arcpy.Clip_analysis(thiessenClip, subAreaIn, thiessenClipSub)
343.         thiessenClip = thiessenClipSub
344.         arcpy.AddMessage(„\nThiessen polygons were potentially clipped
            using the subarea delimitting feature class.“)
345.
346.     else:
347.         arcpy.AddMessage(„\nThiessen polygons are prepared for the
            data comparison.“)
348.
349.
350.     # - - - Creates table where the calculated and field-measured data will
            be compared:
351.     arcpy.env.workspace = cdbase
352.     compTabName = fileName + „X_Comparisons_X“
353.     comparisonTable = cdbase + os.sep + compTabName
354.
355.     # Sets required field names for the Comparisons table:
356.     column1 = „FileName“           # for the name of each processed file with
            individual settings.
357.     column2 = „Measured“           # for the number of field-measured (FM)
            trees.
358.     column3 = „Identified“         # for the number of trees identified by the
            tool.
359.     column4 = „Unmatched“         # for the number of FM trees without
            matching identified trees.
360.     column5 = „Matched“           # for the number of identified trees
            matched to FM trees.
361.     column6 = „Matched_Pct“       # for the percentage of matched trees from
            all FM trees.
362.     column7 = „Redundant“         # for the number of redundantly identified
            trees (not matched).
363.     column8 = „_MAE_“             # for the Mean Absolute Error between field
            measured and counted heights.
364.     column9 = „_RMSE_“           # for the Root Mean Square Error for field
            measured and counted heights.
365.     column10 = „Corr_Coeff“       # for the Pearson's Correlation Coefficient
            for FM and counted heights.
366.     column11 = „R_squared“        # for the Coefficient of Determination for
            FM and counted heights.
367.     column12 = „Stat_Sig_R“       # for the Statistical Significance of the
            Pearson's Correlation Coefficient.
368.     column13 = „Mean_Diff_MT“     # for the Mean Difference between average
            heights for Matched Trees only.
369.     column14 = „Corr_Coeff_MT“    # for the Pearson's Correlation Coefficient
            for Matched Trees only.
370.     column15 = „R_squared_MT“     # for the Coefficient of Determination for
            Matched Trees only.
371.     column16 = „Mean_FM_Ht“       # for the Mean height of FM trees.
372.     column17 = „SD_FM_Ht“        # for the Standard Deviation of heights of
            FM trees.
373.     column18 = „Mean_IT_Ht“       # for the Mean height of identified trees.
374.     column19 = „SD_IT_Ht“        # for the Standard Deviation of heights of
            identified trees.
375.     column20 = „Counts_Diff“      # for the Difference between count of
            identified and FM trees.
376.     column21 = „Heights_Diff“     # for the Difference between mean height
            of identified and FM trees.
377.
378.     if arcpy.Exists(comparisonTable):
379.         arcpy.AddMessage(„\nComparison data will be added to the
            existing table.“)
380.
381.     # Creates the table and defines data types of its columns:

```

```

382.     else:
383.         arcpy.CreateTable_management(cdbase, compTabName)
384.         arcpy.AddField_management(comparisonTable, column1, „TEXT“)
385.         arcpy.AddField_management(comparisonTable, column2, „SHORT“)
386.         arcpy.AddField_management(comparisonTable, column3, „SHORT“)
387.         arcpy.AddField_management(comparisonTable, column4, „SHORT“)
388.         arcpy.AddField_management(comparisonTable, column5, „SHORT“)
389.         arcpy.AddField_management(comparisonTable, column6, „DOUBLE“)
390.         arcpy.AddField_management(comparisonTable, column7, „SHORT“)
391.         arcpy.AddField_management(comparisonTable, column8, „DOUBLE“)
392.         arcpy.AddField_management(comparisonTable, column9, „DOUBLE“)
393.         arcpy.AddField_management(comparisonTable, column10, „DOUBLE“)
394.         arcpy.AddField_management(comparisonTable, column11, „DOUBLE“)
395.         arcpy.AddField_management(comparisonTable, column12, „TEXT“, , 15)
396.         arcpy.AddField_management(comparisonTable, column13, „DOUBLE“)
397.         arcpy.AddField_management(comparisonTable, column14, „DOUBLE“)
398.         arcpy.AddField_management(comparisonTable, column15, „DOUBLE“)
399.         arcpy.AddField_management(comparisonTable, column16, „DOUBLE“)
400.         arcpy.AddField_management(comparisonTable, column17, „DOUBLE“)
401.         arcpy.AddField_management(comparisonTable, column18, „DOUBLE“)
402.         arcpy.AddField_management(comparisonTable, column19, „DOUBLE“)
403.         arcpy.AddField_management(comparisonTable, column20, „SHORT“)
404.         arcpy.AddField_management(comparisonTable, column21, „DOUBLE“)
405.
406.         arcpy.AddMessage („\nComparison table was created as ,“
+ compTabName + „\.”)
407.
408.     arcpy.AddMessage („\n* * * * *”)
409.
410. else:
411.     arcpy.AddMessage („\nField measurement data were not provided.“)
412.     arcpy.AddMessage („\nComparison table was neither created, nor
updated.“)
413.     arcpy.AddMessage („\n* * * * *”)
414.
415.
416. # - - - Corrects the user-defined inputs and writes Warning Messages if
necessary:
417. # Returns a Warning Message when the value of Rasters Cell Size Min is
larger than the value of Rasters Cell Size Max.
418. if outCellSizeMin > outCellSizeMax:
419.     arcpy.AddWarning („\n ! ! ! Minimal cell size cannot be larger than
Maximal cell size ! ! !”)
420.
421. # If the value of Rasters Cell Size Min is set to 0 m, it is changed to
the value of Rasters Cell Size Step:
422. elif outCellSizeMin == 0:
423.     outCellSizeMin = outCellSizeStep
424.     arcpy.AddWarning („\n ! ! ! Minimal cell size was altered from ,0` to
,“ + str(int(outCellSizeMin*100)) + „` cm ! ! !”)
425.
426. # If the value of Rasters Cell Size Step is set to 0 m, it is changed to
the value of 1 m:
427. elif outCellSizeStep == 0:
428.     outCellSizeStep = 1
429.     arcpy.AddWarning („\n ! ! ! Cell size Step cannot be ,0` ! The value
was changed to ,“ + str(outCellSizeStep) + „` ! ! !”)
430.
431. # Returns a Warning Message when the value of Focal Statistics Circle
Radius Min is larger than the value of Focal Statistics Circle Radius Max.
432. elif FScircleRadiusMin > FScircleRadiusMax:
433.     arcpy.AddWarning („\n ! ! ! Minimal FS Circle Radius cannot be larger
than Maximal FS Circle Radius ! ! !”)
434.
435. else:
436.     arcpy.AddMessage („\nInputs were checked and the Inverse Watershed
Segmentation calculations will be performed.“)

```



```

494.
495. arcpy.AddMessage(„\nResolution of outputs was set to „ + resolution
    + „ cm.“)
496.
497. if round(outCellSizeCm) < 10:
498.     resolution = „00“ + resolution
499.
500. elif round(outCellSizeCm) >= 10 and round(outCellSizeCm) < 100:
501.     resolution = „0“ + resolution
502.
503. else:
504.     resolution = resolution
505.
506. # - - - Begins the loop encompassing the Interpolation Methods cycles:
507. for interpolation in interpolationMethodList:
508.
509.     interpolation = interpolation.strip(„`)
510.
511.     arcpy.AddMessage(„\n\n    >> Running IM cycle „
    + str(IMcycleSubtotal) + „ out of „ + str(IMcycleTotal) + „ <<\n“)
512.
513.     # - - - Sets the Interpolation Methods abbreviations:
514.     if interpolation == „BINNING AVERAGE NATURAL_NEIGHBOR“:
515.         intAbbrev = „_BA“
516.     elif interpolation == „BINNING IDW NATURAL_NEIGHBOR“:
517.         intAbbrev = „_BI“
518.     elif interpolation == „BINNING MAXIMUM NATURAL_NEIGHBOR“:
519.         intAbbrev = „_BM“
520.     elif interpolation == „BINNING NEAREST NATURAL_NEIGHBOR“:
521.         intAbbrev = „_BN“
522.     elif interpolation == „TRIANGULATION LINEAR WINDOW_SIZE MAXIMUM 1“:
523.         intAbbrev = „_TLW“ # Thinned
524.     elif interpolation == „TRIANGULATION LINEAR NO_THINNING MAXIMUM 1“:
525.         intAbbrev = „_TLN“ # No Thinning
526.     elif interpolation == „TRIANGULATION NATURAL_NEIGHBOR WINDOW_SIZE
    MAXIMUM 1“:
527.         intAbbrev = „_TNW“ # Thinned
528.     elif interpolation == „TRIANGULATION NATURAL_NEIGHBOR NO_THINNING
    MAXIMUM 1“:
529.         intAbbrev = „_TNN“ # No Thinning
530.     else:
531.         arcpy.AddMessage(„\nIncorrect interpolation method was
    selected!\n“)
532.
533.     intAbb = str(intAbbrev)
534.
535.
536. # - - - Creates Digital Surface Model (DSM) from the *.lasd file:
537. DSM = wdbase + os.sep + fileName + resolution + intAbb + „_DSM“
538.
539.     arcpy.AddMessage(„\n- Interpolation Method applied: „
    + str(interpolation))
540.     arcpy.AddMessage(„- Interpolation Method abbreviation: „
    + str(intAbb))
541.
542.     arcpy.LasDatasetToRaster_conversion(DSM_lasd, DSM, „ELEVATION“,
    interpolation, „FLOAT“, „CELLSIZE“, outCellSize)
543.
544.     DSMresolutionGet = arcpy.GetRasterProperties_management
    (DSM, „CELLSIZEX“)
545.     DSMresolution = float(str(DSMresolutionGet).replace(„,“, „.‘))
546.     # arcpy.AddMessage(„\n- DSM was created with the resolution of „
    + str(int(DSMresolution*100)) + „ cm.“)
547.     arcpy.AddMessage(„\n- DSM was created with the resolution of „
    + str(int(round(DSMresolution*100))) + „ cm.“)
548.
549.

```

```

550.     # - - - Creates Canopy Height Model (CHM) by subtracting DTM
551.     from DSM:
552.     CHM = wdbase + os.sep + fileName + resolution + intAbb + "__CHM"
553.     outMinus = Minus(DSM, DTM)
554.     outMinus.save(CHM)
555.     del outMinus
556.
557.     CHMresolutionGet = arcpy.GetRasterProperties_management
558.     (CHM, "CELLSIZEX")
559.     CHMresolution = float(str(CHMresolutionGet).replace(",","."))
560.     #arcpy.AddMessage("- CHM was created with the resolution of "
561.     + str(int(CHMresolution*100)) + " cm.")
562.     arcpy.AddMessage("- CHM was created with the resolution of "
563.     + str(int(round(CHMresolution*100))) + " cm.")
564.
565.     # - - - Sets the initial values of certain FS variables:
566.     FScircleRadius = FScircleRadiusMin
567.
568.     FScycle = 1
569.
570.     # - - - Begins the loop encompassing the Focal Statistics cycles:
571.     while FScircleRadius <= FScircleRadiusMax:
572.
573.         processedFileName = fileName + resolution + intAbb + "__FS"
574.         + str(FScircleRadius)
575.
576.         arcpy.AddMessage("\n\n    > Running FS cycle "
577.         + str(FScycleSubtotal) + " out of " +
578.         str(FScycleTotal) + " <\n")
579.
580.         # Writes the summary information in the beggining of each FS
581.         cycle:
582.         arcpy.AddMessage("\nInner loop information:")
583.         arcpy.AddMessage("\n~ Processed file: " + processedFileName)
584.         arcpy.AddMessage("\n~ CS Cycle: " + str(CScycleSubtotal)
585.         + " / " + str(CScycleTotal) + " ; IM Cycle: "
586.         + str(IMcycleSubtotal) + " / "
587.         + str(IMcycleTotal) + " ; FS Cycle: "
588.         + str(FScycleSubtotal)
589.         + " / " + str(FScycleTotal)
590.         + " ; FS Subcycle: (" + str(FScycle) + " / "
591.         + str(FScycles) + ")")
592.         arcpy.AddMessage("\n~ Resolution: " + resolutionStr + " cm ;
593.         FS Circle Radius: " + str(FScircleRadius))
594.         arcpy.AddMessage("\n~ IM abbrev.: " + str(intAbb))
595.
596.         # - - - Applies the Focal Statistics to smooth the CHM and to
597.         accentuate its local Maxima:
598.         FS = CHM + "__FS" + str(FScircleRadius)
599.         outFocalStats = FocalStatistics(CHM,
600.         NbrCircle(int(FScircleRadius), "CELL"), "MAXIMUM", "DATA")
601.         outFocalStats.save(FS)
602.         del outFocalStats
603.         arcpy.AddMessage("\n\nFocal Statistics were applied on CHM
604.         using " + str(FScircleRadius) + " cell(s) circle radius.")
605.
606.         # - - - Makes a negative CHM (inverts the CHM smoothed by
607.         Focal Statistics):
608.         Neg = FS + "__neg"
609.         outTimes = Times(FS, -1)
610.         outTimes.save(Neg)
611.         del outTimes

```

```

599.         arcpy.AddMessage(„\nNegatives were counted with the raster
600.         resolution of „ + resolutionStr + „ cm.“)
601.
602.         # - - - Creates Flow Direction raster from the negative CHM:
603.         FDir = Neg + „_FDir“
604.         outFlowDirection = FlowDirection(Neg)
605.         outFlowDirection.save(FDir)
606.         del outFlowDirection
607.         arcpy.AddMessage(„\nFlow Directions were counted with the
608.         raster resolution of „ + resolutionStr + „ cm.“)
609.
610.         # - - - Creates Flow Length raster from the Flow Direction
611.         raster:
612.         FLen = FDir + „_FLen“
613.         outFlowLength = FlowLength(FDir, „DOWNSTREAM“)
614.         outFlowLength.save(FLen)
615.         del outFlowLength
616.         arcpy.AddMessage(„\nFlow Lengths were counted with the raster
617.         resolution of „ + resolutionStr + „ cm.“)
618.
619.         # - - - Reclassifies the Flow Length raster:
620.         Rec = FLen + „_Rec“
621.         outReclass = Reclassify(FLen, „Value“, RemapValue([[0,1]]),
622.         „NODATA“)
623.         outReclass.save(Rec)
624.         del outReclass
625.         arcpy.AddMessage(„\nReclassifications were counted with the
626.         raster resolution of „ + resolutionStr + „ cm.“)
627.
628.         # - - - Converts reclassified rasters to polygons:
629.         Pol = Rec + „_Pgn“
630.         arcpy.RasterToPolygon_conversion(Rec, Pol, „NO_SIMPLIFY“,
631.         „VALUE“)
632.         arcpy.AddMessage(„\nRasters were converted to polygons.“)
633.
634.         # - - - Makes centroid points from the created polygons:
635.         Poi = Pol + „_Pnt“
636.         arcpy.FeatureToPoint_management(Pol, Poi, „CENTROID“)
637.         arcpy.AddMessage(„\nPolygons were converted to points.“)
638.
639.         # - - - Extracts the height values from CHM raster to the
640.         created points:
641.         resultsPathName = rdbase + os.sep + fileName + resolution
642.         + intAbb + „_FS“ + str(FScircleRadius)
643.
644.         ExPoi = resultsPathName + „_CrownTops“
645.         ExtractValuesToPoints(Poi, FS, ExPoi, „NONE“, „VALUE_ONLY“)
646.         arcpy.AddMessage(„\nParticular CHM raster values were extacted
647.         to points.“)
648.
649.         # - - - Creates the crown delineations using the Basin tool:
650.         Bas = FDir + „_Basin“
651.         outBasin = Basin(FDir)
652.         outBasin.save(Bas)
653.         del outBasin
654.         arcpy.AddMessage(„\nBasin raster was created with the
655.         resolution of „ + resolutionStr + „ cm.“)
656.
657.         # - - - Converts Basin raster to simplified polygon feature
658.         class:

```





```

704.         arcpy.AddMessage(„\nCrown Tops within the field measurement
705.         area were identified.“)
706.
707.         # Specifies the environment extent:
708.         if arcpy.Exists(subAreaIn):
709.             arcpy.env.extent = subAreaIn
710.         else:
711.             arcpy.env.extent = DSM
712.
713.         # Sets the cell size for subsequently created rasters:
714.         tempCellSize = 0.1
715.         arcpy.env.cellSize = tempCellSize
716.
717.         # - - - Converts the points containing calculated heights
718.         of trees to raster cells:
719.         treeHeight = „RASTERVALU“
720.         Ras = Poi + „_Ras“
721.         arcpy.FeatureToRaster_conversion(ExPoi, treeHeight, Ras,
722.         tempCellSize)
723.         arcpy.AddMessage(„\nPoints with extracted elevations were
724.         converted to raster cells.“)
725.
726.         # - - - Creates a copy of the previous raster when
727.         replacing NoData with Zero values (necessary for
728.         subsequent calculations):
729.         RasZ = Poi + „_RasZ“
730.         outCon = Con(IsNull(Ras),0, Ras)
731.         outCon.save(RasZ)
732.         del outCon
733.         arcpy.AddMessage(„\nRaster cells with ‚NoData‘ values were
734.         replaced by ‚0‘ values.“)
735.
736.         # - - - Calculates the Zonal Statistics from the raster
737.         cells:
738.         # a) for the area of individual Thiessen polygons around
739.         field measured trees:
740.         compResultsPathName = cdbase + os.sep + fileName +
741.         resolution + intAbb + „_FS“ + str(FScircleRadius)
742.         zoneField = „ID“
743.         zonalTable1 = compResultsPathName + „_ZonalStatsCounts“
744.         zonalTable2 = compResultsPathName + „_ZonalStatsFull“
745.
746.         ZonalStatisticsAsTable(thiessenClip, zoneField, Ras,
747.         zonalTable1, „DATA“, „ALL“) # Includes also NoData values
748.         arcpy.AddMessage(„\nZonal statistics were calculated for
749.         original raster cells using Thiessen polygons.“)
750.
751.         ZonalStatisticsAsTable(thiessenClip, zoneField, RasZ,
752.         zonalTable2, „DATA“, „ALL“) # Includes zeroes instead of
753.         NoData values
754.         arcpy.AddMessage(„\nZonal statistics were calculated for
755.         modified raster cells using Thiessen polygons.“)
756.
757.         # b) for the area of buffered bounding polygon around field
758.         measured trees:
759.         zoneFieldBB = „ORIG_FID“
760.         zonalTable3 = compResultsPathName + „_ZonalStatsUnpaired“
761.         ZonalStatisticsAsTable(boundBuffer, zoneFieldBB, Ras,
762.         zonalTable3, „DATA“, „ALL“)
763.         arcpy.AddMessage(„\nZonal statistics were calculated for
764.         original raster cells using buffered bounding polygon.“)
765.
766.         # - - - Makes comparison of data and counts correlation
767.         coefficients and appropriate error values:

```

```

753.
754. # - - - Joins the field measured trees with the table of
      # calculated trees (without NoData):
755. joinedTrees = processedFileName + „_Joined“
756. fmTabID = „ID“ # field measurements table ID
757. zsTabID = „ID“ # zonal statistics table ID
758.
759. fieldMeasCopy = arcpy.FeatureClassToFeatureClass_conversion
      (fieldMeasurements, cdbase, joinedTrees)
      # Makes a copy of Field Measurements dataset
760. fieldMeasJoin = arcpy.JoinField_management(fieldMeasCopy,
      fmTabID, zonalTable2, zsTabID) # Joins Zonal Statistics
      table to that copy
761. arcpy.AddMessage(„\nThe Field Measurement table and the
      table of calculated tree heights were joined.“)
762.
763.
764. # Names of present and new cols for the Field
      Measurement table including the join:
765. joinCol1 = „Height“ # for field measured (FM) heights
      (existing column)
766. joinCol2 = „MAX“ # for calculated heights
      (existing column)
767. joinCol3 = „Diff“ # for their difference
768. joinCol4 = „Abs_Diff“ # for absolute value of that
      difference
769. joinCol5 = „Diff_sq2“ # for the square of that difference
770. joinCol6 = „No_Max“ # for unidentified trees
771. joinCol7 = „Height_2“ # for FM heights of matched trees
772. joinCol8 = „MAX_2“ # for calculated heights of matched
      trees
773. joinCol9 = „Diff_2“ # for their difference
774.
775. # Adds new columns to the Field Measurement table including
      the join
776. arcpy.AddField_management(fieldMeasJoin, joinCol3, „DOUBLE“)
777. arcpy.AddField_management(fieldMeasJoin, joinCol4, „DOUBLE“)
778. arcpy.AddField_management(fieldMeasJoin, joinCol5, „DOUBLE“)
779. arcpy.AddField_management(fieldMeasJoin, joinCol6, „SHORT“)
780. arcpy.AddField_management(fieldMeasJoin, joinCol7, „DOUBLE“)
781. arcpy.AddField_management(fieldMeasJoin, joinCol8, „DOUBLE“)
782. arcpy.AddField_management(fieldMeasJoin, joinCol9, „DOUBLE“)
783. arcpy.AddMessage(„\nNew columns were added to the Field
      Measurement table with a join.“)
784.
785.
786. # - - - Calculates demanded values in the newly added
      fields:
787. joinFields = [joinCol1, joinCol2, joinCol3, joinCol4,
      joinCol5, joinCol6, joinCol7, joinCol8, joinCol9]
788.
789. with arcpy.da.UpdateCursor(fieldMeasJoin, joinFields) as
      cursor:
790.     for row in cursor:
791.         if row[1] == None:
792.             row[1] = 0
793.             row[5] = 1
794.         elif row[1] == 0: # Marks rows without matching
      trees(with no calculated heights)
795.             row[5] = 1
796.         else:
797.             row[5] = 0
798.             row[2] = row[0] - row[1] # Counts the difference
      between ‚Height‘ field (measured heights)
      and ‚MAX‘ field (calculated heights)
799.             row[3] = abs(row[2]) # Calculates absolute values
      of that difference

```

```

800.         row[4] = row[2]**2 # Calculates the second power
           of that difference
801.         if row[1] > 0:
802.             row[6] = row[0]
803.             row[7] = row[1]
804.             row[8] = row[6] - row[7]
805.         cursor.updateRow(row)
806.
807.     arcpy.AddMessage(„\nDifferences between measured and
           calculated tree heights were counted.“)
808.
809.
810.     # - - - Performs required mathematical and statistical
           calculations using Individual Tree Approach (ITA):
811.     arcpy.AddMessage(„\n* * * * * „)
812.     arcpy.AddMessage(„\nResults of the identified and
           field-measured trees comparisons:“)
813.     arcpy.AddMessage(„\n\n~ Comparisons for Individual Tree
           Approach (paired trees): „)
814.
815.     # Makes arrays from certain columns, to prepare them for
           further calculations:
816.     joinArray1 = arcpy.da.FeatureClassToNumPyArray
           (fieldMeasJoin, joinCol1) # Makes array from ‚Height‘ field
817.     joinArray2 = arcpy.da.FeatureClassToNumPyArray
           (fieldMeasJoin, joinCol2) # Makes array from ‚MAX‘ field
818.
819.     measuredTrees = len(joinArray1)
820.     arcpy.AddMessage(„\nMeasured trees: „ + str(measuredTrees))
821.
822.     # Gets number of identified trees falling into the Thiessen
           polygons (and thus being compared):
823.     zonalCol = „COUNT“
824.     zonalArray = arcpy.da.TableToNumPyArray(zonalTable1,
           zonalCol)
825.     identifiedTrees = zonalArray[zonalCol].sum()
826.     arcpy.AddMessage(„\nIdentified trees: „ +
           str(identifiedTrees))
827.
828.     # Calculates the number of unmatched trees (measured trees
           with no identified tree in their Thiessen polygon):
829.     joinArray3 = arcpy.da.FeatureClassToNumPyArray
           (fieldMeasJoin, joinCol6)
830.     unmatchedTrees = joinArray3[joinCol6].sum()
831.     arcpy.AddMessage(„\nUnmatched trees: „ +
           str(unmatchedTrees))
832.
833.     # Calculates the number of matched trees (paired measured
           and identified trees based on Thiessen polygons):
834.     matchedTrees = measuredTrees - unmatchedTrees
835.     arcpy.AddMessage(„\nMatched trees: „ + str(matchedTrees))
836.
837.     # Calculates the percentage of matched trees out of all
           measured trees:
838.     matchedTreesPerc = float(matchedTrees) /
           float(measuredTrees) * 100
839.     matchedTreesPercRound = round(matchedTreesPerc,2)
840.     arcpy.AddMessage(„\nMatched trees percentage: „
           + str(matchedTreesPercRound) + „ %“)
841.
842.     # Calculates the count of identified without matched trees
           (shows if any redundant trees were identified):
843.     redundantTrees = identifiedTrees - matchedTrees
844.     arcpy.AddMessage(„\nRedundantly identified trees: „
           + str(redundantTrees))
845.
846.     # Calculates the Mean Absolute Error as an average of

```

```

absolute value differences between measured and
calculated tree heights:
847. joinArray4 = arcpy.da.FeatureClassToNumPyArray
      (fieldMeasJoin, joinCol4)
848. absDiffSum = joinArray4[joinCol4].sum()
849. absDiffMean = absDiffSum / len(joinArray4)
850. absDiffMeanRound = round(absDiffMean, 3)
851. arcpy.AddMessage(„\n\nMean Absolute Error (MAE): „
      + str(absDiffMeanRound))

852.
853. # Calculates the Root Mean Square Error from the
      differences between measured and calculated tree heights:
854. joinArray5 = arcpy.da.FeatureClassToNumPyArray
      (fieldMeasJoin, joinCol5)
855. sqDiffSum = joinArray5[joinCol5].sum()
856. sqDiffMean = sqDiffSum / len(joinArray5)
857. sqDiffMeanRoot = sqDiffMean ** 0.5
858. sqDiffMeanRootRound = round(sqDiffMeanRoot, 3)
859. arcpy.AddMessage(„\n\nRoot Mean Square Error (RMSE): „
      + str(sqDiffMeanRootRound))

860.
861. # Calculates Pearson's Correlation Coefficient for measured
      and calculated tree heights:
862. corrCoef = numpy.corrcoef(joinArray1, joinArray2)[0, 1]
863. corrCoefRound = round(corrCoef, 3)
864. arcpy.AddMessage(„\n\nPearson's Correlation Coefficient (R): „
      + str(corrCoefRound))

865.
866. # Calculates Coefficient of determination (R-squared) for
      measured and calculated tree heights:
867. squaredR = corrCoef ** 2
868. squaredRround = round(squaredR, 3)
869. arcpy.AddMessage(„\n\nCoefficient of determination
      (R-squared): „ + str(squaredRround))

870.
871. # Tests for the statistical significance of calculated
      Correlation Coefficient:
872. n = matchedTrees # sample size
873. R = corrCoef # Pearson's Correlation Coefficient
874. T = (R*((n-2)**0.5))/((1-R**2)**0.5) # Test statistic using
      Student's t-distribution

875.
876. dof = n - 2 # degrees of freedom
877.
878. # critical values for alfa = 0.05 for the two-tailed
      test:
879. if dof >= 100:
880.     cv = 1.984
881. elif dof >= 80 and dof < 100:
882.     cv = 1.99
883. elif dof >= 60 and dof < 80:
884.     cv = 2.0
885. elif dof >= 40 and dof < 60:
886.     cv = 2.021
887. elif dof >= 20 and dof < 40:
888.     cv = 2.086
889. elif dof >= 10 and dof < 20:
890.     cv = 2.228
891. elif dof >= 5 and dof < 10:
892.     cv = 2.571
893. elif dof >= 2 and dof < 5:
894.     cv = 4.303
895. else:
896.     cv = 12.706
897.
898. if T > cv:
899.     statSig = „Yes“

```

```

900.         else:
901.             statSig = „No“
902.
903.         arcpy.AddMessage(„\nStatistically significant R: „
+ str(statSig))
904.
905.         # Calculates the Mean Difference between measured and
calculated tree heights of matched trees only (without zero
values):
906.         joinArray6 = arcpy.da.FeatureClassToNumPyArray
(fieldMeasJoin, joinCol9, skip_nulls=True)
907.         diffMatchSum = joinArray6[joinCol9].sum()
908.         diffMatchMean = diffMatchSum / len(joinArray6)
909.         diffMatchMeanRound = round(diffMatchMean, 3)
910.         arcpy.AddMessage(„\n\nMean Difference of average heights
for Matched trees only: „ + str(diffMatchMeanRound))
911.
912.         # Calculates Pearson's Correlation Coefficient for measured
and calculated tree heights of matched trees only
(without zero values):
913.         joinArray7 = arcpy.da.FeatureClassToNumPyArray
(fieldMeasJoin, joinCol7, skip_nulls=True) # Makes array
from FM heights without Zero values.
914.         joinArray8 = arcpy.da.FeatureClassToNumPyArray
(fieldMeasJoin, joinCol8, skip_nulls=True)
# Makes array from calculated heights without Zero values.
915.
916.         if len(joinArray6) < 1:
917.             joinArray7 = [0]
918.             joinArray8 = [0]
919.
920.         corrCoefMatch = numpy.corrcoef(joinArray7, joinArray8)[0,1]
921.         corrCoefMatchRound = round(corrCoefMatch, 3)
922.         arcpy.AddMessage(„\nPearson's Correlation Coefficient (R)
for Matched trees only: „ + str(corrCoefMatchRound))
923.
924.         # Calculates Coefficient of determination (R-squared) for
measured and calculated tree heights of matched trees
only (without zero values):
925.         squaredRmatch = corrCoefMatch ** 2
926.         squaredRmatchRound = round(squaredRmatch, 3)
927.         arcpy.AddMessage(„\nCoefficient of determination (R-squared)
for Matched trees only: „ + str(squaredRmatchRound))
928.
929.         # Calculates the average height of field-measured trees:
930.         fmHeightSum = joinArray1[joinCol1].sum() # sum of field
measured heights
931.         fmHeightMean = fmHeightSum / measuredTrees # mean of field
measured heights
932.         fmHeightMeanRound = round(fmHeightMean, 3)
933.         arcpy.AddMessage(„\n\nAverage height of field-measured
trees: „ + str(fmHeightMeanRound))
934.
935.         # Calculates Standard Deviation (SD) for heights of
field-measured trees:
936.         fmhArray = numpy.asarray(joinArray1, float) # Prepares the
Height array
937.         stDevFMH = numpy.std(fmhArray) #SD of field-measured heights
938.         stDevFMHround = round(stDevFMH, 3)
939.         arcpy.AddMessage(„\nStandard Deviation (SD) of
field-measured heights: „ + str(stDevFMHround))
940.
941.
942.         # - - - Performs required mathematical and statistical
calculations using Area-Based Approach (ABA):
943.         arcpy.AddMessage(„\n\n~ Comparisons for Area-Based Approach
(unpaired trees): „)

```

```

944.
945.     # Calculates average height of identified trees:
946.     unpairCol1 = „MEAN“
947.     unpairArray1 = arcpy.da.TableToNumPyArray(zonalTable3,
948.         unpairCol1) # average height of identified trees in proper
949.         area
950.     unpairArray1Num = unpairArray1[unpairCol1].sum() # one-value
951.         array converted to float number
952.     unpairArray1NumRound = round(unpairArray1Num, 3)
953.     arcpy.AddMessage(„\nAverage height of identified trees: „
954.         + str(unpairArray1NumRound))
955.
956.     # Calculates Standard Deviation for heights of identified
957.     trees:
958.     unpairCol2 = „STD“
959.     unpairArray2 = arcpy.da.TableToNumPyArray(zonalTable3,
960.         unpairCol2) # SD of identified trees heights
961.     unpairArray2Num = unpairArray2[unpairCol2].sum() # one-value
962.         array converted to float number
963.     unpairArray2NumRound = round(unpairArray2Num, 3)
964.     arcpy.AddMessage(„\nStandard Deviation (SD) of calculated
965.         heights: „ + str(unpairArray2NumRound))
966.
967.     # Calculates difference between the counts of identified and
968.     field-measured trees:
969.     countDiff = identifiedTrees - measuredTrees
970.     arcpy.AddMessage(„\nTrees count difference: „
971.         + str(countDiff))
972.
973.     # Calculates difference between average heights of
974.     identified and field-measured trees:
975.     heightDiff = unpairArray1Num - fmHeightMean
976.     heightDiffRound = round(heightDiff, 3)
977.     arcpy.AddMessage(„\nDifference between average heights: „
978.         + str(heightDiffRound))
979.
980.     # - - - Fills the proper values into the comparison table:
981.     inCursor = arcpy.da.InsertCursor(comparisonTable, [column1,
982.         column2, column3, column4, column5, column6, column7,
983.         column8, column9, column10, column11, column12, column13,
984.         column14, column15, column16, column17, column18, column19,
985.         column20, column21])
986.     inCursor.insertRow([processedFileName, measuredTrees,
987.         identifiedTrees, unmatchedTrees, matchedTrees,
988.         matchedTreesPercRound, redundantTrees, absDiffMeanRound,
989.         sqDiffMeanRootRound, corrCoefRound, squaredRround, statSig,
990.         diffMatchMeanRound, corrCoefMatchRound, squaredRmatchRound,
991.         fmHeightMeanRound, stDevFMHround, unpairArray1NumRound,
992.         unpairArray2NumRound, countDiff, heightDiffRound])
993.     del inCursor
994.
995.     arcpy.AddMessage(„\n\nComparison table was filled with
996.         appropriate data.“)
997.     arcpy.AddMessage(„\n* * * * *“)
998.
999.     # Sets back the appropriate Cell Size
1000.    arcpy.env.cellSize = outCellSize
1001.
1002. else:
1003.     arcpy.AddMessage(„\nField measurement data were not
1004.         provided.“)
1005.
1006. # - - - Updates counters before the completion of the FS cycle:

```

```

992.         FScycleResidue = FScycleTotal - FScycleSubtotal
993.
994.         arcpy.AddMessage(„\n\nFS cycle „ + str(FScycleSubtotal)
          + „ completed! Remaining FS cycles: „ + str(FScycleResidue))
995.         arcpy.AddMessage(„\n.....“)
996.
997.         FScircleRadius = FScircleRadius + FScircleRadiusStep
998.
999.         FScycle = FScycle + 1
1000.        FScycleSubtotal = FScycleSubtotal + 1
1001.
1002.        # - - - End of FS cycle.
1003.
1004.
1005.        # - - - Optionally deletes rasters and feature classes from the
          working geodatabase before each IM cycle completes:
1006.        if str(checkBoxDel) == „true“:
1007.
1008.            arcpy.AddMessage(„\nWorking datasets created so far will be
          deleted.“)
1009.            arcpy.env.workspace = wdbase
1010.            fcs = arcpy.ListFeatureClasses()
1011.            rst = arcpy.ListRasters()
1012.
1013.            for fc in fcs:
1014.                arcpy.Delete_management(fc)
1015.
1016.            arcpy.AddMessage(„\nWorking feature classes from IM cycle „
          + str(IMcycleSubtotal) + „ were deleted.“)
1017.
1018.            for rs in rst:
1019.                arcpy.Delete_management(rs)
1020.
1021.            arcpy.AddMessage(„\nWorking rasters from IM cycle „
          + str(IMcycleSubtotal) + „ were deleted.“)
1022.
1023.        else:
1024.            arcpy.AddMessage(„\nWorking datasets were not deleted.“)
1025.
1026.
1027.        # - - - Updates counters before the completion of the IM cycle:
1028.        IMcycleResidue = IMcycleTotal - IMcycleSubtotal
1029.
1030.        arcpy.AddMessage(„\n\nIM cycle „ + str(IMcycleSubtotal)
          + „ completed! Remaining IM cycles: „ + str(IMcycleResidue))
1031.        arcpy.AddMessage(„\n_ _ _ _ _“)
1032.
1033.        IMcycleSubtotal = IMcycleSubtotal + 1
1034.
1035.        # - - - End of IM cycle.
1036.
1037.
1038.        # - - - Updates counters before the completion of the CS cycle:
1039.        CScycleResidue = CScycleTotal - CScycleSubtotal
1040.
1041.        arcpy.AddMessage(„\n\nCS cycle „ + str(CScycleSubtotal)
          + „ completed! Remaining CS cycles: „ + str(CScycleResidue))
1042.        arcpy.AddMessage(„\n* * * * *“)
1043.
1044.        outCellSize = outCellSize + outCellSizeStep
1045.
1046.        CScycleSubtotal = CScycleSubtotal + 1
1047.
1048.
1049.        # - - - Progressively reduces number of FS subcycles, if required:
1050.        if str(checkBoxRFS) == „true“:
1051.            if CScycleResidue < FScycles:

```



```

1052.         FScircleRadiusMax = FScircleRadiusMax - 1
1053.         FScycles = FScycles - 1
1054.         arcpy.AddMessage(„\nNumber of FS subcycles was reduced
          by 1 to actual value of „ + str(FScycles) + „.“)
1055.
1056.         else:
1057.             arcpy.AddMessage(„\nNumber of FS subcycles was maintained
          at „ + str(FScycles) + „.“)
1058.
1059.     else:
1060.         arcpy.AddMessage(„\nNumber of FS subcycles was maintained at „
          + str(FScycles) + „.“)
1061.
1062.     # - - - End of CS cycle.
1063.
1064.
1065. # - - - Recapitulation of the performed cycles counts and checking with
          the expected values:
1066. arcpy.AddMessage(„\n\n    All loops were finished!“)
1067.
1068. arcpy.AddMessage(„\n\nTotal number of CS cycles performed: „
          + str(int(CScycleSubtotal)-1) + „ ; Predicted: „ + str(CScycleTotal))
1069.
1070. arcpy.AddMessage(„\n\nTotal number of IM cycles performed: „
          + str(int(IMcycleSubtotal)-1) + „ ; Predicted: „ + str(IMcycleTotal))
1071.
1072. arcpy.AddMessage(„\n\nTotal number of FS cycles performed: „
          + str(int(FScycleSubtotal)-1) + „ ; Predicted: „ + str(FScycleTotal))
1073.
1074. if str(checkBoxRFS) == ‚true‘:
1075.     arcpy.AddMessage(„\nNumber of potential FS cycles without
          reduction: „ + str(FScycleTotalOrig))
1076.     arcpy.AddMessage(„Number of FS cycles avoided thanks to the
          reduction : „ + str(cycleReductionTotal))
1077.
1078. else:
1079.     arcpy.AddMessage(„\nNumber of FS cycles was not reduced.“)
1080.
1081.
1082. # - - - Exports the comparison table as an Excel file:
1083. if arcpy.Exists(fieldMeasurements):
1084.     arcpy.env.workspace = rtables
1085.     tableName = fileName + „Comparisons.xls“
1086.     arcpy.TableToExcel_conversion(comparisonTable, tableName)
1087.     arcpy.AddMessage(„\n\nComparison table was exported in the „
          + tables + „\ folder as file: „ + tableName + „.“)
1088.
1089. else:
1090.     arcpy.AddMessage(„\n\nNo comparison tables were exported.“)
1091.
1092.
1093. # - - - Optionally deletes the already emptied Working geodatabase:
1094. if str(checkBoxDel) == ‚true‘:
1095.     arcpy.management.Delete(wdbase)
1096.     arcpy.AddMessage(„\n“ + wbase + „ geodatabase was deleted!“)
1097.
1098. else:
1099.     arcpy.AddMessage(„\nGeodatabase with working datasets was
          preserved.“)
1100.
1101. arcpy.AddMessage(„\n\n Je to tam, kemo!\n\n“)
1102.
1103. # - - - End of the script.

```

## Appendix 3

### *User Guide for the UAV Forest Explorer Tool*

#### Table of Contents

1) Introduction .....	II
2) Hardware Requirements .....	II
3) Software Requirements .....	II
4) Installation Instructions .....	II
5) General Tool Description .....	II
6) Usage .....	III
7) Elementary Data Inputs and Processing Principles .....	IV
8) Elementary Data Outputs .....	V
9) Initial Settings of the Tool .....	VI
Workspace Folder .....	VI
Filename (Outputs Prefix) .....	VI
Surface Point Cloud *.las File .....	VII
Las Dataset Name .....	VII
Digital Terrain Model (DTM) .....	VII
Refine DTM Cell Size? (optional) .....	VII
New DTM Cell Size [m] (optional) .....	VII
Rasters Cell Size Min [m] .....	VIII
Rasters Cell Size Max [m] .....	VIII
Rasters Cell Size Step [m] .....	VIII
Interpolation Methods .....	VIII
Focal Statistics Circle Radius Min [Cell] .....	IX
Focal Statistics Circle Radius Max [Cell] .....	IX
Progressively Reduce Focal Statistics Subcycles? (optional) .....	IX
Delimitting Sub-Area (optional) .....	XI
Layer Files Folder (optional) .....	XI
Compare Data with Field-Measured Heights? (optional) .....	XII
Field Measurements Data (optional) .....	XII
Delete Working Datasets? (optional) .....	XII
10) Field-Measurements Data Utilization .....	XIII
11) Suggested workflow .....	XV
12) Legal Information .....	XVII

## 1) Introduction

This User Guide describes the hardware and software requirements, demanded inputs, default and optional data outputs, background of processing principles and instructions for initial settings of the UAV Forest Explorer tool.

## 2) Hardware Requirements

Any personal computer (desktop or notebook PC) capable of running ArcGIS 10 software and its geoprocessing tools should be able to run the UAV Forest Explorer.

## 3) Software Requirements

The tool requires ArcGIS® for Desktop Advanced software by Esri®, version 10.2 or later. The tool was tested on *ArcMap 10.2* with 100% reliability. The stability on newer versions of ArcMap was not fully tested. The tool is running on the *Python version 2.7*.

## 4) Installation Instructions

The tool is to be used similarly like any other tool within ArcGIS Desktop software. The *UAV\_Forest\_Explorer.tbx* file should be saved on a computer hard drive. Then, in ArcCatalog this file should be located and copied. Afterwards, still in ArcCatalog, the path to *Toolboxes/My Toolboxes* should be located and the file should be pasted here.

Since the tool contains the source code (python script) already imported into it, searching for the external \*.py file is not needed. To guarantee maximal universality, the tool does not need to install or manually import any external libraries, packages or modules.

When the \*.tbx file is pasted to the *My Toolboxes* folder, it can be unfolded and the tool in it can be double-clicked. This opens the graphical user interface of the UAV Forest Explorer tool. At this point the tool is ready to be used.

## 5) General Tool Description

This tool serves for thorough exploration of forest stands based on the photogrammetric data gained using an Unmanned Aerial Vehicle (UAV). With the

basic settings the tool is designed to iteratively calculate the Inverse Watershed Segmentation calculations to identify individual trees in the forest stand and to estimate their heights just based on the remote sensing data. Iterations applied each time with different settings help to efficiently discover the best settings suitable for each particular forest stand.

## **6) Usage**

The tool can be used basically in two ways. Either without or with the field measurements ground truth data. The difference is following. When the ground truth data are not provided, the tool automatically processes the remote sensing data, performs Inverse Watershed Segmentation calculations, identifies trees in the area of interest and delineates their crowns. The results then can be assessed chiefly manually and compared between each other mainly visually.

When the field-measurements data are provided by the user, the tool performs all the previous processes as well, but makes also some additional computations. It takes the ground truth data (which have to meet specific conditions), and compares them with the results of its own calculations. Especially it compares the counts and heights of the automatically identified trees with these values of field-measured trees. The tool performs series of mathematical and statistical calculations for this purpose, working on the basis of the Individual Tree Approach (ITA) as well as of the Area-Based Approach (ABA). The exact outputs of this comparisons resulting from each combination of the tool settings are then stored also in a tabular form. The results of tens or hundreds of iterations (settings combinations) can be then assessed by the user easily in this way.

Besides the possibility to use the field-measurements data, the tool offers also some other facultative options. For instance to progressively reduce the number of iterations, when excluding those combinations of settings giving the less valuable results; to refine the cell size of the DTM, if being too coarse; to specify the area of interest to delimit the extent of calculations; to provide layer files, which then can be applied on the demanded feature classes created by the tool; or to choose to delete the working datasets, if preserving them is not necessary.

The tool enables the user to control the processes it makes while running. When the Background Processing is disabled in the Geoprocessing Options of ArcMap, the progress of the tool processing can be watched via Messages continuously displayed in the Progress Dialog Box.

## 7) Elementary Data Inputs and Processing Principles

The tool accepts several data inputs. Some of them are obligatory, some can be provided just optionally. Only two data inputs are required to enable the tool to run and to perform the fundamental operations resulting to identification of trees. These data inputs are following:

- *Point cloud* in the form of \*.las file containing the elevation information of the forest canopy surface covering the area of interest. Dataset should be derived from the photogrammetric processing of the UAV-borne imagery.
- *Digital Terrain Model (DTM)* in the form of a raster dataset with cell values representing the elevation of the terrain below the examined forest stand. Can be obtained from various sources (contours, LiDAR mapping, geodetic survey, etc.). If being too coarse, the spatial resolution of the DTM can be optionally refined by the tool to the desired values.

Based just on these data, the tool is able to identify the treetops in the area of interest and to assign the appropriate heights to them. The number of identified trees depends on the settings of Raster Cell Size(s), Interpolation Method(s) and Focal Statistics Circle Radius(es) applied. Both numerical inputs can be set as a particular value or as a range of values. Then between one to eight interpolation methods can be selected. If only one of each values/methods is set, one calculation is performed during a single tool run. If the ranges of values are defined or multiple interpolation methods are selected, the tool runs iteratively. In such case, tens or hundreds of iterations can be calculated during one tool run easily.

Basically, the tool is performing three inner loops/cycles to process Inverse Watershed Segmentation (IWS) calculations iteratively:

1. *Cell Size cycle* which performs all further calculations for each desired raster cell size (based on Raster Cell Size Min, Max and Step).
2. *Interpolation Method cycle* which is calculated for each particular Cell Size. It creates Digital Surface Model (DSM) from the LAS Dataset using required interpolation method(s). Subsequently a Canopy Height Model (CHM) is created by subtracting the DTM from the DSM.

3. *Focal Statistics cycle* which is calculated for each particular Cell Size and each particular Interpolation Method. It smooths the CHM, calculates the maximum of its cells in the defined neighbourhood and performs the other IWS processes.

Between optional data inputs belongs the delimitting sub-area, which can restrict the calculations for the particular area of interest. It should be provided in the form of polygon feature class. When not provided, the calculations are performed for the whole area covered by the point cloud dataset or the DTM (the smaller of them).

## 8) Elementary Data Outputs

The tool produces several kinds of data outputs. All of them are stored in the user-defined *Workspace Folder*. The outputs are created mostly in the form of feature classes, raster datasets and tables, when some of them are stored in the file geodatabases and some of them just in folders (both are created automatically by the tool). Some data outputs are created by default, some of them can be produced just based on optional settings. Between the elementary data outputs belong:

- *WorkingData.gdb* - a file geodatabase containing working raster files and feature classes created during each Inverse Watershed Segmentation. This geodatabase can optionally be deleted by the tool automatically.
- *IdentifiedTrees.gdb* - a file geodatabase containing following datasets:
  - Point feature classes (*'...CrownTops'*) where points represent the apexes of identified trees. The tree heights, calculated as local maxima of uniquely generated and smoothed Canopy Height Model (CHM), are in the attribute tables of these feature classes stored in the 'RASTERVALU' column.
  - Polygon feature classes (*'...Crowns'*) where polygons represent simplified borderlines between individual tree crowns.

Optionally, when the sample layer files are provided by the user, the tool can also create layer files for both these feature classes. The produced layer files are then stored in the 'LayerFiles' folder.

Besides those basic outputs, the tool can perform also several optional computations and create consequent outputs.

If the user has the field measurement ground truth data available, the tool gives the option to compare the calculation results with them. The field measurement data should be provided in the form of a point feature class, where each point represents the position of a tree and contains the appropriate height as an attribute. The tool then creates additional outputs such as *Comparisons.gdb* file geodatabase or *Tables* folder. The calculations performed by the tool when the field measurement data are provided are thoroughly described later on in the proper part of this document (Chapter 10 - Field-Measurements Data Utilization).

The tool can produce together 4 file geodatabases (*Comparisons.gdb*, *IdentifiedTrees.gdb*, *RefinedDTM.gdb* and *WorkingData.gdb*) and up to two folders (*LayerFiles* and *Tables*) filled with output data.

All outputs of this tool are positioned using S-JTSK Krovak EastNorth coordinate system.

## 9) Initial Settings of the Tool

In this section the initial settings of the UAV Forest Explorer tool is described. Using the graphical user interface of the tool, user can see series of fields to be filled. Some of them are compulsory, some are optional. The names of these fields and their purpose are described one by one.

**Workspace Folder** - The path to a folder on a computer hard drive, where all the tool outputs will be stored. An empty folder is recommended.

**Filename (Outputs Prefix)** - A unique filename, which will be used as a prefix for the names of all the tool outputs. Can express the characterization of the forest stand just being processed (e.g. OldPines) or the description of the location (e.g. Site1) etc.

Most of the tool outputs will consist of this filename, followed by the raster cell size (in cm), interpolation method abbreviation and focal statistics circle radius (in cells) applied in the particular run. This ensures that each settings applied during each iteration generates unique and easily distinguishable results.

For instance 'OldPines\_065\_BM\_FS3\_CrownTops' is the name of the feature class (representing crown tops) created using 65-cm raster cell size, 'Binning' interpolation method with 'Maximum' cell assignment type and 3-cell Focal Statistics circle radius.

! Warning: Filename should not include any spaces or diacritics !

**Surface Point Cloud \*.las File** - A point cloud in the form of \*.las file representing the canopy surface of the forest stand being under investigation. Point cloud should be derived from the photogrammetric processing of the imagery acquired using an UAV.

**Las Dataset Name** - Name of the LAS Dataset (\*.lasd file) created from the provided \*.las file. The default name is 'LasDataset.lasd'.

**Digital Terrain Model (DTM)** - A raster dataset with cell values representing the elevation of the terrain below the investigated forest stand. Can be obtained from various sources (contours, LiDAR mapping, geodetic survey, etc.).

**Refine DTM Cell Size? (optional)** - Gives the option to refine the spatial resolution of the DTM, if being too coarse. The aim is to reduce the differences between neighbouring raster cells in steep areas. When keeping the source elevation information, the refined DTM should better represent the shape of the natural terrain.

If checked, the provided DTM is converted to points and then a new DTM is created using the Spline interpolation ("Interpolates a raster surface from points using a two-dimensional minimum curvature spline technique. The resulting smooth surface passes exactly through the input points."). The new DTM is then stored in the *RefinedDTM.gdb* file geodatabase and its name contains the new DTM cell size (in cm).

**New DTM Cell Size [m] (optional)** - The demanded spatial resolution of the refined DTM. The default value is 1 m. The field is active only when the *Refine DTM Cell Size?* checkbox is checked.



**Rasters Cell Size Min [m]** - The minimal value of the spatial resolution of all the raster files created during the Inverse Watershed Segmentation calculations. The cell size of those rasters has an influence on the number of identified trees. Finer cell size will result in more distinguished trees than a coarser one.

**Rasters Cell Size Max [m]** - The maximal value of the spatial resolution of all the raster files created during the Inverse Watershed Segmentation calculations. When only one particular cell size is desired for the processing, the value should be the same as the value of Raster Cell Size Min.

**Rasters Cell Size Step [m]** - The value of the spatial resolution step added to the previously used value of the raster spatial resolution after each Cell Size cycle. Is relevant only if a range of values is set in the previous two fields (*Raster Cell Size Max* is larger than *Raster Cell Size Min*).

Example: If Raster Cell Size Min is set to 0.2 m, Raster Cell Size Max is set to 0.5 m and Raster Cell Size Step is set to 0.1 m, together four Cell Size cycles will be performed with following raster spatial resolutions: 0.2, 0.3, 0.4 and 0.5 metres.

**Interpolation Methods** - Interpolation Method(s) to be used for the LAS Dataset to Raster conversion. Different interpolation methods may lead to different results concerning the number and heights of the identified trees. Following abbreviations are used in the tool outputs for particular interpolation methods:

- "BA" for BINNING with AVERAGE Cell Assignment Type,
- "BI" for BINNING with IDW Cell Assignment Type,
- "BM" for BINNING with MAXIMUM Cell Assignment Type,
- "BN" for BINNING with NEAREST Cell Assignment Type.

The Void Fill Method applied for Binning interpolations is NATURAL\_NEIGHBOR.

- "TLW" for TRIANGULATION with LINEAR Interpolation Method, WINDOW\_SIZE Point Thinning Type, MAXIMUM Point Selection Method and 1m Resolution,
- "TLN" for TRIANGULATION with LINEAR Interpolation Method and NO\_THINNING Point Thinning Type,
- "TNW" for TRIANGULATION with NATURAL\_NEIGHBOR Interpolation

Method, WINDOW\_SIZE Point Thinning Type, MAXIMUM Point Selection Method and 1m Resolution,

– “TNN” for TRIANGULATION with NATURAL\_NEIGHBOR Interpolation Method and NO\_THINNING Point Thinning Type.

One up to all eight interpolation methods can be selected.

**Focal Statistics Circle Radius Min [Cell]** - The minimal value of Circle Radius as a neighbourhood for Focal Statistics applied on the CHM. The Statistics type is MAXIMUM (“Calculates the largest value of the cells in the neighbourhood area around each cell”).

The local maxima of the CHM (the elevation values of potential tree apexes) are preserved. Using the focal statistics, the surface of the CHM is partly smoothed and the potential noise is reduced. The higher the value of circle radius, the larger smoothing and generalization effect. The accepted values for this field are integers.

**Focal Statistics Circle Radius Max [Cell]** - The maximal value of Circle Radius as a neighbourhood for Focal Statistics applied on the CHM. When only one particular Focal Statistics Circle Radius value is desired for the processing, the value should be the same as the value of *Focal Statistics Circle Radius Min*.

The value of *Focal Statistics Circle Radius Step* is by default 1 Cell. Therefore when for instance the value of Focal Statistics Circle Radius Min is set to 1 and the value of Focal Statistics Circle Radius Max is set to 5, together five Focal Statistics cycles will be performed. The outputs will then contain abbreviations from \_FS1 to \_FS5 in their names. The accepted values for this field are integers.

**Progressively Reduce Focal Statistics Subcycles? (optional)** - Gives the option to progressively reduce the number of Focal Statistics (FS) subcycles to significantly decrease the computation time. It is meaningful when large number of iterations should be calculated, but not all combinations of Cell Size (CS) values and FS Circle Radius values are desired. Especially the combinations of large Cell Sizes and large FS Circle Radiuses can be found inessential.

When this option is checked, the tool potentially reduces the value of Focal Statistics Circle Radius Max for the cycles with largest Cell Sizes. When the

particular conditions are met, the value is reduced by 1 cell after each Cell Size cycle, but the value is never reduced below 1 cell. It is ensured by the fact, that the reduction will begin only in such CS cycle, when the number of remaining CS cycles is smaller than the number of FS subcycles (number of FS subcycles is the difference between FS Circle Radius Max and FS Circle Radius Min).

The following examples should enable to better understand the effect of the reduction of FS subcycles performed when this option is chosen.

*Example1:*

Rasters Cell Size Min is set to 0.1 m, Rasters Cell Size Max is set to 0.5 m and Rasters Cell Size Step is set to 0.1 m. The number of CS cycles to be performed is therefore 5. Only one Interpolation Method is selected, FS Circle Radius Min is set to 1 and FS Circle Radius Max is set to 4. The number of FS subcycles to be performed within each Interpolation Method (IM) cycle is therefore 4. In normal case (without reduction) 1 IM cycle would be performed within each CS cycle and 4 FS subcycles would be performed within each IM cycle. That makes together 20 FS cycles to be performed during one tool run. When the option to reduce FS subcycles will be checked, the cycles will be performed as follows:

CS cycle 1: performed 1 IM cycle and 4 FS subcycles (FS1, FS2, FS3, FS4),  
CS cycle 2: performed 1 IM cycle and 4 FS subcycles (FS1, FS2, FS3, FS4),  
CS cycle 3: performed 1 IM cycle and 3 FS subcycles (FS1, FS2, FS3),  
CS cycle 4: performed 1 IM cycle and 2 FS subcycles (FS1, FS2),  
CS cycle 5: performed 1 IM cycle and 1 FS subcycle (FS1).

The number of FS cycles performed during the tool run is then 14. That means that together 6 FS cycles were avoided thanks to the reduction. Namely following combinations were not processed: CS 0.3 and FS 4; CS 0.4 and FS 3 and FS 4; CS 0.5 and FS 2, FS 3 and FS 4, where CS 0.3 is the Cell Size cycle with 0.3 m spatial resolution and FS 4 is Focal Statistics with a 4-cell circle radius used for the CHM smoothing. All other combinations were processed as usually.

*Example 2:*

Rasters Cell Size Min is set to 0.05 m, Rasters Cell Size Max is set to 1 m and Rasters Cell Size Step is set to 0.05 m. The number of CS cycles to be performed is therefore 20. All 8 interpolation methods are selected, FS Circle Radius Min is set to 1 cell and FS Circle Radius Max is set to 10 cells. The number of FS subcycles to be performed within each Interpolation Method (IM) cycle is therefore 10. In normal case (without reduction) 8 IM cycles would be performed within each CS cycle and 10 FS subcycles would be performed within each IM cycle. That makes together 1600 FS cycles to be performed during one tool run. When the option to reduce FS subcycles is checked, the cycles are performed as follows:

CS cycle 1 to CS cycle 11: performed 8 IM cycles and 10 FS subcycles (FS1 to FS10), which makes 80 processed FS cycles per each CS cycle.

CS cycle 12 to CS cycle 20: performed 8 IM cycles and 9 down to 1 FS subcycles decreasing by 1 in each CS cycle (it means cycles FS1 to FS9 in CS cycle 12; FS1 to FS8 in CS cycle 13; ... FS1 to FS5 in CS cycle 16; ... FS1 to FS2 in CS cycle 19; and only FS1 in CS cycle 20).

The number of FS cycles performed during the tool run is then 1240. That means that together 360 FS cycles were avoided thanks to the reduction. Just combinations of the largest Cell Sizes with largest FS circle radiuses were gradually avoided, since those combinations would provide the less usable results. The computation time needed for running the tool can be decreased markedly this way.

**Delimiting Sub-Area (optional)** - Optionally provided polygon feature class which defines the extent of a particular area of interest. All the calculations will be then processed only in this area. Useful to delimit e.g. just the area of the selected study plot. Most of the processed data will be copied and clipped by this feature class, if being larger. This limitation can reduce the computation time significantly. If not filled, the calculations will be processed for the whole area of the provided point cloud or DTM (the one which is smaller).

**Layer Files Folder (optional)** - The path to the folder containing sample layer files. One layer file should represent the demanded style of point feature

classes created by the tool as 'CrownTops'. Such layer file should be named '*Point\_Layer\_File.lyr*'. Another layer file should represent the demanded style of polygon feature classes created by the tool as 'Crowns'. This layer file should be named '*Polygon\_Layer\_File.lyr*'.

If provided, the tool creates additional outputs in the new 'LayerFiles' folder, which is situated in the Workspace Folder. The advantage is, that all outputs stored in the 'IdentifiedTrees.gdb' will have their equivalent layer files with demanded properties created in this folder. This facilitates visual comparisons of the results, if needed. For instance the sample layer files provided together with UAV Forest Explorer are coloured light green, to be easily visible above the background orthophoto images, and the polygons are hollow. The user then does not need to set such properties to all the feature classes. All the identified tree tops and all distinguished tree crowns, created under particular settings, can then be easily compared with other layer files, which represent feature classes resulting from different settings.

**Compare Data with Field-Measured Heights? (optional)** - Gives the option to provide field-measured positions and heights of trees and to compare the results of the tool calculations with this ground-truth data. If checked, the following field (Field Measurements Data) becomes active.

**Field Measurements Data (optional)** - Optionally provided point feature class containing the field-measured positions of trees and their heights. This ground truth data then will be used by the tool to be compared with the results of its own calculations and trees identification.

In the attribute table of this feature class a column named '*Height*' has to be present. This column should be containing the heights of trees (in metres) measured e.g. by hypsometer. The tool then compares the counts and heights of trees from both sources, i.e. calculated ones with field-measured ones.

**Delete Working Datasets? (optional)** - Gives the option to sequentially delete the Inverse Watershed Segmentation calculations working datasets. Those datasets are the most space-demanding of all the results created by the tool (for large areas or for hundreds of iterations they can reach the level of tens of gigabytes). At

the same time these datasets do not have to be necessarily preserved. This option therefore enables to not excessively occupy the hard drive space.

If checked, all the rasters and feature classes are deleted from the working geodatabase before each IM cycle is completed. Before the entire tool run is finished, also the WorkingData.gdb geodatabase is deleted completely.

## 10) Field-Measurements Data Utilization

This chapter is devoted to explanation of the tool processing principles which are applied when the ground truth data are provided by the user in the initial settings of the tool. The tool in such case performs series of mathematical and statistical calculations, which enable efficiently compare the results of automatic trees identification with the data measured in the field. The calculations are performed on the basis of two principles:

1) On the basis of the Individual Tree Approach, when the trees are paired. It means that Thiessen polygons are created around the field-measured (FM) trees and the tool is looking for the highest identified tree within each Thiessen polygon to be matched with appropriate FM tree. Also the number of trees identified in the area of Thiessen polygons is taken into consideration to provide maximally reliable results.

2) On the basis of the Area-Based Approach, when the trees are not paired. Instead the number of identified trees within the area of interest (i.e. area defined by the field-measured trees) is calculated together with the average height of those trees. Both values are then compared with corresponding data of the FM trees.

When the field measurements data are employed, the tool creates the following additional outputs:

- *Comparisons.gdb* - a file geodatabase containing:

- Point feature class ('...*Identified*') with trees identified by the tool just in the area of field measurements and with their calculated heights stored in the attribute table.

- Point feature class (*'...Joined'*) with points corresponding to the field measurement trees. The attribute table contains calculations comparing field-measured heights with calculated heights of paired trees.

- Tables (*'...ZonalStatsCounts'*, *'...ZonalStatsFull'*, *'...ZonalStatsUnpaired'*) containing summary statistics calculated for identified trees, either paired or unpaired with the field measurement data.

- Table (*'...X\_Comparisons\_X'*) encompassing the overall results of comparisons from all iterations performed by the tool under the specified Filename. Each row of the table stores data calculated for each unique combination of tool settings (each one iteration) which are written into the following 21 fields (columns) of the table:

- 1) Processed filename, unique for outputs of each combination of tool settings, the abbreviations of which it contains;
- 2) Number of field-measured trees;
- 3) Number of trees identified by the tool;
- 4) Number of unmatched (unpaired) trees, i.e. FM trees without any matching identified tree;
- 5) Number of matched (paired) trees;
- 6) Percentage of matched trees (from the amount of FM trees);
- 7) Number of redundant trees (i.e. identified trees which were not matched to any FM trees);
- 8) Mean Absolute Error (MAE) as an average of absolute value differences between measured and calculated tree heights;
- 9) Root Mean Square Error (RMSE) calculated from the differences between measured and calculated tree heights;
- 10) Pearson's Correlation Coefficient (R);
- 11) Coefficient of determination (R-squared), similarly as R also computed as a relation of measured and calculated tree heights;
- 12) Statistical significance of the Pearson's Correlation Coefficient (as 'Yes' for statistically significant R and 'No' for statistically insignificant R);
- 13) Mean Difference between average heights calculated for matched trees only;

- 14) Pearson's Correlation Coefficient calculated for matched trees only;
- 15) Coefficient of Determination calculated for matched trees only.

All these values were counted on the basis of individual tree crown approach. The last six values in the table are then calculated on the basis of the area-based approach:

- 16) Mean height of field-measured trees;
- 17) Standard Deviation of heights of field-measured trees;
- 18) Mean height of identified trees;
- 19) Standard Deviation of heights of identified trees;
- 20) Count difference between the quantities of identified and field measured trees;
- 21) Height difference between average heights of identified and field measured trees.

- *Tables* folder - folder in which the Comparisons table is automatically exported in the form of an \*.xls file. The table then serves as a well arranged dataset where all the results of all different settings applied by the tool, can be easily seen and compared. The settings giving the best results either on the ITA or ABA basis, can be then selected efficiently.

## 11) Suggested workflow

The recommended workflow could be shown on a following model example: A large forest stand is to be investigated and the field measurements were performed on a representative site(s) inside that stand. The user can delimit a subset area just around the area of field measurements and apply required amount of iterations with various settings on it. This can be done in more steps, to find the optimal settings (mainly the range of Cell Size values).

First a large range of Cell Size values can be tested with only one Interpolation Method selected and only 1 cell given for the Circle Radius of the Focal Statistics. For instance the Raster Cell Size Min can be set to 0.1 m, Raster Cell Size Max set to 2.0 m and Raster Cell Size Step set to 0.1 m, which will process 20 iterations.



From the Comparisons table the suitable range of Cell Size values giving the best results can be selected (e.g. we can see that meaningful results are given only for the resolutions below 0.6 m).

Then in second step the range of Cell Size values can be limited to maximally 0.6 m, the Rasters Cell Size Min can be decreased to 0.05 m and the same value can receive the Rasters Cell Size Step. Then all 8 Interpolation Methods can be selected and the range of Focal Statistics Circle Radiuses can be set e.g. from 1 to 10 with progressive reduction of the Focal Statistics subcycles. Such settings will cause to process 600 iterations within one tool run (360 iterations are avoided thanks to the reduction option). Processing so many iterations on the area of the whole forest stand could be unwantedly demanding on the computation time, but when processed on the subset area, the time consumption is significantly lowered.

When all the calculations are performed and the tool run is completed, the results can be evaluated. All the data outputs are stored in the Workspace Folder in the appropriate geodatabases or folders. To compare some of the results visually, the feature classes in the *IdentifiedTrees.gdb* file geodatabase can be accessed, or the corresponding layer files in the *LayerFiles* folder can be displayed, in the case that the sample layer files were provided in the initial settings.

In the next step the Comparisons table can be examined (either as a *...X\_Comparisons\_X* table in ArcMap or as an *...Comparisons.xls* table e.g. in Excel). Here two kinds of results can be sought. First of all the best result for the ITA method, i.e. calculated for the paired trees. Such result can be characterised by the high values of statistically significant Pearson's Correlation Coefficient and Coefficient of determination, low values of Mean Error, Mean Absolute Error and Root Mean Square Error. At the same time the number of identified and matched trees should be noticed. For instance only results with at least 90 % of matched trees and at the same time with maximally 10 % of redundant trees (counted from the number of field-measured trees) can be taken into consideration. Then result meeting the best all these conditions can be selected.

The second kind of results is the one calculated for ABA method, i.e. for the unpaired trees. In this case fewer values are being investigated. One value is the Counts Difference, where for example the range corresponding to 10 %

of field measured trees can be decided as convenient. Then the mean height of identified trees can be compared with the mean height of field-measured trees and the lowest height difference can be searched between the results meeting the first condition. Then also the standard deviations of the heights of identified trees can be compared with standard deviation of the heights of field-measured trees. The result with the lowest Count difference, Height Difference and possibly also the Standard Deviation can be then selected as the most suitable one for the ABA method.

When the best result is selected for each method, the settings used for acquiring those results should be highlighted. These settings can be subsequently applied on the area of the whole forest stand, if needed. This enables to calculate the counts and heights of trees very fast even for large areas, and if the forest stand is homogenous, also with high reliability.

## **12) Legal Information**

The tool was created in the scope of the Dissertation Thesis called “Design of Application for Assessing the Height of Trees in Forest Stands Based on Images from an Unmanned Aerial Vehicle” which was produced within the Applied Geoinformatics doctoral study program at the Department of Forest Management and Applied Geoinformatics at Mendel University in Brno, Czech Republic.

Author: Ing. Martin Machala

Supervisor: doc. Ing. Martin Klimánek, Ph.D.

This version of the tool is for non-commercial use only.

Not to be distributed without the awareness of the author.

Support: [xmachala@mendelu.cz](mailto:xmachala@mendelu.cz)

© Martin Machala 2014 - 2016

## Appendix 4 – Best Results of UAV Forest Explorer Runs

Plot I.		Best Parameter	CS	IM	FS	Mea- sured	Identi- fied	Un- matched	Matched	Matched %	Redun- dant	MAE	RMSE	R	R <sup>2</sup>	Stat Sig R	Mean Diff (MT)	R (MT)	R <sup>2</sup> (MT)	Mean FM Ht	SD FM Ht	Mean IT Ht	SD IT Ht	Count Diff	Height Diff
All Field-Measured (FM) Trees	Individual Tree App. Smaller Range	RMSE & R	20	TNN	2	93	93	24	69	74.19	24	7.819	<b>10.194</b>	<b>0.117</b>	0.014	No	-4.541	0.134	0.018	17.022	4.586	21.666	1.184	0	4.644
		RMSE	20	TNN	2	93	93	24	69	74.19	24	7.819	<b>10.194</b>	0.117	0.014	No	-4.541	0.134	0.018	17.022	4.586	21.666	1.184	0	4.644
		R	20	TNN	2	93	93	24	69	74.19	24	7.819	10.194	<b>0.117</b>	0.014	No	-4.541	0.134	0.018	17.022	4.586	21.666	1.184	0	4.644
		R for MT	30	TNW	1	93	91	28	65	69.89	26	8.583	10.995	0.053	0.003	No	-4.734	<b>0.165</b>	0.027	17.022	4.586	21.715	1.218	-2	4.693
	Larger Range	RMSE	5	BI	9	93	102	19	74	79.57	28	7.181	<b>9.489</b>	0.125	0.016	No	-4.601	0.121	0.015	17.022	4.586	21.763	1.182	9	4.741
		R	5	BA	10	93	83	28	65	69.89	18	8.338	10.707	<b>0.131</b>	0.017	No	-4.643	0.128	0.016	17.022	4.586	21.890	1.216	-10	4.869
		R for MT	35	BI	1	93	68	35	58	62.37	10	10.221	12.616	-0.139	0.019	No	-5.404	<b>0.275</b>	0.076	17.022	4.586	21.813	1.199	-25	4.791
	Area-Based Approach	Count Diff (0)	20	TNN	2	93	93	24	69	74.19	24	7.819	10.194	0.117	0.014	No	-4.541	0.134	0.018	17.022	4.586	21.666	1.184	0	<b>4.644</b>
		Count Diff (±1)	30	TNN	1	93	94	26	67	72.04	27	8.034	10.494	0.105	0.011	No	-4.496	0.097	0.009	17.022	4.586	21.641	1.212	1	<b>4.620</b>
		Height Diff	5	TNN	1	93	1684	0	93	100.00	1591	5.181	6.706	0.145	0.021	No	-4.913	0.145	0.021	17.022	4.586	20.326	1.506	1591	<b>3.305</b>
		SD IT Ht	20	TLN	2	93	92	25	68	73.12	24	7.963	10.343	0.113	0.013	No	-4.548	0.163	0.027	17.022	4.586	21.678	<b>1.179</b>	-1	4.657

Plot I.		Best Parameter	CS	IM	FS	Mea- sured	Identi- fied	Un- matched	Matched	Matched %	Redun- dant	MAE	RMSE	R	R <sup>2</sup>	Stat Sig R	Mean Diff (MT)	R (MT)	R <sup>2</sup> (MT)	Mean FM Ht	SD FM Ht	Mean IT Ht	SD IT Ht	Count Diff	Height Diff
Reduced Number of FM Trees	Individual Tree App. Smaller Range	RMSE & R	40	BI	1	68	64	17	51	75.00	13	6.907	<b>10.194</b>	<b>0.059</b>	0.003	No	-2.359	0.193	0.037	19.368	2.759	21.732	1.188	-4	2.364
		RMSE	40	BI	1	68	64	17	51	75.00	13	6.907	<b>10.194</b>	0.059	0.003	No	-2.359	0.193	0.037	19.368	2.759	21.732	1.188	-4	2.364
		R	40	BI	1	68	64	17	51	75.00	13	6.907	10.194	<b>0.059</b>	0.003	No	-2.359	0.193	0.037	19.368	2.759	21.732	1.188	-4	2.364
		R for MT	35	BA	1	68	66	18	50	73.53	16	7.477	10.917	-0.121	0.015	No	-2.801	<b>0.422</b>	0.178	19.368	2.759	21.756	1.160	-2	2.388
	Larger Range	RMSE	5	BN	9	68	101	9	59	86.76	42	5.191	<b>7.939</b>	0.040	0.002	No	-2.652	0.244	0.060	19.368	2.759	21.800	1.185	33	2.433
		R	55	TLW	1	68	47	30	38	55.88	9	9.953	12.962	<b>0.172</b>	0.030	No	-2.529	0.201	0.040	19.368	2.759	22.120	1.128	-21	2.753
		R for MT	15	BI	4	68	60	22	46	67.65	14	8.536	11.815	-0.076	0.006	No	-3.024	<b>0.458</b>	0.210	19.368	2.759	22.031	1.127	-8	2.664
	Area-Based Approach	Count Diff (0)	35	BI	1	68	68	17	51	75.00	17	7.178	10.591	-0.093	0.009	No	-2.752	0.404	0.163	19.368	2.759	21.813	1.199	0	<b>2.445</b>
		Count Diff (±1)	35	BI	1	68	68	17	51	75.00	17	7.178	10.591	-0.093	0.009	No	-2.752	0.404	0.163	19.368	2.759	21.813	1.199	0	<b>2.445</b>
		Height Diff	5	TNN	1	68	1678	0	68	100.00	1610	3.082	3.884	0.237	0.056	No	-2.782	0.237	0.056	19.368	2.759	20.326	1.507	1610	<b>0.958</b>
SD IT Ht		25	TNW	2	68	68	18	50	73.53	18	7.442	10.630	0.008	0.000	No	-2.782	0.277	0.077	19.368	2.759	21.920	<b>1.109</b>	0	2.553	

Plot II.		Best Parameter	CS	IM	FS	Mea- sured	Identi- fied	Un- matched	Matched	Matched %	Redun- dant	MAE	RMSE	R	R <sup>2</sup>	Stat Sig R	Mean Diff (MT)	R (MT)	R <sup>2</sup> (MT)	Mean FM Ht	SD FM Ht	Mean IT Ht	SD IT Ht	Count Diff	Height Diff
All Field-Measured (FM) Trees	Individual Tree App. Smaller Range	RMSE & R	25	BM	1	98	99	32	66	67.35	33	7.548	<b>9.883</b>	<b>0.414</b>	0.172	Yes	-4.017	0.496	0.246	17.061	5.281	22.226	1.508	1	5.165
		RMSE	25	BM	1	98	99	32	66	67.35	33	7.548	<b>9.883</b>	0.414	0.172	Yes	-4.017	0.496	0.246	17.061	5.281	22.226	1.508	1	5.165
		R	25	BM	1	98	99	32	66	67.35	33	7.548	9.883	<b>0.414</b>	0.172	Yes	-4.017	0.496	0.246	17.061	5.281	22.226	1.508	1	5.165
		R for MT	10	TLN	4	98	94	34	64	65.31	30	7.945	10.313	0.377	0.142	Yes	-4.102	<b>0.551</b>	0.303	17.061	5.281	22.131	1.518	-4	5.070
	Larger Range	RMSE	25	TLW	1	98	105	30	68	69.39	37	7.467	<b>9.806</b>	0.383	0.147	Yes	-4.153	0.536	0.287	17.061	5.281	22.101	1.464	7	5.040
		R	30	BM	1	98	78	40	58	59.18	20	7.881	10.258	<b>0.516</b>	0.266	Yes	-3.340	0.487	0.237	17.061	5.281	22.365	1.505	-20	5.304
		R for MT	25	BA	1	98	107	33	65	66.33	42	7.672	9.983	0.405	0.164	Yes	-3.805	<b>0.587</b>	0.345	17.061	5.281	21.799	1.526	9	4.737
	Area-Based Approach	Count Diff (0)	10	BN	4	98	99	32	66	67.35	33	7.788	10.171	0.359	0.129	Yes	-4.140	0.504	0.254	17.061	5.281	22.152	1.548	1	<b>5.091</b>
		Count Diff (±1)	10	BN	4	98	99	32	66	67.35	33	7.788	10.171	0.359	0.129	Yes	-4.140	0.504	0.254	17.061	5.281	22.152	1.548	1	<b>5.091</b>
		Height Diff	5	BM	1	98	1181	2	96	97.96	1085	5.564	7.318	0.269	0.072	Yes	-5.227	0.440	0.194	17.061	5.281	20.542	2.143	1083	<b>3.480</b>
		SD IT Ht	25	BM	1	98	99	32	66	67.35	33	7.548	9.883	0.414	0.172	Yes	-4.017	0.496	0.246	17.061	5.281	22.226	<b>1.508</b>	1	5.165

Plot II.		Best Parameter	CS	IM	FS	Mea- sured	Identi- fied	Un- matched	Matched	Matched %	Redun- dant	MAE	RMSE	R	R <sup>2</sup>	Stat Sig R	Mean Diff (MT)	R (MT)	R <sup>2</sup> (MT)	Mean FM Ht	SD FM Ht	Mean IT Ht	SD IT Ht	Count Diff	Height Diff
Reduced Number of FM Trees	Individual Tree App- Smaller Range	RMSE & R	10	BA	5	57	58	13	44	77.19	14	4.903	8.363	0.733	0.537	Yes	-0.879	0.582	0.339	20.860	3.075	22.631	1.499	1	1.771
		RMSE	15	BN	4	57	54	11	46	80.70	8	4.540	<b>7.858</b>	0.656	0.431	Yes	-1.136	0.546	0.298	20.860	3.075	22.710	1.527	-3	1.850
		R	35	BM	1	57	52	15	42	73.68	10	5.364	8.905	<b>0.792</b>	0.627	Yes	-0.778	0.595	0.354	20.860	3.075	22.809	1.473	-5	1.949
		R for MT	35	BM	1	57	52	15	42	73.68	10	5.364	8.905	0.792	0.627	Yes	-0.778	<b>0.595</b>	0.354	20.860	3.075	22.809	1.473	-5	1.949
	Larger Range	RMSE	15	BA	2	57	111	5	52	91.23	59	2.963	<b>5.500</b>	0.556	0.310	Yes	-1.278	0.641	0.411	20.860	3.075	21.790	1.865	54	0.930
		R	10	BM	7	57	45	16	41	71.93	4	5.648	9.246	<b>0.798</b>	0.636	Yes	-0.727	0.587	0.344	20.860	3.075	22.998	1.483	-12	2.138
		R for MT	5	TNN	7	57	106	7	50	87.72	56	3.419	6.330	0.604	0.364	Yes	-1.188	<b>0.679</b>	0.461	20.860	3.075	21.962	1.681	49	1.103
	Area-Based Approach	Count Diff (0)	25	BA	2	57	57	14	43	75.44	14	5.416	8.992	0.655	0.429	Yes	-0.859	0.529	0.279	20.860	3.075	22.460	1.486	0	<b>1.600</b>
		Count Diff (±1)	35	BA	1	57	58	13	44	77.19	14	5.197	8.759	0.613	0.375	Yes	-0.862	0.542	0.294	20.860	3.075	22.358	1.492	1	<b>1.498</b>
		Height Diff	10	BA	1	57	500	2	55	96.49	445	2.541	4.302	0.421	0.177	Yes	-1.721	0.649	0.421	20.860	3.075	20.877	1.990	443	<b>0.018</b>
		SD IT Ht	35	TNW	1	57	57	14	43	75.44	14	5.396	8.930	0.677	0.458	Yes	-1.014	0.506	0.256	20.860	3.075	22.632	<b>1.463</b>	0	1.773

Plot III.		Best Parameter	CS	IM	FS	Mea- sured	Identi- fied	Un- matched	Matched	Matched %	Redun- dant	MAE	RMSE	R	R <sup>2</sup>	Stat Sig R	Mean Diff (MT)	R (MT)	R <sup>2</sup> (MT)	Mean FM Ht	SD FM Ht	Mean IT Ht	SD IT Ht	Count Diff	Height Diff
All Field-Measured (FM) Trees	Individual Tree App- Smaller Range	RMSE & R	25	BI	2	64	66	23	41	64.06	25	9.153	<b>11.846</b>	0.252	0.063	No	-3.216	0.042	0.002	18.766	5.556	22.885	1.806	2	4.119
		RMSE	25	BI	2	64	66	23	41	64.06	25	9.153	<b>11.846</b>	0.252	0.063	No	-3.216	0.042	0.002	18.766	5.556	22.885	1.806	2	4.119
		R	10	TLN	6	64	61	26	38	59.38	23	9.852	12.454	<b>0.259</b>	0.067	No	-3.241	-0.071	0.005	18.766	5.556	23.358	1.669	-3	4.592
		R for MT	15	BN	4	64	63	27	37	57.81	26	10.405	13.045	0.181	0.033	No	-3.784	<b>0.082</b>	0.007	18.766	5.556	23.438	1.522	-1	4.673
	Larger Range	RMSE	25	BA	2	64	70	21	43	67.19	27	8.971	<b>11.565</b>	0.219	0.048	No	-3.083	0.086	0.007	18.766	5.556	22.704	2.021	6	3.938
		R	10	BA	7	64	48	30	34	53.13	14	10.228	12.900	<b>0.326</b>	0.106	No	-2.912	-0.059	0.003	18.766	5.556	23.522	1.496	-16	4.756
		R for MT	15	BA	4	64	56	28	36	56.25	20	11.402	14.061	0.004	0.000	No	-4.561	<b>0.144</b>	0.021	18.766	5.556	23.341	1.538	-8	4.575
	Area-Based Approach	Count Diff (0)	35	BM	1	64	64	25	39	60.94	25	10.009	12.709	0.171	0.029	No	-3.617	-0.052	0.003	18.766	5.556	23.246	1.900	0	<b>4.480</b>
		Count Diff (±1)	40	TNW	1	64	64	21	43	67.19	21	9.733	12.461	0.055	0.003	No	-4.153	0.006	0.000	18.766	5.556	23.268	1.703	0	<b>4.502</b>
		Height Diff	5	BN	1	64	1545	0	64	100.00	1481	5.684	7.367	0.052	0.003	No	-4.545	0.052	0.003	18.766	5.556	21.167	3.061	1481	<b>2.402</b>
		SD IT Ht	10	TNW	6	64	64	28	36	56.25	28	10.752	13.456	0.139	0.019	No	-4.036	0.017	0.000	18.766	5.556	23.551	<b>1.387</b>	0	4.785

Plot III.		Best Parameter	CS	IM	FS	Mea- sured	Identi- fied	Un- matched	Matched	Matched %	Redun- dant	MAE	RMSE	R	R <sup>2</sup>	Stat Sig R	Mean Diff (MT)	R (MT)	R <sup>2</sup> (MT)	Mean FM Ht	SD FM Ht	Mean IT Ht	SD IT Ht	Count Diff	Height Diff
Reduced Number of FM Trees	Individual Tree App- Smaller Range	RMSE & R	45	BN	1	43	46	12	31	72.09	15	7.881	11.474	<b>0.253</b>	0.064	No	-0.973	0.068	0.005	21.930	3.187	23.354	1.848	3	1.424
		RMSE	20	BM	3	43	48	10	33	76.74	15	7.315	<b>10.615</b>	0.228	0.052	No	-0.951	0.012	0.000	21.930	3.187	23.324	1.907	5	1.394
		R	45	BN	1	43	46	12	31	72.09	15	7.881	11.474	<b>0.253</b>	0.064	No	-0.973	0.068	0.005	21.930	3.187	23.354	1.848	3	1.424
		R for MT	20	BA	3	43	48	13	30	69.77	18	8.838	12.665	-0.014	0.000	No	-1.630	<b>0.130</b>	0.017	21.930	3.187	23.499	1.536	5	1.569
	Larger Range	RMSE	15	BM	4	43	60	9	34	79.07	26	6.876	<b>10.125</b>	0.220	0.048	No	-0.986	0.013	0.000	21.930	3.187	23.388	1.743	17	1.458
		R	40	BN	1	43	58	10	33	76.74	25	7.148	10.453	<b>0.271</b>	0.074	No	-0.765	-0.034	0.001	21.930	3.187	23.212	1.858	15	1.282
		R for MT	55	BN	1	43	32	15	28	65.12	4	9.593	13.452	0.007	0.000	No	-1.767	<b>0.243</b>	0.059	21.930	3.187	23.637	1.457	-11	1.706
	Area-Based Approach	Count Diff (0)	45	BM	1	43	43	11	32	74.42	11	7.704	11.085	0.226	0.051	No	-1.086	0.050	0.003	21.930	3.187	23.474	1.737	0	<b>1.544</b>
		Count Diff (±1)	45	BI	1	43	42	14	29	67.44	13	9.192	12.961	0.028	0.001	No	-1.206	0.100	0.010	21.930	3.187	23.036	1.852	-1	<b>1.106</b>
		Height Diff	10	BN	1	43	415	1	42	97.67	373	3.471	4.981	0.072	0.005	No	-1.654	0.076	0.006	21.930	3.187	21.971	2.825	372	<b>0.041</b>
		SD IT Ht	10	TLN	7	43	44	12	31	72.09	13	8.168	11.747	0.154	0.024	No	-1.373	0.055	0.003	21.930	3.187	23.649	<b>1.475</b>	1	1.719

Plot IV.		Best Parameter	CS	IM	FS	Mea- sured	Identi- fied	Un- matched	Matched	Matched %	Redun- dant	MAE	RMSE	R	R <sup>2</sup>	Stat Sig R	Mean Diff (MT)	R (MT)	R <sup>2</sup> (MT)	Mean FM Ht	SD FM Ht	Mean IT Ht	SD IT Ht	Count Diff	Height Diff	
All Field-Measured (FM) Trees	Individual Tree App.	Smaller Range	RMSE & R	10	BI	5	64	67	19	45	70.31	22	7.046	<b>10.302</b>	<b>0.543</b>	0.295	Yes	-1.869	0.561	0.315	20.938	5.841	24.160	2.432	3	3.222
			RMSE	10	BA	5	64	67	19	45	70.31	22	7.047	<b>10.302</b>	0.543	0.295	Yes	-1.870	0.561	0.315	20.938	5.841	24.160	2.431	3	3.222
		R	10	BA	5	64	67	19	45	70.31	22	7.047	10.302	<b>0.543</b>	0.295	Yes	-1.870	0.561	0.315	20.938	5.841	24.160	2.431	3	3.222	
		R for MT	10	TNN	5	64	69	20	44	68.75	25	7.305	10.770	0.513	0.263	Yes	-2.005	<b>0.652</b>	0.425	20.938	5.841	24.096	2.436	5	3.159	
	Larger Range	RMSE	10	BA	5	64	67	19	45	70.31	22	7.047	<b>10.302</b>	0.543	0.295	Yes	-1.870	0.561	0.315	20.938	5.841	24.160	2.431	3	3.222	
		R	20	TNN	3	64	45	27	37	57.81	8	8.767	12.309	<b>0.555</b>	0.308	Yes	-1.353	0.557	0.310	20.938	5.841	24.569	2.605	-19	3.632	
	Area-Based Approach	R for MT	10	TNN	6	64	45	27	37	57.81	8	9.059	12.760	0.479	0.229	Yes	-1.804	<b>0.658</b>	0.434	20.938	5.841	24.549	2.731	-19	3.611	
		Count Diff (0)	40	BN	1	64	64	20	44	68.75	20	8.010	11.390	0.410	0.168	Yes	-2.292	0.449	0.202	20.938	5.841	24.291	2.556	0	<b>3.353</b>	
		Count Diff (±1)	40	BN	1	64	64	20	44	68.75	20	8.010	11.390	0.410	0.168	Yes	-2.292	0.449	0.202	20.938	5.841	24.291	2.556	0	<b>3.353</b>	
		Height Diff	5	BM	1	64	1629	0	64	100.00	1565	4.888	6.908	0.396	0.156	Yes	-4.344	0.396	0.156	20.938	5.841	21.986	3.143	1565	<b>1.049</b>	
		SD IT Ht	40	BN	1	64	64	20	44	68.75	20	8.010	11.390	0.410	0.168	Yes	-2.292	0.449	0.202	20.938	5.841	24.291	<b>2.556</b>	0	3.353	

Plot IV.		Best Parameter	CS	IM	FS	Mea- sured	Identi- fied	Un- matched	Matched	Matched %	Redun- dant	MAE	RMSE	R	R <sup>2</sup>	Stat Sig R	Mean Diff (MT)	R (MT)	R <sup>2</sup> (MT)	Mean FM Ht	SD FM Ht	Mean IT Ht	SD IT Ht	Count Diff	Height Diff	
Reduced Number of FM Trees	Individual Tree App.	Smaller Range	RMSE & R	55	TNN	1	40	35	11	29	72.50	6	7.332	12.207	0.462	0.214	Yes	-0.064	0.827	0.683	24.600	3.025	24.917	2.633	-5	0.317
			RMSE	50	BA	1	40	39	9	31	77.50	8	6.201	<b>11.161</b>	0.401	0.161	Yes	0.107	0.854	0.730	24.600	3.025	24.360	2.606	-1	-0.240
		R	30	TNW	2	40	35	12	28	70.00	7	8.040	12.744	<b>0.478</b>	0.228	Yes	-0.187	0.711	0.505	24.600	3.025	25.166	2.668	-5	0.566	
		R for MT	45	TNW	1	40	37	12	28	70.00	9	8.197	13.338	0.255	0.065	No	-0.672	<b>0.877</b>	0.769	24.600	3.025	25.141	2.477	-3	0.541	
	Larger Range	RMSE	20	TLW	2	40	76	2	38	95.00	38	2.824	<b>5.703</b>	0.393	0.155	Yes	-0.251	0.715	0.512	24.600	3.025	24.111	2.456	36	-0.489	
		R	30	TNW	2	40	35	12	28	70.00	7	8.040	12.744	<b>0.478</b>	0.228	Yes	-0.187	0.711	0.505	24.600	3.025	25.166	2.668	-5	0.566	
	Area-Based Approach	R for MT	40	TLN	2	40	28	15	25	62.50	3	9.770	14.954	0.236	0.056	No	-0.659	<b>0.920</b>	0.846	24.600	3.025	25.187	2.841	-12	0.587	
		Count Diff (0)	45	TNN	1	40	40	11	29	72.50	11	7.631	12.534	0.356	0.126	No	-0.150	0.684	0.468	24.600	3.025	24.572	2.747	0	<b>-0.028</b>	
		Count Diff (±1)	20	TLN	3	40	40	10	30	75.00	10	7.110	12.063	0.315	0.099	No	-0.322	0.743	0.552	24.600	3.025	24.807	2.649	0	<b>0.207</b>	
		Height Diff	30	BI	2	40	41	8	32	80.00	9	5.781	10.717	0.342	0.117	No	-0.141	0.852	0.725	24.600	3.025	24.582	2.583	1	<b>-0.018</b>	
SD IT Ht	45	TLN	1	40	39	13	27	67.50	12	8.645	13.743	0.302	0.092	No	-0.586	0.867	0.751	24.600	3.025	24.871	<b>2.487</b>	-1	0.271			

Plot V.		Best Parameter	CS	IM	FS	Mea- sured	Identi- fied	Un- matched	Matched	Matched %	Redun- dant	MAE	RMSE	R	R <sup>2</sup>	Stat Sig R	Mean Diff (MT)	R (MT)	R <sup>2</sup> (MT)	Mean FM Ht	SD FM Ht	Mean IT Ht	SD IT Ht	Count Diff	Height Diff	
All Field-Measured (FM) Trees	Individual Tree App.	Smaller Range	RMSE & R	15	BA	3	72	73	25	47	65.28	26	7.027	9.807	<b>0.519</b>	0.269	Yes	-2.817	0.349	0.122	17.931	5.360	22.647	1.503	1	4.716
			RMSE	10	BA	5	72	72	23	49	68.06	23	7.029	<b>9.741</b>	0.475	0.226	Yes	-3.267	0.327	0.107	17.931	5.360	22.743	1.477	0	4.812
		R	15	BA	3	72	73	25	47	65.28	26	7.027	9.807	<b>0.519</b>	0.269	Yes	-2.817	0.349	0.122	17.931	5.360	22.647	1.503	1	4.716	
		R for MT	20	BA	2	72	77	23	49	68.06	28	7.880	10.730	0.287	0.083	Yes	-3.757	<b>0.422</b>	0.178	17.931	5.360	22.532	1.475	5	4.601	
	Larger Range	RMSE	10	BA	5	72	72	23	49	68.06	23	7.029	<b>9.741</b>	0.475	0.226	Yes	-3.267	0.327	0.107	17.931	5.360	22.743	1.477	0	4.812	
		R	20	TNW	3	72	50	32	40	55.56	10	8.133	10.883	<b>0.559</b>	0.312	Yes	-2.563	0.388	0.151	17.931	5.360	22.957	1.355	-22	5.026	
	Area-Based Approach	R for MT	40	BI	1	72	50	34	38	52.78	12	8.671	11.577	0.489	0.239	Yes	-2.372	<b>0.521</b>	0.271	17.931	5.360	22.546	1.522	-22	4.615	
		Count Diff (0)	10	BA	5	72	72	23	49	68.06	23	7.029	9.741	0.475	0.226	Yes	-3.267	0.327	0.107	17.931	5.360	22.743	1.477	0	<b>4.812</b>	
		Count Diff (±1)	15	BA	3	72	73	25	47	65.28	26	7.027	9.807	0.519	0.269	Yes	-2.817	0.349	0.122	17.931	5.360	22.647	1.503	1	<b>4.716</b>	
		Height Diff	5	BN	1	72	1560	1	71	98.61	1489	5.335	7.376	0.133	0.018	No	-4.914	0.373	0.139	17.931	5.360	21.164	2.241	1488	<b>3.234</b>	
SD IT Ht	10	TLN	5	72	73	25	47	65.28	26	7.598	10.354	0.435	0.189	Yes	-3.425	0.287	0.082	17.931	5.360	22.928	<b>1.388</b>	1	4.997			

Plot V.		Best Parameter	CS	IM	FS	Mea- sured	Identi- fied	Un- matched	Matched	Matched %	Redun- dant	MAE	RMSE	R	R <sup>2</sup>	Stat Sig R	Mean Diff (MT)	R (MT)	R <sup>2</sup> (MT)	Mean FM Ht	SD FM Ht	Mean IT Ht	SD IT Ht	Count Diff	Height Diff	
Reduced Number of FM Trees	Individual Tree App.	Smaller Range	RMSE & R	15	TNN	4	53	53	17	36	67.92	17	7.379	10.997	0.466	0.217	Yes	-1.557	0.369	0.136	20.632	2.867	23.013	1.224	0	2.381
			RMSE	40	TLN	1	53	57	14	39	73.58	18	6.428	<b>10.013</b>	0.445	0.198	Yes	-1.661	0.399	0.159	20.632	2.867	22.749	1.422	4	2.117
			R	20	TNW	3	53	48	17	36	67.92	12	7.318	10.909	<b>0.505</b>	0.255	Yes	-1.672	0.329	0.108	20.632	2.867	22.989	1.374	-5	2.357
		R for MT	25	BA	2	53	48	21	32	60.38	16	8.721	12.398	0.428	0.183	Yes	-1.407	<b>0.487</b>	0.237	20.632	2.867	22.810	1.345	-5	2.178	
		Larger Range	RMSE	10	TNW	5	53	77	9	44	83.02	33	5.176	<b>8.425</b>	0.327	0.107	Yes	-2.019	0.363	0.132	20.632	2.867	22.901	1.512	24	2.269
			R	20	BA	3	53	43	19	34	64.15	9	7.871	11.536	<b>0.511</b>	0.261	Yes	-1.323	0.369	0.136	20.632	2.867	22.818	1.325	-10	2.186
	R for MT		40	BI	1	53	47	18	35	66.04	12	7.800	11.535	0.391	0.153	Yes	-1.410	<b>0.500</b>	0.250	20.632	2.867	22.594	1.557	-6	1.962	
	Area-Based Approach	Count Diff (0)	15	TNN	4	53	53	17	36	67.92	17	7.379	10.997	0.466	0.217	Yes	-1.557	0.369	0.136	20.632	2.867	23.013	1.224	0	<b>2.381</b>	
		Count Diff (±1)	20	TLN	3	53	54	17	36	67.92	18	7.487	11.135	0.422	0.178	Yes	-1.738	0.319	0.102	20.632	2.867	22.985	1.313	1	<b>2.353</b>	
		Height Diff	5	BN	1	53	1514	0	53	100.00	1461	2.677	3.732	0.294	0.086	Yes	-2.485	0.294	0.086	20.632	2.867	21.169	2.265	1461	<b>0.537</b>	
		SD IT Ht	15	TNN	4	53	53	17	36	67.92	17	7.379	10.997	0.466	0.217	Yes	-1.557	0.369	0.136	20.632	2.867	23.013	<b>1.224</b>	0	2.381	

Plot VI.		Best Parameter	CS	IM	FS	Mea- sured	Identi- fied	Un- matched	Matched	Matched %	Redun- dant	MAE	RMSE	R	R <sup>2</sup>	Stat Sig R	Mean Diff (MT)	R (MT)	R <sup>2</sup> (MT)	Mean FM Ht	SD FM Ht	Mean IT Ht	SD IT Ht	Count Diff	Height Diff	
All Field-Measured (FM) Trees	Individual Tree App.	Smaller Range	RMSE & R	10	TNW	3	79	77	22	57	72.15	20	10.675	14.349	0.104	0.011	No	-4.734	0.420	0.177	24.323	5.960	28.866	2.632	-2	4.543
			RMSE	10	TLW	3	79	83	19	60	75.95	23	10.125	<b>13.734</b>	0.081	0.007	No	-4.849	0.401	0.161	24.323	5.960	28.822	2.585	4	4.499
			R	20	TNW	1	79	84	24	55	69.62	29	10.874	14.557	<b>0.150</b>	0.023	No	-4.461	0.376	0.141	24.323	5.960	28.759	2.520	5	4.436
		R for MT	5	BA	8	79	75	26	53	67.09	22	11.417	15.076	0.147	0.022	No	-4.868	<b>0.572</b>	0.327	24.323	5.960	29.035	2.390	-4	4.713	
		Larger Range	RMSE	30	TNN	1	79	64	26	53	67.09	11	10.577	<b>14.276</b>	0.278	0.077	Yes	-3.982	0.569	0.324	24.323	5.960	28.893	2.266	-15	4.570
			R	15	TNN	3	79	58	30	49	62.03	9	11.243	14.876	<b>0.340</b>	0.115	Yes	-3.794	0.537	0.288	24.323	5.960	29.091	2.275	-21	4.768
	R for MT		35	BA	1	79	59	29	50	63.29	9	11.523	15.243	0.228	0.052	No	-4.164	<b>0.643</b>	0.414	24.323	5.960	28.951	2.177	-20	4.628	
	Area-Based Approach	Count Diff (0)	10	TNW	3	79	77	22	57	72.15	20	10.675	14.349	0.104	0.011	No	-4.734	0.420	0.177	24.323	5.960	28.866	2.632	-2	<b>4.543</b>	
		Count Diff (±1)	10	TLW	3	79	83	19	60	75.95	23	10.125	13.734	0.081	0.007	No	-4.849	0.401	0.161	24.323	5.960	28.822	2.585	4	<b>4.499</b>	
		Height Diff	5	BM	1	79	1880	0	79	100.00	1801	6.041	7.936	0.219	0.048	No	-5.353	0.219	0.048	24.323	5.960	26.915	2.572	1801	<b>2.592</b>	
		SD IT Ht	10	TNW	3	79	77	22	57	72.15	20	10.675	14.349	0.104	0.011	No	-4.734	0.420	0.177	24.323	5.960	28.866	<b>2.632</b>	-2	4.543	

Plot VI.		Best Parameter	CS	IM	FS	Mea- sured	Identi- fied	Un- matched	Matched	Matched %	Redun- dant	MAE	RMSE	R	R <sup>2</sup>	Stat Sig R	Mean Diff (MT)	R (MT)	R <sup>2</sup> (MT)	Mean FM Ht	SD FM Ht	Mean IT Ht	SD IT Ht	Count Diff	Height Diff	
Reduced Number of FM Trees	Individual Tree App.	Smaller Range	RMSE & R	15	BI	5	40	37	8	32	80.00	5	6.837	12.782	0.394	0.155	Yes	-0.269	0.598	0.358	29.688	2.176	30.100	1.928	-3	0.412
			RMSE	15	TLN	4	40	43	6	34	85.00	9	5.481	<b>11.107</b>	0.359	0.129	Yes	-0.332	0.626	0.392	29.688	2.176	29.795	2.073	3	0.108
			R	20	TNN	4	40	35	9	31	77.50	4	7.423	13.464	<b>0.448</b>	0.201	Yes	-0.231	0.618	0.382	29.688	2.176	30.165	1.944	-5	0.478
		R for MT	30	BN	2	40	36	8	32	80.00	4	6.723	12.814	0.383	0.147	Yes	-0.198	<b>0.703</b>	0.494	29.688	2.176	30.029	2.051	-4	0.342	
		Larger Range	RMSE	5	TNN	7	40	79	0	40	100.00	39	1.636	<b>2.053</b>	0.552	0.304	Yes	-0.303	0.552	0.304	29.688	2.176	28.577	2.716	39	-1.111
			R	5	TLN	7	40	84	0	40	100.00	44	1.668	2.106	<b>0.559</b>	0.312	Yes	-0.220	0.559	0.312	29.688	2.176	28.622	2.818	44	-1.066
	R for MT		30	BN	2	40	36	8	32	80.00	4	6.723	12.814	0.383	0.147	Yes	-0.198	<b>0.703</b>	0.494	29.688	2.176	30.029	2.051	-4	0.342	
	Area-Based Approach	Count Diff (0)	30	BA	2	40	40	6	34	85.00	6	5.491	11.141	0.343	0.118	No	-0.108	0.612	0.374	29.688	2.176	29.663	2.093	0	<b>-0.025</b>	
		Count Diff (±1)	35	BA	2	40	40	7	33	82.50	7	6.228	12.114	0.310	0.096	No	-0.100	0.586	0.343	29.688	2.176	29.651	2.049	0	<b>-0.036</b>	
		Height Diff	35	BI	2	40	39	7	33	82.50	6	6.191	12.110	0.318	0.101	No	-0.038	0.619	0.383	29.688	2.176	29.682	2.075	-1	<b>-0.005</b>	
		SD IT Ht	45	TNN	1	40	41	6	34	85.00	7	5.434	11.128	0.348	0.121	Yes	-0.145	0.650	0.423	29.688	2.176	29.737	<b>1.982</b>	1	0.049	

Plot VII.		Best Parameter	CS	IM	FS	Mea- sured	Identi- fied	Un- matched	Matched	Matched %	Redun- dant	MAE	RMSE	R	R <sup>2</sup>	Stat Sig R	Mean Diff (MT)	R (MT)	R <sup>2</sup> (MT)	Mean FM Ht	SD FM Ht	Mean IT Ht	SD IT Ht	Count Diff	Height Diff		
All Field-Measured (FM) Trees	Individual Tree App- Smaller Range	RMSE & R	25	BA	4	60	62	11	49	81.67	13	5.697	11.564	<b>0.657</b>	0.431	Yes	0.172	0.448	0.200	29.925	2.398	30.300	1.024	2	0.375		
		RMSE	25	BI	4	60	63	10	50	83.33	13	5.335	<b>11.061</b>	0.617	0.380	Yes	0.081	0.399	0.159	29.925	2.398	30.307	1.042	3	0.382		
		R	25	BA	4	60	62	11	49	81.67	13	5.697	11.564	<b>0.657</b>	0.431	Yes	0.172	0.448	0.200	29.925	2.398	30.300	1.024	2	0.375		
		R for MT	80	BN	1	60	63	14	46	76.67	17	7.424	13.784	0.418	0.175	Yes	-0.089	<b>0.527</b>	0.278	29.925	2.398	30.355	1.232	3	0.430		
		RMSE	25	BI	4	60	63	10	50	83.33	13	5.335	<b>11.061</b>	0.617	0.380	Yes	0.081	0.399	0.159	29.925	2.398	30.307	1.042	3	0.382		
		R	25	BA	4	60	62	11	49	81.67	13	5.697	11.564	<b>0.657</b>	0.431	Yes	0.172	0.448	0.200	29.925	2.398	30.300	1.024	2	0.375		
	Area-Based Approach	Larger Range	R for MT	75	BI	1	60	54	17	43	71.67	11	8.931	15.338	0.386	0.149	Yes	0.412	<b>0.598</b>	0.358	29.925	2.398	29.821	1.167	-6	-0.104	
			Count Diff (0)	45	BA	2	60	60	15	45	75.00	15	8.122	14.452	0.345	0.119	Yes	0.174	0.218	0.048	29.925	2.398	29.990	1.144	0	<b>0.065</b>	
			Count Diff (±1)	70	BA	1	60	60	12	48	80.00	12	6.830	12.976	0.300	0.090	Yes	0.199	0.342	0.117	29.925	2.398	29.825	1.172	0	<b>-0.100</b>	
		Area-Based Approach	Larger Range	Height Diff	80	BI	1	60	50	17	43	71.67	7	9.011	15.439	0.341	0.116	Yes	0.423	0.576	0.331	29.925	2.398	29.922	1.161	-10	<b>-0.003</b>
				SD IT Ht	30	TNN	4	60	59	11	49	81.67	10	5.961	11.941	0.502	0.252	Yes	-0.225	0.291	0.085	29.925	2.398	30.573	<b>1.076</b>	-1	0.648

Plot VII.		Best Parameter	CS	IM	FS	Mea- sured	Identi- fied	Un- matched	Matched	Matched %	Redun- dant	MAE	RMSE	R	R <sup>2</sup>	Stat Sig R	Mean Diff (MT)	R (MT)	R <sup>2</sup> (MT)	Mean FM Ht	SD FM Ht	Mean IT Ht	SD IT Ht	Count Diff	Height Diff		
Reduced Number of FM Trees	Individual Tree App- Smaller Range	RMSE & R	30	TLN	4	56	60	9	47	83.93	13	5.509	11.741	<b>0.436</b>	0.190	Yes	-0.084	0.384	0.148	30.446	1.426	30.689	1.105	4	0.242		
		RMSE	25	BA	4	56	61	6	50	89.29	11	4.090	<b>9.720</b>	0.285	0.081	Yes	0.112	0.401	0.160	30.446	1.426	30.320	0.989	5	-0.126		
		R	30	TLN	4	56	60	9	47	83.93	13	5.509	11.741	<b>0.436</b>	0.190	Yes	-0.084	0.384	0.148	30.446	1.426	30.689	1.105	4	0.242		
		R for MT	30	TLW	4	56	54	12	44	78.57	10	7.254	14.022	0.143	0.020	No	-0.258	<b>0.538</b>	0.290	30.446	1.426	30.787	1.191	-2	0.341		
		RMSE	25	BA	4	56	61	6	50	89.29	11	4.090	<b>9.720</b>	0.285	0.081	Yes	0.112	0.401	0.160	30.446	1.426	30.320	0.989	5	-0.126		
		R	100	TLW	1	56	40	23	33	58.93	7	12.738	19.003	<b>0.521</b>	0.272	Yes	0.360	0.445	0.198	30.446	1.426	30.497	1.187	-16	0.051		
	Area-Based Approach	Larger Range	R for MT	30	TLW	4	56	54	12	44	78.57	10	7.254	14.022	0.143	0.020	No	-0.258	<b>0.538</b>	0.290	30.446	1.426	30.787	1.191	-2	0.341	
			Count Diff (0)	35	TNN	3	56	56	10	46	82.14	10	6.209	12.682	0.232	0.054	No	-0.025	0.460	0.211	30.446	1.426	30.448	1.168	0	<b>0.001</b>	
			Count Diff (±1)	15	BA	8	56	55	11	45	80.36	10	6.655	13.217	0.295	0.087	Yes	0.035	0.462	0.213	30.446	1.426	30.451	1.101	-1	<b>0.004</b>	
		Area-Based Approach	Larger Range	Height Diff	35	TNN	3	56	56	10	46	82.14	10	6.209	12.682	0.232	0.054	No	-0.025	0.460	0.211	30.446	1.426	30.448	1.168	0	<b>0.001</b>
				SD IT Ht	35	BI	3	56	55	11	45	80.36	10	6.791	13.406	0.151	0.023	No	0.207	0.404	0.163	30.446	1.426	30.177	<b>1.026</b>	-1	-0.270

Plot VIII.		Best Parameter	CS	IM	FS	Mea- sured	Identi- fied	Un- matched	Matched	Matched %	Redun- dant	MAE	RMSE	R	R <sup>2</sup>	Stat Sig R	Mean Diff (MT)	R (MT)	R <sup>2</sup> (MT)	Mean FM Ht	SD FM Ht	Mean IT Ht	SD IT Ht	Count Diff	Height Diff		
All Field-Measured (FM) Trees	Individual Tree App- Smaller Range	RMSE & R	25	BA	2	68	70	18	50	73.53	20	7.878	13.311	0.548	0.300	Yes	-1.940	0.756	0.572	28.669	9.122	32.073	4.380	2	3.403		
		RMSE	10	BI	6	68	73	17	51	75.00	22	7.505	<b>12.806</b>	0.576	0.332	Yes	-2.210	0.750	0.563	28.669	9.122	32.833	4.188	5	4.164		
		R	10	BA	6	68	72	20	48	70.59	24	7.932	13.473	<b>0.603</b>	0.364	Yes	-1.833	0.739	0.545	28.669	9.122	32.702	4.201	4	4.033		
		R for MT	25	BI	2	68	72	18	50	73.53	22	7.891	13.313	0.548	0.301	Yes	-1.979	<b>0.757</b>	0.572	28.669	9.122	32.066	4.344	4	3.397		
		RMSE	10	BI	6	68	73	17	51	75.00	22	7.505	<b>12.806</b>	0.576	0.332	Yes	-2.210	0.750	0.563	28.669	9.122	32.833	4.188	5	4.164		
		R	45	TNN	1	68	60	23	45	66.18	15	8.669	14.124	<b>0.632</b>	0.399	Yes	-1.273	0.775	0.600	28.669	9.122	32.836	3.987	-8	4.167		
	Area-Based Approach	Larger Range	R for MT	45	BI	1	68	56	22	46	67.65	10	8.585	14.287	0.582	0.339	Yes	-1.251	<b>0.827</b>	0.684	28.669	9.122	32.473	4.201	-12	3.804	
			Count Diff (0)	40	TNN	1	68	69	21	47	69.12	22	8.430	14.160	0.566	0.321	Yes	-1.735	0.721	0.519	28.669	9.122	32.563	4.171	1	<b>3.894</b>	
			Count Diff (±1)	40	TNN	1	68	69	21	47	69.12	22	8.430	14.160	0.566	0.321	Yes	-1.735	0.721	0.519	28.669	9.122	32.563	4.171	1	<b>3.894</b>	
		Area-Based Approach	Larger Range	Height Diff	5	BM	1	68	2376	0	68	100.00	2308	5.820	9.815	0.488	0.238	Yes	-5.615	0.488	0.238	28.669	9.122	30.094	5.115	2308	<b>1.425</b>
				SD IT Ht	15	TNN	4	68	69	18	50	73.53	19	8.441	13.896	0.489	0.240	Yes	-2.988	0.604	0.365	28.669	9.122	33.172	<b>3.700</b>	1	4.503

Plot VIII.		Best Parameter	CS	IM	FS	Mea- sured	Identi- fied	Un- matched	Matched	Matched %	Redun- dant	MAE	RMSE	R	R <sup>2</sup>	Stat Sig R	Mean Diff (MT)	R (MT)	R <sup>2</sup> (MT)	Mean FM Ht	SD FM Ht	Mean IT Ht	SD IT Ht	Count Diff	Height Diff
Reduced Number of FM Trees	Individual Tree App- Smaller Range	RMSE & R	45	TNN	1	54	56	12	42	77.78	14	7.714	14.362	<b>0.533</b>	0.284	Yes	-0.401	0.838	0.702	32.963	3.581	33.516	2.802	2	0.553
		RMSE	10	TNW	7	54	58	9	45	83.33	13	6.504	<b>12.964</b>	0.372	0.138	Yes	-1.106	0.803	0.644	32.963	3.581	33.845	2.877	4	0.882
		R	45	TNN	1	54	56	12	42	77.78	14	7.714	14.362	<b>0.533</b>	0.284	Yes	-0.401	0.838	0.702	32.963	3.581	33.516	2.802	2	0.553
		R for MT	20	BA	3	54	55	15	39	72.22	16	9.446	16.551	0.426	0.182	Yes	-0.642	<b>0.900</b>	0.811	32.963	3.581	33.478	2.920	1	0.515
	Larger Range	RMSE	35	BI	1	54	71	8	46	85.19	25	5.673	<b>11.990</b>	0.422	0.178	Yes	-0.355	0.789	0.623	32.963	3.581	32.566	3.053	17	-0.397
		R	25	TLN	3	54	45	17	37	68.52	8	10.416	17.228	<b>0.564</b>	0.318	Yes	-0.644	0.858	0.736	32.963	3.581	34.133	2.963	-9	1.170
		R for MT	20	BI	4	54	38	20	34	62.96	4	12.189	19.052	0.487	0.237	Yes	-0.661	<b>0.903</b>	0.815	32.963	3.581	34.534	2.764	-16	1.572
	Area-Based Approach	Count Diff (0)	30	TNN	2	54	54	14	40	74.07	14	9.055	16.125	0.381	0.145	Yes	-0.827	0.892	0.795	32.963	3.581	33.728	2.778	0	<b>0.765</b>
		Count Diff (±1)	40	BI	1	54	55	12	42	77.78	13	7.755	14.713	0.437	0.191	Yes	-0.151	0.849	0.721	32.963	3.581	33.199	2.905	1	<b>0.236</b>
		Height Diff	25	BI	2	54	66	10	44	81.48	22	6.644	13.223	0.487	0.237	Yes	-0.359	0.832	0.692	32.963	3.581	32.944	3.021	12	<b>-0.019</b>
		SD IT Ht	30	TNN	2	54	54	14	40	74.07	14	9.055	16.125	0.381	0.145	Yes	-0.827	0.892	0.795	32.963	3.581	33.728	<b>2.778</b>	0	0.765

Plot IX.		Best Parameter	CS	IM	FS	Mea- sured	Identi- fied	Un- matched	Matched	Matched %	Redun- dant	MAE	RMSE	R	R <sup>2</sup>	Stat Sig R	Mean Diff (MT)	R (MT)	R <sup>2</sup> (MT)	Mean FM Ht	SD FM Ht	Mean IT Ht	SD IT Ht	Count Diff	Height Diff
All Field-Measured (FM) Trees	Individual Tree App- Smaller Range	RMSE & R	15	BN	4	71	72	13	58	81.69	14	5.015	<b>9.865</b>	0.668	0.446	Yes	-1.210	0.634	0.402	28.549	6.577	31.171	2.999	1	2.622
		RMSE	15	BN	4	71	72	13	58	81.69	14	5.015	<b>9.865</b>	0.668	0.446	Yes	-1.210	0.634	0.402	28.549	6.577	31.171	2.999	1	2.622
		R	35	BM	1	71	74	15	56	78.87	18	5.455	10.447	<b>0.697</b>	0.486	Yes	-1.097	0.633	0.400	28.549	6.577	31.276	3.008	3	2.727
		R for MT	15	TLN	4	71	69	15	56	78.87	13	5.803	11.113	0.610	0.372	Yes	-1.194	<b>0.644</b>	0.415	28.549	6.577	31.075	3.120	-2	2.525
	Larger Range	RMSE	10	TNW	5	71	77	13	58	81.69	19	4.938	<b>9.599</b>	0.694	0.481	Yes	-1.328	0.588	0.345	28.549	6.577	31.284	2.860	6	2.734
		R	10	TLN	8	71	55	18	53	74.65	2	6.121	11.343	<b>0.726</b>	0.527	Yes	-0.782	0.649	0.422	28.549	6.577	31.870	2.390	-16	3.321
		R for MT	20	TNN	3	71	61	18	53	74.65	8	6.287	11.640	0.695	0.482	Yes	-0.636	<b>0.688</b>	0.473	28.549	6.577	31.359	2.906	-10	2.809
	Area-Based Approach	Count Diff (0)	15	BI	4	71	71	19	52	73.24	19	7.183	12.806	0.589	0.347	Yes	-0.784	0.595	0.354	28.549	6.577	31.131	2.772	0	<b>2.582</b>
		Count Diff (±1)	45	BI	1	71	72	17	54	76.06	18	6.453	11.564	0.644	0.415	Yes	-0.123	0.511	0.261	28.549	6.577	30.705	2.487	1	<b>2.156</b>
		Height Diff	5	TNW	2	71	846	0	71	100.00	775	3.413	6.502	0.522	0.272	Yes	-3.141	0.522	0.272	28.549	6.577	28.563	3.618	775	<b>0.014</b>
		SD IT Ht	45	BI	1	71	72	17	54	76.06	18	6.453	11.564	0.644	0.415	Yes	-0.123	0.511	0.261	28.549	6.577	30.705	<b>2.487</b>	1	2.156

Plot IX.		Best Parameter	CS	IM	FS	Mea- sured	Identi- fied	Un- matched	Matched	Matched %	Redun- dant	MAE	RMSE	R	R <sup>2</sup>	Stat Sig R	Mean Diff (MT)	R (MT)	R <sup>2</sup> (MT)	Mean FM Ht	SD FM Ht	Mean IT Ht	SD IT Ht	Count Diff	Height Diff
Reduced Number of FM Trees	Individual Tree App- Smaller Range	RMSE & R	10	TNW	7	57	56	4	53	92.98	3	2.677	7.396	0.605	0.366	Yes	-0.467	0.927	0.859	31.307	2.605	31.950	2.395	-1	0.643
		RMSE	10	TLN	8	57	55	4	53	92.98	2	2.620	<b>7.389</b>	0.604	0.365	Yes	-0.367	0.928	0.861	31.307	2.605	31.870	2.390	-2	0.563
		R	30	BM	2	57	57	6	51	89.47	6	3.668	9.070	<b>0.632</b>	0.399	Yes	-0.512	0.919	0.845	31.307	2.605	32.062	2.313	0	0.755
		R for MT	40	TNW	1	57	62	5	52	91.23	10	3.072	8.358	0.594	0.353	Yes	-0.316	<b>0.950</b>	0.902	31.307	2.605	31.438	2.936	5	0.131
	Larger Range	RMSE	10	TNW	5	57	77	2	55	96.49	22	1.690	<b>5.070</b>	0.656	0.431	Yes	-0.438	0.928	0.861	31.307	2.605	31.284	2.860	20	-0.023
		R	30	TLW	4	57	41	16	41	71.93	0	8.596	15.264	<b>0.699</b>	0.488	Yes	-0.356	0.931	0.867	31.307	2.605	32.673	2.257	-16	1.366
		R for MT	60	TNW	1	57	48	10	47	82.46	1	5.753	12.472	0.445	0.198	Yes	-0.317	<b>0.951</b>	0.904	31.307	2.605	32.005	2.468	-9	0.698
	Area-Based Approach	Count Diff (0)	40	BN	2	57	57	7	50	87.72	7	4.110	9.985	0.584	0.341	Yes	-0.146	0.927	0.860	31.307	2.605	31.656	2.413	0	<b>0.349</b>
		Count Diff (±1)	10	TNN	7	57	57	5	52	91.23	5	3.164	8.517	0.532	0.283	Yes	-0.348	0.928	0.861	31.307	2.605	31.672	2.529	0	<b>0.365</b>
		Height Diff	50	TLN	1	57	56	11	46	80.70	10	6.225	12.836	0.545	0.298	Yes	0.157	0.898	0.806	31.307	2.605	31.313	2.744	-1	<b>0.006</b>
		SD IT Ht	20	BA	4	57	56	8	49	85.96	7	4.799	10.792	0.553	0.306	Yes	0.007	0.844	0.712	31.307	2.605	31.601	<b>2.243</b>	-1	0.294



Plot X.		Best Parameter	CS	IM	FS	Mea- sured	Identi- fied	Un- matched	Matched	Matched %	Redun- dant	MAE	RMSE	R	R <sup>2</sup>	Stat Sig R	Mean Diff (MT)	R (MT)	R <sup>2</sup> (MT)	Mean FM Ht	SD FM Ht	Mean IT Ht	SD IT Ht	Count Diff	Height Diff
All Field-Measured (FM) Trees	Individual Tree App- Smaller Range	RMSE & R	30	TLW	1	92	93	7	85	92.39	8	1.409	<b>4.037</b>	0.769	0.591	Yes	-0.283	0.956	0.913	19.467	2.688	20.021	1.918	1	0.554
		RMSE	30	TLW	1	92	93	7	85	92.39	8	1.409	<b>4.037</b>	0.769	0.591	Yes	-0.283	0.956	0.913	19.467	2.688	20.021	1.918	1	0.554
		R	15	TNN	3	92	95	13	79	85.87	16	2.375	5.684	<b>0.800</b>	0.641	Yes	-0.134	0.958	0.918	19.467	2.688	19.993	1.686	3	0.526
		R for MT	15	TNN	3	92	95	13	79	85.87	16	2.375	5.684	0.800	0.641	Yes	-0.134	<b>0.958</b>	0.918	19.467	2.688	19.993	1.686	3	0.526
		RMSE	30	TLW	1	92	93	7	85	92.39	8	1.409	<b>4.037</b>	0.769	0.591	Yes	-0.283	0.956	0.913	19.467	2.688	20.021	1.918	1	0.554
		R	10	TNN	5	92	86	12	80	86.96	6	2.198	5.366	<b>0.812</b>	0.660	Yes	-0.177	0.959	0.919	19.467	2.688	20.280	1.565	-6	0.813
	Area-Based Approach	R for MT	15	BN	4	92	79	16	76	82.61	3	2.985	6.641	0.751	0.563	Yes	-0.265	<b>0.967</b>	0.935	19.467	2.688	20.457	1.609	-13	0.990
		Count Diff (0)	35	BA	1	92	92	12	80	86.96	12	2.769	5.718	0.740	0.547	Yes	0.864	0.737	0.543	19.467	2.688	19.008	1.892	0	<b>-0.460</b>
		Count Diff (±1)	15	TLN	3	92	92	11	81	88.04	11	2.064	5.169	0.787	0.620	Yes	-0.241	0.925	0.856	19.467	2.688	20.066	1.786	0	<b>0.599</b>
		Height Diff	15	BI	3	92	96	11	81	88.04	15	2.358	5.485	0.702	0.493	Yes	0.146	0.797	0.635	19.467	2.688	19.486	1.970	4	<b>0.019</b>
		SD IT Ht	5	BI	10	92	92	8	84	91.30	8	1.670	4.399	0.750	0.562	Yes	-0.413	0.934	0.872	19.467	2.688	20.252	<b>1.668</b>	0	0.785

Plot X.		Best Parameter	CS	IM	FS	Mea- sured	Identi- fied	Un- matched	Matched	Matched %	Redun- dant	MAE	RMSE	R	R <sup>2</sup>	Stat Sig R	Mean Diff (MT)	R (MT)	R <sup>2</sup> (MT)	Mean FM Ht	SD FM Ht	Mean IT Ht	SD IT Ht	Count Diff	Height Diff
Reduced Number of FM Trees	Individual Tree App- Smaller Range	RMSE & R	35	TLW	1	85	84	5	80	94.12	4	1.310	4.180	0.668	0.446	Yes	-0.207	0.966	0.933	20.035	1.709	20.251	1.768	-1	0.215
		RMSE	5	BI	10	85	90	3	82	96.47	8	1.039	<b>3.419</b>	0.563	0.317	Yes	-0.358	0.940	0.884	20.035	1.709	20.330	1.601	5	0.295
		R	10	TLN	5	85	85	6	79	92.94	6	1.541	4.593	<b>0.671</b>	0.451	Yes	-0.240	0.963	0.927	20.035	1.709	20.414	1.539	0	0.378
		R for MT	30	BM	1	85	87	7	78	91.76	9	1.807	5.058	0.643	0.413	Yes	-0.366	<b>0.971</b>	0.942	20.035	1.709	20.363	1.758	2	0.328
	Area-Based Approach	RMSE	30	TNW	1	85	91	3	82	96.47	9	0.917	<b>3.295</b>	0.641	0.411	Yes	-0.217	0.971	0.942	20.035	1.709	20.116	1.823	6	0.080
		R	10	BN	7	85	73	13	72	84.71	1	3.026	6.963	<b>0.694</b>	0.481	Yes	-0.293	0.960	0.922	20.035	1.709	20.734	1.419	-12	0.699
		R for MT	5	TNW	9	85	91	4	81	95.29	10	1.183	3.809	0.635	0.404	Yes	-0.328	<b>0.972</b>	0.944	20.035	1.709	20.187	1.888	6	0.151
		Count Diff (0)	10	TLN	5	85	85	6	79	92.94	6	1.541	4.593	0.671	0.451	Yes	-0.240	0.963	0.927	20.035	1.709	20.414	1.539	0	<b>0.378</b>
		Count Diff (±1)	40	TLN	1	85	84	6	79	92.94	5	1.663	4.659	0.637	0.405	Yes	0.171	0.913	0.834	20.035	1.709	20.002	1.509	-1	<b>-0.033</b>
		Height Diff	15	TNN	3	85	94	6	79	92.94	15	1.535	4.614	0.658	0.433	Yes	-0.134	0.958	0.918	20.035	1.709	20.030	1.656	9	<b>-0.005</b>
SD IT Ht	40	TLN	1	85	84	6	79	92.94	5	1.663	4.659	0.637	0.405	Yes	0.171	0.913	0.834	20.035	1.709	20.002	<b>1.509</b>	-1	-0.033		

Plot XI.		Best Parameter	CS	IM	FS	Mea- sured	Identi- fied	Un- matched	Matched	Matched %	Redun- dant	MAE	RMSE	R	R <sup>2</sup>	Stat Sig R	Mean Diff (MT)	R (MT)	R <sup>2</sup> (MT)	Mean FM Ht	SD FM Ht	Mean IT Ht	SD IT Ht	Count Diff	Height Diff
All Field-Measured (FM) Trees	Individual Tree App- Smaller Range	RMSE & R	70	BA	1	60	61	17	43	71.67	18	10.652	<b>16.024</b>	0.336	0.113	Yes	-1.285	-0.134	0.018	31.050	5.400	31.835	5.227	1	0.785
		RMSE	70	BA	1	60	61	17	43	71.67	18	10.652	<b>16.024</b>	0.336	0.113	Yes	-1.285	-0.134	0.018	31.050	5.400	31.835	5.227	1	0.785
		R	65	TLN	1	60	56	21	39	65.00	17	12.035	17.741	<b>0.360</b>	0.130	Yes	-3.091	0.506	0.256	31.050	5.400	34.705	4.696	-4	3.655
		R for MT	65	TLN	1	60	56	21	39	65.00	17	12.035	17.741	0.360	0.130	Yes	-3.091	<b>0.506</b>	0.256	31.050	5.400	34.705	4.696	-4	3.655
		RMSE	70	BA	1	60	61	17	43	71.67	18	10.652	<b>16.024</b>	0.336	0.113	Yes	-1.285	-0.134	0.018	31.050	5.400	31.835	5.227	1	0.785
		R	65	TLN	1	60	56	21	39	65.00	17	12.035	17.741	<b>0.360</b>	0.130	Yes	-3.091	0.506	0.256	31.050	5.400	34.705	4.696	-4	3.655
	Area-Based Approach	R for MT	55	TNN	2	60	42	27	33	55.00	9	14.882	20.426	0.300	0.090	No	-3.021	<b>0.605</b>	0.366	31.050	5.400	34.622	5.335	-18	3.572
		Count Diff (0)	20	BA	5	60	60	21	39	65.00	21	13.284	19.065	0.080	0.006	No	-3.481	-0.078	0.006	31.050	5.400	33.512	4.795	0	<b>2.462</b>
		Count Diff (±1)	70	BA	1	60	61	17	43	71.67	18	10.652	16.024	0.336	0.113	Yes	-1.285	-0.134	0.018	31.050	5.400	31.835	5.227	1	<b>0.785</b>
		Height Diff	30	BI	1	60	237	6	54	90.00	183	6.495	10.879	0.186	0.035	No	-3.123	-0.041	0.002	31.050	5.400	31.032	6.662	177	<b>-0.018</b>
		SD IT Ht	15	BI	7	60	61	21	39	65.00	22	13.496	19.310	0.034	0.001	No	-3.977	-0.051	0.003	31.050	5.400	34.108	<b>4.571</b>	1	3.058

Plot XI.		Best Parameter	CS	IM	FS	Mea- sured	Identi- fied	Un- matched	Matched	Matched %	Redun- dant	MAE	RMSE	R	R <sup>2</sup>	Stat Sig R	Mean Diff (MT)	R (MT)	R <sup>2</sup> (MT)	Mean FM Ht	SD FM Ht	Mean IT Ht	SD IT Ht	Count Diff	Height Diff	
Reduced Number of FM Trees	Individual Tree App.	Smaller Range	RMSE & R	65	TLN	1	58	56	19	39	67.24	17	12.191	17.981	0.278	0.077	No	-3.091	0.506	0.256	31.862	3.174	34.705	4.696	-2	2.843
			RMSE	70	BA	1	58	61	15	43	74.14	18	10.760	<b>16.229</b>	0.180	0.032	No	-1.285	-0.134	0.018	31.862	3.174	31.835	5.227	3	-0.027
			R	70	TNN	1	58	54	19	39	67.24	15	12.154	17.930	<b>0.292</b>	0.085	No	-2.952	0.462	0.214	31.862	3.174	34.619	4.820	-4	2.757
			R for MT	70	TLN	1	58	56	19	39	67.24	17	12.703	18.499	0.099	0.010	No	-3.477	<b>0.556</b>	0.310	31.862	3.174	34.681	4.719	-2	2.819
		Larger Range	RMSE	70	BA	1	58	61	15	43	74.14	18	10.760	<b>16.229</b>	0.180	0.032	No	-1.285	-0.134	0.018	31.862	3.174	31.835	5.227	3	-0.027
			R	55	TLN	2	58	43	26	32	55.17	11	15.380	20.838	<b>0.355</b>	0.126	No	-2.907	0.591	0.350	31.862	3.174	34.812	5.322	-15	2.950
			R for MT	35	BN	3	58	47	23	35	60.34	12	14.650	20.107	0.173	0.030	No	-3.711	<b>0.662</b>	0.438	31.862	3.174	35.125	5.156	-11	3.263
	Area-Based Approach	Count Diff (0)	30	TNN	3	58	58	19	39	67.24	19	12.808	18.648	0.046	0.002	No	-3.575	0.286	0.082	31.862	3.174	34.299	6.390	0	<b>2.437</b>	
		Count Diff (±1)	25	BA	4	58	59	19	39	67.24	20	12.329	18.076	0.229	0.052	No	-2.271	0.074	0.005	31.862	3.174	33.294	4.890	1	<b>1.432</b>	
		Height Diff	70	BA	1	58	61	15	43	74.14	18	10.760	16.229	0.180	0.032	No	-1.285	-0.134	0.018	31.862	3.174	31.835	5.227	3	<b>-0.027</b>	
		SD IT Ht	65	BN	1	58	58	20	38	65.52	20	13.125	18.862	0.135	0.018	No	-3.456	0.398	0.159	31.862	3.174	34.779	<b>4.624</b>	0	2.917	

Plot XII.		Best Parameter	CS	IM	FS	Mea- sured	Identi- fied	Un- matched	Matched	Matched %	Redun- dant	MAE	RMSE	R	R <sup>2</sup>	Stat Sig R	Mean Diff (MT)	R (MT)	R <sup>2</sup> (MT)	Mean FM Ht	SD FM Ht	Mean IT Ht	SD IT Ht	Count Diff	Height Diff	
All Field-Measured (FM) Trees	Individual Tree App.	Smaller Range	RMSE & R	15	BI	6	60	61	15	45	75.00	16	5.964	<b>8.671</b>	0.418	0.174	Yes	-2.059	0.269	0.072	17.942	2.569	19.902	3.212	1	1.961
			RMSE	15	BI	6	60	61	15	45	75.00	16	5.964	<b>8.671</b>	0.418	0.174	Yes	-2.059	0.269	0.072	17.942	2.569	19.902	3.212	1	1.961
			R	15	BN	5	60	55	17	43	71.67	12	7.018	9.401	<b>0.434</b>	0.188	Yes	-3.348	0.335	0.112	17.942	2.569	21.307	3.155	-5	3.366
			R for MT	10	TLW	7	60	65	15	45	75.00	20	6.956	9.418	0.257	0.066	No	-3.464	<b>0.714</b>	0.509	17.942	2.569	21.196	3.364	5	3.254
		Larger Range	RMSE	20	BA	4	60	66	14	46	76.67	20	5.803	<b>8.458</b>	0.381	0.145	Yes	-1.599	0.211	0.045	17.942	2.569	19.519	3.271	6	1.578
			R	55	TNN	1	60	66	20	40	66.67	26	7.073	9.828	<b>0.487</b>	0.237	Yes	-2.130	0.143	0.020	17.942	2.569	20.008	3.270	6	2.067
			R for MT	10	TLW	7	60	65	15	45	75.00	20	6.956	9.418	0.257	0.066	No	-3.464	<b>0.714</b>	0.509	17.942	2.569	21.196	3.364	5	3.254
	Area-Based Approach	Count Diff (0)	60	TLN	1	60	60	21	39	65.00	21	8.183	10.954	0.134	0.018	No	-2.834	0.257	0.066	17.942	2.569	20.053	3.236	0	<b>2.112</b>	
		Count Diff (±1)	15	BI	6	60	61	15	45	75.00	16	5.964	8.671	0.418	0.174	Yes	-2.059	0.269	0.072	17.942	2.569	19.902	3.212	1	<b>1.961</b>	
		Height Diff	45	BA	1	60	95	8	52	86.67	43	4.722	7.320	0.070	0.005	No	-0.763	0.200	0.040	17.942	2.569	17.944	3.218	35	<b>0.003</b>	
		SD IT Ht	40	TNN	2	60	61	18	42	70.00	19	7.006	9.752	0.336	0.113	Yes	-2.711	0.430	0.185	17.942	2.569	20.450	<b>3.058</b>	1	2.508	

Plot XII.		Best Parameter	CS	IM	FS	Mea- sured	Identi- fied	Un- matched	Matched	Matched %	Redun- dant	MAE	RMSE	R	R <sup>2</sup>	Stat Sig R	Mean Diff (MT)	R (MT)	R <sup>2</sup> (MT)	Mean FM Ht	SD FM Ht	Mean IT Ht	SD IT Ht	Count Diff	Height Diff	
Reduced Number of FM Trees	Individual Tree App.	Smaller Range	RMSE & R	10	TLN	8	58	57	16	42	72.41	15	7.132	9.659	0.322	0.104	Yes	-3.268	0.456	0.208	18.190	2.173	21.290	3.151	-1	3.100
			RMSE	15	BI	6	58	61	13	45	77.59	16	5.799	<b>8.576</b>	0.320	0.103	Yes	-2.059	0.269	0.072	18.190	2.173	19.902	3.212	3	1.713
			R	60	BN	1	58	54	16	42	72.41	12	6.717	9.427	<b>0.373</b>	0.139	Yes	-2.607	0.260	0.068	18.190	2.173	20.738	3.169	-4	2.548
			R for MT	45	BM	1	58	63	12	46	79.31	17	6.275	8.643	0.289	0.083	No	-3.370	<b>0.606</b>	0.368	18.190	2.173	21.251	3.162	5	3.062
		Larger Range	RMSE	15	BI	6	58	61	13	45	77.59	16	5.799	<b>8.576</b>	0.320	0.103	Yes	-2.059	0.269	0.072	18.190	2.173	19.902	3.212	3	1.713
			R	25	BI	4	58	41	22	36	62.07	5	8.070	10.897	<b>0.387</b>	0.150	Yes	-1.284	0.165	0.027	18.190	2.173	19.953	2.299	-17	1.763
			R for MT	45	BM	1	58	63	12	46	79.31	17	6.275	8.643	0.289	0.083	No	-3.370	<b>0.606</b>	0.368	18.190	2.173	21.251	3.162	5	3.062
	Area-Based Approach	Count Diff (0)	50	TNW	1	58	58	15	43	74.14	15	6.986	9.566	0.230	0.053	No	-3.290	0.477	0.227	18.190	2.173	21.116	3.112	0	<b>2.926</b>	
		Count Diff (±1)	40	BI	2	58	57	17	41	70.69	16	6.927	10.087	0.122	0.015	No	-1.240	0.277	0.077	18.190	2.173	18.770	3.397	-1	<b>0.581</b>	
		Height Diff	80	BA	1	58	35	28	30	51.72	5	9.806	12.613	0.229	0.053	No	0.434	0.287	0.082	18.190	2.173	18.174	2.761	-23	<b>-0.015</b>	
		SD IT Ht	10	TNN	8	58	59	12	46	79.31	13	6.178	8.735	0.195	0.038	No	-3.155	0.507	0.257	18.190	2.173	20.983	<b>3.097</b>	1	2.793	

Plot XIII.		Best Parameter	CS	IM	FS	Mea- sured	Identi- fied	Un- matched	Matched	Matched %	Redun- dant	MAE	RMSE	R	R <sup>2</sup>	Stat Sig R	Mean Diff (MT)	R (MT)	R <sup>2</sup> (MT)	Mean FM Ht	SD FM Ht	Mean IT Ht	SD IT Ht	Count Diff	Height Diff	
All Field-Measured (FM) Trees	Individual Tree App- Smaller Range	RMSE & R	35	TNW	1	62	60	19	43	69.35	17	6.961	10.966	0.527	0.278	Yes	-3.026	0.356	0.127	21.250	7.701	26.117	3.734	-2	4.867	
		RMSE	15	TLN	3	62	66	16	46	74.19	20	6.265	<b>9.989</b>	0.549	0.302	Yes	-2.900	0.242	0.059	21.250	7.701	25.450	4.760	4	4.200	
		R	35	TLW	1	62	57	20	42	67.74	15	6.924	10.927	<b>0.560</b>	0.314	Yes	-2.808	0.240	0.057	21.250	7.701	26.213	3.795	-5	4.963	
		R for MT	35	BN	1	62	66	18	44	70.97	22	8.156	12.278	0.334	0.112	Yes	-4.039	<b>0.482</b>	0.232	21.250	7.701	25.154	5.629	4	3.904	
		RMSE	15	TLN	3	62	66	16	46	74.19	20	6.265	<b>9.989</b>	0.549	0.302	Yes	-2.900	0.242	0.059	21.250	7.701	25.450	4.760	4	4.200	
		R	25	BM	2	62	56	20	42	67.74	14	6.532	10.463	<b>0.612</b>	0.374	Yes	-2.560	0.144	0.021	21.250	7.701	26.745	1.487	-6	5.495	
	Area-Based Approach	Larger Range	R for MT	35	BN	1	62	66	18	44	70.97	22	8.156	12.278	0.334	0.112	Yes	-4.039	<b>0.482</b>	0.232	21.250	7.701	25.154	5.629	4	3.904
			Count Diff (0)	40	BI	1	62	62	21	41	66.13	21	8.884	12.759	0.337	0.114	Yes	-2.175	0.247	0.061	21.250	7.701	24.140	3.844	0	<b>2.890</b>
			Count Diff (±1)	40	BI	1	62	62	21	41	66.13	21	8.884	12.759	0.337	0.114	Yes	-2.175	0.247	0.061	21.250	7.701	24.140	3.844	0	<b>2.890</b>
	Area-Based Approach	Larger Range	Height Diff	5	TLW	1	62	1031	0	62	100.00	969	5.756	8.989	0.473	0.223	Yes	-5.466	0.473	0.223	21.250	7.701	21.368	8.087	969	<b>0.118</b>
			SD IT Ht	35	TLN	1	62	62	16	46	74.19	16	7.273	11.359	0.384	0.148	Yes	-3.656	0.441	0.194	21.250	7.701	25.703	<b>3.709</b>	0	4.453

Plot XIII.		Best Parameter	CS	IM	FS	Mea- sured	Identi- fied	Un- matched	Matched	Matched %	Redun- dant	MAE	RMSE	R	R <sup>2</sup>	Stat Sig R	Mean Diff (MT)	R (MT)	R <sup>2</sup> (MT)	Mean FM Ht	SD FM Ht	Mean IT Ht	SD IT Ht	Count Diff	Height Diff	
Reduced Number of FM Trees	Individual Tree App- Smaller Range	RMSE & R	60	TLN	1	43	40	8	35	81.40	5	5.259	<b>10.819</b>	0.425	0.181	Yes	-0.326	0.758	0.575	26.244	1.757	26.795	1.277	-3	0.551	
		RMSE	60	TLN	1	43	40	8	35	81.40	5	5.259	<b>10.819</b>	0.425	0.181	Yes	-0.326	0.758	0.575	26.244	1.757	26.795	1.277	-3	0.551	
		R	65	BN	1	43	38	10	33	76.74	5	6.461	12.041	<b>0.494</b>	0.244	Yes	-0.343	0.678	0.460	26.244	1.757	26.763	1.397	-5	0.519	
		R for MT	10	TLN	8	43	40	9	34	79.07	6	6.038	11.645	0.352	0.124	Yes	-0.829	<b>0.808</b>	0.653	26.244	1.757	27.162	1.260	-3	0.918	
		RMSE	10	TLN	6	43	49	5	38	88.37	11	3.852	<b>8.651</b>	0.347	0.120	Yes	-0.822	0.762	0.581	26.244	1.757	26.924	1.356	6	0.680	
		R	65	BN	1	43	38	10	33	76.74	5	6.461	12.041	<b>0.494</b>	0.244	Yes	-0.343	0.678	0.460	26.244	1.757	26.763	1.397	-5	0.519	
	Area-Based Approach	Larger Range	R for MT	10	TLN	8	43	40	9	34	79.07	6	6.038	11.645	0.352	0.124	Yes	-0.829	<b>0.808</b>	0.653	26.244	1.757	27.162	1.260	-3	0.918
			Count Diff (0)	50	TNN	1	43	43	9	34	79.07	9	6.089	11.913	0.190	0.036	No	-0.259	0.774	0.598	26.244	1.757	26.360	1.506	0	<b>0.115</b>
			Count Diff (±1)	15	BA	5	43	42	9	34	79.07	8	6.497	12.006	0.149	0.022	No	0.097	0.378	0.143	26.244	1.757	26.192	1.713	-1	<b>-0.052</b>
	Area-Based Approach	Larger Range	Height Diff	10	TLW	5	43	56	5	38	88.37	18	4.172	9.108	0.086	0.007	No	-1.005	0.591	0.349	26.244	1.757	26.237	3.796	13	<b>-0.007</b>
			SD IT Ht	30	BM	2	43	42	9	34	79.07	8	6.109	11.701	0.320	0.102	No	-0.873	0.792	0.627	26.244	1.757	27.136	<b>1.256</b>	-1	0.891

Plot XIII.		Best Parameter	CS	IM	FS	Mea- sured	Identi- fied	Un- matched	Matched	Matched %	Redun- dant	MAE	RMSE	R	R <sup>2</sup>	Stat Sig R	Mean Diff (MT)	R (MT)	R <sup>2</sup> (MT)	Mean FM Ht	SD FM Ht	Mean IT Ht	SD IT Ht	Count Diff	Height Diff	
Modified Positions of Trees	Individual Tree App- Smaller Range	RMSE & R	60	TNN	1	43	42	3	40	93.02	2	2.238	5.884	<b>0.758</b>	0.574	Yes	0.056	0.766	0.586	26.244	1.757	26.476	1.371	-1	0.231	
		RMSE	20	TNW	3	43	45	2	41	95.35	4	1.867	<b>4.965</b>	0.623	0.388	Yes	-0.653	0.844	0.712	26.244	1.757	26.974	1.345	2	0.730	
		R	60	TNN	1	43	42	3	40	93.02	2	2.238	5.884	<b>0.758</b>	0.574	Yes	0.056	0.766	0.586	26.244	1.757	26.476	1.371	-1	0.231	
		R for MT	60	TLW	1	43	39	6	37	86.05	2	3.951	9.036	0.586	0.343	Yes	-0.441	<b>0.847</b>	0.718	26.244	1.757	27.027	1.238	-4	0.783	
		RMSE	35	TLN	1	43	65	0	43	100.00	22	0.824	<b>1.048</b>	0.840	0.706	Yes	-0.436	0.840	0.706	26.244	1.757	25.252	4.713	22	-0.992	
		R	40	BM	1	43	51	0	43	100.00	8	0.939	1.159	<b>0.862</b>	0.742	Yes	-0.740	0.862	0.742	26.244	1.757	26.918	1.446	8	0.674	
	Area-Based Approach	Larger Range	R for MT	75	BM	1	43	32	11	32	74.42	0	7.091	12.789	0.425	0.181	Yes	-0.780	<b>0.890</b>	0.793	26.244	1.757	27.405	1.279	-11	1.160
			Count Diff (0)	20	BI	4	43	43	6	37	86.05	6	4.421	9.327	0.456	0.208	Yes	0.209	0.545	0.297	26.244	1.757	26.152	1.722	0	<b>-0.092</b>
			Count Diff (±1)	15	BA	5	43	44	4	39	90.70	5	3.204	7.366	0.561	0.315	Yes	0.140	0.541	0.293	26.244	1.757	26.204	1.735	1	<b>-0.040</b>
	Area-Based Approach	Larger Range	Height Diff	20	BA	5	43	38	8	35	81.40	3	5.582	10.832	0.450	0.203	Yes	0.197	0.508	0.258	26.244	1.757	26.238	1.756	-5	<b>-0.006</b>
			SD IT Ht	35	TLN	2	43	42	4	39	90.70	3	2.798	7.005	0.716	0.512	Yes	-0.349	0.798	0.637	26.244	1.757	26.899	<b>1.224</b>	-1	0.654

Plot XIV.	Best Parameter	CS	IM	FS	Mea-sured	Identi-fied	Un-matched	Matched	Matched %	Redun-dant	MAE	RMSE	R	R <sup>2</sup>	Stat Sig R	Mean Diff (MT)	R (MT)	R <sup>2</sup> (MT)	Mean FM Ht	SD FM Ht	Mean IT Ht	SD IT Ht	Count Diff	Height Diff		
All Field-Measured (FM) Trees	Individual Tree App.	Smaller Range	RMSE & R	45	TNN	1	67	64	11	56	83.58	8	3.628	7.219	<b>0.608</b>	0.370	Yes	-0.902	0.223	0.050	21.142	4.172	22.932	1.665	-3	1.790
			RMSE	35	TNW	1	67	72	8	59	88.06	13	3.619	<b>7.130</b>	0.437	0.191	Yes	-1.619	0.515	0.266	21.142	4.172	23.014	2.235	5	1.872
		R	45	TNN	1	67	64	11	56	83.58	8	3.628	7.219	<b>0.608</b>	0.370	Yes	-0.902	0.223	0.050	21.142	4.172	22.932	1.665	-3	1.790	
		R for MT	20	TLN	3	67	64	12	55	82.09	9	4.555	8.582	0.419	0.176	Yes	-1.477	<b>0.586</b>	0.344	21.142	4.172	23.088	2.294	-3	1.947	
	Larger Range	RMSE	35	TLW	1	67	74	6	61	91.04	13	3.101	<b>6.373</b>	0.439	0.193	Yes	-1.605	0.534	0.285	21.142	4.172	22.925	2.283	7	1.783	
		R	45	TNN	1	67	64	11	56	83.58	8	3.628	7.219	<b>0.608</b>	0.370	Yes	-0.902	0.223	0.050	21.142	4.172	22.932	1.665	-3	1.790	
	Area-Based Approach	R for MT	20	TLN	3	67	64	12	55	82.09	9	4.555	8.582	0.419	0.176	Yes	-1.477	<b>0.586</b>	0.344	21.142	4.172	23.088	2.294	-3	1.947	
		Count Diff (0)	10	TNN	6	67	67	12	55	82.09	12	4.251	8.054	0.535	0.286	Yes	-1.345	0.576	0.332	21.142	4.172	23.101	2.230	0	<b>1.959</b>	
		Count Diff (±1)	45	BI	1	67	66	13	54	80.60	12	4.749	8.675	0.439	0.193	Yes	-0.377	0.184	0.034	21.142	4.172	22.170	1.855	-1	<b>1.029</b>	
		Height Diff	20	TLN	1	67	222	1	66	98.51	156	2.550	5.157	0.218	0.047	No	-2.109	0.464	0.216	21.142	4.172	21.149	4.464	155	<b>0.008</b>	
		SD IT Ht	45	BI	1	67	66	13	54	80.60	12	4.749	8.675	0.439	0.193	Yes	-0.377	0.184	0.034	21.142	4.172	22.170	<b>1.855</b>	-1	1.029	

Plot XIV.	Best Parameter	CS	IM	FS	Mea-sured	Identi-fied	Un-matched	Matched	Matched %	Redun-dant	MAE	RMSE	R	R <sup>2</sup>	Stat Sig R	Mean Diff (MT)	R (MT)	R <sup>2</sup> (MT)	Mean FM Ht	SD FM Ht	Mean IT Ht	SD IT Ht	Count Diff	Height Diff		
Reduced Number of FM Trees	Individual Tree App.	Smaller Range	RMSE & R	50	TLW	1	56	53	7	49	87.50	4	3.407	7.674	0.484	0.234	Yes	-0.786	0.857	0.735	22.786	1.281	23.655	1.289	-3	0.869
			RMSE	45	TNN	1	56	60	4	52	92.86	8	2.226	<b>5.870</b>	0.409	0.167	Yes	-0.476	0.797	0.635	22.786	1.281	23.140	1.501	4	0.354
		R	15	TNW	5	56	52	9	47	83.93	5	4.265	8.701	<b>0.516</b>	0.267	Yes	-0.952	0.838	0.703	22.786	1.281	23.887	1.198	-4	1.101	
		R for MT	20	TNN	4	56	52	8	48	85.71	4	3.792	8.359	0.372	0.138	Yes	-0.750	<b>0.879</b>	0.773	22.786	1.281	23.607	1.259	-4	0.821	
	Larger Range	RMSE	35	TLW	1	56	69	3	53	94.64	16	2.062	<b>5.255</b>	0.296	0.088	Yes	-0.896	0.860	0.740	22.786	1.281	23.178	2.148	13	0.392	
		R	80	TLN	1	56	41	17	39	69.64	2	7.032	12.030	<b>0.572</b>	0.327	Yes	-0.360	0.741	0.548	22.786	1.281	23.579	1.157	-15	0.794	
	Area-Based Approach	R for MT	20	TNN	4	56	52	8	48	85.71	4	3.792	8.359	0.372	0.138	Yes	-0.750	<b>0.879</b>	0.773	22.786	1.281	23.607	1.259	-4	0.821	
		Count Diff (0)	45	TLW	1	56	56	8	48	85.71	8	3.839	8.344	0.389	0.151	Yes	-0.814	0.859	0.739	22.786	1.281	23.349	2.267	0	<b>0.563</b>	
		Count Diff (±1)	50	TLN	1	56	57	8	48	85.71	9	3.706	8.352	0.364	0.132	Yes	-0.608	0.869	0.756	22.786	1.281	23.088	2.186	1	<b>0.303</b>	
		Height Diff	25	TLN	2	56	69	6	50	89.29	19	3.214	7.454	0.197	0.039	No	-0.876	0.820	0.672	22.786	1.281	22.787	3.421	13	<b>0.001</b>	
SD IT Ht	10	TLW	7	56	55	9	47	83.93	8	4.368	8.884	0.374	0.140	Yes	-0.992	0.843	0.710	22.786	1.281	23.777	<b>1.236</b>	-1	0.991			

Plot XIV.	Best Parameter	CS	IM	FS	Mea-sured	Identi-fied	Un-matched	Matched	Matched %	Redun-dant	MAE	RMSE	R	R <sup>2</sup>	Stat Sig R	Mean Diff (MT)	R (MT)	R <sup>2</sup> (MT)	Mean FM Ht	SD FM Ht	Mean IT Ht	SD IT Ht	Count Diff	Height Diff		
Modified Positions of Trees	Individual Tree App.	Smaller Range	RMSE & R	60	TLN	1	56	58	3	53	94.64	5	1.666	4.705	0.664	0.441	Yes	-0.510	0.833	0.693	22.786	1.281	23.296	1.346	2	0.511
			RMSE	10	BA	7	56	61	2	54	96.43	7	1.502	<b>3.909</b>	0.625	0.391	Yes	-0.722	0.851	0.724	22.786	1.281	23.209	2.243	5	0.423
		R	10	BI	7	56	60	3	53	94.64	7	1.844	4.734	<b>0.671</b>	0.450	Yes	-0.729	0.841	0.707	22.786	1.281	23.255	2.243	4	0.469	
		R for MT	35	TNN	2	56	56	4	52	92.86	4	2.190	5.724	0.514	0.264	Yes	-0.703	<b>0.888</b>	0.789	22.786	1.281	23.472	1.398	0	0.686	
	Larger Range	RMSE	20	BI	3	56	66	0	56	100.00	10	0.797	<b>0.999</b>	0.797	0.635	Yes	-0.353	0.797	0.635	22.786	1.281	22.816	1.675	10	0.030	
		R	10	BA	6	56	71	0	56	100.00	15	0.850	1.056	<b>0.850</b>	0.723	Yes	-0.758	0.850	0.723	22.786	1.281	23.005	2.164	15	0.219	
	Area-Based Approach	R for MT	20	TNN	3	56	62	1	55	98.21	7	1.167	3.099	0.433	0.187	Yes	-0.773	<b>0.895</b>	0.800	22.786	1.281	23.465	1.347	6	0.679	
		Count Diff (0)	55	BI	1	56	56	6	50	89.29	6	3.171	7.026	0.590	0.349	Yes	0.412	0.608	0.370	22.786	1.281	22.443	1.803	0	<b>-0.343</b>	
		Count Diff (±1)	35	BI	2	56	57	6	50	89.29	7	3.040	7.160	0.454	0.206	Yes	-0.087	0.716	0.513	22.786	1.281	22.817	1.659	1	<b>0.031</b>	
		Height Diff	40	BI	2	56	53	7	49	87.50	4	3.423	7.572	0.583	0.340	Yes	0.050	0.657	0.431	22.786	1.281	22.796	1.714	-3	<b>0.010</b>	
SD IT Ht	35	BN	2	56	55	5	51	91.07	4	2.640	6.332	0.578	0.334	Yes	-0.827	0.862	0.744	22.786	1.281	23.730	<b>1.217</b>	-1	0.945			

Plot XV.	Best Parameter	CS	IM	FS	Mea-sured	Identi-fied	Un-matched	Matched	Matched %	Redun-dant	MAE	RMSE	R	R <sup>2</sup>	Stat Sig R	Mean Diff (MT)	R (MT)	R <sup>2</sup> (MT)	Mean FM Ht	SD FM Ht	Mean IT Ht	SD IT Ht	Count Diff	Height Diff		
All Field-Measured (FM) Trees	Individual Tree App.	Smaller Range	RMSE & R	35	TNN	1	61	64	18	43	70.49	21	9.750	<b>15.790</b>	0.323	0.105	Yes	-1.888	0.447	0.199	29.262	7.850	31.829	2.440	3	2.567
			RMSE	35	TNN	1	61	64	18	43	70.49	21	9.750	<b>15.790</b>	0.323	0.105	Yes	-1.888	0.447	0.199	29.262	7.850	31.829	2.440	3	2.567
		R	35	TNN	1	61	64	18	43	70.49	21	9.750	15.790	<b>0.323</b>	0.105	Yes	-1.888	0.447	0.199	29.262	7.850	31.829	2.440	3	2.567	
		R for MT	15	TNN	3	61	66	19	42	68.85	24	10.313	16.627	0.265	0.070	No	-2.299	<b>0.614</b>	0.377	29.262	7.850	32.126	2.433	5	2.864	
	Larger Range	RMSE	40	BI	1	61	50	18	43	70.49	7	8.862	<b>14.654</b>	0.470	0.221	Yes	-0.593	0.309	0.096	29.262	7.850	31.822	2.395	-11	2.559	
		R	40	BI	1	61	50	18	43	70.49	7	8.862	14.654	<b>0.470</b>	0.221	Yes	-0.593	0.309	0.096	29.262	7.850	31.822	2.395	-11	2.559	
	Area-Based Approach	R for MT	10	BI	6	61	47	22	39	63.93	8	11.391	17.699	0.274	0.075	No	-2.245	<b>0.623</b>	0.388	29.262	7.850	32.656	2.230	-14	3.393	
		Count Diff (0)	10	TNN	5	61	61	21	40	65.57	21	11.286	17.691	0.223	0.050	No	-2.579	0.562	0.316	29.262	7.850	32.183	2.436	0	<b>2.921</b>	
		Count Diff (±1)	10	TNN	5	61	61	21	40	65.57	21	11.286	17.691	0.223	0.050	No	-2.579	0.562	0.316	29.262	7.850	32.183	2.436	0	<b>2.921</b>	
		Height Diff	5	BM	1	61	2584	0	61	100.00	2523	4.143	8.231	0.381	0.145	Yes	-3.825	0.381	0.145	29.262	7.850	29.416	2.789	2523	<b>0.154</b>	
		SD IT Ht	25	BN	2	61	62	19	42	68.85	20	10.567	16.940	0.225	0.051	No	-2.655	0.451	0.203	29.262	7.850	32.385	<b>2.255</b>	1	3.123	

Plot XV.	Best Parameter	CS	IM	FS	Mea-sured	Identi-fied	Un-matched	Matched	Matched %	Redun-dant	MAE	RMSE	R	R <sup>2</sup>	Stat Sig R	Mean Diff (MT)	R (MT)	R <sup>2</sup> (MT)	Mean FM Ht	SD FM Ht	Mean IT Ht	SD IT Ht	Count Diff	Height Diff		
Reduced Number of FM Trees	Individual Tree App.	Smaller Range	RMSE & R	35	BI	1	55	58	14	41	74.55	17	8.282	14.741	<b>0.609</b>	0.370	Yes	0.305	0.717	0.514	31.682	2.936	31.563	2.596	3	-0.119
			RMSE	40	BI	1	55	50	13	42	76.36	8	8.069	<b>14.230</b>	0.587	0.345	Yes	0.400	0.389	0.151	31.682	2.936	31.822	2.395	-5	0.140
		R	35	BI	1	55	58	14	41	74.55	17	8.282	14.741	<b>0.609</b>	0.370	Yes	0.305	0.717	0.514	31.682	2.936	31.563	2.596	3	-0.119	
		R for MT	10	BA	6	55	50	18	37	67.27	13	10.470	17.314	0.452	0.205	Yes	-0.455	<b>0.817</b>	0.667	31.682	2.936	32.496	2.327	-5	0.814	
	Larger Range	RMSE	35	TNN	1	55	63	13	42	76.36	21	7.969	<b>14.114</b>	0.619	0.384	Yes	-0.001	0.464	0.216	31.682	2.936	31.876	2.430	8	0.195	
		R	45	BA	1	55	41	20	35	63.64	6	11.530	17.834	<b>0.638</b>	0.407	Yes	0.656	0.658	0.433	31.682	2.936	32.172	2.178	-14	0.490	
	Area-Based Approach	R for MT	15	BI	4	55	46	18	37	67.27	9	10.504	17.360	0.436	0.190	Yes	-0.491	<b>0.824</b>	0.679	31.682	2.936	32.660	2.288	-9	0.978	
		Count Diff (0)	35	BA	1	55	55	16	39	70.91	16	9.354	15.959	0.566	0.320	Yes	0.179	0.778	0.606	31.682	2.936	31.623	2.584	0	<b>-0.059</b>	
		Count Diff (±1)	25	BA	2	55	54	14	41	74.55	13	8.267	14.921	0.542	0.294	Yes	0.104	0.776	0.602	31.682	2.936	31.906	2.363	-1	<b>0.224</b>	
		Height Diff	5	TLW	8	55	106	5	50	90.91	56	4.271	8.999	0.442	0.195	Yes	-0.675	0.499	0.249	31.682	2.936	31.685	2.495	51	<b>0.003</b>	
SD IT Ht	25	TNN	2	55	54	15	40	72.73	14	9.065	15.780	0.431	0.186	Yes	-0.427	0.650	0.422	31.682	2.936	32.378	<b>2.195</b>	-1	0.696			

Plot XV.	Best Parameter	CS	IM	FS	Mea-sured	Identi-fied	Un-matched	Matched	Matched %	Redun-dant	MAE	RMSE	R	R <sup>2</sup>	Stat Sig R	Mean Diff (MT)	R (MT)	R <sup>2</sup> (MT)	Mean FM Ht	SD FM Ht	Mean IT Ht	SD IT Ht	Count Diff	Height Diff		
Modified Positions of Trees	Individual Tree App.	Smaller Range	RMSE & R	40	TLN	1	55	52	9	46	83.64	6	5.371	11.086	0.761	0.579	Yes	-0.111	0.722	0.522	31.682	2.936	32.487	2.250	-3	0.805
			RMSE	10	TNN	5	55	60	6	49	89.09	11	4.000	<b>9.152</b>	0.646	0.417	Yes	-0.744	0.815	0.664	31.682	2.936	32.349	2.410	5	0.667
		R	40	BN	1	55	53	11	44	80.00	9	6.189	12.290	<b>0.804</b>	0.646	Yes	-0.246	0.877	0.769	31.682	2.936	32.608	2.164	-2	0.926	
		R for MT	10	BA	6	55	51	9	46	83.64	5	5.260	11.278	0.703	0.494	Yes	-0.364	<b>0.902</b>	0.814	31.682	2.936	32.617	2.251	-4	0.935	
	Larger Range	RMSE	10	TLN	5	55	64	5	50	90.91	14	3.607	<b>8.439</b>	0.602	0.362	Yes	-0.887	0.782	0.612	31.682	2.936	32.260	2.504	9	0.579	
		R	40	BN	1	55	53	11	44	80.00	9	6.189	12.290	<b>0.804</b>	0.646	Yes	-0.246	0.877	0.769	31.682	2.936	32.608	2.164	-2	0.926	
	Area-Based Approach	R for MT	10	BA	6	55	51	9	46	83.64	5	5.260	11.278	0.703	0.494	Yes	-0.364	<b>0.902</b>	0.814	31.682	2.936	32.617	2.251	-4	0.935	
		Count Diff (0)	25	TNW	2	55	55	10	45	81.82	10	5.856	11.908	0.725	0.525	Yes	-0.554	0.834	0.696	31.682	2.936	32.700	2.374	0	<b>1.018</b>	
		Count Diff (±1)	25	TLW	2	55	55	10	45	81.82	10	5.855	11.908	0.724	0.525	Yes	-0.563	0.835	0.697	31.682	2.936	32.709	2.370	0	<b>1.027</b>	
		Height Diff	35	BA	1	55	56	10	45	81.82	11	5.974	12.050	0.676	0.457	Yes	0.197	0.826	0.682	31.682	2.936	31.689	2.609	1	<b>0.007</b>	
SD IT Ht	15	BM	4	55	54	13	42	76.36	12	7.448	13.837	0.716	0.512	Yes	-0.650	0.828	0.685	31.682	2.936	33.009	<b>2.158</b>	-1	1.327			

Plot XVI.	Best Parameter	CS	IM	FS	Measured	Identified	Un-matched	Matched	Matched %	Redundant	MAE	RMSE	R	R <sup>2</sup>	Stat Sig R	Mean Diff (MT)	R (MT)	R <sup>2</sup> (MT)	Mean FM Ht	SD FM Ht	Mean IT Ht	SD IT Ht	Count Diff	Height Diff		
All Field-Measured (FM) Trees	Individual Tree App.	Smaller Range	RMSE & R	10	BN	5	66	70	2	64	96.97	6	0.933	<b>3.094</b>	0.732	0.537	Yes	-0.258	0.967	0.935	21.864	2.005	22.018	1.957	4	0.155
			RMSE	10	BN	5	66	70	2	64	96.97	6	0.933	<b>3.094</b>	0.732	0.537	Yes	-0.258	0.967	0.935	21.864	2.005	22.018	1.957	4	0.155
		R	45	TNN	1	66	62	5	61	92.42	1	1.730	4.962	<b>0.752</b>	0.565	Yes	0.310	0.959	0.920	21.864	2.005	21.797	1.742	-4	-0.066	
		R for MT	35	TNW	1	66	64	4	62	93.94	2	1.412	4.579	0.683	0.467	Yes	-0.083	<b>0.978</b>	0.957	21.864	2.005	22.073	1.888	-2	0.209	
	Larger Range	RMSE	10	BN	5	66	70	2	64	96.97	6	0.933	<b>3.094</b>	0.732	0.537	Yes	-0.258	0.967	0.935	21.864	2.005	22.018	1.957	4	0.155	
		R	50	TNW	1	66	59	7	59	89.39	0	2.189	5.975	<b>0.767</b>	0.588	Yes	0.008	0.973	0.947	21.864	2.005	22.280	1.663	-7	0.417	
	Area-Based Approach	R for MT	35	TNW	1	66	64	4	62	93.94	2	1.412	4.579	0.683	0.467	Yes	-0.083	<b>0.978</b>	0.957	21.864	2.005	22.073	1.888	-2	0.209	
		Count Diff (0)	15	BA	4	66	66	4	62	93.94	4	1.459	4.557	0.673	0.453	Yes	0.053	0.965	0.931	21.864	2.005	21.875	1.772	0	<b>0.011</b>	
		Count Diff (±1)	10	BA	6	66	66	3	63	95.45	3	1.166	3.838	0.704	0.495	Yes	-0.050	0.961	0.924	21.864	2.005	21.954	1.846	0	<b>0.090</b>	
		Height Diff	15	BI	4	66	67	3	63	95.45	4	1.156	3.834	0.705	0.497	Yes	0.032	0.966	0.932	21.864	2.005	21.866	1.789	1	<b>0.002</b>	
		SD IT Ht	15	BA	4	66	66	4	62	93.94	4	1.459	4.557	0.673	0.453	Yes	0.053	0.965	0.931	21.864	2.005	21.875	<b>1.772</b>	0	0.011	

Plot XVI.	Best Parameter	CS	IM	FS	Measured	Identified	Un-matched	Matched	Matched %	Redundant	MAE	RMSE	R	R <sup>2</sup>	Stat Sig R	Mean Diff (MT)	R (MT)	R <sup>2</sup> (MT)	Mean FM Ht	SD FM Ht	Mean IT Ht	SD IT Ht	Count Diff	Height Diff		
Reduced Number of FM Trees	Individual Tree App.	Smaller Range	RMSE & R	40	BN	1	59	63	0	59	100.00	4	0.354	<b>0.438</b>	<b>0.969</b>	0.939	Yes	0.187	0.969	0.939	22.322	1.567	21.963	1.738	4	-0.359
			RMSE	40	BN	1	59	63	0	59	100.00	4	0.354	<b>0.438</b>	0.969	0.939	Yes	0.187	0.969	0.939	22.322	1.567	21.963	1.738	4	-0.359
		R	40	BN	1	59	63	0	59	100.00	4	0.354	0.438	<b>0.969</b>	0.939	Yes	0.187	0.969	0.939	22.322	1.567	21.963	1.738	4	-0.359	
		R for MT	35	TNW	1	59	63	1	58	98.31	5	0.631	2.631	0.626	0.392	Yes	-0.064	<b>0.971</b>	0.944	22.322	1.567	22.134	1.839	4	-0.188	
	Larger Range	RMSE	10	BA	6	59	65	0	59	100.00	6	0.317	<b>0.395</b>	0.968	0.937	Yes	0.018	0.968	0.937	22.322	1.567	22.011	1.802	6	-0.311	
		R	40	BN	1	59	63	0	59	100.00	4	0.354	0.438	<b>0.969</b>	0.939	Yes	0.187	0.969	0.939	22.322	1.567	21.963	1.738	4	-0.359	
	Area-Based Approach	R for MT	40	TLN	2	59	53	7	52	88.14	1	2.810	7.326	0.432	0.186	Yes	0.220	<b>0.973</b>	0.946	22.322	1.567	22.182	1.580	-6	-0.140	
		Count Diff (0)	45	TLW	1	59	59	1	58	98.31	1	0.660	2.638	0.634	0.402	Yes	-0.016	0.966	0.933	22.322	1.567	22.309	1.709	0	<b>-0.013</b>	
		Count Diff (±1)	10	TLN	7	59	59	3	56	94.92	3	1.366	4.683	0.510	0.260	Yes	-0.116	0.967	0.934	22.322	1.567	22.337	1.768	0	<b>0.015</b>	
		Height Diff	20	BI	5	59	50	10	49	83.05	1	3.865	8.708	0.483	0.233	Yes	0.175	0.960	0.921	22.322	1.567	22.321	1.543	-9	<b>-0.001</b>	
SD IT Ht	50	TNN	1	59	60	1	58	98.31	2	0.774	2.665	0.602	0.362	Yes	0.333	0.953	0.909	22.322	1.567	21.937	<b>1.553</b>	1	-0.385			

Plot XVII.	Best Parameter	CS	IM	FS	Measured	Identified	Un-matched	Matched	Matched %	Redundant	MAE	RMSE	R	R <sup>2</sup>	Stat Sig R	Mean Diff (MT)	R (MT)	R <sup>2</sup> (MT)	Mean FM Ht	SD FM Ht	Mean IT Ht	SD IT Ht	Count Diff	Height Diff		
All Field-Measured (FM) Trees	Individual Tree App.	Smaller Range	RMSE & R	25	TNW	1	110	106	8	102	92.73	4	1.509	3.793	0.731	0.534	Yes	0.443	<b>0.951</b>	0.905	16.986	1.690	16.687	1.473	-4	-0.299
			RMSE	25	BI	1	110	114	7	103	93.64	11	1.551	<b>3.672</b>	0.653	0.426	Yes	0.511	0.906	0.820	16.986	1.690	16.323	1.657	4	-0.663
		R	15	TLW	2	110	114	9	101	91.82	13	1.611	3.954	<b>0.756</b>	0.571	Yes	0.369	0.871	0.759	16.986	1.690	16.610	1.521	4	-0.377	
		R for MT	25	TNW	1	110	106	8	102	92.73	4	1.509	3.793	0.731	0.534	Yes	0.443	<b>0.951</b>	0.905	16.986	1.690	16.687	1.473	-4	-0.299	
	Larger Range	RMSE	15	BI	2	110	121	6	104	94.55	17	1.361	<b>3.373</b>	0.646	0.418	Yes	0.365	0.870	0.756	16.986	1.690	16.333	1.706	11	-0.653	
		R	30	BI	1	110	98	15	95	86.36	3	2.511	5.252	<b>0.801</b>	0.641	Yes	0.691	0.958	0.918	16.986	1.690	16.671	1.325	-12	-0.315	
	Area-Based Approach	R for MT	15	TNN	3	110	96	16	94	85.45	2	2.521	5.520	0.761	0.580	Yes	0.472	<b>0.959</b>	0.920	16.986	1.690	16.902	1.316	-14	-0.084	
		Count Diff (0)	5	TNW	7	110	112	10	100	90.91	12	1.708	4.235	0.750	0.562	Yes	0.375	0.945	0.892	16.986	1.690	16.644	1.562	2	<b>-0.342</b>	
		Count Diff (±1)	5	TLW	7	110	112	9	101	91.82	11	1.610	4.068	0.718	0.515	Yes	0.372	0.940	0.884	16.986	1.690	16.623	1.595	2	<b>-0.364</b>	
		Height Diff	35	BI	2	110	75	35	75	68.18	0	5.412	8.795	0.672	0.452	Yes	0.721	0.935	0.874	16.986	1.690	16.986	1.067	-35	<b>0.000</b>	
SD IT Ht	5	TNW	7	110	112	10	100	90.91	12	1.708	4.235	0.750	0.562	Yes	0.375	0.945	0.892	16.986	1.690	16.644	<b>1.562</b>	2	-0.342			

Plot XVII.		Best Parameter	CS	IM	FS	Mea- sured	Identi- fied	Un- matched	Matched	Matched %	Redun- dant	MAE	RMSE	R	R <sup>2</sup>	Stat Sig R	Mean Diff (MT)	R (MT)	R <sup>2</sup> (MT)	Mean FM Ht	SD FM Ht	Mean IT Ht	SD IT Ht	Count Diff	Height Diff
Reduced Number of FM Trees	Individual Tree App- Smaller Range	RMSE & R	25	TNW	1	101	106	2	99	98.02	7	0.833	<b>2.298</b>	0.601	0.362	Yes	0.486	0.957	0.915	17.347	1.194	16.687	1.473	5	-0.659
		RMSE	25	TNW	1	101	106	2	99	98.02	7	0.833	<b>2.298</b>	0.601	0.362	Yes	0.486	0.957	0.915	17.347	1.194	16.687	1.473	5	-0.659
		R	20	BI	2	101	97	6	95	94.06	2	1.460	3.815	<b>0.628</b>	0.394	Yes	0.555	0.953	0.907	17.347	1.194	16.830	1.306	-4	-0.517
		R for MT	30	TNN	1	101	102	6	95	94.06	7	1.470	3.854	0.604	0.365	Yes	0.562	<b>0.962</b>	0.926	17.347	1.194	16.665	1.487	1	-0.682
	Larger Range	RMSE	15	TLW	2	101	114	2	99	98.02	15	0.801	<b>2.290</b>	0.599	0.359	Yes	0.440	0.955	0.913	17.347	1.194	16.610	1.521	13	-0.737
		R	15	BM	4	101	83	18	83	82.18	0	3.187	6.707	<b>0.689</b>	0.475	Yes	0.377	0.943	0.890	17.347	1.194	17.297	1.074	-18	-0.049
		R for MT	30	TNN	1	101	102	6	95	94.06	7	1.470	3.854	0.604	0.365	Yes	0.562	<b>0.962</b>	0.926	17.347	1.194	16.665	1.487	1	-0.682
	Area-Based Approach	Count Diff (0)	10	TLN	4	101	100	6	95	94.06	5	1.413	3.883	0.572	0.327	Yes	0.453	0.952	0.907	17.347	1.194	16.853	1.349	-1	<b>-0.493</b>
		Count Diff (±1)	25	BM	1	101	102	6	95	94.06	7	1.386	3.900	0.560	0.314	Yes	0.403	0.946	0.894	17.347	1.194	16.842	1.441	1	<b>-0.505</b>
		Height Diff	20	BM	3	101	78	23	78	77.23	0	3.999	7.709	0.652	0.425	Yes	0.356	0.945	0.892	17.347	1.194	17.356	1.087	-23	<b>0.009</b>
		SD IT Ht	10	TLN	4	101	100	6	95	94.06	5	1.413	3.883	0.572	0.327	Yes	0.453	0.952	0.907	17.347	1.194	16.853	<b>1.349</b>	-1	-0.493

Plot XVIII.		Best Parameter	CS	IM	FS	Mea- sured	Identi- fied	Un- matched	Matched	Matched %	Redun- dant	MAE	RMSE	R	R <sup>2</sup>	Stat Sig R	Mean Diff (MT)	R (MT)	R <sup>2</sup> (MT)	Mean FM Ht	SD FM Ht	Mean IT Ht	SD IT Ht	Count Diff	Height Diff
All Field-Measured (FM) Trees	Individual Tree App- Smaller Range	RMSE & R	10	TNW	5	63	68	11	52	82.54	16	4.015	<b>8.416</b>	<b>0.745</b>	0.555	Yes	-0.601	0.936	0.876	24.103	3.099	25.025	2.349	5	0.922
		RMSE	10	TNW	5	63	68	11	52	82.54	16	4.015	<b>8.416</b>	0.745	0.555	Yes	-0.601	0.936	0.876	24.103	3.099	25.025	2.349	5	0.922
		R	10	TNW	5	63	68	11	52	82.54	16	4.015	8.416	<b>0.745</b>	0.555	Yes	-0.601	0.936	0.876	24.103	3.099	25.025	2.349	5	0.922
		R for MT	10	BI	6	63	58	13	50	79.37	8	4.590	9.331	0.733	0.537	Yes	-0.370	<b>0.953</b>	0.908	24.103	3.099	25.155	2.257	-5	1.052
	Larger Range	RMSE	10	TNW	5	63	68	11	52	82.54	16	4.015	<b>8.416</b>	0.745	0.555	Yes	-0.601	0.936	0.876	24.103	3.099	25.025	2.349	5	0.922
		R	55	BI	1	63	46	18	45	71.43	1	6.268	10.817	<b>0.867</b>	0.751	Yes	0.674	0.937	0.879	24.103	3.099	24.960	1.749	-17	0.857
		R for MT	45	TNN	1	63	52	16	47	74.60	5	5.560	10.595	0.714	0.510	Yes	-0.029	<b>0.972</b>	0.944	24.103	3.099	25.057	2.272	-11	0.954
	Area-Based Approach	Count Diff (0)	35	BI	1	63	64	11	52	82.54	12	4.106	8.755	0.649	0.422	Yes	0.015	0.929	0.863	24.103	3.099	24.144	2.731	1	<b>0.041</b>
		Count Diff (±1)	35	BI	1	63	64	11	52	82.54	12	4.106	8.755	0.649	0.422	Yes	0.015	0.929	0.863	24.103	3.099	24.144	2.731	1	<b>0.041</b>
		Height Diff	5	TNN	8	63	119	6	57	90.48	62	2.775	6.385	0.621	0.386	Yes	-0.908	0.855	0.730	24.103	3.099	24.099	2.418	56	<b>-0.004</b>
		SD IT Ht	35	BI	1	63	64	11	52	82.54	12	4.106	8.755	0.649	0.422	Yes	0.015	0.929	0.863	24.103	3.099	24.144	<b>2.731</b>	1	0.041

Plot XVIII.		Best Parameter	CS	IM	FS	Mea- sured	Identi- fied	Un- matched	Matched	Matched %	Redun- dant	MAE	RMSE	R	R <sup>2</sup>	Stat Sig R	Mean Diff (MT)	R (MT)	R <sup>2</sup> (MT)	Mean FM Ht	SD FM Ht	Mean IT Ht	SD IT Ht	Count Diff	Height Diff
Reduced Number of FM Trees	Individual Tree App- Smaller Range	RMSE & R	65	BA	1	42	42	2	40	95.24	2	2.237	5.545	0.422	0.178	Yes	1.107	0.916	0.838	25.917	1.512	24.715	1.721	0	-1.202
		RMSE	50	BI	1	42	45	1	41	97.62	4	1.267	<b>4.171</b>	0.322	0.103	Yes	0.589	0.940	0.884	25.917	1.512	25.081	1.850	3	-0.835
		R	30	BN	3	42	37	6	36	85.71	1	3.783	9.337	<b>0.469</b>	0.220	Yes	-0.243	0.980	0.959	25.917	1.512	26.264	1.627	-5	0.347
		R for MT	35	TNW	2	42	37	6	36	85.71	1	3.814	9.369	0.449	0.202	Yes	-0.299	<b>0.983</b>	0.966	25.917	1.512	26.306	1.645	-5	0.389
	Larger Range	RMSE	25	TLN	2	42	67	1	41	97.62	26	0.968	<b>4.115</b>	0.322	0.104	Yes	-0.168	0.970	0.940	25.917	1.512	24.911	2.283	25	-1.006
		R	75	BM	1	42	29	13	29	69.05	0	8.034	13.800	<b>0.577</b>	0.333	Yes	-0.533	0.980	0.961	25.917	1.512	26.964	1.396	-13	1.047
		R for MT	40	TNW	3	42	29	13	29	69.05	0	8.002	13.947	0.470	0.221	Yes	-0.350	<b>0.986</b>	0.972	25.917	1.512	26.660	1.508	-13	0.743
	Area-Based Approach	Count Diff (0)	20	TNN	4	42	42	3	39	92.86	3	2.086	6.701	0.370	0.137	Yes	-0.234	0.978	0.957	25.917	1.512	25.927	1.855	0	<b>0.010</b>
		Count Diff (±1)	20	BN	4	42	42	4	38	90.48	4	2.683	7.695	0.397	0.157	Yes	-0.308	0.981	0.962	25.917	1.512	25.947	1.950	0	<b>0.030</b>
		Height Diff	10	TNN	8	42	43	3	39	92.86	4	2.180	6.792	0.327	0.107	Yes	-0.285	0.969	0.940	25.917	1.512	25.911	1.937	1	<b>-0.005</b>
		SD IT Ht	30	BA	3	42	42	1	41	97.62	1	1.029	4.124	0.309	0.095	No	0.257	0.956	0.914	25.917	1.512	25.574	<b>1.678</b>	0	-0.342

Plot IX.		Best Parameter	CS	IM	FS	Mea- sured	Identi- fied	Un- matched	Matched	Matched %	Redun- dant	MAE	RMSE	R	R <sup>2</sup>	Stat Sig R	Mean Diff (MT)	R (MT)	R <sup>2</sup> (MT)	Mean FM Ht	SD FM Ht	Mean IT Ht	SD IT Ht	Count Diff	Height Diff
All Field-Measured (FM) Trees	Individual Tree App- Smaller Range	RMSE & R	30	TLN	1	74	74	17	57	77.03	17	3.779	6.969	0.668	0.446	Yes	-0.798	0.621	0.386	17.784	4.109	19.319	2.620	0	1.535
		RMSE	5	TLN	9	74	79	13	61	82.43	18	3.281	<b>6.137</b>	0.648	0.420	Yes	-1.243	0.631	0.399	17.784	4.109	19.500	2.530	5	1.716
		R	30	BI	1	74	71	19	55	74.32	16	4.022	7.215	<b>0.708</b>	0.501	Yes	-0.350	0.769	0.592	17.784	4.109	19.051	2.171	-3	1.267
		R for MT	30	BI	1	74	71	19	55	74.32	16	4.022	7.215	0.708	0.501	Yes	-0.350	<b>0.769</b>	0.592	17.784	4.109	19.051	2.171	-3	1.267
	Larger Range	RMSE	5	TLN	9	74	79	13	61	82.43	18	3.281	<b>6.137</b>	0.648	0.420	Yes	-1.243	0.631	0.399	17.784	4.109	19.500	2.530	5	1.716
		R	35	TLW	1	74	56	20	54	72.97	2	4.023	7.245	<b>0.783</b>	0.613	Yes	-0.236	0.667	0.444	17.784	4.109	19.823	2.793	-18	2.039
		R for MT	40	TNN	1	74	53	24	50	67.57	3	4.671	8.047	0.767	0.588	Yes	-0.147	<b>0.915</b>	0.837	17.784	4.109	19.874	1.584	-21	2.090
		Area-Based Approach	Count Diff (0)	30	TLN	1	74	74	17	57	77.03	17	3.779	6.969	0.668	0.446	Yes	-0.798	0.621	0.386	17.784	4.109	19.319	2.620	0
	Count Diff (±1)		5	BA	9	74	75	15	59	79.73	16	4.049	7.417	0.485	0.235	Yes	-1.320	0.654	0.427	17.784	4.109	19.249	2.824	1	<b>1.465</b>
	Height Diff		5	BI	5	74	223	1	73	98.65	150	2.331	4.343	0.410	0.168	Yes	-2.004	0.686	0.470	17.784	4.109	17.777	3.350	149	<b>-0.007</b>
	SD IT Ht		5	BN	9	74	73	15	59	79.73	14	3.937	7.063	0.560	0.313	Yes	-1.361	0.676	0.457	17.784	4.109	19.772	<b>1.791</b>	-1	1.988

Plot IX.		Best Parameter	CS	IM	FS	Mea- sured	Identi- fied	Un- matched	Matched	Matched %	Redun- dant	MAE	RMSE	R	R <sup>2</sup>	Stat Sig R	Mean Diff (MT)	R (MT)	R <sup>2</sup> (MT)	Mean FM Ht	SD FM Ht	Mean IT Ht	SD IT Ht	Count Diff	Height Diff
Reduced Number of FM Trees	Individual Tree App- Smaller Range	RMSE & R	10	TNW	5	53	56	1	52	98.11	4	0.807	<b>2.475</b>	0.632	0.399	Yes	-0.406	0.956	0.914	19.991	1.512	20.282	1.608	3	0.291
		RMSE	10	TNW	5	53	56	1	52	98.11	4	0.807	<b>2.475</b>	0.632	0.399	Yes	-0.406	0.956	0.914	19.991	1.512	20.282	1.608	3	0.291
		R	10	TNW	6	53	54	3	50	94.34	4	1.447	4.166	<b>0.644</b>	0.415	Yes	-0.411	0.949	0.900	19.991	1.512	20.384	1.544	1	0.393
		R for MT	35	TNW	1	53	56	2	51	96.23	5	1.103	3.685	0.477	0.227	Yes	-0.294	<b>0.960</b>	0.921	19.991	1.512	20.149	1.606	3	0.158
	Larger Range	RMSE	5	TLN	9	53	76	1	52	98.11	24	0.800	<b>2.474</b>	0.631	0.399	Yes	-0.388	0.955	0.912	19.991	1.512	19.745	1.735	23	-0.245
		R	10	TNW	6	53	54	3	50	94.34	4	1.447	4.166	<b>0.644</b>	0.415	Yes	-0.411	0.949	0.900	19.991	1.512	20.384	1.544	1	0.393
		R for MT	35	TNW	1	53	56	2	51	96.23	5	1.103	3.685	0.477	0.227	Yes	-0.294	<b>0.960</b>	0.921	19.991	1.512	20.149	1.606	3	0.158
		Area-Based Approach	Count Diff (0)	45	TLW	1	53	53	5	48	90.57	5	2.072	5.593	0.575	0.330	Yes	-0.270	0.944	0.891	19.991	1.512	19.931	2.821	0
	Count Diff (±1)		25	BA	2	53	53	4	49	92.45	4	1.984	5.520	0.224	0.050	No	-0.044	0.857	0.735	19.991	1.512	19.917	1.439	0	<b>-0.073</b>
	Height Diff		25	BI	2	53	52	4	49	92.45	3	1.984	5.521	0.223	0.050	No	-0.080	0.855	0.731	19.991	1.512	19.981	1.436	-1	<b>-0.009</b>
	SD IT Ht		15	BI	4	53	52	5	48	90.57	4	2.287	5.989	0.309	0.096	Yes	-0.214	0.868	0.754	19.991	1.512	20.167	<b>1.354</b>	-1	0.176

Plot XX.		Best Parameter	CS	IM	FS	Mea- sured	Identi- fied	Un- matched	Matched	Matched %	Redun- dant	MAE	RMSE	R	R <sup>2</sup>	Stat Sig R	Mean Diff (MT)	R (MT)	R <sup>2</sup> (MT)	Mean FM Ht	SD FM Ht	Mean IT Ht	SD IT Ht	Count Diff	Height Diff
All Field-Measured (FM) Trees	Individual Tree App- Smaller Range	RMSE & R	20	BA	3	62	62	14	48	77.42	14	7.302	12.666	0.482	0.232	Yes	0.945	0.834	0.696	28.137	3.910	26.314	5.932	0	-1.823
		RMSE	45	TNN	1	62	64	13	49	79.03	15	6.780	<b>12.559</b>	0.334	0.111	Yes	-0.346	0.803	0.645	28.137	3.910	27.416	5.601	2	-0.721
		R	15	BI	4	62	63	17	45	72.58	18	8.193	13.647	<b>0.544</b>	0.296	Yes	0.529	0.805	0.648	28.137	3.910	26.752	5.923	1	-1.385
		R for MT	45	BN	1	62	61	15	47	75.81	14	7.019	12.855	0.489	0.239	Yes	-0.407	<b>0.856</b>	0.732	28.137	3.910	28.183	5.625	-1	0.046
	Larger Range	RMSE	45	TNN	1	62	64	13	49	79.03	15	6.780	<b>12.559</b>	0.334	0.111	Yes	-0.346	0.803	0.645	28.137	3.910	27.416	5.601	2	-0.721
		R	55	BI	1	62	51	18	44	70.97	7	9.091	13.873	<b>0.663</b>	0.439	Yes	2.407	0.830	0.689	28.137	3.910	26.633	4.197	-11	-1.504
		R for MT	25	BN	2	62	68	15	47	75.81	21	7.116	13.112	0.426	0.182	Yes	-0.530	<b>0.873</b>	0.762	28.137	3.910	28.560	4.444	6	0.422
		Area-Based Approach	Count Diff (0)	15	TNN	4	62	62	16	46	74.19	16	7.676	13.560	0.525	0.276	Yes	0.246	0.630	0.396	28.137	3.910	27.862	5.609	0
	Count Diff (±1)		45	BN	1	62	61	15	47	75.81	14	7.019	12.855	0.489	0.239	Yes	-0.407	0.856	0.732	28.137	3.910	28.183	5.625	-1	<b>0.046</b>
	Height Diff		10	TLN	5	62	69	15	47	75.81	22	7.423	13.365	0.462	0.213	Yes	-0.026	0.599	0.359	28.137	3.910	28.138	5.470	7	<b>0.001</b>
	SD IT Ht		45	BI	1	62	61	16	46	74.19	15	8.721	13.887	0.427	0.182	Yes	1.740	0.783	0.613	28.137	3.910	25.602	<b>5.252</b>	-1	-2.535



Plot XX.	Best Parameter	CS	IM	FS	Mea- sured	Identi- fied	Un- matched	Matched	Matched %	Redun- dant	MAE	RMSE	R	R <sup>2</sup>	Stat Sig R	Mean Diff (MT)	R (MT)	R <sup>2</sup> (MT)	Mean FM Ht	SD FM Ht	Mean IT Ht	SD IT Ht	Count Diff	Height Diff		
Reduced Number of FM Trees	Individual Tree App- Smaller Range	RMSE & R		35	TNN	2	47	46	8	39	82.98	11.831	0.397	0.157	Yes	0.441	0.948	0.899	29.755	2.826	28.953	3.069	-1	-0.802		
		RMSE		55	BI	1	47	51	6	41	41	87.23	<b>10.983</b>	0.340	0.116	Yes	2.354	0.828	0.685	29.755	2.826	26.633	4.197	4	-3.122	
		R		20	TNN	4	47	43	9	38	38	80.85	6.470	12.968	<b>0.450</b>	0.203	Yes	0.805	0.693	0.480	29.755	2.826	28.918	5.025	-4	-0.837
		R for MT		30	BM	2	47	48	8	39	39	82.98	5.333	11.815	0.383	0.147	Yes	-0.200	<b>0.968</b>	0.936	29.755	2.826	29.891	2.827	1	0.135
	Larger Range	RMSE		15	BA	4	47	63	5	42	42	89.36	<b>9.623</b>	0.373	0.139	Yes	0.869	0.858	0.736	29.755	2.826	26.830	5.864	16	-2.925	
		R		15	BN	7	47	35	13	34	34	72.34	8.116	14.659	<b>0.549</b>	0.301	Yes	-0.059	0.961	0.924	29.755	2.826	30.469	2.519	-12	0.714
		R for MT		50	BM	1	47	41	10	37	37	78.72	6.422	12.975	0.466	0.217	Yes	-0.330	<b>0.970</b>	0.941	29.755	2.826	29.636	5.020	-6	-0.119
		Count Diff (0)		45	BM	1	47	47	11	36	36	76.60	7.172	13.877	0.378	0.143	Yes	-0.360	0.966	0.934	29.755	2.826	29.386	4.806	0	<b>-0.369</b>
	Area-Based Approach	Count Diff (±1)		30	BM	2	47	48	8	39	39	82.98	5.333	11.815	0.383	0.147	Yes	-0.200	0.968	0.936	29.755	2.826	29.891	2.827	1	<b>0.135</b>
		Height Diff		45	TLN	2	47	38	9	38	38	80.85	6.056	12.464	0.416	0.173	Yes	0.350	0.951	0.904	29.755	2.826	29.742	2.706	-9	<b>-0.014</b>
		SD IT Ht		30	BM	2	47	48	8	39	39	82.98	5.333	11.815	0.383	0.147	Yes	-0.200	0.968	0.936	29.755	2.826	29.891	<b>2.827</b>	1	0.135

### Explanatory note:

CS - Cell Size,

IM - Interpolation Method,

FS - Focal Statistics Circle Radius,

**Measured** - number of field-measured (FM) trees,

**Identified** - number of trees identified within Thiessen polygons,

**Unmatched** - number of FM trees without any matching identified tree,

**Matched** - number of FM trees matched with (i.e. paired to) identified trees,

**Matched %** - percentage of matched trees from all FM trees,

**Redundant** - number of redundantly identified trees (not matched),

**MAE** - Mean Absolute Error for FM and counted heights,

**RMSE** - Root Mean Square Error for FM and counted heights,

**R** - Pearson's Correlation Coefficient for FM and counted heights,

**R<sup>2</sup>** - Coefficient of Determination for FM and counted heights,

**Stat Sig R** - Statistical Significance of the Pearson's Correlation Coefficient,

**Mean Diff (MT)** - Mean Difference between average values of FM and counted heights for Matched Trees (MT) only,

**R (MT)** - Pearson's Correlation Coefficient for Matched Trees only,

**R<sup>2</sup> (MT)** - Coefficient of Determination for Matched Trees only,

**Mean FM Ht** - Mean height of FM trees,

**SD FM Ht** - Standard Deviation of heights of FM trees,

**Mean IT Ht** - Mean height of Identified Trees (IT),

**SD IT Ht** - Standard Deviation of heights of identified trees,

**Count Diff** - Difference between count of identified and FM trees,

**Height Diff** - Difference between mean height of identified and FM trees.